

HEMOZOIN: A PARADIGM FOR BIOMINERALIZATION IN DISEASE

By

Melissa D. Carter

Dissertation

Submitted to the Faculty of the
Graduate School of Vanderbilt University
in partial fulfillment of the requirements

for the degree of

DOCTOR OF PHILOSOPHY

in

Chemistry

August, 2009

Nashville, Tennessee

Approved:

Dr. David W. Wright

Dr. Richard N. Armstrong

Dr. John A. McLean

Dr. Craig W. Lindsley

To my core few —

My parents Allen and Linda Carter —

Two people who counted each blessing and taught me to do the same.

My Savior Jesus Christ —

The cornerstone of all grace, love and mercy.

ACKNOWLEDGEMENTS

This work would not have been possible without the financial support of Vanderbilt University, the National Institutes of Health (R03AI060827 and U54AI057157) and the Department of Defense (W81XWH-07-ACA-0092) from the Army Medical Material Research Command. NIAID Contract N01-A1-30026 of the NIAID Schistosomiasis Resource Center under the direction of Fred Lewis enabled the use of a *S. mansoni* infected Swiss Webster murine model. Vanderbilt's large collaborative cores were also crucial in the compilation of this body of work. The Vanderbilt Mass Spectrometry Research Center and staff, especially Dr. David Hachey, Dr. Wade Calcutt and Ms. Dawn Overstreet, were significant resources in several analyses. The Vanderbilt Division of Animal Care and Institute of Animal Care and Use Committee, especially Ms. Paula Austin and Dr. Yasin Kokoye, made possible our on-campus mouse studies. The Vanderbilt High Throughput Screening Facility and the Vanderbilt Institute of Chemical Biology, especially Mrs. Lisa Wright, Mr. Daniel Dorset and Mrs. Michelle Lewis, enabled our screening of over 100,000 compounds for activity against β -hematin crystallization *in vitro*. The Vanderbilt Institute of Nanoscale Science and Engineering, especially Dr. Anthony Hmelo, provided access to sensitive imaging instruments such as the scanning electron microscope. The Vanderbilt Medical Center Cell Imaging Shared Resource, especially Mr. Sean Schaffer, enabled the imaging of several light and confocal images.

This work would also not have been possible without the advisement of my Ph.D. Committee members. To my advisor, David W. Wright, I would like to say thank you for

your. . . “exhilaration” toward our work. You have been at my side and heels the entire step of the way, like a housed jack russell. No matter the American Doll compensation, I maintain that Ella should have a pony; we had one; why shouldn’t she? Furthermore, I am very happy that I was able to return the favor of several morning scares one Saturday morning; I would say you averaged a three inch jump, and you deserved it. Thank you for always “encouraging” me to think harder and smarter about my project(s) by whatever means necessary. To Dr. Richard N. Armstrong, I began my graduate career with a rotation in your research group, and like Dr. Wright, you have known my work the longest while at Vanderbilt. During my qualifying exam, you asked me about the excretion of antimalarials in patients, and I remember blinking/gulping at my own ignorance for not considering the travel of the compounds I would be identifying in my proposed assays. Thank you. To Dr. Craig W. Lindsley, you were an addition to my committee as we began to consider developing assays worthy of high throughput screening. You introduced me to the NCGC website and consequently, Z’ factors. In short, had I not met with you a month prior to my qualifying exam and the proposal of my assays as high throughput screens, that exam could have been disastrous. Thank you. Last but not least is Dr. John A. McLean. Dr. McLean, thank you for always reading my written submissions thoroughly; you were quick to inquire on the difference between HeNe1 and HeNe2 lasers and considerately waited as I fumbled over my idea of their difference before disclosing that in fact, there was no difference. We began our Vanderbilt careers the same year, and yet, you have always made time to meet with me and attend my committee meetings with interest. Thank you.

Outside of graduate school, I am grateful for the many teachers who have guided me in my career. The first are my parents. You gave me life, guided my every step and never abandoned my side no matter my scorn or immaturity. You held my hand when I was scared, held my hair when I was sick and held me when only a parents' love could save. I praise you for your wisdom, sacrifice, persistence and most of all, love. You told me once, "You can quit or you can press on, but you are not going to sit there and cry about it." Your girl's got grit. Thank you. I would also like to thank my large extended family for their love and support. I have felt the comfort of your presence for many years, if only everyone could be so fortunate. Perhaps the most adoring addition to my family, Buddy, always listened to my concerns and provided a means of procrastination in physics class. There is a long list preceding him deserving of my deep appreciation, too, and they are: Taff, Red, Blacky, Thumper, Cottontail, O'Hare McGregor, Tangerine, Sherbet, Daffodil, Rooster Cogbourne, several Goldies and a couple of Kermets.

There have been many teachers who spent tireless hours training me; I am sorry that I can only compose a list here: Mrs. Rosemary Trent, Mrs. Paula Cates, Ms. Rhonda, Ms. Margaret, Ms. Jackie, Ms. Teresa Weatherford, Mrs. Bayes, Mrs. Seal, Mrs. Edwards, Mrs. Grigsby, Mrs. Stout, Mr. Small, Mr. & Mrs. Herron, Mrs. Greer, Mrs. Cloud, Mr. & Mrs. Ketron, Mrs. Lotts, Ms. Hughes, Mr. Welch, Mrs. Hall, Mrs. Evers, Mrs. Dorothy Hanner-Ratcliff, Mrs. Louise Dickson, Mrs. Melita Warner-Brock, Mrs. Bentzen, Mrs. Bovender, Mrs. Wiseman, Mr. Lafe Cook, Mr. Bill Martin, Mr. Wilson, Mrs. Woods, Miss Lisa Jones, Prof. Gerald Seebach, Prof. Carl Heltzel, Prof. Eva Csuهاي, Prof. Alan Goren, Prof. Kimberley Williams, Prof. Kathleen Jagger, Prof. Peggy

Palombi, Prof. Ben Hawkins, Prof. Forlami Ladipo, Prof. Norman Loney, Ms. Kim Williams, Pastor Frank and Master Shin. Thank you.

Certainly, an acknowledgements section would not be complete without paying homage to my long-standing friendships. To Megan Griffin, thank you for being my best friend. Consequently, you are also the recipient of my longest-lasting friendship; God bless you! You sent me off to college with a year's subscription to Cosmopolitan to counterbalance my otherwise sheltered countenance. To Jamie Wilhite, you were my college lab partner and fellow sufferer of several physical chemistry lab reports. You introduced me to the art of random questions and taught me there's never a moment of stress that can't be relieved by a good laugh. Thank you. To Tina Thrasher-Shelton, you were originally my strict boss and ultimately, a very dear and trusted friend. You are like family to me, and through you, I have witnessed and learned to appreciate the home-game glory of Alabama's best.

My lab has a "full disclosure" quote board at its doorway, and that is how I choose to remember everyone— out of context and in the funniest of moments. After all, these are what ultimately chase away the apathy, and for those many endearing days, I am eternally grateful. To Clare Kenny Carney, I am thankful for my recruitment into the Wright lab and your crying son who rescued me from a \$180 speeding ticket. I'm thankful to Scott Miller for his direct frankness and his ability to roll with the New Orleans festivities. Elizabeth Bentzen baked decadent cakes and was fierce as a poker player. Malgorzata Broncel was behind many successful experiments in our lab and introduced us all to the finer tastes of tea-time. Aren Gerdon was the analytical chemist within us all and always seemed to know what to say or ask in order to inspire us. Many

thanks to Sarah Sewell-Pierce for always reminding me that “grad school is not a race, it’s a marathon” and for introducing me to MySpace and Facebook. My advisor read that last sentence and may be exploding. To Ryan Rutledge and Alex Schrimpe-Rutledge who threw an awesome ugly sweater party and managed to have a minor marital tiff over monopoly real estate, you deserve muchos kudos for remaining happy while both working and living together. To Kristin Halfpenny, my dissertation writing buddy, who joined me for some intense mileage at the gym and broke up a dog fight in the middle of the street that consequently scared a mailman back into his mail truck, thanks for being a fun rotation mentor and for all the Facebook bumper stickers. To Leila Deravi: Roll Tide! We hung in there little root, and we learned so much. Thank you for forgiving me.

To Anh Hoang, my baymate and the woman who beat the guys at fantasy football two years in a row, thank you for all your kindness. Vanessa Scott is an individual all to herself: a punk, owner of a 12 ft. Burmese python and zombie movie junkie. It’s been fun. Josh Swartz reminds me of Scott Miller in so many ways, but now he is hemozoin so who knows, that may all change. To Stephen Jackson, you are probably the only person I know who is awesome enough to have an adopted elephant, Willie. To Rebecca Sandlin, it has been a pleasure working with you, and I wish you all the best with your future hemozoin discoveries and just to be safe, better “balance”. John Stone, thank you for always bringing a smile to my face. I just wish we could have played tennis once or twice. To Catherine Prudom, many thanks for your friendship, from sharing in Newton and Darwin’s puppy days to your generous advice on phage.

This brings me to my final Wright lab salutes. The first of which goes to S. Reese Harry, a very dear friend who helped me find my color. His, he said, was gray. Mine, I

couldn't decide and am therefore, left with an eclectic dark brown pigment, only slightly ironic given four years of hemozoin studies. You were my first baymate; you "expanded" my vocabulary and introduced me to some of life's more entertaining vices. In short, you are the brother I may have asked for at some point. You were a shoulder to lean on, an ear that cared and a firm dose of reality when needed. Thank you. Finally, there's Jonas Perez, or Jon-ass as I knew him initially. There are some people in life you meet who you weren't trying to meet, but God sits them right in your path, and Jonas, you are one of those. I had forgotten something very important to me, and simply put, you reminded me, and for that, I am more grateful than these words of gratitude will ever read. Thank you. Oh, but please don't go digging up anymore backyards; that freaked me out a little. So Reese and Jonas- I love you guys; now wipe the tears and pop a top! I know Thursdays will never be the same, but stay strong; you're up next, and you can profess your undying gratitude soon, too.

For most graduate students, there are other graduate students, outside of their research group, that play a large role in their success. I have at least four of these people to thank. The first is Vanessa Phelan, the New Yorker who braved a Tennessee graduate school. You made a wonderful football, baseball and concert buddy, and at the end of the day, we saw each other at the best and worst of moments but still triumphed. To Brooke Gliga, you may just be one of the most random people (that is a compliment) as well as one of the sweetest. Thank you for bringing humor to mouse day and sharing so much. To Dan Brown, thank you for your plethora of advice on assay screening. To Blake Branson, we spent an exhausting amount of time trying to coax beautiful spectra from an aging XRD; thank you for all your help.

Finally, there is my church family. It wasn't until my last year in graduate school that I had a come-to-Jesus-experience and there, I found some of my most cherished friends. Thank you Melita Thomas for always having a quirky sense of humor and grounded spirit. Thank you Cheri Viar for sharing in my love of shoes and for joining in the many Friday movie ventures. And broadly (because I'm running out of room), thank you Ashley Edmiston, Jimmy and Kristen Jernigan, Trent and Kara Mitchell, Nancy Carver, Katie Dobyys, Denise Zannino, Kim Williams, Adam King, Lea Ann Henderson, Andrew and Pam Smith and Cherilyn Crowe. Thank you all; I couldn't ask for better friends.

TABLE OF CONTENTS

	Page
DEDICATION	ii
ACKNOWLEDGEMENTS	iii
LIST OF TABLES	xiii
LIST OF FIGURES	xiv
LIST OF SCHEMES	xvii
Chapter	
I. INTRODUCTION	1
Hemozoin: A Paradigm for Biominerals in Disease	1
Heme Homeostasis	2
Biomineralization	5
Search for Hemozoin's Bionucleating Template	7
Target of Antimalarials	10
Hemozoin Characterization	13
Identification of Native Lipid Components of Hemozoin	16
Chemical Reactivity and Immunomodulation	17
Conclusions	21
II. IDENTIFICATION OF HYDROXYEICOSATETRAENOIC ACID COMPONENTS OF SCHISTOSOMAL HEMOZOIN	24
Experimental	25
Results and Discussion	29
Conclusions	38
III. IMMUNOMODULATORY ACTIVITY OF HEMOZOIN	39
Experimental	41
Results and Discussion	48
Conclusions	61
IV. <i>IN SITU</i> ISOLATION OF SCHISTOSOMAL HEMOZOIN	63
Experimental	66

Results and Discussion	73
Conclusions	89
V. LIPOPHILIC MEDIATED ASSAYS FOR β-HEMATIN INHIBITORS	91
Experimental	94
Results and Discussion	97
Conclusions	107
VI. HIGH THROUGHPUT SCREENS FOR LEAD SMALL-MOLECULE INHIBITORS OF β-HEMATIN CRYSTALLIZATION	109
Experimental	111
Results and Discussion	112
Conclusions	123
 Appendix	
A. CELL AND TISSUE CULTURE PROTOCOLS AND ASSAYS	126
Cell Culture, Counting and Plating	126
Griess Assay	131
Cytochrome C Superoxide Assay	132
Amplex Red Hydrogen Peroxide Assay	135
Alternatively Activated Macrophages	136
B. SCHISTOSOMIASIS STUDY PROTOCOLS	139
Murine Model Infection	139
Observed Disease Progression	140
Schistosome Perfusion	141
Hemozoin Isolation	143
Thromboxane Assay for Mouse Urine	144
Anti-HNE Immunostaining of Thin Tissue Sections	147
C. β-HEMATIN ASSAY PROTOCOLS	150
Dehydrohalogenation β -Hematin Synthesis	150
Crystal Extension Assay	151
Lipid-Mediated Crystallization Assay	153
Detergent-Mediated Crystallization Assay	155
BH Assay Development and Optimization	158
Hydrogen Peroxide Degradation Assay	161
D. HTS PRELIMINARY HITS OF THE NP-40 MEDIATED BH CRYSTALLIZATION ASSAY	164

BIBLIOGRAPHY	176
CURRICULUM VITAE	192

LIST OF TABLES

Table		Page
1.	Lipophilic Mediators of BH Formation	99
2.	Efficacy of Known BH Inhibitors in the Lipophilic Mediated Assays	101
3.	Evaluation of Common Interfering Agents	104
4.	Results of Follow-Up Screen Concentration Response Curves	124
5.	Cell Plating Values for Optimal Cell Confluence	130
6.	Chloroquine-Inhibited Neutral Lipid BH Assay's Response to pH and Ionic Strength	158
7.	Amodiaquine-Inhibited Neutral Lipid BH Assay's Response to pH and Ionic Strength	159
8.	Chloroquine-Treated NP-40 BH Assay's Response to pH and Ionic Strength	159

LIST OF FIGURES

Figure	Page
1. Modes of hemozoin inhibition	11
2. Hemozoin-chloroquine binding model	12
3. Physical characterization of hemozoin	15
4. Hemozoin from <i>S. mansoni</i>	29
5. IR and XRD of HZ	30
6. HETE-containing lipid coat of native <i>SmHZ</i>	31
7. Extracted ion profile of <i>SmHZ</i> lipid coat	32
8. Chiral-RP-LC-MS/MS of <i>SmHZ</i> lipid coat	33
9. Hemozoin-mediated lipid peroxidation of arachidonic acid	35
10. Extracted ion profile of HETEs from the BH-AA reaction	36
11. Extracted ion profile of HETEs from the <i>SmHZ</i> -AA reaction	37
12. Impact of native <i>SmHZ</i> and components on iNOS activity	38
13. Effect of BH on the production of ROS and RNS	49
14. Effect of preincubation of RAW cells with BH on RNS production as measured by the Griess assay	50
15. Degradation of BH	52
16. Colocalization of BH inside acidic vacuoles	54
17. Confocal images of BH degradation inside RAW cells	56
18. Concentration-dependent effect of HNE treatment on oxidative burst	57
19. Concentration-dependent effect of 15-HETE treatment on oxidative burst	59
20. Effect of the products of ghost and BH interactions on oxidative burst	60

21.	Growth of <i>S. mansoni</i> -infected livers and spleens through 8 weeks p.i.	75
22.	Variation in mice and organ weight	76
23.	Hematoxylin and eosin (H&E) immunostaining of liver and spleen tissue	77
24.	Physical characterization of isolated schistosomal HZ	79
25.	Quantification of HZ isolated from livers and spleens	80
26.	ICP-MS determined iron content of collected livers and spleens	81
27.	Anti-4-HNE immunostaining of liver and spleen tissue sections	84
28.	LC-MS/MS identification of IsoKs from BH reaction with AA	85
29.	IsoK immunostaining of liver and spleen tissue sections	87
30.	Measurement of IsoP and IsoF levels in livers and spleens	88
31.	Assay development and validation pathway	92
32.	Powder XRD of Bohle and NP-40 BH products	98
33.	Assay optimization of substrate heme and lipophilic mediator	100
34.	Amodiaquine CRCs of neutral lipid and NP-40 mediated BH assays	102
35.	Assessment of plate uniformity	103
36.	Natural product extracts in BH crystallization screens	106
37.	Red Cinchona bark extract in BH crystallization assay	107
38.	Calculation of Z' values during assay cross validation	113
39.	CRC of amodiaquine in the NP-40 BH assay	113
40.	Small molecule library screens in the NP-40 BH assay	114
41.	Structural trends in the preliminary hits from the NP-40 BH assay screens	119
42.	Azole trends in the preliminary hits from the NP-40 BH assay screens	121
43.	Concentration response curve of preliminary hit	122

44.	Hemocytometer grid	129
45.	Percutaneous tail infection of Swiss Webster mice with <i>S. mansoni</i> cercariae ..	139
46.	Increase in abdominal circumference in disease progression	141
47.	<i>S. mansoni</i> collection from infected Swiss Webster mice	142
48.	Structure of 11-dehydro-thromboxane B ₂ (TxB ₂)	145
49.	Mouse urine TxB ₂ levels during <i>S. mansoni</i> infection	147
50.	CRCs from BH crystal extension assay	151
51.	Cross validation of BH crystal extension assay	152
52.	Inhibition studies of neutral lipid blend mediated BH assays	154
53.	CRCs of NP-40 mediated BH assays	156
54.	HTS plate layout of the NP-40 BH assay	157
55.	Quantification of BH formed at varying pH and buffer ionic strength	160
56.	Kinetic and heme-dose response studies in the BH crystallization assays	161
57.	H ₂ O ₂ degradation of BH produced from varying templates	163
58.	Numerical plot of structural trends of preliminary hits in the NP-40 BH assay screens	164

LIST OF SCHEMES

Scheme	Page
1. Ordered pathway of hemoglobin catabolism	3
2. Hemozoin-mediated lipid peroxidation	18
3. Purported pathways of heme degradation by H ₂ O ₂	53
4. Initiation of lipid peroxidation by HZ redox cycling	65
5. Potential lipid peroxidation products of arachidonic acid	82
6. IC _{MAX} hits identified in the preliminary screens of the NP-40 BH assay	116
7. Chemical properties of the BH assay controls amodiaquine and chloroquine ...	117
8. Azole structures observed in preliminary hits of the NP-40 BH assay screens ..	120
9. Structures searched in preliminary hits from NP-40 BH assay screens	122
10. Griess reaction scheme	131
11. Cytochrome c reduction by superoxide	133
12. Amplex red oxidation to fluorescent resorufin	135
13. Th1 and Th2 stimulant response pathway in macrophage cells	137
14. KMnO ₄ standardization	161
15. H ₂ O ₂ standardization	162
16. Complete list of preliminary hits identified in the NP-40 mediated BH crystallization assay small molecule library screens	165

CHAPTER I

INTRODUCTION

Hemozoin: A Paradigm for Biominerals in Disease^{1,2}

Biom mineralization is the biologic formation of organic-inorganic composites generally organized on a nucleating template of organic material. During bone and teeth formation, hydroxyapatite, which is a calcium phosphate derivative enriched with carbonate, mineralizes on a template of collagen fibrils and other proteins.³ Likewise, calcium oxalate monohydrate crystals mineralize on a biologic matrix of proteins in both plants and humans. Although these crystals function as tissue support in plants,⁴ they cause painful inflammation in humans.⁵ In fact, biom mineralization is associated with several human diseases. Nephrolithiasis is the mineralization of calcium oxalate monohydrate in the urinary tract of patients as kidney stones. In gout or metabolic arthritis, monosodium urate crystals accumulate in the articular joints. A patient's innate immune response or the on-rush of monocytes and neutrophils at the sites of crystal sedimentation causes the characteristic tissue inflammation and pain associated with these diseases. Biom mineralization can also contribute to the pathology of parasitic diseases like malaria and schistosomiasis. When the malarial protozoa *Plasmodium falciparum* deposits heme-derived aggregates in host vasculature, these aggregates travel through the bloodstream and collect in the brain, spleen and liver. When they are phagocytosed by innate immune cells such as monocytes and neutrophils, the cells'

ability to produce reactive oxygen and nitrogen species is impaired. This immunomodulation is typical of the pathogenesis caused by many biomineral-associated diseases.

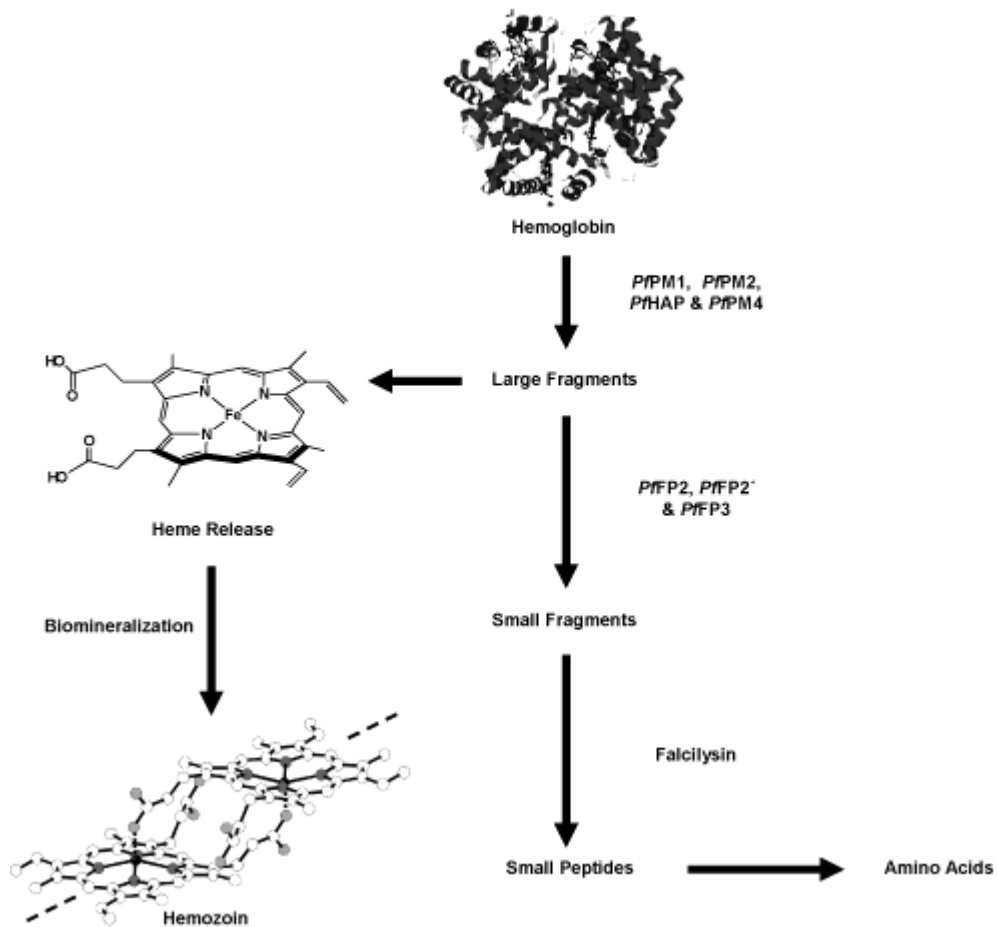
Heme Homeostasis

Over 40% of the world's population is at risk from malaria. The disease causes severe illness in over 500 million people and results in over 1.7 million deaths each year. Transmission is most prevalent in the world's poorest countries, predominantly sub-Saharan Africa, and accounts for 40% of public healthcare costs. In addition, a 2007 World Health Organization report estimates a 1.3% decline in annual economic growth for countries with high rates of malarial infection. Compounded over time, this drop contributes significantly to GDP disparities between those countries where malarial infection is endemic and those where it is not.

Over 100 *Plasmodium* species contribute to the spread of malaria, but only four of these (*P. falciparum*, *P. vivax*, *P. ovale*, and *P. malariae*) account for human infection, the deadliest being *P. falciparum*. The malaria life cycle exists first in a mosquito, and then it passes to a human host. An infected female *Anopheles* mosquito is the host of the parasite's sporogonic life cycle. Mature *P. falciparum* sporozoites reach the salivary glands of the mosquito, and the parasite is transmitted to a human host when the mosquito feeds. During this blood meal, sporozoites are released into the bloodstream where they penetrate hepatic cells and mature into schizonts. The liver cells rupture after approximately two weeks, discharging merozoites into the bloodstream whereupon they

infect red blood cells (RBCs). Every 48 to 78 hours, mature merozoites rupture from spent RBCs and either they differentiate into gametocytes or they infect more RBCs. This blood stage is responsible for the clinical manifestation of the disease.⁶

P. falciparum ingest and degrade up to 80% of host erythrocyte hemoglobin (Hb) to provide the parasite with essential amino acids for growth and maturation.⁶ During high parasitemia (20%), up to 100 g of the 750 g of circulating host Hb can be catabolized by the parasite.⁶



Scheme 1 Ordered pathway of hemoglobin catabolism. Host Hb cleavage is initiated by *Pf*PM1 and *Pf*PM2. Hb unfolds, releases heme and exposes other peptide bonds to the falcipains. Resultant protein fragments are degraded even more by falcilysin and transported to the cytosol where they are broken down into needed amino acids. The heme released in the first step aggregates via biominerallization to form HZ.

Hb is broken down in the parasite's acidic (pH 4.5-5.2) digestive food vacuole (DV) by a suite of proteinases that includes four aspartic acid proteinases (plasmepsins *PfPM1*, *PfPM2*, *PfHAP*, and *PfPM4*), three cysteine proteinases (falcipains *PfFP2*, *PfFP2'*, and *PfFP3*), and a metalloproteinase (falcilysin) (Scheme 1).⁷ This ordered catabolic process is initiated by *PfPM1* and *PfPM2*, which cleave between residues $\alpha 33\text{Phe}$ and $\alpha 34\text{Leu}$ in the hinge region of Hb. Recent quadruple knockout studies show individual plasmepsin redundancy and suggest that although each aspartic proteinase may not be essential to the intraerythrocytic stage, they could play unique roles outside Hb digestion. On plasmepsin cleavage, the protein unfolds, which releases free heme and exposes other peptide bonds to the cysteine proteinases. Knockout studies suggest gene redundancy between *PfFP2* and *PfFP2'*, which shows no effect on parasite development with changes in the falcipain present. In the complete absence of cysteine proteinases, however, undigested Hb accumulates in the parasite's DV and causes lysis. After falcipain cleavage, subsequent protein fragments are broken down by falcilysin. The remaining peptide fragments are transported from the DV to the cytoplasm where they are degraded into the final amino acids needed by the parasite.⁷

The French military physician Charles Louis Alphonse Laveran was credited with the 1880 discovery of the malaria protozoa *Oscillaria malariae*, which was later termed *Plasmodium*. In malaria necropsies, Laveran noted the presence of dark pigmented bodies in the bloodstream and in the brain, spleen, and liver.⁸ This pigmented body was later characterized as a unique biomineral composed of a dimeric ferriprotoporphyrin IX (Fe(III)PPIX) aggregate, which is known commonly as hemozoin (HZ).

Although the nutritional needs of *P. falciparum* are met by Hb catabolism, the parasite is endangered by the release of heme. During intraerythrocytic phases, free heme can accumulate at concentrations that reach 400 mM in the DV. Subsequently, the heme can cause disruption of cellular function by the inhibition of enzymes, the generation of oxidative free radicals, and the peroxidation of membranes,⁶ which leads ultimately to parasite death. Unlike higher organisms, *P. falciparum* lacks a heme-oxygenase pathway for the cellular disposal of heme. Rather, the protozoa achieves effective detoxification by removing the heme from solution through biomineralization mechanisms, which results in crystalline HZ.⁹

Biomineralization

Over 570 million years, the complex process of organizing inorganic molecules, which generally contain calcium, iron or silicon, into crystal aggregates evolved as a protective mechanism for organisms. Fossil records show that biomineralization surfaced first in the form of organism scales and skeletons during the neoproterozoic era,¹⁰ and now, biominerals are recognized commonly in a range of functional structures including shells,¹¹ vertebrate teeth, and bone,^{12,13} diatom silicates¹⁴ and unicellular silver deposits.¹⁵ The formation of these materials is attributed to two processes: 1) biologically-induced mineralization, which is the deposition of minerals via adventitious precipitation¹⁶ and 2) biologically-controlled mineralization, which is the regulated formation of minerals that have a specific function and structure.¹⁷ Generally, induced minerals are heterogenous in

character, whereas minerals that result from cellularly controlled processes exhibit uniform composition and morphology.³

The processes of crystal nucleation and growth are driven by the basic laws of thermodynamics in which a greater free energy must exist in the original solution phase than the resultant crystalline phase.¹⁸ However, it must be noted that the free energy distribution at the crystal surface differs from these phases.⁵ Since molecules on the crystal surface are not bound as strongly as molecules in the preliminary bulk solution, their free energy contribution to the system is greater. This energy difference between molecules at the surface and in solution is known as the interfacial free energy. Acting on the destabilization of crystal nuclei, the interfacial free energy can cause either nucleus dissolution or growth of the nucleus to a large enough size that its stability prevails over the affects of surface free energy, and a crystal is formed. The nucleation pathways that lead to the most stable crystal phase are the foundations of the Ostwald-Lussac law of phases, which explains that nucleation occurs in a series of pathways with increasing stability before reaching the final crystalline state.⁵ The propagation and continued growth of a stable crystal is attributable to a uniform nucleation template from which a new phase is formed from an old phase that has become higher in free energy.^{5,19}

In the context of crystal nucleation and growth, the formation of biominerals can be cast as a three-step process that involves the supermolecular preorganization of a template, the interfacial molecular recognition of crystal nuclei and the cellular processing of resultant aggregates.²⁰ The first-order assembly of organic matrices such as protein and lipid networks provides a foundation for the second-order assembly of inorganic species. Typically, these frameworks have functionalized surfaces that behave

as templates for inorganic nucleation and are governed by electrostatic, structural and stereochemical complementarity at the organic-inorganic interface. Without cellular intervention to control the flux of metal ions, crystal nuclei would continue to grow along these scaffolds, proceeding to their bulk state. Clearly, such unconstrained growth represents a danger to cellular integrity. The final stage of biomineral construction is cellular processing, which is often the distinguishing step between native biomineral morphology and that of its synthetic analogs. The intracellular or extracellular environment in which a crystal grows ultimately influences its crystallographic structure and morphology²⁰ and ensures the function of laden cells.

Search for Hemozoin's Bionucleating Template

Investigations into the mechanisms of HZ formation have centered on protein or lipid-rich nucleating templates. Early hypotheses of a catalytic heme-polymerase in trophozoite lysates were abandoned because of failed attempts at identification and purification of the enzymatic activity. An alternative to such a heme polymerase was proposed by Sullivan²¹ from their investigations of a family of histidine-rich proteins (HRP) isolated from the DVs of *P. falciparum*. HRPII is a 30 kDa protein with 76% of its composition being His or Ala residues. HRPIII is 27 kDa and is 56% His or Ala residues. Both proteins have repeats of the tripeptide Ala-His-His, 51 repeats in HRPII and 28 repeats in HRPIII. This Ala-His-His recurring domain provides an archetypal biomineralization scaffold for the nucleation and propagation of free heme into HZ. When HRPII or HRPIII were incubated with heme in aqueous acetate solution, the

protein templates bound 17 molecules of heme, mediated the formation of HZ and was inhibited by the antimalarial drug chloroquine.

This HRP nucleating domain was explored even more by Ziegler *et al.*²² who used template design principles to construct a dendrimer-based template model system. These bionucleating templates (BNT I and II) were composed of the nucleating domain of HRPII of *P. falciparum* coupled to a tetralysine dendrimer core. The templates could bind to near stoichiometric amounts of Fe(III)PPIX, although substrate specificity experiments suggested that substrate recognition was dependent on the porphyrin moiety rather than specific metal recognition. Moreover, HRP substrate recognition was not shown to be mediated by histidine axial ligation to a metal ion, but rather it was attributed to π -stacking and electrostatic interactions. Chloroquine inhibition of the bionucleating templates was comparable with HRP II and III impaired formation of HZ when treated with the antimalarial.²²

These templates, like HRPII, were shown to promote HZ formation at a parasite DV relevant pH 4.0-4.5. In fact, HRPII is active from pH 4.5 to pH 6.0. HZ formation slows at pH values below 2.0 and above 5.0.²³ Although an increase in pH does cause an increase in binding of heme to HRPII, the HZ produced actually decreases leading, instead, to the formation of μ -oxo-heme dimers.²³ Therefore, the bis-histidyl heme binding observed on other proteins like histidine-rich glycoprotein (HRG) at physiologic pH 7.0 differs from the HRPII nucleation of HZ in the parasite's acidic DV,²⁴ although a pH 7 HRPII model was attempted by Schneider and Marletta in 2005.²⁵ At this pH, binding is consistent with a nucleating template that serves as an organizing function rather than a tight heme-binding function.

Subsequent experiments revealed, however, that the HRP's were not the likely template for HZ formation. Double deletion mutants of HRPII and HRPIII did not prevent the formation of HZ in the DV,²¹ which suggests the existence of an alternative template. In addition, HRPII is not located solely in the DV, but rather it is secreted into the serum of victims at high concentrations. Histology labeling experiments show that HRPs in the DV are simply captured during the endocytosis of host Hb and not specifically targeted to the DV.²¹ Such surreptitious colocalization would also suggest the existence of a non-HRP template. In light of these experimental results, the search for HZ's biomineralization template turned toward other possibilities.

Lipids are a possible template for HZ biomineralization. As a bionucleating template, lipids can increase the solubility of Fe(III)PPIX, localize high concentrations of Fe(III)PPIX with iron-hydrophobic headgroup interactions and provide a layer of free heme intercalation. The propionate groups of free heme within the lipid layer draw into their positively charged Fe(III) centers, which weakens any hydrogen bonds of Fe(III)PPIX dimers. Fitch *et al.*²⁶ showed that HZ formation could be mediated at pH 5.0 in the presence of fatty acids like arachidonic acid and glycerols of oleic acid as well as detergents like polyoxyethylene sorbitan monooleate (TWEEN 80). Increasing support for a lipid template led to the membrane sacrifice theory by Hemplemann *et al.*,²⁷ which suggested that inner membranes of RBC transport vesicles in the parasite cytosome were degraded by free heme, releasing lipids that increase heme solubility and aggregation. In the sacrifice of the inner membrane, the outer membrane is preserved to prevent additional oxidative damage to the parasite.²⁷ *In vitro* lipid-initiated HZ crystallization was reported by Egan *et al.*²⁸ using a range of lipids that includes myristoyl, oleoyl and

palmitoyl glycerides; phosphocholines and cholesterol to initiate HZ formation along the lipid-water interface. Simulation of HZ formation in these studies indicated that the hydrophobic Fe(III)PPIX dimer was more stable in the lipid layer to foster hydrogen bonds between the protonated propionic acid groups and thus, HZ crystal assembly.²⁸ Transmission electron microscopy images of HZ localized in lipid nanospheres within an infected trophozoite stage RBC provided increased support of a lipid-mediated HZ bionucleating process. The extraction of these fatty acyl glycerides (including monostearic, monopalmitic, dipalmitic, dioleic and dilinoleic glycerols) and their incubation with substrate hemin developed a competent *in vitro* template for HZ formation.²⁹

Target of Antimalarials

Interruption of the parasite heme biomineralization pathway is a logical target of antimalarial drug development. As antimalarials amass in the parasite's DV, HZ formation is inhibited, and the parasite becomes flooded in toxic heme. Beginning with the hypothesis that neutral lipid droplets indeed serve as biomineralization templates for the formation of HZ, a variety of limiting cases exist in which inhibitors may disrupt the aggregation of HZ (Figure 1). An inhibitor may bind the heme substrate in such a manner that the heme-inhibitor complex cannot be recognized by the template. Alternately, a drug could interact with the template, blocking the heme binding site. Finally, a HZ aggregation inhibitor might trap the heme bound to the template, which prevents formation of the dimeric unit or nucleation of the extended crystal. These

possible modalities, which are derived from the paradigm of biomineral formation, can be used to understand the mechanism of action of some antimalarial compounds.

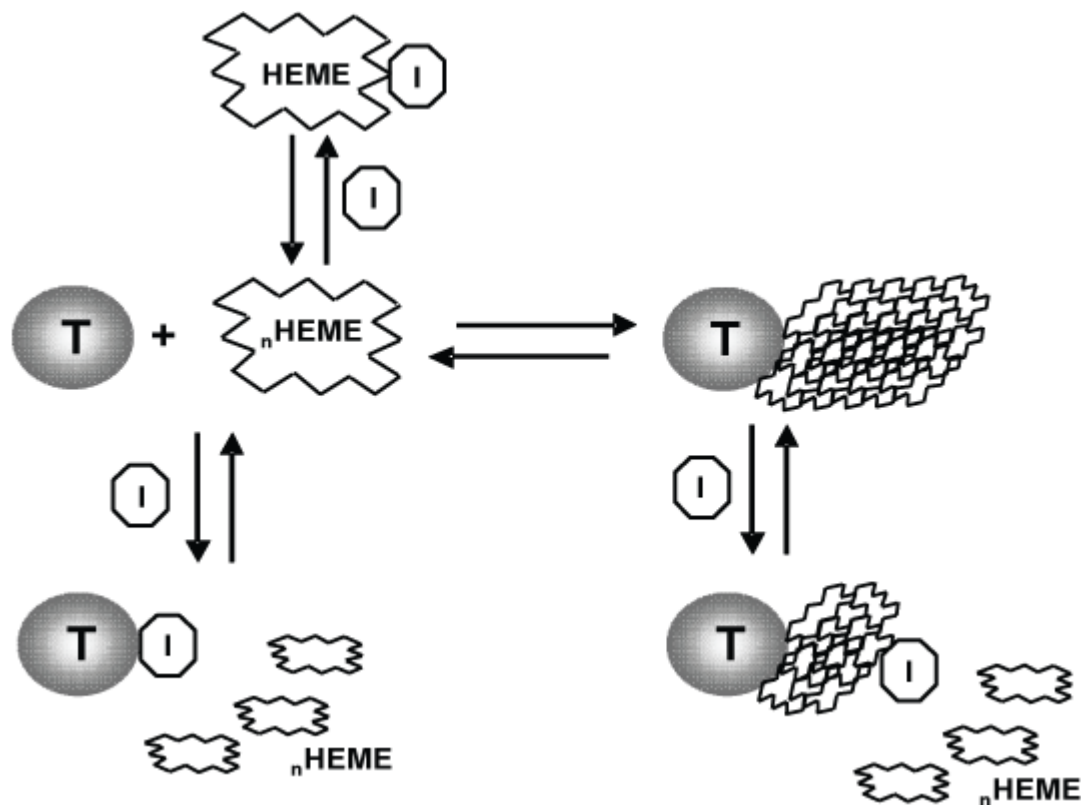


Figure 1 Modes of hemozoin inhibition. On a neutral lipid droplet template (T), heme can aggregate to form the biomineral HZ. Antimalarials may inhibit this aggregation by binding heme substrate, interacting with the lipid template or trapping heme bound to the template. All actions serve to prevent the formation of HZ.

Well-known quinoline-based drugs like chloroquine and amodiaquine are thought to target this HZ biomineralization pathway. These drugs have been the standards in treatment of malaria, but growing parasite resistance threatens their use. Quinoline-based drugs include the well-known 4-aminoquinoline derivatives chloroquine, amodiaquine, halofantrine, quinine and bisquinoline.³⁰ These drugs are thought to cap monomeric heme or bind the μ -oxo-dimer of oxidized heme to prevent HZ formation. The π - π

interactions at the $\{010\}$ heme face control resultant adduct formation. Computational models of HZ and quinoline interactions indicated that drug adsorption occurred on the $\{001\}$ and $\{011\}$ crystal faces (Figure 2).³¹ These highly symmetrical crystals also showed tapering at each drug-bound $\{001\}$ or $\{011\}$ ledge, which suggested weakening of the quinoline inhibition along the crystal's c-axis which resulted in thinner crystal cross-sections.³¹

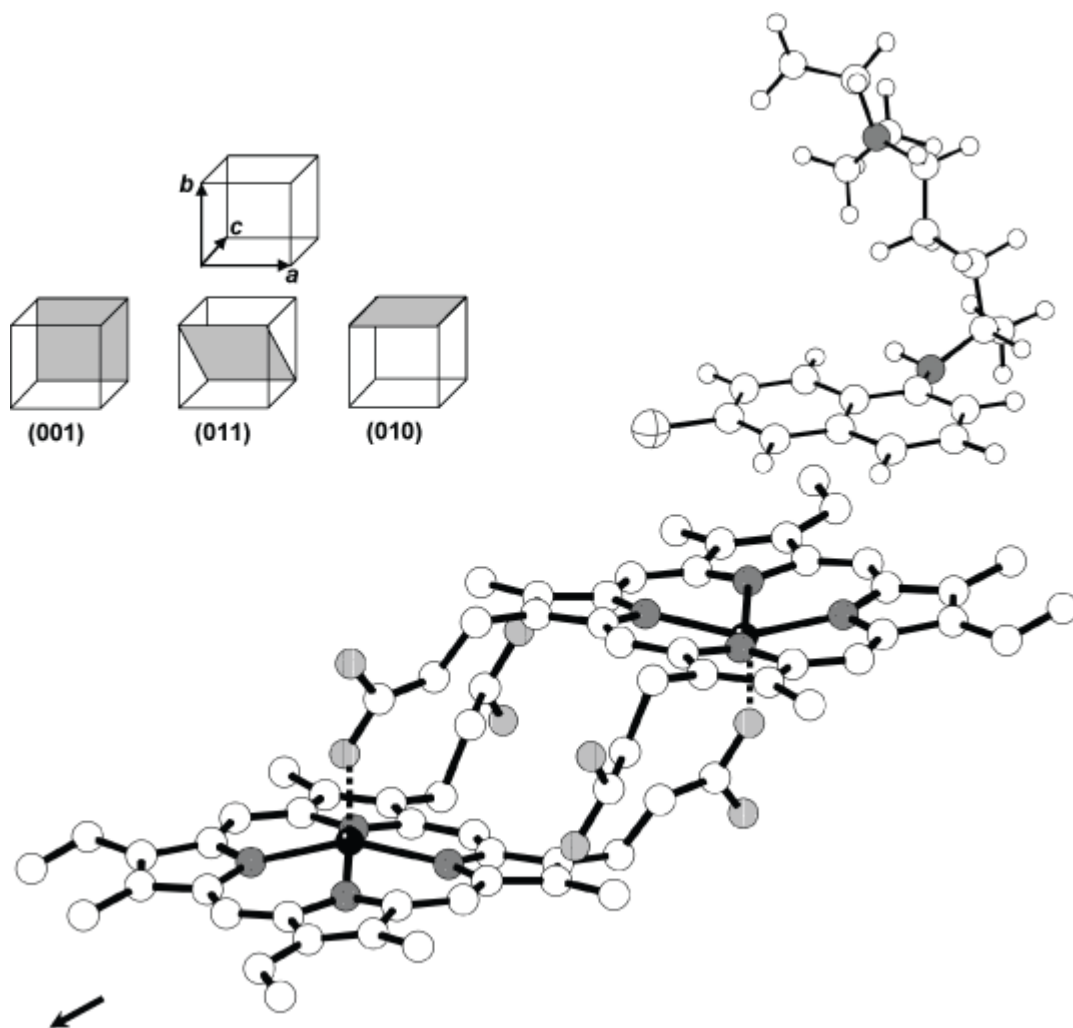


Figure 2 Hemozoin-chloroquine binding model. Chloroquine is thought to bind to the $\{001\}$ and $\{011\}$ faces of heme as well as π - π stacking at the $\{010\}$ face. To prevent HZ formation completely, chloroquine would have to bind both faces of each heme monomer or crystal extension would be blocked in only one direction as shown.

Other inhibitors of HZ formation are thought to act similarly to the quinoline family. Binding of the antifungal azole-based drugs (clotrimazole, ketoconazole and miconazole) to heme is thought to damage parasite cell membranes and cause death.³⁰ The isonitrile terpenes (diisocyanoadociane and axisonitrile-2), isolated from marine sponges and the synthetically derived methylene blue analogs (azures A, B and C; thion; celestine blue; and phenosaphranin) most likely prohibit HZ formation by binding monomeric heme. The xanthone family of antimalarials, such as the hydroxyxanthenes and the bis-(N,N-diethylamino)-ethoxy xanthenes, were found also to bind at the HZ crystal faces $\{001\}$ and $\{011\}$. Specifically, the drugs' terminal groups bind the carboxyl group exposed at each face, which inhibits the nucleation and growth of the crystal.³¹ The crystal engineering prospect of future drug design is an interesting one that beckons additional exploration and promises applications in a variety of biomineral-associated diseases.

Hemozoin Characterization

Prior to the definitive X-ray powder diffraction characterization of HZ, the true structure of the aggregate remained elusive because of its limited solubility. HZ was soluble only in NaOH, which completely degraded the structure and prevented any attempt to determine the intramolecular atomic interactions. The insolubility of the product rendered useless many “standard” experimental methods for the characterization of bioinorganic systems. This aspect of the biomineral's identification undoubtedly

contributed to Ridley's description of HZ as "a black insoluble mass of material that can be soul-destroying to work with".³²

Studies by Slater *et al.*³³ provided an initial "fingerprint" of HZ's chemical structure by applying Fourier-transform IR (FT-IR) spectroscopy to intact HZ crystals. The IR spectrum of HZ revealed intense absorbance patterns at 1664 and 1211 cm^{-1} , which indicate the axial propionate C=O and C-O stretching, respectively (Figure 3A). These peaks were absent from the spectra of the synthetic substrates hemin chloride and hemein. These data suggested a direct coordination between the carboxylate of one heme monomer and the iron center of another, which rules out a direct iron-carbon bond that would have characteristic stretching near 1900 cm^{-1} . Imagining a long carboxyl-propagated "polymer," this structure accounted for the aggregate's insolubility.

Using field emission inlens scanning electron microscopy, gross physical analysis of isolated HZ crystals obtained from mammalian *Plasmodium* species show a uniform morphology that resembles smooth-sided bricks arranged at right angles.³⁴ Unlike the smooth, flat sides of the aggregates, the crystals' tapering, square ends indicate a face of continuous nucleation and growth. The average dimensions of these crystals were 100 nm x 100 nm x 300-500 nm. Even strains of *P. falciparum* that lack HRPII or HRPIII were shown to produce uniform HZ crystals.³⁴ This observed consistency in morphology is caused by the final step of *in vivo* biomineralization, which is cellular processing. In this stage, cells organize HZ crystals to best fit the confines of their storage vacuole as illustrated in an *in situ* HZ RBC electron micrograph image (Figure 3C).²⁴ This differs from the seemingly less-ordered *in vitro* production of HZ's synthetic analog, which is

known as β -hematin (BH), in a reaction vessel, which fosters continued crystal extension without cellular restraint (Figure 3D).

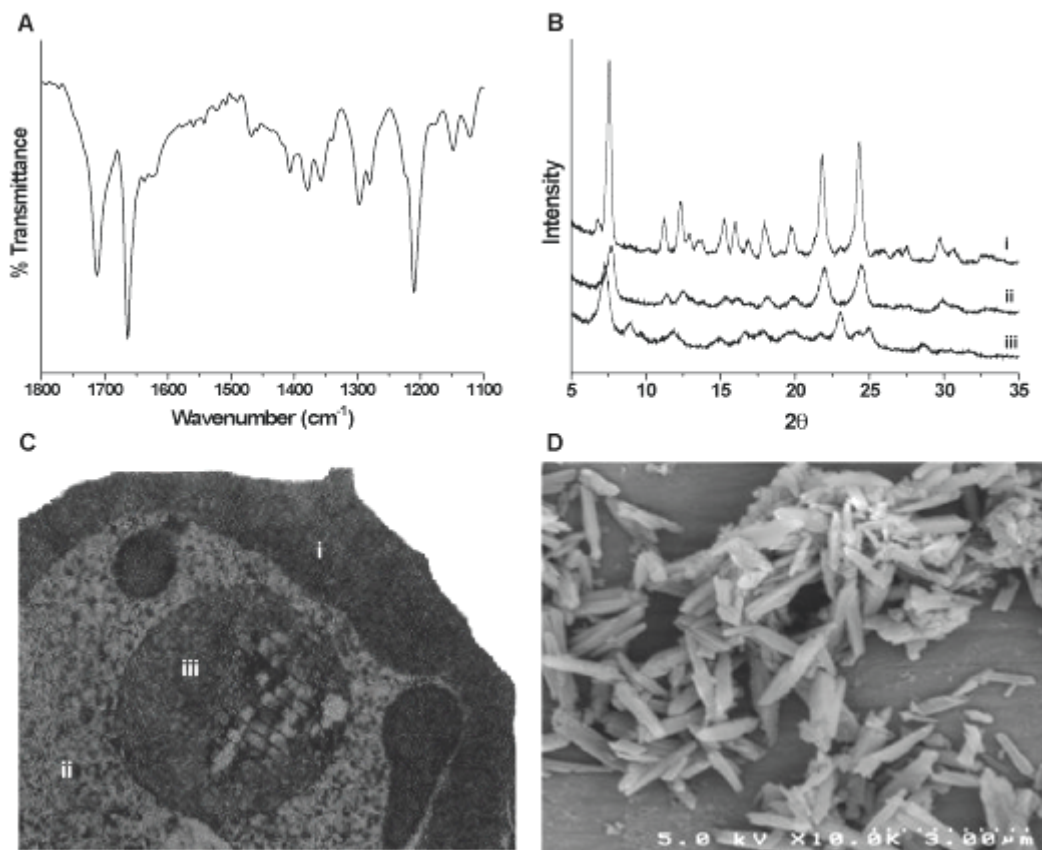


Figure 3 Physical characterization of hemozoin. (A) The axial propionate linkages between heme units in HZ are seen by FT-IR fingerprints of C=O and C-O stretching at 1664 and 1211 cm^{-1} , respectively. (B) Characteristic 2:1 peaks are seen at 7° : 21° and 24° 2θ for (i) native and (ii) synthetic HZ. Absent from these aggregates is the 23° 2θ peak observed in the diffraction pattern of (iii) substrate hemin chloride. (C) Electron micrograph of HZ in *P. falciparum* infected RBC where (i) is the host RBC, (ii) is the parasite and (iii) is the DV. Image courtesy of Daniel E. Goldberg. (D) SEM image of uniform BH crystals.

The introduction of high-resolution synchrotron X-ray radiation enabled the X-ray powder diffraction of both native HZ and BH. Their structure was determined using simulated annealing techniques on the diffraction data.³⁵ This method included the use of the Le Bail algorithm to compare integrated peak intensities, the Rietveld refinement of the structure's molecular bonding geometry and Fourier difference calculations of atomic

positions. The resultant diffraction pattern confirmed a triclinic unit cell with a space group of P-1, which demonstrates an inversion of symmetry between the unit cells of the Fe(III)PPIX dimer (Figure 3B). This pattern led to the definitive structure of a five-coordinate Fe(III)PPIX dimer bound by reciprocal monodentate carboxylate interactions with the propionic side chains of each PPIX. Hydrogen bonding between these heme dimers accounted for the aggregate's stable, extended crystalline network. Importantly, this work established that HZ and BH were crystallographically, chemically and spectroscopically identical.³⁵

Identification of Native Lipid Components of Hemozoin

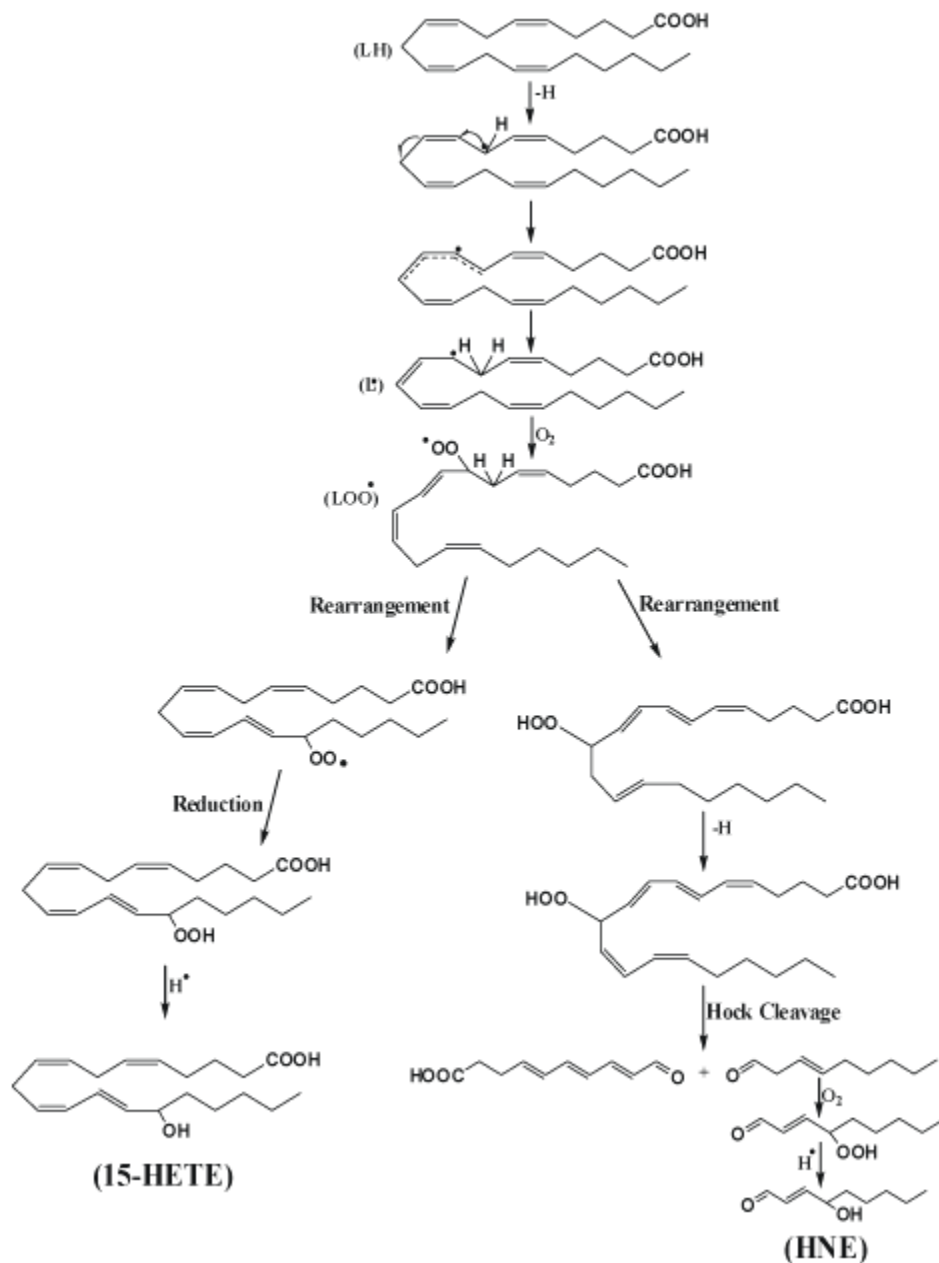
In vivo native HZ transmission electron microscopy images from trophozoite-infected RBCs depicted the localization of HZ crystals within neutral lipid nanospheres.²⁹ Trophozoite DVs were isolated using Percoll/sucrose bottom separation techniques, and the lipid content of these isolates was extracted by Bligh-Dyer (chloroform/methanol) lipid extraction. Methyl ester fatty acid characterization by gas chromatography-MS (GC-MS) and lithium (Li⁺) adduct electrospray ionization mass spectrometry of trophozoite fractions revealed a suite of neutral lipids adhered to the crystal's surface. When these lipid extracts (a ratio of 4 monostearic-: 2 monopalmitic-: 1 dipalmitic-: 1 dioleic-: and 1 dilinoleic glycerol) were incubated in the presence of substrate hemin, HZ formation was observed.²⁹ This competent nucleating template of fatty acyl glycerides is consistent with the hypothesis of a lipid scaffold for heme aggregation in *P. falciparum*.

Also extracted from native HZ were polar hydroxylated fatty acids derived presumably from cellular arachidonic and linoleic acids. Native HZ was purified from infected RBCs by a series of centrifugation steps followed by organic extraction of its lipid coat. Analysis of the lipid coat revealed the presence of hydroxylated polyunsaturated fatty acids. These polar lipids were separated using reverse phase-, normal phase- and chiral phase high performance liquid chromatography and subsequently examined by GC-MS. Native HZ lipid coat GC-MS analysis revealed the presence of 15-, 12-, 11-, 9-, 8- and 5-hydroxyeicosatetraenoic acids (HETEs) as well as 13- and 9-hydroxyoctadecadienoic acids (HODEs).³⁶

Chemical Reactivity and Immunomodulation

Native HZ produced in the parasite DV most likely encounters cellular debris such as arachidonic and linoleic fatty acids or other lipids when released from a bursting RBC. Redox cycling of surface exposed heme units within HZ can lead to the initiation of lipid peroxidation (LPO). Abstraction of a bisallylic hydrogen atom from a fatty acid such as arachidonic acid results in an unpaired electron on the methylene carbon.³⁷ This unpaired electron promotes the rearrangement of the double bonds adjacent to the methylene group that produces an alkyl radical (L•). In the presence of oxygen, alkyl radicals react to form peroxy radicals (LOO•) that can abstract a hydrogen atom that yields a lipid peroxide (LOOH) and can propagate more reactions. Reduction of the peroxy radical would result in the production of racemic mixtures of hydroxylated fatty acids like the HETEs and HODEs described previously in the HZ lipid coat. Secondary

oxidation and chain β -cleavage results in reactive 4-hydroxy-2-nonenal (HNE) (Scheme 2).



Scheme 2 Hemozoin-mediated lipid peroxidation. Redox cycling of iron in complexes like HZ can initiate lipid peroxidation of fatty acids like arachidonic acid (LH). Abstraction of the bisallylic hydrogen leaves an unpaired electron on the methylene carbon that can rearrange to form a reactive alkyl radical (L•). Oxidation of this radical leads to a peroxy radical (LOO•), and upon reduction, forms a lipid peroxide (LOOH) that can undergo additional reactions to yield a variety of secondary oxidation products.

Lipid peroxidation was demonstrated *in vitro* by reacting arachidonic acid with native HZ purified of all cellular lipid and protein content.³⁸ Resultant HETE products were extracted from the reaction supernatant and identified using reverse phase high performance liquid chromatography.³⁸ Recent studies of BH reactions with arachidonic acid revealed an identical reaction profile to that of HZ with all six positional HETE isomers identified by ultra high pressure reverse phase and chiral phase liquid chromatography tandem MS/MS (chiral-RP-LC-MS/MS).³⁹ LC-MS analysis has enabled the separation and identification of these cellular metabolites at femtomole levels of detection. The presence of these oxidation products in the lipid coat of native HZ and their formation upon arachidonic acid incubation with purified HZ and BH strongly supports the HZ-mediated LPO of cellular fatty acids. Additionally, the known immunomodulatory activity of these lipid peroxidation products is intriguing given the reported ability of HZ to disrupt the function of innate immune cells.

Once thought to be a simple “inert” detoxification biomineral, an increasing appreciation exists of HZ’s reactivity and subsequent perturbation of the host immune response. HZ reactivity in the modulation of innate and adaptive immunity has been attributed to a range of effects that include toll-like receptor 9 (TLR9) activation, cytokine production, LPO and dendritic cell development. Recent studies found that the *P. falciparum* DNA that remained on native HZ extracts was the true source of TLR9 activation, and once native HZ was treated with nuclease, no activation was observed.⁴⁰ HZ disruption of dendritic cell function was shown to cause a decline in T cell activation that led to a weakened adaptive immune response. The role of HZ as an immunoreactive

aggregate may impact the high rates of patient secondary infection as well as the decline in vaccine efficacy.

Functionally, phagocytosis of HZ has been reported to impair macrophage oxidative burst, to downregulate inducible nitric oxide synthase (iNOS) activation, and to perturb cytokine profiles in infected patients. It has also been shown to correlate with increased levels of immunomodulatory LPO products such as prostaglandin E₂ (PGE₂), HNE and HETEs in monocytes.⁴¹ The biologic activity of these compounds is generally derived from either of two mechanisms. In the first mode of action, the reactive intermediates or products may form adducts to DNA or proteins. Thus, a variety of chain-terminating reactions of peroxy, alkoxy or epoxyperoxy radicals can result in oxidative cross-links to DNA or proteins. Furthermore, the electrophilic alkenals, such as HNE, readily form Schiff-base adducts to lysine residues and Michael addition adducts to histidine and cysteine residues to perturb the function of many proteins.⁴² In the second mode of action, the LPO products may act as alternate ligands to several different proteins and receptors to initiate an ultimately pathogenic signaling cascade. The hydroxylated fatty acids 9- and 13-HODE, as well as 15-HETE, have all been found to be activators of the important nuclear receptor protein PPAR- γ , which is involved in key cellular regulatory and differentiation functions in monocytes.⁴³ 15-HETE has also been found to stimulate RBC adherence to capillary endothelia, to enhance vascular permeability and edema and to induce chemotaxis and chemokinesis, although the precise pathways remain unclear. From these examples, it is easy to imagine how such promiscuous reactivity often manifests itself in the pathogenesis of disease states. These

findings suggest that HZ's ability to rectify cellular responses may actually be caused by formation of primary and secondary LPO products.⁴¹

To study this hypothesis, BH was incubated with ghost RBC membrane lipids, which are similar to those that the native biomineral would be exposed to upon RBC rupture.⁴¹ RAW macrophage-like cells were treated with the supernatant of this reaction, and reactive oxygen and nitrogen species (ROS and RNS) produced via the NADPH oxidase and iNOS pathways were inhibited. The levels of inhibition paralleled the effects of individual LPO products such as 15-HETE or HNE at pathologically reported concentrations. Additionally, treatment of cells with either BH or unreacted ghost supernatant did not cause a decrease in ROS and RNS production, which indicates that the products of HZ-mediated LPO were responsible for the observed disruption of macrophage function, not the dimeric heme component of the aggregate itself.⁴¹ Mechanisms for such malarial host-pathogen interactions and, more broadly, biomineral-to-cell relationships are primarily undefined, which creates a significant treatment barrier. Unraveling the formation and role of HZ in the pathogenesis of *P. falciparum* infection may provide additional insight into the prevention and treatment of a variety of diseases that result from pathogenic biominerals.

Conclusions

Biomineralization results in an expansive array of complex materials. These natural biominerals often represent unique crystal forms that extend over several size domains that are synthesized under ambient conditions. Increasingly, it is understood

that biomineralization processes play important roles in the pathologies of several diseases. In malaria, the parasite forms the HZ biomineral in response to the heme released during hemoglobin catabolism. HZ serves an important detoxification role that allows the organism to maintain homeostasis during its intraerythrocytic phases. Despite the fact that HZ represents a validated drug target for *P. falciparum*, many fundamental questions remain concerning its formation; questions such as how or if the parasite assembles neutral lipid droplets specifically, how the heme is transported and deposited in these lipid domains, and whether new strategies exist that could be used to design drugs to disrupt this process. Tackling the rational drug design problem from a crystal engineering perspective offers an interesting direction for drug discovery, whether designing crystal-specific antibodies or fabricating selectively binding compounds. Consequently, studies on the *in vivo* formation of HZ afford an opportunity for chemists with a variety of interests (e.g., organic, inorganic, biologic, supramolecular, materials) to make significant contributions in attacking this neglected and devastating disease.

A second, emerging area of research is the pathophysiologic responses between biominerals and immune cells. A commonality between the diseases that maintain a pathogenic biomineral is the inflammatory response. Be it an autoimmune reaction, as in the case of gout, or down-regulation of the innate immune system as in malaria, it is clear that the interface between biominerals and cells is important in mitigating these responses. In the case of HZ, growing evidence suggests that the biomineral reacts with cellular fatty acids to produce a suite of reactive oxidized eicosanoids. The immunoreactivity of these oxidation products is likely a significant contributor to the inflammation and discomfort experienced by patients. Developing therapies for these

effects and for the cause of infection could provide a dual approach in the treatment of many pathogenic biominerals and proffers the potential for novel initiatives in disease prevention and treatment.

CHAPTER II

IDENTIFICATION OF HYDROXYEICOSATETRAENOIC ACID COMPONENTS OF SCHISTOSOMAL HEMOZOIN^{39,44}

Schistosomiasis is a parasitic disease that chronically infects over 200 million people in 74 countries and is responsible for more than 200,000 deaths each year.⁴⁵⁻⁴⁷ Based on recent reports, schistosomiasis ranks second only to malaria as a cause for chronic morbidity among tropical diseases.⁴⁸ Parasitic infection by *Schistosoma mansoni* occurs via a complex digenetic life cycle. In order to obtain requisite amino acids for growth and development, the blood fluke catabolizes host Hb from RBCs. Adult female schistosomes consume an estimated 330,000 RBCs per hour.⁴⁹ Erythrocytic Hb is broken down by proteolytic enzymes in the gut releasing significant quantities of potentially toxic free heme.⁵⁰ To avoid these cytotoxic effects,^{38,51} blood feeding organisms have developed novel mechanisms for heme detoxification.

In the protozoan *P. falciparum*, toxic free heme accumulates in the DV and is sequestered by aggregation into an inert crystalline pigment, HZ.⁵² *S. mansoni* appears to employ a similar heme detoxification pathway. During Hb catabolism in the digestive cavity of the trematode, free heme aggregates, and the subsequent pigment is regurgitated by the parasite into the surrounding host vasculature. This dark-brown pigment was recently characterized by Oliveira and coworkers as being structurally identical to *P. falciparum* HZ (PfHZ) and its synthetic analogue BH.^{53,54}

HZ has long been considered an inert, detoxification end-product, but recent studies suggest that native *Pf*HZ is capable of modulating host immunity. Schwarzer and coworkers showed that phagocytosis of native *Pf*HZ by human monocytes disrupts the normal cellular function of professional phagocytes.^{36,55} The accumulation of native HZ in circulating monocytes and neutrophils inhibits normal phagocytic function by inducing oxidative stress and down-regulating intercellular mechanisms that generate potent oxidative molecules used to defend against foreign invaders, namely ROS and RNS.⁵⁶ Furthermore, HZ has been shown to induce lipid peroxidation of polyunsaturated fatty acids (PUFAs) resulting in the formation of potentially cytotoxic and immunomodulatory molecules including HETEs^{36,38,57} and HNE.^{58,59} Consequently, HZ-mediated production of arachidonic acid (AA) metabolites, such as HETEs and HNE, are of significant interest in schistosomiasis since that role of HZ in the disease's pathogenesis remains largely unexplored.

Experimental

β -Hematin synthesis. BH was synthesized via dehydrohalogenation of hemin, as described by Bohle.⁶⁰ The reaction vessel was sealed, protected from light and stood undisturbed for three months. The resulting mixture was filtered, and the precipitate was washed exhaustively with methanol, 0.1 M sodium bicarbonate (pH 9.1) and deionized water. The purified product was dried under vacuum at 150°C for 48 h and stored under dessicant.

SmHZ isolation. Adult schistosomes were obtained by mesenteric perfusion of mice 42 days post-infection.⁶¹ Cultivated adult female worms were homogenized in phosphate buffered saline (PBS, pH 7.4) using a 15 mL glass homogenizer. Homogenate was centrifuged twice at 1000 x g for 60 s, and the tissue pellet was discarded. The supernatant was centrifuged 2 h at 5445 x g. The resulting dark-brown pellet was resuspended in 5 mL sterile PBS after vortexing and gentle sonication for 5 min. *SmHZ* recovery was quantified as described by Sullivan *et al.*⁶² with 20 mM NaOH, 2% SDS at 25°C for 2 h. Heme content was determined from absorbance at 400 nm ($\epsilon = 1 \times 10^5 \text{ M}^{-1} \text{ cm}^{-1}$) using an Agilent 8453 UV-Visible Spectrophotometer.

Native SmHZ lipid extraction. The native *SmHZ* lipid component was extracted twice from 2.5 mg/mL native *SmHZ* in 25 mM chelexed-phosphate buffer (pH 7.4) using 1:1 (v/v) ethyl acetate. The emulsion was vortexed 60 s and centrifuged 30 min at 5445 x g. The organic layer was removed and evaporated under nitrogen. The lipids were reconstituted in 1 mL of ethanol and stored at -80°C.

In vitro HZ-mediated HETE production. Purified native *SmHZ*, complete removal of lipids confirmed by NP-HPLC, was used in these experiments. The reaction was performed by adding 5.32 mM AA to a 2 mL suspension of either *SmHZ* or BH (0.3 mg/mL) in 25 mM chelexed-phosphate buffer (pH 7.4) for 4 h at 25°C. Reaction products were extracted with ethyl acetate and stored in ethanol at -80°C.

LC-MS/MS HETE identification. HETE standards and lipid samples were dried under nitrogen and resuspended in acetonitrile/water (30:70), 10 mM ammonium carbonate and 0.1 M BHT prior to injection. The LC-MS/MS analysis was performed on a Waters Acquity UPLC system (Waters, Milford, MA) connected to a Thermo Fisher

Scientific, Waltham, MA) using a Thermo Hypersil Gold C18 column (1.9 μm , 2.1 x 150 mm). LC conditions were as follows: solvent A contained 10 mM ammonium carbonate in acetonitrile/water (10:90) and solvent B contained 10 mM ammonium carbonate in acetonitrile/water (10:90). The following gradient program was used with a flow rate of 600 $\mu\text{L}/\text{min}$: 0-0.25 min, 30% B; 0.25-9 min, linear gradient 30-45%; 9-10 min, 45% B; 10-10.50 min, linear gradient 45-30% B; 10.50-17 min, 30% B. Sample injection volume was 10 μL . The following optimized parameters were used for the detection of analyte and internal standard: N_2 sheath gas 36 psi; N_2 auxiliary gas 20 psi; capillary temperature 300°C; source voltage 3.8 kV; source current 100 μA ; skimmer offset 0.00 V; capillary offset -44.00 V; tube lens offset -103.30 V; activation time 30 ms (MS), 50 ms (MS^2); isolation width 1 m/z (MS), 2 m/z (MS^2). Data acquisition and quantitative spectral analysis was conducted using the Thermo-Finnigan Xcaliber software, version 2.0 Sur 1.

LC-MS/MS chiral separation. Normal phase LC (NP-LC) analysis was performed prior to chiral RP-LC-MS/MS in order to isolate HETE isomers for individual analysis. The NP-LC was performed on a Waters 600 HPLC connected to a Waters 996 photodiode array (Waters, Milford, MA) using a Beckman Ultrasphere silica column (5 μm , 4.6 mm x 25 cm; Beckman Coulter, Fullerton, CA). An isocratic gradient of 98.8% hexane, 1.2% isopropanol and 0.1% acetic acid was used at a flow rate of 1.00 mL/min. HETE absorbance was detected at 237 nm.

Chiral-RP-LC-MS/MS. The LC-MS/MS analysis was performed as before using a CHIRALPAK AD-RH column (5 μm , 2.1 mm x 150 mm; Chiral Technologies, Inc., West Chester, PA). LC conditions were as follows: solvent A contained 0.25% formic acid in acetonitrile/water (5:95) and solvent B contained 0.25% formic acid in

acetonitrile/water (95:5). The following gradient program was used with a flow rate of 200 $\mu\text{L}/\text{min}$: 0-5 min, 50% B; 5-20 min, linear gradient 50-100% B; 30-32 min, 50% B. The following optimized parameters were used for the detection of analyte and internal standard: N_2 sheath gas 36 psi; N_2 auxiliary gas 20 psi; capillary temperature 300°C; source voltage 3.8 kV; source current 100 μA ; skimmer offset 0.00 V; capillary offset -44.00 V; tube lens offset -103.30 V; activation time 30 ms (MS), 50 ms (MS^2); isolation width 1 m/z (MS), 2 m/z (MS^2). Data acquisition and quantitative spectral analysis were conducted using Thermo-Finnigan Xcaliber version 2.0 Sur 1.

iNOS inhibition. Effects of 5-, 12- and 15-*S*-HETE, HNE and *SmHZ* on LPS-stimulated *iNOS* activity in RAW 264.7 cells (1×10^5 cells/well in 96-well culture plates at 37°C in 5% CO_2 for ≥ 8 h) was examined. Cell viability was confirmed using Trypan Blue exclusion. Stock solutions of 5-, 12- and 15-*S*-HETE were prepared by evaporating each 100 μg vial to near dryness under nitrogen and reconstituting in RPMI complete medium (ethanol concentrations below 0.5%). Additionally, 0.1 mg/mL stock solutions of native *SmHZ*, BH and 17.5 μM HNE were prepared in RPMI complete medium. Following stock solution treatment in the presence of LPS (1 $\mu\text{g}/\text{mL}$), cell cultures were incubated at 37°C in 5% CO_2 for 24 h. The Griess reaction was used to measure nitrite concentration.⁶³ Absorbance of the resultant *azo* complex was measured at 540 nm using a Bio-Tek Synergy HT Multidetector Microplate Reader.

SEM. Dry purified *SmHZ* was suspended in ethanol, sonicated for 10 min, applied to a polished aluminum specimen mount and dried at 25°C overnight. Each sample was sputter-coated with gold for 20 s and imaged using a Hitachi S4200 scanning electron microscope at 5.0 kV accelerating voltage.

Results and Discussion

Schistosomal pigment (*SmHZ*) is typically found accumulated in resident tissue macrophages of the liver. Adult worm pairs reside in the hepatic portal system of the host and regurgitate hemozoin and cellular debris into the surrounding vasculature. Adult female worms exhibit a much heavier degree of pigmentation relative to males due to the nutritional demands of oogenesis (Figure 4A). Following perfusion of the hepatic portal vein in *S. mansoni*-infected Swiss Webster mice, adult female and male worms were separated, counted and homogenized to determine *SmHZ* burden per worm as previously described.⁶² On average, adult females were found to accumulate $1.729 \pm 0.29 \mu\text{g}$ of hemozoin while the adult males were found to amass only $0.114 \pm 0.07 \mu\text{g}$ per worm.

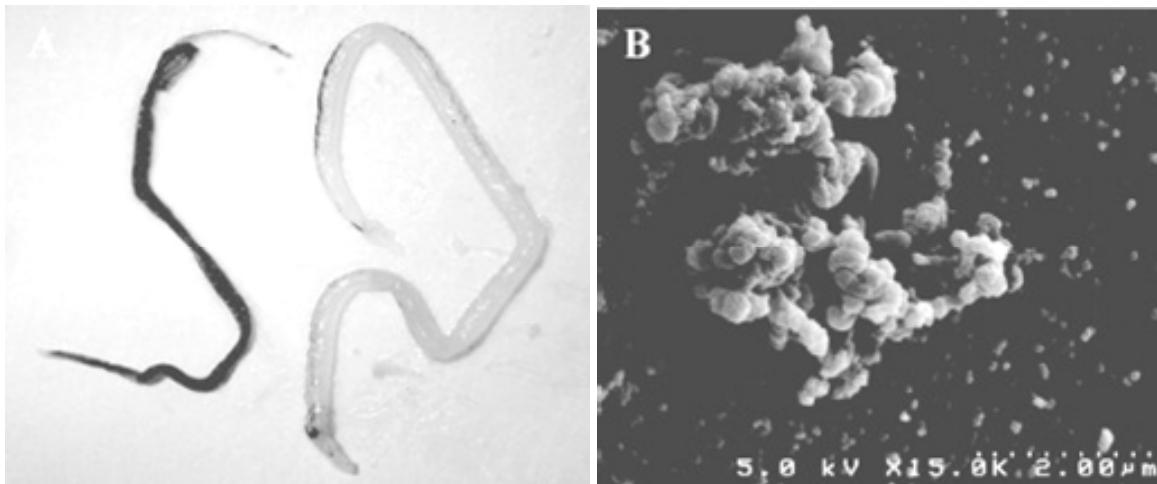


Figure 4 Hemozoin from *S. mansoni*. (A) Adult female (left) and male (right) *S. mansoni* laden with hemozoin. Female worms accumulate a heavier hemozoin burden, as seen by their darker pigmentation, due to the nutritional demands of oogenesis. (B) SEM image of schistosomal hemozoin isolated from homogenized *S. mansoni*.

Isolated *SmHZ* was purified and characterized using X-ray powder diffraction (characteristic 2:1 intensity of the signature 2θ peaks at 7° : 21° and 24°) and Fourier

transform infrared spectroscopy (1664 and 1211 cm^{-1} of C=O and C-O stretching) confirming a dimeric ferriprotoporphyrin IX aggregate identical to *PfHZ* and BH (Figure 5). While *PfHZ* and BH SEM images portray a biomineral of elongated rectangular crystals with well-defined crystal facets, *SmHZ* images depict the characteristic heterogeneous morphology and large size distribution often attributed to the extracellular environment of HZ formation in *S. mansoni* (Figure 4B).⁵⁴

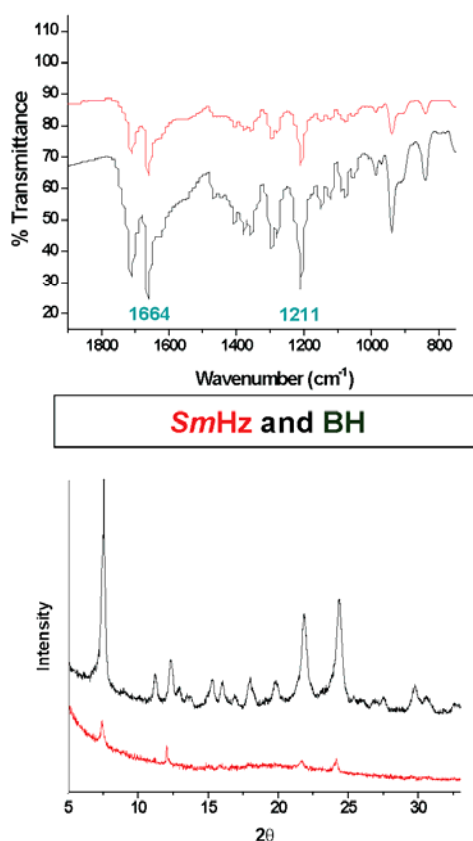


Figure 5 IR and XRD of HZ. (A) The presence of axial propionate linkages in HZ's dimeric ferriprotoporphyrin IX structure was confirmed using infrared spectroscopy showing the C-O stretching at 1211 cm^{-1} and C=O stretching at 1664 cm^{-1} . (B) Characterization by powder x-ray diffraction (Cu K α radiation) reveals the 2:1 intensity of 2 θ peaks at 7°: 21° and 24°. Reduced peak distinction compared to BH in *SmHZ* pattern is attributed to limited sample size.

The nature and function of the lipid environment surrounding the heme aggregate of native HZ is complex. In a recent study, transmission electron microscopy (TEM) showed the localization of *Sm*HZ at the hydrophilic-hydrophobic interface of lipid droplets in the *S. mansoni* gut lumen.⁶⁴ Similarly, Pisciotta and coworkers extracted a suite of neutral lipids coating native HZ from the digestive food vacuole of *P. falciparum*.²⁹ In both cases, the lipid extracts provided a competent scaffold for hemozoin formation *in vitro*.^{29,64} Polar hydroxylated fatty acids derived from arachidonic and linoleic acids have also been extracted from native *Pf*HZ, as has the secondary oxidation product HNE.^{36,38,59} These compounds have been shown to be capable of significantly altering the function of macrophage cells during the course of malarial infection.

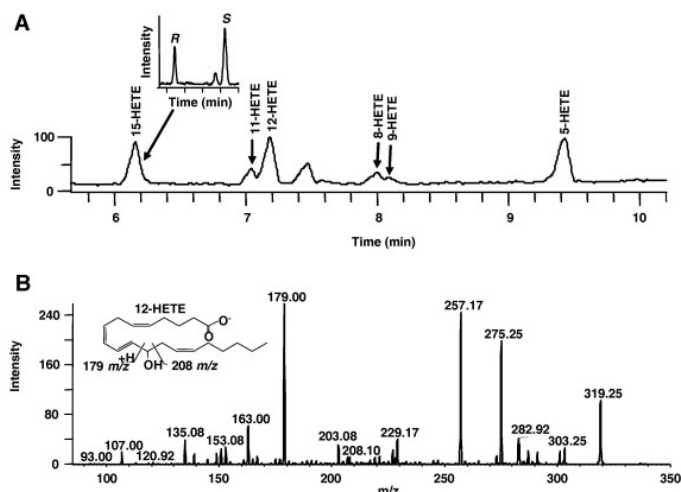


Figure 6 HETE-containing lipid coat of native *Sm*HZ. (A) Lipids were extracted from native *Sm*HZ using ethyl acetate, blown dry under $N_2(g)$ and redissolved in RP-LC-MS/MS mobile phase. All six hydroxylated fatty acid derivatives of arachidonic acid were identified (15-, 11-, 12-, 8-, 9- and 5-HETE). Insert shows the representative chiral resolution for 15-HETE (11.5 min. *R* and 14.5 min. *S*). (B) Representative MS/MS fragmentation for 12-HETE. All isomers were confirmed using authentic standards and extracted ion profiles from MS/MS.

To investigate the presence of biologically active AA metabolites in native *SmHz*, the hydroxylated fatty acid component of native *SmHz* was isolated and analyzed by liquid chromatography-tandem mass spectrometry (LC-MS/MS). The identification of each HETE positional isomer peak was achieved using time dependent MS/MS in which the isobaric carboxylate $[M-H]^-$, 319 m/z , precursor ion was trapped and subsequently

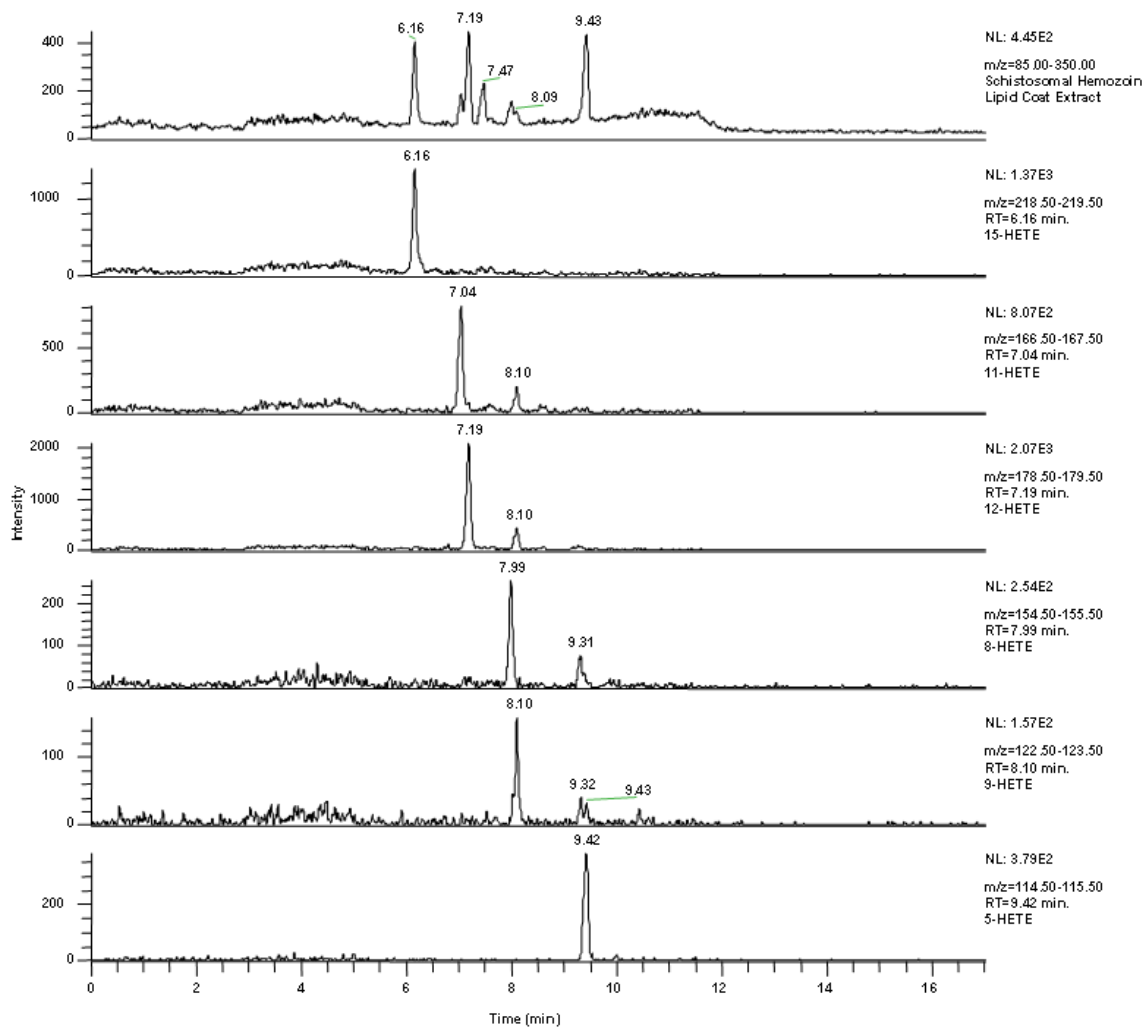


Figure 7 Extracted ion profile of *SmHz* lipid coat. The identification of all six positional isomers of HETE in the *SmHz* lipid coat was achieved by extracting the characteristic MS/MS fragment masses of each isomer from the collected 319 m/z reverse-phase-LC-MS ions. Individual isomers from the total ion chromatogram (A) of the *SmHz* lipid coat are shown: (B) 15-HETE at 6.16 min., (C) 11-HETE at 7.04 min., (D) 12-HETE at 7.19 min., (E) 8-HETE at 7.99 min., (F) 9-HETE at 8.10 min. and (G) 5-HETE at 9.42 min. Characteristic MS/MS fragments were confirmed using authentic HETE standards.

fragmented to give product ions of each HETE isomer (Figure 6). All six HETE positional isomers derived from AA were observed in the *Sm*HZ lipid extract, with the most abundant species being 15-, 12- and 5-HETE ([M-ROH]⁺: 219, 179 and 115 *m/z*, respectively) (Figure 7). In contrast to previous HETE identifications in hemozoin producing parasites,³⁶ the LC-MS/MS method presented herein is a marked advancement

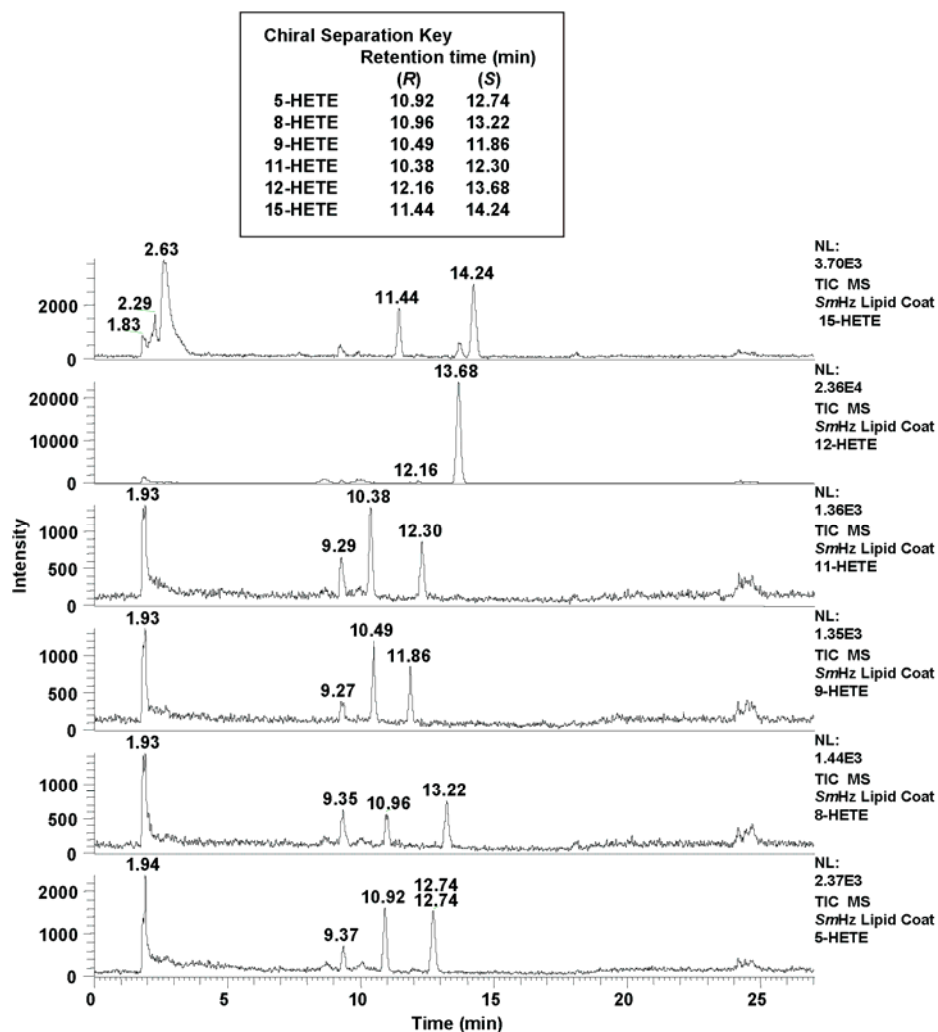


Figure 8 Chiral-RP-LC-MS/MS of *Sm*HZ lipid coat. *R* and *S* HETE enantiomers were separated using chiral-reverse-phase-LC-MS/MS (*R*- and *S*-HETE retention times shown in figure key). Each HETE isomer was identified by its characteristic MS/MS fragment masses as determined from authentic HETE standards. A 1:1 ratio was observed for all HETE enantiomers with the exception of 12-HETE which exhibited a 70:1 distribution of 12-*S*-HETE to 12-*R*-HETE.

including MS/MS confirmation of all identified HETEs during separation and an increased instrument sensitivity reaching the femtomole range. Such a limit of detection is especially important when working with the extracted lipids of limited native HZ samples, as is the case of *S. mansoni* yields from Swiss Webster mice (1 mg *SmHZ*/ 60 mice).

Chiral purity of biologically derived hydroxylated fatty acids is typically attributed to the lipoxygenase (Lox) family⁶⁵⁻⁷² with preference usually shown for *S*-stereo-isomer products. In the absence of Lox, however, free radical-mediated peroxidation of AA can yield a racemic mixture of each hydroxylated isomer. Given the presence of all six HETE isomers in the *SmHZ* lipid coat, additional chiral analysis was performed to examine the enantiomeric chiral analysis was performed to examine the enantiomeric distribution of the monohydroxy derivatives. Chiral LC-MS/MS of the *SmHZ* lipid extract revealed an equivalent stereoselective distribution of all HETEs with the exception of 12-*S*-HETE (Figure 8). Based on integrated peak area, a 70:1 abundance of 12-*S*-HETE to 12-*R*-HETE was observed suggesting accumulation of enzymatically produced HETE. This is in marked contrast to the equivalent stereoisomeric ratios observed for the 12-HETEs in the lipid coat of *PfHZ*.³⁶ Previously, murine host 12-Lox activity has been described in the immunomodulation of schistosomiasis.^{73,74} Three types of murine 12-Lox (epidermal-, leukocyte- and platelet-type 12-Lox) have been reported, but none of these were observed in a recent proteomic analysis of gut contents from *S. mansoni*.^{73,75} In *S. mansoni*, only the activity of a 15-*S*-Lox has been reported, although sequence analysis of the partially sequenced *S. mansoni* genome⁷⁶ suggests the possible presence of a 12-*S*-Lox gene. Regardless of the origin of the observed 12-*S*-HETE, the

racemic mixture of all other HETE isomers is indicative of HZ-mediated lipid peroxidation of fatty acids.

In order to confirm the expected HZ-driven lipid peroxidation of fatty acids, *in vitro*, reactions of AA incubated with either purified *SmHZ* or BH were performed under aerobic conditions. The resultant oxidized lipids were extracted and characterized by RP- and chiral-LC-MS/MS. Relative to AA controls, both purified *SmHZ* and BH produced significant quantities of the six HETE positional hydroxylation isomers, with 15- and 5-HETE as the most prominent (Figure 9-11).

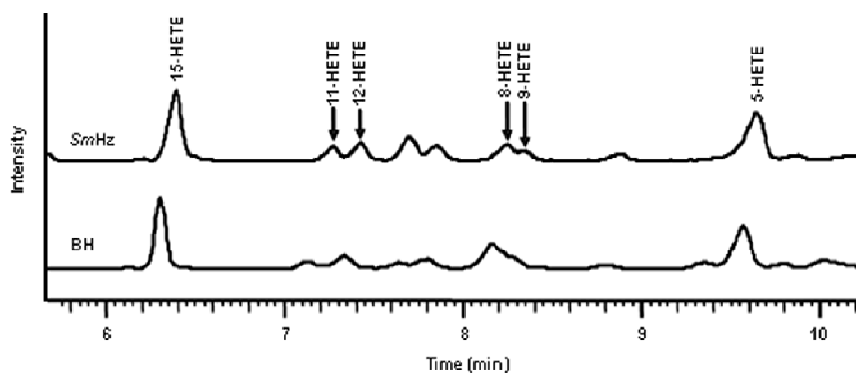


Figure 9 Hemozoin-mediated lipid peroxidation of arachidonic acid. Oxidation studies by incubation of 0.3 mg/mL BH or *SmHZ* with 5.32 mM AA were conducted. The hydroxylated fatty acid isomers 15-, 11-, 12-, 8-, 9- and 5-HETE were identified in the reactions' lipid extracts using RP-LC-MS/MS.

These findings are in good agreement with earlier literature concerning the reactivity of both purified *PfHZ* and BH.^{38,77} Upon subsequent chiral analysis, the positional HETE isomers were separated with a stereoselective ratio of nearly 1, suggesting no preferential stereochemical orientation of the substrate during oxidation. As expected, the stereoselective bias for 12-*S*-HETE seen in the native *SmHZ* lipid coat was absent in the

reaction of either purified *SmHZ* or BH with AA. Taken together, these results demonstrate that *SmHZ* mediated peroxidation of PUFAs is the likely source for the

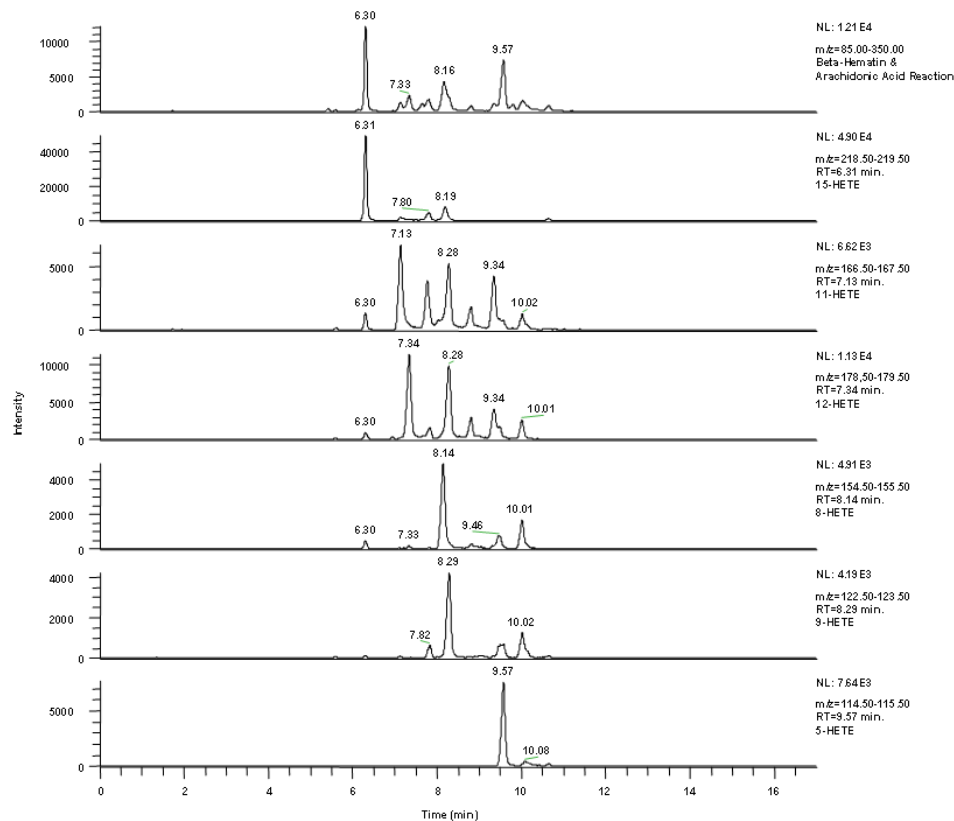


Figure 10 Extracted ion profile of HETEs from the BH-AA reaction. All six positional isomers of HETEs were extracted and confirmed by MS/MS from the BH-AA reaction.

enantiomeric population of observed HETE isomers in the lipid coat.

Lipid metabolites have been shown to elicit immunomodulatory effects ranging from impairment of both PMA-stimulated oxidative burst and nitric oxide (NO) production in macrophages to altering endothelial cell permeability and initiating chemotaxis.^{36,41,78} Investigation of the HETE isomers' individual effects on macrophage-like cell function following LPS challenge revealed that the predominate 5-, 12- and 15-*S*-HETEs impaired NO production in a dose-dependent manner (Figure 12A). 12-*S*-

HETE was the most potent inhibitor of iNOS, attenuating NO production by 50%. The immunosuppressive activity of native *SmHZ*'s hydroxylated fatty acids suggest that

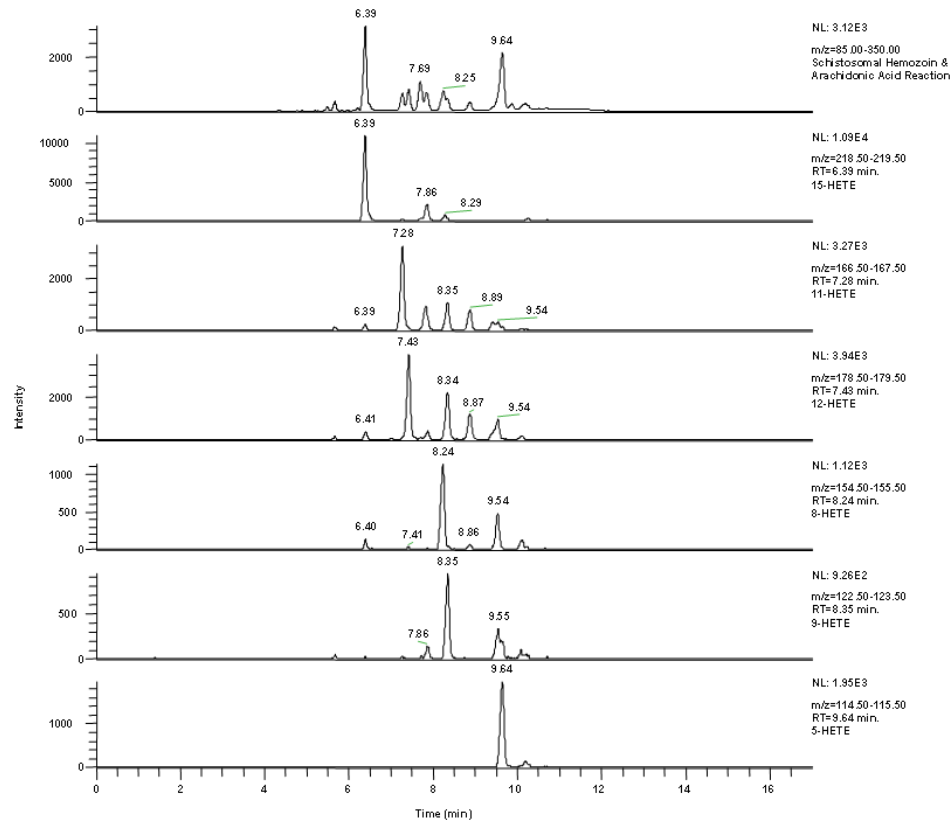


Figure 11 Extracted ion profile of HETEs from the *SmHZ*-AA reaction. All six positional isomers of HETEs were extracted and confirmed by MS/MS from the *SmHZ*-AA reaction.

phagocytosis of native *SmHZ* by resident macrophages may partially disrupt the innate immune response. In fact, further study revealed a 25% reduction in NO production in lipid-coated *SmHZ*-laden macrophages relative to control experiments, implicating native *SmHZ* as a biologically active agent (Figure 12B).

The lipid coat of native *SmHZ* is a complex mixture of both neutral lipids and PUFA peroxidation products. Previous analysis of the neutral lipids revealed the presence of monopalmitic-, monostearic-, dipalmitic-, dioleic- and dilinoleic glycerols.²⁹

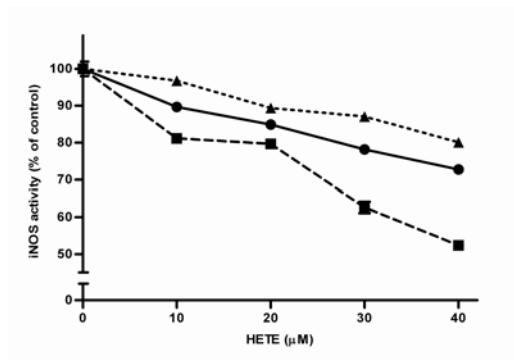
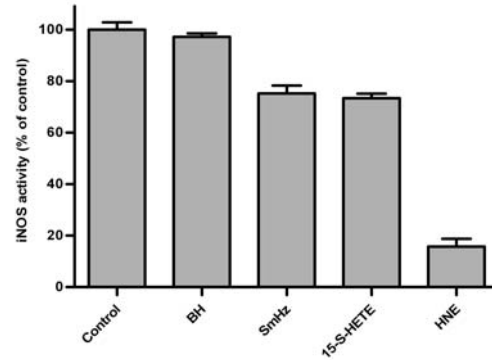
A**B**

Figure 12 Impact of native *SmHZ* and components on iNOS activity. (A) RNS production in macrophage cells monitored following treatment with increasing concentrations of (●) 15-, (■) 12- and (▲) 5-S-HETE by the Griess assay. (B) Cells were treated with 0.1 mg/mL BH or *SmHZ*, as well as 40 μM 15-S-HETE or HNE. The activity of cells stimulated with LPS was used as a control.

Conclusions

Herein, the composition of the arachidonate metabolites has been determined to consist of an enantiomeric mixture of all positional hydroxylated isomers with 15-, 12- and 5-HETE as the dominant species. These findings are consistent with HZ-mediated lipid peroxidation of host arachidonate. Additional chiral analysis revealed an accumulation of a biologically derived 12-S-HETE of an unknown origin. When the immunosuppressive activity of native *SmHZ* and its major HETE components was examined in macrophage-like cells, iNOS activity was impaired. Further exploration of this unique biomineral's composition and its ability to modulate host immunity is crucial in developing a better understanding of the possible role of hemozoin in the host-pathogen interactions involving *S. mansoni*.

CHAPTER III

IMMUNOMODULATORY ACTIVITY OF HEMOZOIN^{41,79}

The most common and deadly form of the malaria parasite, *Plasmodium falciparum*, is responsible for 1.5-2.7 million deaths and 300-500 million acute illnesses annually.^{80,81} These statistics combined with the development of drug-resistant parasitic strains and vectors place a multibillion dollar annual burden on precisely those populations least capable of shouldering it.⁸¹⁻⁸³ According to the World Health Organization,⁸¹ malaria is considered to be one of the major public health challenges responsible for inhibiting development in underdeveloped regions of the world side by side with HIV/AIDS and tuberculosis. Consequently, despite its absence in the developed world, malaria represents a significant global health issue. Historically, the disease was thought to stem from fetid marshes and was thus named *mal aria*, literally bad air.⁸¹ In truth, malaria is a parasitic disease of the genus *Plasmodium* that is transmitted to humans through the bite of an infected female *Anopheles* mosquito. The parasitic lifecycle inside the host is complex, and it is the intraerythrocytic stage that is of interest herein.

During this stage, nourishing amino acids are acquired when hemoglobin is catabolized within the acidic lysosome known as the digestive food vacuole (DV).⁸⁴ As a result, toxic free heme is released as well, and its accumulation leads to lipid peroxidation,³⁸ DV protease inhibition, oxidized free radicals^{85,86} and finally, parasite lysis.⁸⁷ Therefore, the parasite has evolved a detoxification pathway leading to the

aggregation of heme into the insoluble biomineral known as hemozoin.⁸⁸ When HZ is formed, it remains in the infected RBC until the cell bursts, releasing the parasite and the HZ along with the cell's lipid membrane and other debris into the host vasculature.⁸² The host's innate immune system launches a defensive surge of monocytes and neutrophils in order to phagocytose and destroy the dispersed particulate. Ideally, these phagocytes would then activate the NADPH oxidase and inducible nitric oxide synthase (iNOS) pathways which would produce ROS and RNS, respectively. It is these reactive species that possess the ability to destroy the engulfed material during oxidative burst.⁸⁹

Recent images with confocal microscopy, however, have shown that *Pf*HZ can withstand the ROS and RNS onslaught by macrophages up to 72 hours.⁹⁰ Additionally, engulfed HZ has been linked to impaired phagocyte function, including PMA induced oxidative burst,^{55,59} rephagocytosis,^{55,91} interferon γ response⁹² and the destruction of other particulate such as bacteria, fungi or tumor cells.⁹³ Altered cytokine production and an upregulation of PGE₂ molecules have also been reported.⁹¹ Likewise, HZ phagocytosis *in vivo* has been shown to correlate with increased levels of HNE⁵⁹ and hydroxylated fatty acids.^{36,78} In support of these findings, *in vitro* work with BH, the synthetic form of HZ, has demonstrated that the biomineral does indeed have the ability to mediate the oxidation of polyunsaturated fatty acids (PUFAs) into hydroxylated fatty acids^{36,39} and HNE.⁵⁸

Controversy over the immunosuppressive nature of HZ and BH litters earlier works. While HZ has since been acknowledged as an immunomodulatory agent, reports on the behavior and effects of BH have varied greatly. Whether inflammatory⁹⁴⁻⁹⁶ or anti-inflammatory,^{92,97-99} the response of the immune system to HZ and BH, two

structurally identical biominerals, should differ only in their external composition, or coat. This coat contains lipids in the case of HZ because it has been exposed to a lipid-rich cell environment during formation and cell rupture. The synthetic BH produced *in vitro* in the laboratory would be absent of this lipid component. Therefore, a look at these lipid constituents on macrophage function was explored in order to examine more carefully the source of HZ's immunomodulatory activity.

Experimental

BH preparation and characterization. BH was synthesized via dehydrohalogenation of hemin, as described by Bohle.⁶⁰ The reaction vessel was sealed, protected from light and stood undisturbed for three months. The resulting mixture was filtered, and the precipitate was washed exhaustively with methanol, 0.1 M sodium bicarbonate (pH 9.1) and deionized water. The purified product was dried under vacuum at 150°C for 48 h and stored under dessicant. The BH was characterized using FT-IR, SEM and XRD and compared to previously reported spectra.³³⁻³⁵

Cell culture. Adherent murine macrophage cell line, RAW 264.7, was maintained in continuous culture with RPMI 1640 medium, supplemented with 10% (v/v) heat-inactivated fetal bovine serum and 100 µg/mL penicillin/streptomycin in an atmosphere of 5% CO₂, 5% humidity at 37°C. Cell viability was determined by Trypan Blue exclusion using a hemocytometer.

Measurement of ROS and RNS production. Measurement of ROS was accomplished using luminol-dependent luminescence. In these experiments, RAW 264.7

cells were plated overnight in complete medium at a density of 4×10^6 cells/well in a 6-well plate. The following day, the medium was removed, the cells gently washed with phosphate-buffered saline (PBS) and treated. After 3 hours of incubation at 5% CO₂, 5% humidity at 37°C, the supernatant was removed and cells gently washed with PBS, and NADPH oxidase was activated by the addition of 1.0 mL of 100 nM PMA in PBS. After 4 minutes, 950 µL of this supernatant was collected into a luminescence tube followed by the addition of 50 µL of 1.0 mM luminol (in PBS). Luminescence was immediately measured using a Monolight 3010 luminometer for 10 seconds. Alternatively, ROS were monitored using dichlorofluorescein diacetate (DCF-DA). In these reactions, cells were plated overnight in complete medium at a density of 5×10^5 cells/well in a 24-well plate. The next morning, the cells were washed, then treated with HNE and 15-HETE, 100 nM PMA in PBS and 8 µM (final) DCF-DA for 1 hour at 37°C and 5% CO₂, 5% humidity. The formation of the fluorescent dichlorofluorescein was monitored with the Bio-Tek Synergy HT multidetection microplate reader using a 485/20 excitation filter and a 528/20 emission filter. It is important to recognize that this assay, unlike the luminol assay described earlier, does not involve pre-incubation of the cells with HNE or 15-HETE. All assays were performed in triplicate, and the average value reported with standard deviation.

Triplicate measurement of RNS was accomplished using the Griess assay.⁶³ For these experiments, RAW 264.7 cells were plated overnight in complete medium at a density of 5×10^5 cells/well in a 24-well plate. The next day, cells were treated and then stimulated by the addition of 10 µL of 50 µg/mL LPS (1 µg/mL final) followed by incubation in 5% CO₂, 5% humidity at 37°C. After 24 hours, 300 µL of the supernatant

was removed from the cells and spun down at 13,200 rpm for 5 minutes. A 100 μ L aliquot of the supernatant was then transferred to a 96-well plate, and the production of NO was monitored using the Griess assay. For this assay, 100 μ L of each sample was reacted with 50 μ L of 1% sulfanilimide in 5% phosphoric acid, followed by 50 μ L of 0.1% NED. After 5 minutes, the absorbance of the resulting *azo* complex was measured at 540 nm using a Bio-Tek Synergy HT multidetection microplate reader. To investigate the effect of BH on the production of ROS and RNS, 120 μ g/mL (final) of BH was suspended in complete medium and used in all cases unless otherwise noted.

Degradation of BH by ROS. To study the ability of ROS to degrade BH *in vitro*, reactions between BH and standardized 0-100 mM hydrogen peroxide¹⁰⁰ and 0-10 mM sodium hypochlorite¹⁰¹ were prepared in triplicate. Briefly, to a 1.5 mL microcentrifuge tube, 100 μ L of a 2.0 mg/mL suspension of BH in 100 mM sodium acetate buffer pH 4.8 was added to 300 μ L of sodium acetate buffer, followed by addition of 100 μ L of the appropriate concentration of hydrogen peroxide or sodium hypochlorite. Prior to incubation in a 37°C water bath for 20 h, the solutions were capped, covered with parafilm and vortexed. After incubation, the samples were centrifuged at $16.1 \times 10^3 \times g$ for 30 minutes to pellet the remaining BH. The clear supernatant was removed, and the pellet was washed once with DI water and re-centrifuged. Finally, the BH was dissociated into free heme by dissolving the pellet in 1.0 mL of 1.0 M NaOH, and the absorbance of free heme was monitored at 400 nm using a Bio-Tek Synergy HT multidetection microplate reader to quantify the remaining heme.

Degradation of BH by RNS. To study the ability of RNS to degrade BH *in vitro*, reactions between BH and 0-100 mM DeaNO, a nitric oxide releasing agent, were

prepared in triplicate. Briefly, to a 1.5 mL microcentrifuge tube, 100 μ L of a 2.0 mg/mL suspension of BH in 100 mM sodium phosphate buffer pH 7.4 was added to 390 μ L of sodium phosphate buffer, followed by the addition of 10 μ L of the appropriate concentration of DeaNO. Prior to incubation in a 37°C water bath for 20 h, the solutions were capped, covered with parafilm and vortexed. After incubation, the samples were centrifuged at $16.1 \times 10^3 \times g$ for 30 minutes to pellet the remaining BH. The brown supernatant was removed and the pellet washed once with deionized water and re-centrifuged. Finally, the BH was dissociated into free heme by dissolving the pellet in 1.0 mL of 1.0 M NaOH and the absorbance of free heme was monitored at 400 nm using a Bio-Tek Synergy HT multidetection microplate reader. At DeaNO concentrations of 25 mM or greater, it was necessary to add 10 μ L of 5.0 M NaOH and allow the tube to rotate overnight to obtain complete dissociation of the BH pellet. Finally, the absorbance of free heme was monitored at 400 nm using a Bio-Tek Synergy HT multidetection microplate reader in order to quantify the remaining BH. Additionally, FT-IR was used to analyze the formation of a Fe-NO complex at the 50 mM DeaNO concentration. The amount of NO released by DeaNO in this experiment was verified by running a series of control reactions. Here, the samples were prepared and treated exactly as those described earlier except that the 100 μ L of BH was replaced with 100 μ L of sodium phosphate buffer. To analyze the amount of NO produced, the Griess assay⁶³ was employed. It should be noted that Fe(III)PPIX solutions may absorb onto plasticware and can exist in different aggregation states, resulting in minor changes in absorbance.

Confocal microscopy. The localization of BH inside an acidic phagolysosome was demonstrated using lysotracker, a pH-sensitive dye. Here, 5×10^4 cells were plated

overnight, followed by gentle PBS wash. Next, the cells were treated with 100 μ L of 0.12 mg/mL BH suspended in complete medium and allowed to phagocytose in an atmosphere of 5% CO₂, 5% humidity at 37°C. After 1.5 h, the cells were washed twice with PBS and were treated with 2 mL of 100 nM PMA diluted in complete medium. After 10 minutes at 5% CO₂, 5% humidity at 37°C, the PMA was removed, the sample washed with PBS and covered with 2 mL of fresh PBS. Approximately 5 minutes prior to imaging, 4 μ L of 20 μ M lysotracker diluted in PBS was added to the dish. Fluorescence imaging of BH was accomplished by excitation at 514 nm followed by collection using a band-pass filter from 533.2 to 542.9 nm. Lysotracker fluorescence was obtained by excitation at 543 nm followed by the use of a long-pass 585 nm filter for emission. The images were stacked into a composite figure in order to determine colocalization.

Confocal microscopy was also utilized to determine the fate of BH that has been phagocytosed by RAW 264.7 macrophage-like cells. Cells were plated and treated with BH as before. The incubation of these dishes was varied at 0, 48 and 72 hour increments in an atmosphere of 5% CO₂, 5% humidity at 37°C. At each time point, the samples were gently washed once with PBS, covered with 2 mL of fresh PBS and immediately imaged on the Zeiss LSM 510 Meta inverted confocal microscope using the same parameters as before. In order to quantify the fluorescence emission from the samples, projections were made of the z-stacks from 200-300 cells per sample, and Metamorph software was used to quantify the amount of fluorescence above the background threshold.

*Superoxide Cytochrome C Assay.*¹⁰² A non-differentiated human myeloblastic HL60 (ndHL60) cell line was differentiated with 1.3% DMSO for five days. Cell suspensions (100 μ L of 1E5 cells/well) in phenol red-free media were added to black 96-well plates and incubated 30 min. Prepared reaction mixtures, 150 μ L of 32 μ M PMA, 320 μ M cytochrome c, and 20 μ L of 10,000 U/mL of SOD in HBSS, were added to the appropriate wells. The plate was incubated another 30 min at 37°C and read at 550 nm. To measure the inhibition of superoxide, varying concentrations of HNE were incubated 4 h in the cell suspensions before addition of reaction mixtures.

*H₂O₂ Amplex Red Assay.*¹⁰³ Five day differentiated HL60 cells (20 μ L) were added to black 96 well plates at 1.5E4 cells/well in phenol red-free RPMI 1640. Prepared reaction mixture (100 μ L of 50 μ M Amplex Red reagent, 0.1 U/mL HRP, and 16 μ M PMA in KRPG) was added to the wells. The plates were incubated 30 min. at 37°C before fluorescence readings were taken at an excitation 530/25 and emission 590/35. To measure the inhibition of H₂O₂, varying concentrations of HNE were incubated 30 min in the cell suspensions before addition of reaction mixtures.

Reaction of HNE and 15-HETE on stimulated RAW 264.7 cells. The ability of HNE and 15-HETE to inhibit PMA and LPS stimulated oxidative burst was analyzed. To examine the effects of HNE and 15-HETE on the activation of NADPH oxidase, 5x10⁵ cells/well were plated in 24-well plates. The following day, the cells were treated in triplicate with HNE (0-100 μ M) or 15-HETE (0-12 μ M) and incubated in 5% CO₂, 5% humidity at 37°C. After 1 hour, the cells were examined for NADPH oxidase activity using DCF-DA, a dye that is converted to the fluorescent dichlorofluorescein in the presence of oxidizing species (described earlier). To investigate LPS inhibition, 5x10⁵

cells/well were plated in 24-well plates overnight. Subsequently, the cells were washed once with PBS, followed by treatment with HNE (0-20.5 μ M) or 15-HETE (0-20 μ M), followed by stimulation of iNOS with LPS (1 μ g/mL final). These samples were allowed to incubate for 24 hours before analysis of the supernatant via the Griess assay.

Ghost cell preparation. Red blood cell ghosts were prepared from expired whole blood obtained from the Vanderbilt Medical Center Blood Bank.^{104,105} Whole blood was kept at 4°C until use and mixed inside the bag before use. A 22 gauge needle fitted to a disposable syringe was used to draw 3 mL of whole blood which was then expelled into a 15 mL polypropylene centrifuge tube. PBS (11 mL) was added, and the tube was gently inverted to mix. The solution was then centrifuged at 1000 x g for 10 minutes. The supernatant was discarded in bleach, and this wash was repeated until the supernatant appeared clear. The RBCs were then lysed by dissolving the pellet in 0°C 5 mM sodium phosphate buffer in 50 mL polypropylene tubes and vortexing. The solution was centrifuged at 10,000 x g, the supernatant was discarded, and wash repeated until no trace of red could be seen in the membrane pellet. The pellet was then dissolved in a minimum amount of PBS and stored at -80°C. A Biorad assay was used to determine the protein content of the final solution. Briefly, standards were made with bovine serum albumin from 1.5 mg/mL to 0.2 mg/mL. Standards and samples were pipetted (5 μ L) into a clear 96 well plate. Bio-rad reagent A (25 μ L), an alkaline copper tartrate solution, was added to each sample followed by 200 μ L of reagent B, a dilute 1,2-naphthoquinone-4-sulfonate solution. The plate was allowed to sit for 15 minutes at room temperature, after which the absorbance was read at 750 nm. RBC ghosts were used for reactions at protein concentrations of 1 mg/mL.

Reactions between RBC ghosts and BH were prepared in test tubes with a total volume of 2 mL. RBC ghosts, normalized to an absorbance of 0.7 at 280 nm, were added first, followed by 500 μ L of 3 mg/mL BH (0.75 mg/mL final), and the samples were taken up to 2 mL total volume with RPMI 1640 complete medium. After stirring for 24 hours at room temperature, the reaction mixtures were centrifuged for 15 minutes at 5,445 x g to pellet ghost membranes and BH. RAW 264.7 murine macrophage cells were then treated in triplicate with varying amounts of the supernatant (from 0 to 100%). Luminol-dependent luminescence was used to measure the effect of the supernatant of the ghost-BH reaction on the production of ROS and the Griess assay was used to monitor the effects on the production of RNS.

Results and Discussion

Biologically, the production of ROS and RNS in phagocytic cells is predominantly mediated by the action of two enzymes: NADPH oxidase and iNOS. The production of ROS during oxidative burst is a result of the activation of NADPH oxidase. Activation of this constitutively expressed enzyme results in the reduction of molecular oxygen to the superoxide anion which is rapidly converted to secondary species such as hypochlorous acid (HOCl), the hydroxyl radical (\cdot OH) and hydrogen peroxide (H_2O_2).¹⁰⁶⁻
¹⁰⁸ RNS are initiated by the induction of nitric oxide synthase. Once translated, iNOS produces nitric oxide, which in turn can react with molecular oxygen to form a variety of derivatives, including NO_2 , N_2O_3 , NO_2^- and NO_3^- .⁶³ Together, these species act to degrade foreign pathogens. Considering the innate toxicity of these reactive microbicidal

agents, their modulation is an important component in establishing a successful parasitic infection.

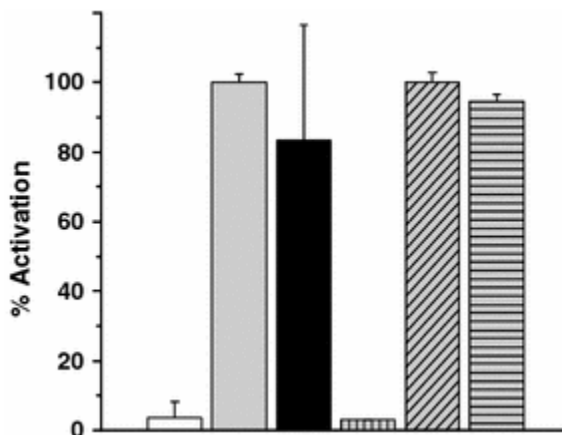


Figure 13 Effect of BH on the production of ROS and RNS. ROS production was assessed by DCF-DA (first 3 columns), showing the percent activity of (**white**) unstimulated cells, (**gray**) cells stimulated with PMA and (**black**) cells treated with BH and stimulated with PMA. The Griess assay was used to measure RNS production (last 3 columns), showing (**gray with vertical lines**) unstimulated cells, (**gray with diagonal lines**) cells stimulated with LPS and (**gray with horizontal lines**) cells treated with BH and stimulated with LPS.

BH's ability to modulate the activity of NADPH oxidase was examined. As shown, BH does not inhibit the production of ROS in PMA-stimulated RAW macrophage-like cells (Figure 13). Pre-incubation with up to 0.4 mg/mL BH showed no inhibitory effect on superoxide anion production as measured by luminol-enhanced luminescence. Reports have similarly indicated no inhibition of ROS in mouse macrophage-like B10R, BV2 microglial and peritoneal macrophage cell lines.^{99,109} In contrast, phagocytosis of native HZ by human monocyte-derived macrophages resulted in inhibition of PMA-stimulated NADPH oxidase^{55,59} in a dose-dependent fashion.

Challenge of LPS-stimulated iNOS in RAW macrophage-like cells with BH does not inhibit the production of RNS either (Figure 13). In control reactions with unstimulated cells, levels of detected NO increased as levels of BH were increased,

owing to particulate activation (data not shown), indicating healthy, functioning macrophage cells. Additionally, 24 hour pre-incubation of RAW macrophage cells with BH does not inhibit re-stimulation with LPS (Figure 14). The results shown in Figure 16 are consistent with studies in macrophage-like B10R and N11 microglial cells which show no BH-dependent inhibition¹¹⁰ of NO but are contradictory to a report with murine peritoneal macrophages that appears to indicate BH inhibition of NO.⁹⁷ Further, HZ directly isolated and exhaustively purified to remove all absorbed proteins, lipids and carbohydrates consistently has been shown not to inhibit NO production in human peripheral blood mononuclear cells and macrophage B10R microglial cells.^{110,111}

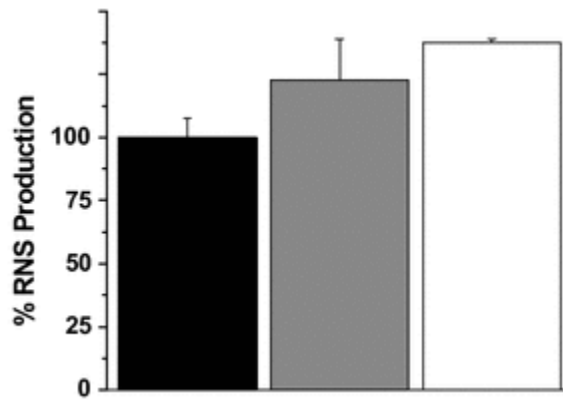


Figure 14 Effect of preincubation of RAW cells with BH on RNS production as measured by the Griess assay. The **black** column corresponds to RNS production of cells stimulated with LPS, the **gray** column is cells treated simultaneously with BH and LPS and the **white** column represents cells first treated for 24 hr with BH, followed by restimulation with LPS for another 24 hr.

Consequently, the results presented herein and the preponderance of published data suggest that NO production is not inhibited by BH treatment. In contrast, native (crude) HZ has been shown to decrease NO production in peritoneal macrophages.¹¹² The stark contrast concerning the immunoreactivity of BH versus native HZ with regards to modulating ROS and RNS production implies that there exists a biochemical distinction

between the two. If BH does not effectively inhibit the intracellular production of ROS and RNS, then these molecules should be available to react with the phagocytosed heme aggregate; however, experiments suggest that hemozoin can persist for up to 72 hours within the phagolysosome.⁹⁰ Consequently, the effects of these microbicidal agents on BH stability may provide some degree of insight into the apparent biochemical differences between BH and hemozoin. In a series of *in vitro* studies, BH stability was examined in the presence of HOCl, H₂O₂ and NO.

BH displays a marked sensitivity to HOCl at pH 4.8, the pH of the phagolysosome, with an EC₅₀ of 5.5 mM (Figure 15A). Its degradation in the presence of HOCl results in the loss of aggregate integrity and formation of an insoluble orange product. The HOCl-mediated oxidation of the protoporphyrin IX methylene bridge likely results in the opening of the ring and release of iron. The consequence of such a reaction would be the dissolution of the aggregate and formation of a product similar to bilirubin, the tetrapyrrole end product of biological heme degradation by heme oxygenase.¹¹³ Analysis of the orange product by UV-Vis spectroscopy is consistent with the production of such an oxidized pyrrole-base material (data not shown).

Reactions between BH and H₂O₂ at pH 4.8 also show BH degradation with increasing concentrations of the reactive agents (Figure 15B), with an EC₅₀ of 38 mM. This value is consistent with H₂O₂ degradation of BH reported by Chen et al.,¹¹⁴ who examined pigment stability in the context of Hb catabolism within the digestive vacuole. Reactions between Fe(III)PPIX and H₂O₂ have been reported to result in formation of four dipyrrolic propentdyopents, hematinic acid and methylvinylmaleimide.¹¹⁵ Heme-Fe(III) can react with H₂O₂ to generate a formal perferryl species¹¹⁶ [⁺heme-Fe(IV)=O or

heme-Fe(V)=O] which can then react with the olefinic porphyrin bridge to form a glycol and regenerate the ferric heme (Scheme 3). The ferric heme reacts with another molecule of H₂O₂ to cleave the glycol and form an amide and an α -formyl pyrrolic species.

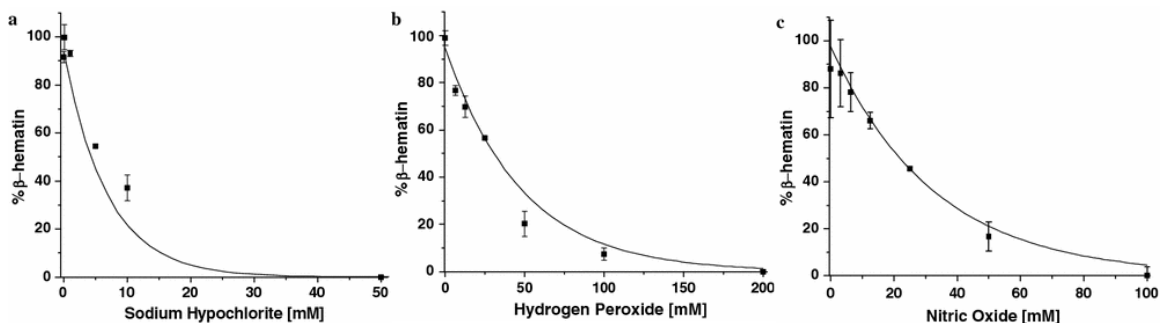
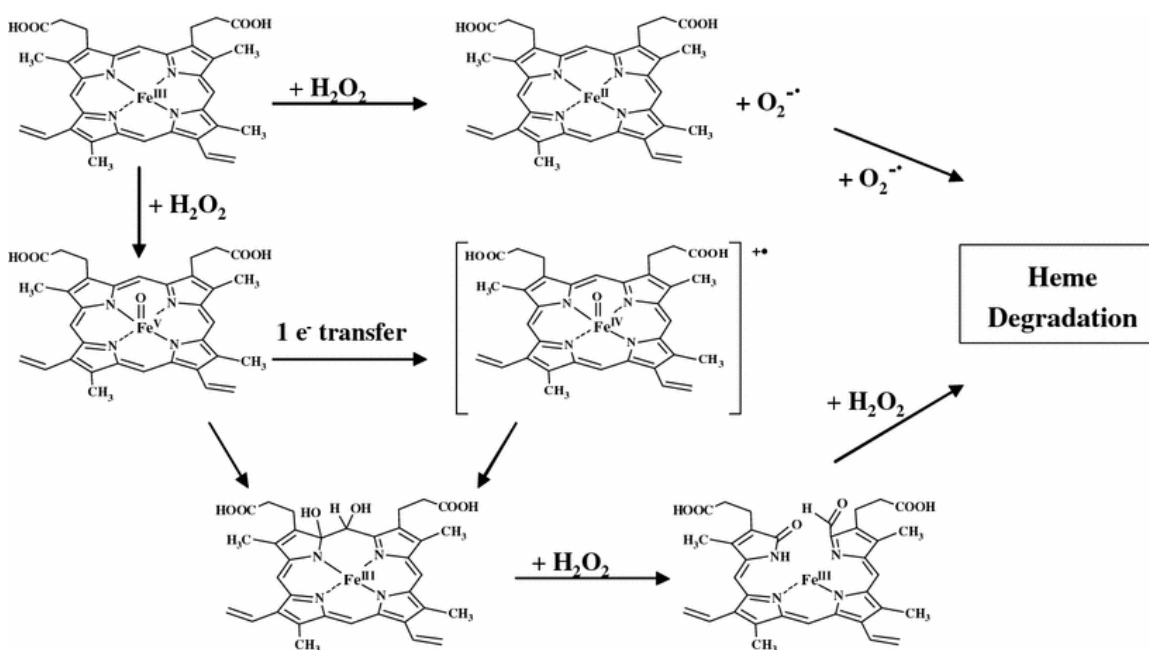


Figure 15 Degradation of BH in the presence of (a) sodium hypochlorite, (b) hydrogen peroxide and (c) nitric oxide.

Repeating this reaction in other methene bridges results in the breakdown of the porphyrin to dipyrroles and monopyrroles.^{115,116} Further enhancement of the degradation process is obtained when the reaction of heme-Fe(III) and H₂O₂ results in the formation of heme-Fe(II) and the superoxide anion. The superoxide anion is able to oxidize the tetrapyrrole rings of heme, leading to the degradation of heme and the release of iron.¹¹⁷ With hemozoin being a dimer consisting of Fe(III)PPIX units, it is plausible that its degradation process in the presence of H₂O₂ is similar to those described for other metal-containing porphyrin systems.

To examine BH sensitivity to RNS, DeaNO, a surrogate for nitric oxide release was employed. Exposure to NO was found to degrade BH in a concentration-dependent manner with an EC₅₀ of 33 mM (Figure 15C). NO binding to ferric heme and formation of a ferric nitrosyl complex likely results in the spontaneous autoreduction of the iron to the ferrous state.¹¹⁸ In terms of stability, reduction of the iron will result in an increased

radius, weakening the iron-nitrogen bonds of the porphyrin. Further, NO acts as an extremely strong ligand and its binding to the iron of heme groups has been shown to exert a large repulsive force on the ligand *trans* to the NO,¹¹⁹ potentially disrupting the reciprocating propionate linkages within the crystal lattice of hemozoin. IR analysis of isolated reaction products prior to complete degradation revealed a vibration at 1636 cm⁻¹ consistent with NO coordination in Fe(II) porphyrin complex (data not shown).¹¹⁸



Scheme 3 Purported pathways of heme degradation by hydrogen peroxide.¹¹³⁻¹¹⁵

Regardless of the potential mechanisms of degradation, the insoluble BH biomineral is sensitive to the ROS and RNS that are generated upon phagocytosis. Further, it is recognized that the crystals of BH are large enough to allow water into the lattice.¹²⁰ Therefore, it is feasible that small molecules such as HOCl, H₂O₂ and NO work their way into the crystal lattice, disrupting the structural integrity of hemozoin from within as well as on the surface. The lower EC₅₀ value (5.5 mM) of HOCl

compared with that of H₂O₂ (38.0 mM) is consistent with it being a much more reactive microbicidal agent.¹⁰⁸ Additionally, the ability of H₂O₂ to degrade heme is known to decrease in acidic environments, whereas HOCl degradation is inversely affected by the acidity.¹²¹ NO is not a particularly strong microbicidal agent either, so it is not surprising that its EC₅₀ value is also higher than that of HOCl.⁸⁹ Finally, it is important to note that the concentration regimes of HOCl, H₂O₂ and NO examined here are relevant to biologically reported concentrations produced within professional phagocytic cells.^{89,122} To investigate the fate of BH inside RAW cells, BH was phagocytosed and its *in vivo* stability examined by confocal microscopy.

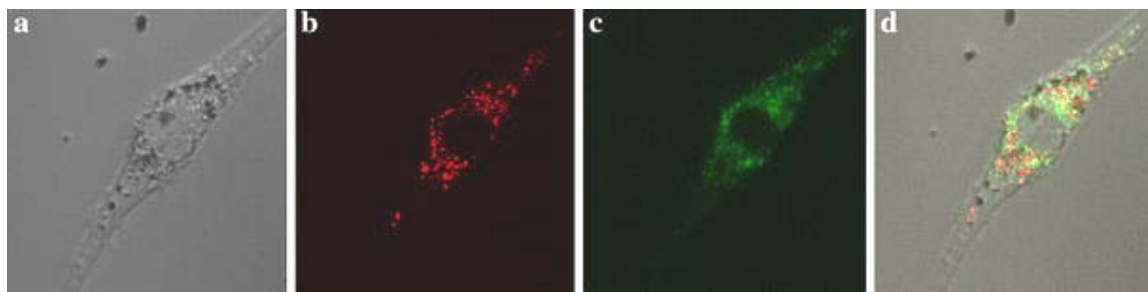


Figure 16 Colocalization of BH inside the acidic vacuoles as examined by confocal microscopy at x40 magnification. (A) The differential interference contrast image of the cell. (B) Excitation at 514 nm followed by emission using a band-pass filter from 533.2-542.9 nm allowed for the imaging of BH fluorescence. (C) Excitation at 543 nm followed by the use of a long-pass 585 nm filter for emission allows for visualization of the lysotracker fluorescence. (D) Composite figure of A-C demonstrating the colocalization of BH inside the acidic vacuoles.

RAW macrophage cells were treated with BH and allowed to phagocytose for 1.5 h. The co-localization of BH inside the acidic vacuoles was shown using the innate fluorescence of BH and a dye specific to acidic compartments such as the phagolysosome (Figure 16). Here, the images of HZ fluorescence and the fluorescence of the lysotracker dye clearly show BH co-localizing to acidic vacuoles of the macrophage cells. No bleed-through was found to occur between the two channels, indicating the fluorescence

intensity obtained from one setting was not being contaminated by fluorescence from the other. The orthogonal slices (*XY* and *XZ*) of the confocal image also revealed segregation of BH exclusively within the cell, confirming that it had indeed been phagocytosed.⁹⁰

The quantitative analysis of BH stability as a function of time was probed at 0, 48 and 72 h. Normalizing the fluorescence at time zero, we determined that by 48 h, BH had been degraded by $67.2 \pm 6.5\%$ and that by 72 h, it had been degraded by $76.8 \pm 2.7\%$. Visually, the results clearly show diminishing fluorescence (Figure 17), noted by a marked decrease in the amount of red fluorescence over the time course of the experiment. Controls in the absence of cells showed that BH fluorescence itself did not decrease with time, indicating the degradation observed was not due to photobleaching of BH (data not shown). The *in vivo* degradation of phagocytosed BH is at odds with the apparent stability of native HZ within human peripheral blood monocytes.^{90,123} These results, together with the observation that the ROS and RNS production was not inhibited by BH, and that the model reactions highlight BH sensitivity to microbicidal agents, indicate that the fate of BH is vastly different from that of native HZ despite the structural identity of the heme dimer core.

Associated with HZ phagocytosis in the pathophysiology of malaria are high levels of HNE and 15-HETE.^{59,78} Recently, it has been determined that HZ is able to nonenzymatically generate significant quantities of hydroxylated fatty acids^{36,38} and to mediate the oxidation of fatty acids such as arachidonic and linoleic acid to produce secondary oxidation products like HNE.⁵⁸ Levels of HNE and 15-HETE within HZ-laden macrophages have been found up to be 230 nmol per 10^{10} cells⁵⁹ and 33-39 μM ,³⁶ respectively. At relatively low concentrations, HNE disrupts cytoskeletal integrity,

impairs mitochondrial respiration, inhibits DNA, RNA and protein synthesis, stimulates neutrophil chemotaxis, and modulates platelet aggregation and changes in response to second messenger pathways.¹²⁴ Similarly, 15-HETE has been shown to generate pathophysiological effects such as altered permeability of endothelial cells, edema, increased adherence of RBCs and induced chemotaxis and chemokinesis.^{36,38} Consequently, macrophage function may be impaired by the presence of these immunoreactive molecules.

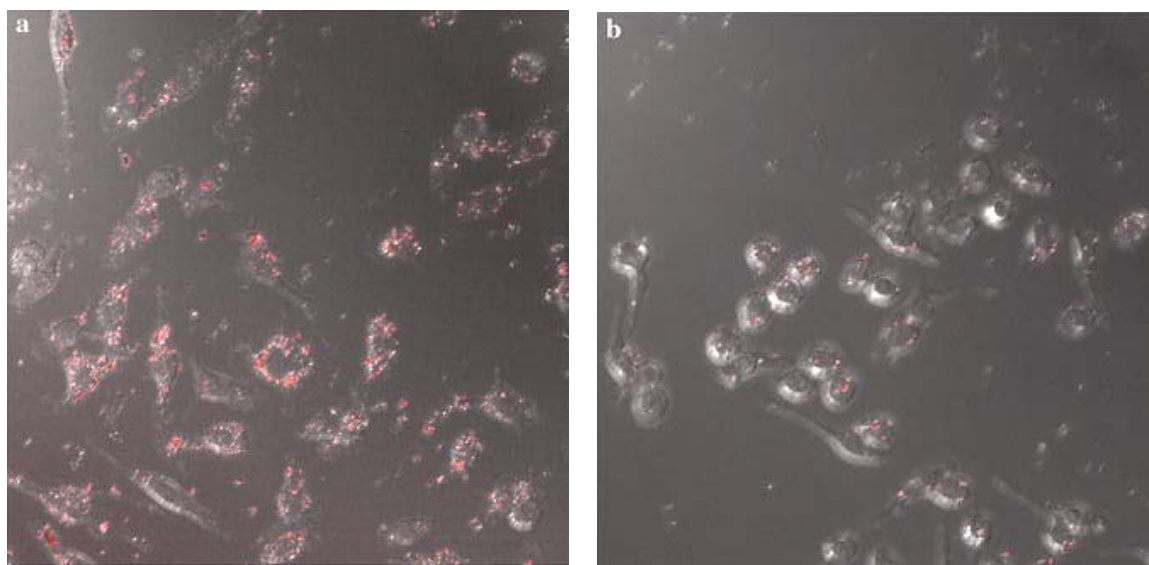


Figure 17 Confocal images (x40 magnification) of BH degradation inside RAW cells at time zero (A) and after 72 hr (B). Fluorescence images were obtained by excitation at 514 nm followed by collection of the emission spectra using a band-pass filter from 533.2 to 542.9 nm.

The cytochrome c superoxide assay and amplex red H₂O₂ assay were optimized to measure the effects of HNE on cellular superoxide. These assays were conducted on human myeloblastic neutrophil-differentiated HL60 cells and showed EC₅₀ values of 4.6 μM and 1.1 μM, respectively (Figure 18A&B). Low EC₅₀ values were indicative of the significant cellular sensitivity to the cytotoxic HNE. RAW cells treated with HNE

followed by stimulation with PMA demonstrated a concentration-dependent inhibition of oxidative burst (Figure 18C). As the concentration of HNE increased up to 100 μM , stimulation of NADPH oxidase was inhibited, with an EC_{50} value of 45.9 μM . Studies of HNE inhibition of superoxide in human neutrophils have shown a similar response, with an EC_{50} value of 27 μM , consistent with the results reported here for macrophage cells.¹²⁵ LPS-activated iNOS was similarly inhibited by HNE in a concentration-dependent manner, with EC_{50} values of 9.2 μM (Figure 18D).

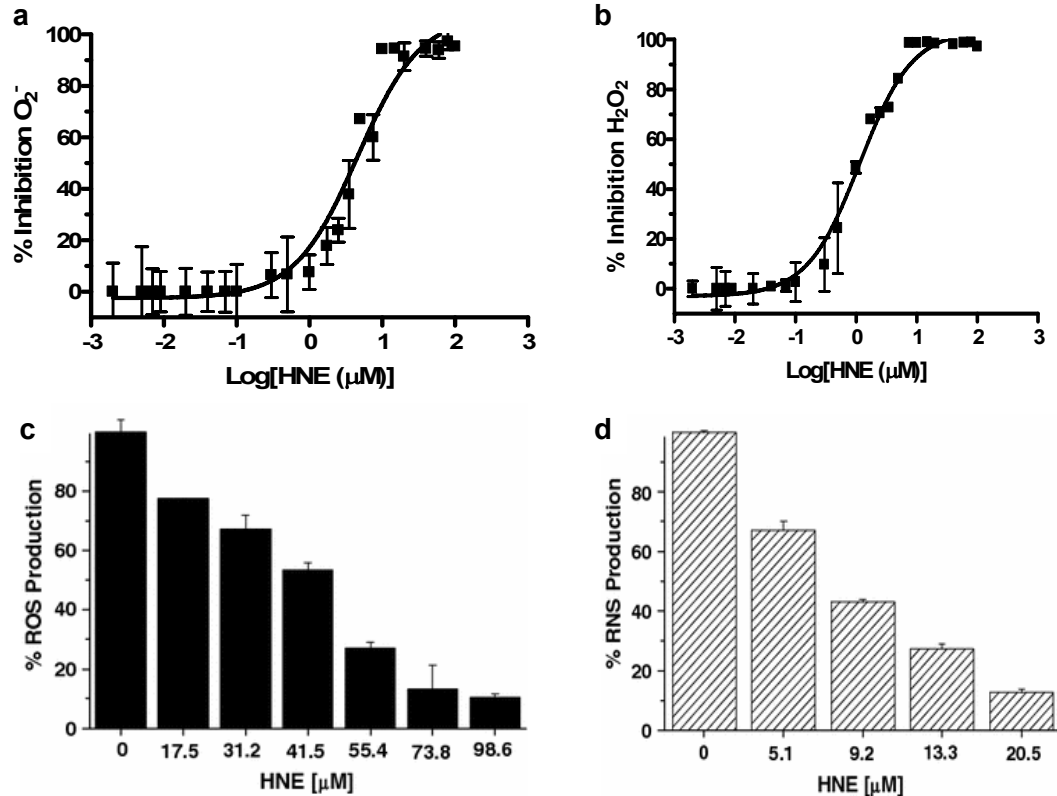


Figure 18 Concentration-dependent effect of HNE treatment on oxidative burst. (A) Inhibition of superoxide production with increasing concentrations of HNE in differentiated HL60 cells was measured using the cytochrome c superoxide assay. Dosing revealed an EC_{50} of 4.6 μM . (B) Inhibition of H_2O_2 production with increasing concentrations of HNE in differentiated HL60 cells was monitored by the Amplex Red H_2O_2 assay. Dosing revealed an EC_{50} of 1.1 μM . (C) Inhibition of ROS production with increasing concentrations of HNE in RAW 264.7 cells as assessed by DCF-DA. Dosing indicated an EC_{50} of 45.9 μM . (D) Inhibition of RNS production with increasing concentrations of HNE in RAW 264.7 cells as assessed by the Griess assay. Dosing indicated an EC_{50} of 9.2 μM .

Generated from the most abundant class of PUFAs, HNE contains three functional groups, is lipophilic and easily diffusible, and highly reactive with cellular components, all characteristics that make HNE an efficient means of disrupting the host immune system.¹²⁶ Previous reports have demonstrated that at concentrations over 10 μM , HNE is capable of inhibiting the activity of protein kinase C, a key signaling protein in NADPH oxidase activation.⁵⁹ HNE is highly reactive with proteins, disrupting function by forming adducts on cysteine, lysine and histidine residues.¹²⁶ In fact, there has been a suggestion of the possible formation of HNE adducts on protein kinase C.^{59,127} This is just one potential target that HNE may interact with once inside the macrophage that may lead to inhibition of oxidative burst.

The cytochrome c assay was used to measure the effects of 15-(S)-HETE, but collected data showed variable inhibition from 0-5 μM and were completely inhibited from 5-25 μM . A similar incongruous pattern was observed using the amplex red H_2O_2 assay. Cells exposed to 15-(S)-HETE showed an increase in H_2O_2 rather than the expected inhibition seen in assays with HNE. Since HETEs are known to cause degranulation in neutrophils,¹²⁸ the 15-(S)-HETE was hypothesized to have caused degranulation and disrupted the assay readings through the release of lysozymes. Similarly, incubation with 15-HETE resulted in a concentration-dependent inhibition of PMA-stimulated burst, with an EC_{50} value of 8.0 μM (Figure 19A). Human monocytes treated with 15-HETE have displayed a similar trend, with 100% inhibition of ROS production at 15 μM 15-HETE.^{36,78} LPS-activated iNOS was also inhibited up to 28.5% in the presence of 15-HETE (Figure 19B). While treatment of phagocytic cells with 15-HETE clearly results in the loss of ROS and RNS production, the mechanism of

inhibition is not immediately obvious other than by subsequent degradation of 15-HETE to HNE. The inhibition of oxidative burst with these highly reactive agents points toward the importance of HZ not as a toxic substance itself, but rather as a mediator of the oxidation of fatty acids to form highly reactive and toxic molecules such as HNE and 15-HETE. Additionally, the particulate nature of the detoxification biomineral ensures that it will be targeted by the innate immune system.

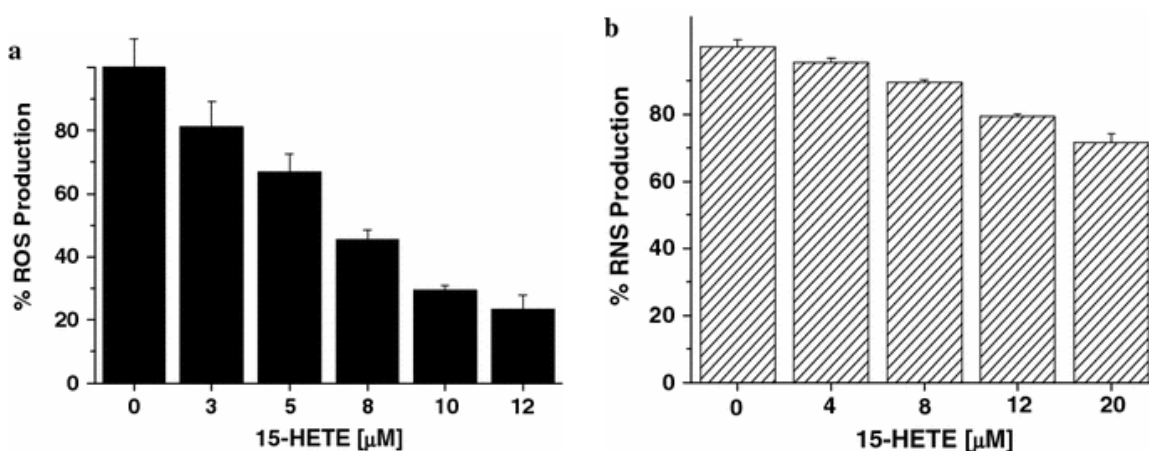


Figure 19 Concentration-dependent effect of 15-HETE treatment on oxidative burst. (A) Inhibition of ROS production with increasing concentrations of 15-HETE in RAW 264.7 cells as assessed by DCF-DA. (B) Inhibition of RNS production with increasing concentrations of 15-HETE as assessed by the Griess assay.

The aforementioned results suggest that the inhibitory effects of HZ are due to its ability to react with membrane lipids and form highly reactive, immunosuppressive molecules. To examine the effects of the constitutive components of the malaria pigment on macrophage response in an appropriate model system, BH was reacted with membrane lipids from erythrocyte ghosts. Following the overnight reaction, RAW macrophage cells were treated with the reaction supernatant. NADPH oxidase in PMA-activated RAW cells was inhibited in a concentration-dependent manner (Figure 20A), as

was the activation of iNOS in LPS-activated cells (Figure 20B). There was no detectable inhibition of ROS or RNS production upon treatment of BH or ghost supernatants alone,

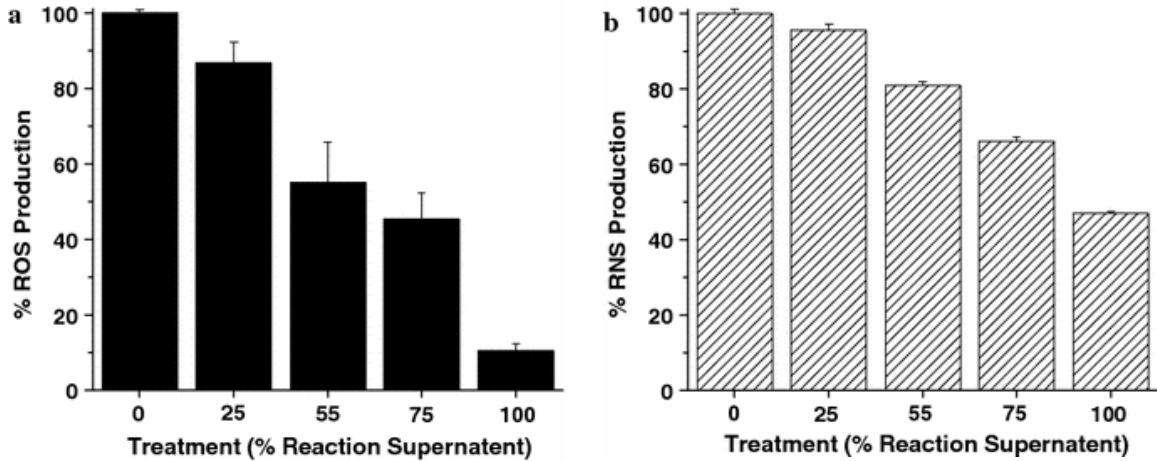


Figure 20 Inhibitory effect of the products of ghost and BH interactions on oxidative burst. (A) Inhibition of ROS production was obtained using luminol-enhanced chemiluminescence and **(B)** inhibition of RNS was obtained using the Griess assay.

indicating that it is the products from the reaction between the two that cause the inhibition (data not shown). These results strongly suggest that erythrocytic rupture releases the detoxification product HZ into a milieu of cellular debris, providing the substrate for the nonenzymatic, heme-catalyzed peroxidation that results in a toxic gradient of primary and secondary fatty acid oxidation products (data not shown). Although the precise mechanism and cellular targets remain unclear, it is indeed these products, not the aggregate of dimeric heme units, which effectively inhibit RAW NADPH oxidase and iNOS activity within macrophage cells.

Conclusions

The composition of native HZ released upon RBC rupture has been reported to be 65.1% proteins, 15.5% Fe(III)PPIX, 5.9% carbohydrates and less than 1% lipids and nucleic acids.^{122,129} Both HZ and BH are able to interact with membrane lipids to generate high levels of reactive secondary metabolites such as HNE and 15-HETE. Inside HZ-laden macrophages, levels of these agents reach between 20 and 40 μM .^{36,59} These molecules act as immunosuppressive agents that are capable of disrupting oxidative burst (both NADPH oxidase and iNOS-activated) and represent the key to understanding reactivity differences between structurally identical native HZ and BH. Clearly, native HZ inhibits the activation of oxidative burst and is stable inside macrophages for long periods of time.^{59,90} In contrast, BH is sensitive to the microbicidal agents of oxidative burst, and macrophages are capable of degrading this material. Significantly, native HZ which has been thoroughly washed to remove debris from RBC rupture (including lipids) reacts in a fashion identical to BH, where it does not inhibit oxidative burst.

Native HZ is a complex material with a similarly complex reactivity. By systematically examining each of the malaria pigment's components, we have been able to dissect their impact on the immune reactivity of a macrophage cell line. Further, via the reaction between synthetic BH and RBC ghosts, we were able to effectively reconstruct the observed immunomodulating reactivity of native HZ. In this fashion, we propose that HZ functions to construct a toxic minefield which disrupts the immune response to the parasitic infection. The presence of particulate HZ and RBC debris

invites the professional phagocytic cells to the site, trapping the cells into a veritable sea of reactive and toxic species which freely diffuse across the cell membrane and/or are brought inside as HZ is phagocytosed. Once there, the highly reactive molecules, generated from the HZ-mediated oxidation of membrane lipids, disrupt macrophage function.

The HZ-mediated immunomodulation presented here represents but one aspect of how this biomineral helps regulate the host/parasite interaction. Recent results also suggest a role for immunomodulation activity originating from the dimer heme moiety in Toll-like receptor 9 activation¹³⁰ and cytokine production perturbation.^{92,96} HZ has also been shown to suppress the adaptive immune system by modulating dendritic cell function and maturation, thus allowing further evasion of the immune system. T cells which are subsequently activated by these modulated dendritic cells are characterized by decreased proliferation and effector functions. This modulation of adaptive immune system activation may contribute to the reduced vaccine efficacy and increased secondary infection seen in malaria-endemic areas.¹³¹ Thus, the parasitic survival strategy involves native HZ modulation of the host immune system on multiple fronts, innate and adaptive, ensuring parasitic success throughout the centuries despite host adaptations. Continued efforts to elucidate the exact mechanisms behind these immunomodulations are critical for the development of new approaches to fighting this disease.

CHAPTER IV

IN SITU ISOLATION OF SCHISTOSOMAL HEMOZOIN

Endemic in 74 countries, 650 million people live at risk of Schistosomiasis infection.¹³² Of the 200 million people infected, 120 million are symptomatic and 20 million of those suffer from severe pathology.¹³² The disease is caused by the parasitic bloodfluke *Schistosoma spp.*, first identified by a German physician and parasitologist Theodore Bilharz in 1851. In his letters to his former professor, Bilharz described the worms as containing “numerous blood corpuscles throughout its whole length.”¹³³ These “blood corpuscles” have since been characterized as aggregates of dimeric ferriprotoporphyrin IX (Fe(III)PPIX), biominerals commonly called hemozoin (HZ).^{44,54,114}

HZ and its synthetic analog, β -hematin (BH), are chemically, crystallographically and spectroscopically identical.³⁵ The aggregate is composed of five-coordinate Fe(III)PPIX dimers stabilized by hydrogen bonding. Binding between the monomeric Fe(III)PPIX units occurs by way of reciprocal monodentate carboxylate interactions between each PPIX and its propionic side chains. Consequently, the resultant HZ is a stable and primarily insoluble crystal,³² resisting the onslaught of professional phagocytes and persisting in liver and spleen macrophages 6-9 months following parasite clearance.¹³⁴

During *Schistosoma spp.* infection, HZ forms as a detoxification byproduct of the schistosomes' catabolism of host hemoglobin and subsequent release of toxic free heme.

While the exact method of HZ formation *in vivo* remains elusive, recent transmission electron micrographs (TEMs) revealed HZ localized along nanosphere neutral lipid droplets of the worms' gut lumen.⁶⁴ HZ accumulates in the gut until the worm regurgitates the excess pigment into the host vasculature. It is in the vasculature that the HZ is recognized as a foreign particulate, attacked and engulfed by professional phagocytes.^{122,135} The number of HZ-laden phagocytes continues to grow as the worms feed, causing a concentration of dark brown pigment in the host tissue as observable in the liver and spleen.^{135,136}

Already burdened by the hepatomegaly caused from schistosomal egg deposition, the spleen and primarily the liver suffer from an inexorable fibrosis that can eventually cause hepatic portal vein occlusion, hypertension and gastrointestinal varices.¹³⁷ The most common and more subtle effects of the disease include anemia, abdominal pain and cognitive impairment.¹³⁸ These side effects have been linked to the initial immune response of reactive oxygen species (ROS) released by the concentrate of eosinophils attacking eggs trapped in the tissue.¹³⁹ The accumulation of released superoxide anions ($O_2^{\cdot-}$) and hydroxyl radicals ($\cdot OH$) in tissues can initiate lipid peroxidation of surrounding fatty acids, ultimately leading to a fibrogenesis cascade.¹³⁹⁻¹⁴¹ In fact, antioxidant studies with a *S. mansoni*-infected murine model revealed that mice receiving doses of the free radical scavenger melatonin showed restored levels of nitric oxide (NO), glutathione (GSH) and superoxide dismutase (SOD) compared to controls.¹³⁹ Consequently, the melatonin-treated mice showed reduced liver granuloma formation, fewer spleen megakaryocytes and near-normal kidney tubule structure.¹³⁹ It is this familiar gap

‘inert’ byproduct of hemophagous parasites,¹⁴⁶ HZ has surfaced, in this respect, as a proinflammatory mediator in infection.^{41,147}

HZs oxidation *in vitro* of the cellular fatty acids arachidonate and linoleate has been shown to form a variety of lipoxidation products including hydroxyeicosatetraenoic acids (HETEs),³⁹ hydroxyoctadecadienoic acids (HODEs) and the secondary oxidation product 4-hydroxy-2-nonenal (HNE).^{36,43,58} Additionally, these lipids have been identified in the extracted lipid coat of native HZ, and also from the lipid coat of BH incubated with red blood cell ghosts (RBCGs). These lipid products have been shown to be inflammatory and in many cases, inhibit cellular function. As more is understood of HZ’s reactivity *in vitro* and its ability to mediate lipid peroxidation,^{39,41,58} intrigue into its reactivity *in vivo* continues to grow. Using a *S. mansoni*-infected murine model, we present herein an 8-week time study in which we monitored both the accumulation of HZ and the swell of HNE *in situ*.

Experimental

Schistosomiasis-infected murine model. Female Swiss Webster mice were infected with 150 *S. mansoni* cercariae via percutaneous exposure of the tail. The schistosomiasis life cycle and infection was completed by the Schistosomiasis Resource Center of the Biomedical Research Institute, Rockville, MD under the direction Dr. Fred Lewis.

β -Hematin synthesis. BH was synthesized via dehydrohalogenation of hemin, as described by Bohle.⁶⁰ The reaction vessel was sealed, protected from light and stood

undisturbed for three months. The resulting mixture was filtered, and the precipitate was washed exhaustively with methanol, 0.1 M sodium bicarbonate (pH 9.1) and deionized water. The purified product was dried under vacuum at 150°C for 48 h and stored under desiccant.

Schistosome HZ isolation. Adult schistosomes were obtained by mesenteric perfusion of mice 42 days post-infection.⁶¹ Cultivated adult female worms were homogenized in phosphate buffered saline (PBS, pH 7.4) using a 15 mL glass homogenizer. Homogenate was centrifuged twice at 1000 x g for 60 s, and the tissue pellet was discarded. The supernatant was centrifuged 2 h at 5445 x g. The resulting dark-brown pellet was resuspended in 5 mL sterile PBS after vortexing and gentle sonication for 5 min. *SmHZ* recovery was quantified as described by Sullivan *et al.*⁶² with 20 mM NaOH, 2% SDS at 25°C for 1 h. Heme content was determined from absorbance at 400 nm ($\epsilon=1 \times 10^5 \text{ M}^{-1} \text{ cm}^{-1}$) using an Agilent 8453 UV-Visible Spectrophotometer.

Tissue HZ isolation. Hemozoin was isolated from collected liver and spleens by homogenizing the organ samples with an electric homogenizer for 45 seconds in 50 mL of DI water. This mixture was centrifuged at 1000 x g for 2 minutes. The tissue pellet was discarded, and the supernatant was centrifuged at 5445 x g for 2 hours. The resulting dark brown pellet was gingerly vortexed with 1 mL of PBS to remove the top layer of gray tissue. Afterwards, the lower layer of dark HZ was resuspended in 5 mL sterile PBS and 5 mL of ethyl acetate after vortexing and gentle sonication for 5 min. A series of 20 minute centrifugations at 5445 x g were then carried out in this 1:1 PBS, ethyl acetate wash solution in order to remove as much lipidous tissue as possible. The HZ was finally

quantified as described by Sullivan *et al.*⁶² with 20 mM NaOH, 2% SDS at 25°C for 1 h. Heme content was determined from absorbance at 400 nm ($\epsilon=1 \times 10^5 \text{ M}^{-1} \text{ cm}^{-1}$) using an Agilent 8453 UV-Visible Spectrophotometer.

HZ purification. Isolated schistosomal HZ was purified following the method of Chen *et al.*¹¹⁴ Briefly, HZ was suspended in 5 mg/mL proteinase K buffer containing 10 mM TrisHCl, pH 8, 0.5% SDS and 1 mM CaCl₂. The mixture was incubated at 37°C for 24 h under constant agitation. The sample was then washed thrice with 2% SDS, centrifuging at 16.1×10^3 for 5 min to precipitate the HZ. The HZ was resuspended in 6 M urea and incubated 3 h at 37°C under constant agitation. This suspension was washed thrice more with 2% SDS, centrifuging at 16.1×10^3 for 5 min to precipitate the HZ. The sample was then washed 8 times with DI water. The final HZ pellet was dried under argon and stored under desiccant at -20°C.

XRD characterization. Powder x-ray diffraction with Cu K α radiation was used to confirm HZ structure. Purified HZ was suspended densely in DI water and a droplet placed on the Si XRD wafer and dried at 100°C.

SEM characterization. Dry purified SmHZ was suspended in ethanol, sonicated for 10 min, applied to a polished aluminum specimen mount and dried at 25°C overnight. Each sample was sputter-coated with gold for 20 s and imaged using a Hitachi S4200 scanning electron microscope at 5.0 kV accelerating voltage.

Ion-Coupled Plasma Mass Spectrometry (ICP-MS). For ICP-MS analysis, all glassware was washed in a 1.9 M potassium hydroxide, ethanol base bath. Livers and spleens from each week were homogenized in a sterile environment (biosafety cabinet). A 10 mg sample of homogenate was added to a conical Wheaton vial along with 1 mL of

concentrated HNO₃, covered with parafilm and allowed to sit at room temperature for 3 h. When dissolved, 10 mL of DI water was added to the sample in a 15 mL Falcon polypropylene tube, therefore containing 5.9% HNO₃ (upper limit of tube resilience). These solutions were filtered through a Millipore 50 mL (0.22 μm) steriflip tube, capped and stored at -40°C until further dilution for analysis. Ultimately, 1 mL of this defrosted sample was diluted to 10 mL in DI water prior to analysis. The final concentration of the sample prior to analysis was 0.59%. The iron content of these samples were determined.

Tissue-section preparation. Tissues were perfused and placed into 15 times the volume of 10% formalin fixative to tissue overnight at room temperature. Tissues were sent to Vanderbilt University Immunohistochemistry Core to be sectioned into 5μm paraffin slices with two tissue slices per slide; one for a negative control and the other for staining sample. Hematoxylin & eosin (H&E) tissue stains were performed by the Vanderbilt University Immunohistochemistry Core, following standard protocols.¹⁴⁸

Anti-4-Hydroxy-2-nonenal tissue stains. A R&D Systems monoclonal anti-HNE primary antibody was used to label HNE present in liver and spleen tissue sections as previously described.¹⁴⁹ Briefly, a R&D Systems HRP-AEC system was used to stain the tissue sections, in which detection is obtained from the formed avidin-biotin complex with the anti-HNE. Horseradish peroxidase (HRP) enzymatic conversion of 3-amino-9-ethylcarbazole (AEC) yielded the red precipitate seen with bright field microscopy. Initially, samples were blocked with 3% H₂O₂ to cover the sample, followed by mouse serum blocking reagent, avidin blocking reagent (avidin, 0.1% NaN₃) and biotin blocking reagent (biotin, 0.1% NaN₃). Between washes, samples were rinsed with phosphate buffered saline (PBS), pH 7.4. Samples were incubated at 37°C with primary HNE

antibody (25 μ L of 25 μ g/mL stock) for 1 h. Samples were rinsed with PBS and incubated with a biotinylated secondary anti-mouse antibody for 1 h at 37°C. The samples were rinsed again with PBS and incubated at 37°C for 30 min. in a high sensitivity streptavidin-HRP (HSS-HRP) solution. Following rinses with PBS, the sample was incubated at 37°C for 1.5 h in 0.08% AEC, 0.1% H₂O₂ acetate buffer. The sample was rinsed with DI water and mounted with aqueous mounting medium. All samples were imaged with an Olympus BH2-RFCA light microscope with Olympus DP70 camera equipped with DP controller software.

Isoketal (IsoK) analysis of BH reaction with arachidonic acid. Lipid peroxidation was initiated by the addition of 0.48 mM β -hematin to 10 mM arachidonic acid (Nu-Chek Prep, Inc., Elysian, MN) in 5 mL of 100 mM phosphate buffer (pH 7.4) for 2 h while stirring. Pyridoxamine (PM) (100 μ M final concentration) (Sigma-Aldrich, St. Louis, MO) was added to scavenge isoketals (IsoK) and the reaction was stirred for an additional 2 h before extraction with diethyl ether (2 \times 2 mL). Combined organic layers were condensed, and the residue was reconstituted in 200 μ L of acetonitrile. IsoK-PM-lactam adducts were analyzed by LC-MS/MS using a Magic Bullet C18AQ micro column (3 μ m, 100 Å , Michrom BioResources, Auburn, CA) with the gradient programmed from 100% solvent A (5 mM ammonium acetate with 0.1% acetic acid) to 100% solvent B (acetonitrile/methanol 95:5) from 0.5 min to 3 min and then continuing at 100% B for an additional 1.5 min. The column was then equilibrated to 100% A for 2.5 min. The flow rate was set to 190 μ L/min and the injection volume was 5 μ L. Eluant was directly coupled to a ThermoFinnigan TSQ Quantum triple quadrupole mass spectrometer (San Jose, CA) equipped with a standard electrospray ionization source.

Nitrogen was used for both the sheath and auxiliary gas. The mass spectrometer was operated in the positive ion mode and the electrospray needle was maintained at 3700 V. The heated capillary was operated at 35 V and 210 °C and the tube lens voltage was set to 90 V. Source CID was 5 V and the collisional energy for all transitions was 30 eV. Product scan spectra of the IsoK-PM-lactam adduct ($[M+H]^+$ m/z 501) were acquired from 50 m/z to 520 m/z . Selective reaction monitoring was used to identify m/z 501 \rightarrow m/z 152 and m/z 501 \rightarrow m/z 332 transitions, calculated as -17 Da (deamidation by fragmentation of the β -amine) from the parent IsoK-PM-lactam mass.

Isoketal (IsoK) immunohistochemistry. Tissues were placed in paraffin blocks, sliced into 5 μ m sections and air dried onto slides. Slides were treated with xylene (5 min., 3x), 100% ethanol (2 min., 2x), 95% ethanol (2 min., 1x), 0.3% hydrogen peroxide in methanol (20 min., 1x) and PBS (2 min., 3x). Incubated slides 20 min. at room temperature in a humid chamber in Dako protein block (Dako Cat #X0909) and rinsed in PBS for 2min. 100 μ L of antibody (20 μ g/mL) D11 ScFv (provided by Dr. L.J Roberts, Vanderbilt University Medical Center, Nashville, TN) diluted in PBS was added to one of the tissue slices while PBS only was added to the second tissue slice and incubated overnight at 4°C in a humid chamber. Slides were rinsed with PBS (2 min., 3x) and added 100 μ L 1:500 dilution of anti-E/HRP (Pharmacia cat #27-9413-01) in Dako antibody diluent (Dako cat #S0809). Samples were incubated 1 h at 37°C and rinsed with PBS (2 min., 3x) and developed with DAB liquid chromogen solution (Sigma D6067) and liquid buffer solution (Sigma D6067) for 7 min. and rinsed with water to stop the reaction.

Isoprostane (IsoP) and isofuran (IsoF) analyses. Tissues were homogenized and F₂-isoprostane and isofuran were purified and analyzed as described in Morrow *et al.*¹⁵⁰ and Fessel *et al.*¹⁵¹ Samples of liver and spleen tissue (0.05-1 g) were homogenized in 20 mL of ice-cold Folch solution (chloroform/methanol, 2:1 v/v) containing 0.005% BHT. Following a 1 h incubation at room temperature under nitrogen, 4 mL of 0.9% sodium chloride was added and the solution vortexed, centrifuged for 10 minutes at 800 x g and the lower organic layer separated from the semisolid proteinaceous layer. The organic layer contains the extracted lipids and was transferred to a 100 mL conical bottom flask and evaporated to dryness under vacuum. The sample was redissolved in 4 mL of methanol, 0.005% BHT and 4 mL of 15% potassium hydroxide, incubated at 37°C for 30 min., which causes hydrolysis and release of F₂-IsoPs. The mixture was acidified to pH 3 with 1 M HCl and diluted to a final volume of 80 mL with pH 3 water in preparation for extraction of free F₂-IsoPs.

The F₂-IsoPs were quantified by GC-negative ion chemical ionization-MS with detection limits reaching 1-5 pg. To a sample, 200-1000 pg of a deuterated standard ([²H₄]8-iso-PGF_{2α}) was added (Cayman Chemical, Ann Arbor, MI). The mixture was vortexed and ran through a C₁₈ Sep-Pak column (Waters Associates, Milford, MA) preconditioned with 5 mL of methanol and 5 mL of pH 3 water. Samples and subsequent solvents were eluted through a Sep-Pak with 10 mL plastic syringe. Column washes were sequential rinses with 10 mL of pH 3 washes and 10 mL heptane, and the F₂-IsoPs were eluted with 10 mL ethyl acetate/heptane (50:50 v/v). The eluant was dried over anhydrous sodium sulfate and applied to a silica Sep-Pak (Waters Associates). The cartridge was washed with 5 mL of ethyl acetate followed by elution of F₂-IsoPs with 5

mL ethyl acetate/methanol (50:50 v/v) which were dried under nitrogen. The F₂-IsoPs were converted to pentafluorobenzyl (PFB) esters via reaction with a mixture of 40 μL of 10% PFB bromide (PFBB) in acetonitrile and 20 μL of 10% *N,N*-diisopropylethylamine in acetonitrile at room temperature for 30 min. This process was repeated and samples were subjected to TLC on chloroform/ethanol (93:7 v/v). The samples are visible upon a spray of 10% solution of phosphomolybdic acid in ethanol and heating.

The PGF_{2α} band was scraped and extracted with ethyl acetate, dried under nitrogen and converted to trimethylsilyl ether derivatives upon addition of 20 μL *N,O*-bis(trimethylsilyl)-trifluoroacetamide (BSTFA) and 10 μL dimethylformamide with incubation at 40°C for 20 min. This was dried under nitrogen and redissolved in 10 μL calcium hydride-dried undecane for GC-MS analysis. Separation is achieved on a 15 m DB1701 fused silica capillary column (J and W Scientific, Folsom, CA). Column temperature was from 190°C to 300°C at a rate of 20°C/minute. The carrier gas was methane at a flow rate of 1 mL/min., and the ion source temperature was 250°C. The electron energy was 70 eV and filament current was 0.25 mA. For F₂-IsoPs and IsoFs, the carboxylate anions at 569 *m/z* and 585 *m/z*, respectively, were monitored for the [M-181] loss of ·CH₂C₆F₅ fragments.

Results and Discussion

Schistosomal inflammation and hence, disease-induced oxidative stress has been the topic of extensive inquiry as it relates to host immunity and clinical treatment. As a result, much of the previous focus has centered on the role of granulomas in egg

deposition and the ensuing loss of tissue function. These studies have revealed a range of schistosomal-induced stresses, including tissue decreases in antioxidant activity,¹⁵²⁻¹⁵⁵ losses in micronutrient levels,^{139,153} changes in regulatory enzymes,^{139,155} reports of DNA genotoxicity^{152,156} and rises in lipid peroxide products.^{139,155,157} It is this lipid peroxidation that occurs in the membranes of the cell and subcellular organelles that has been proposed as the primary source of lost membrane and tissue function in chronic liver diseases like schistosomiasis.¹⁵⁴ Stimulated initially by the antigens released at the surface of the egg, eosinophil peroxidase induces the production of the $O_2^{\cdot-}$ and $\cdot OH$ radicals capable of initiating a reported 2-fold increase in lipid peroxidation.¹⁵⁵ These enzyme-induced ROS are diffuse throughout the granulomatous tissue, but recent studies have noted a fibrotic “barrier” trapping the ROS to the area of the collagen-rich granuloma and protecting the surrounding tissue from the intensity of this oxidative stress.^{155,158} Herein, an 8-week murine schistosomiasis study was undertaken in order to evaluate the progression of oxidative stress as it may relate to the accumulation of tissue-deposited HZ.

S. mansoni-infected mice in this study developed distended abdomens during disease progression as compared to controls. The livers and spleens were measured at each week’s collection (Figure 21 A-L). Compared to uninfected controls, livers and spleens were noted to darken and become thicker and more fibrotic to the touch. The 8 week p.i. liver was an unhealthy, densely-pigmented organ as compared to the uninfected, smooth pink liver. The measured length of the liver at 8 weeks p.i. was approximately 5 cm while the uninfected liver was 3 cm, indicating a 67% increase in size. Similarly, the size

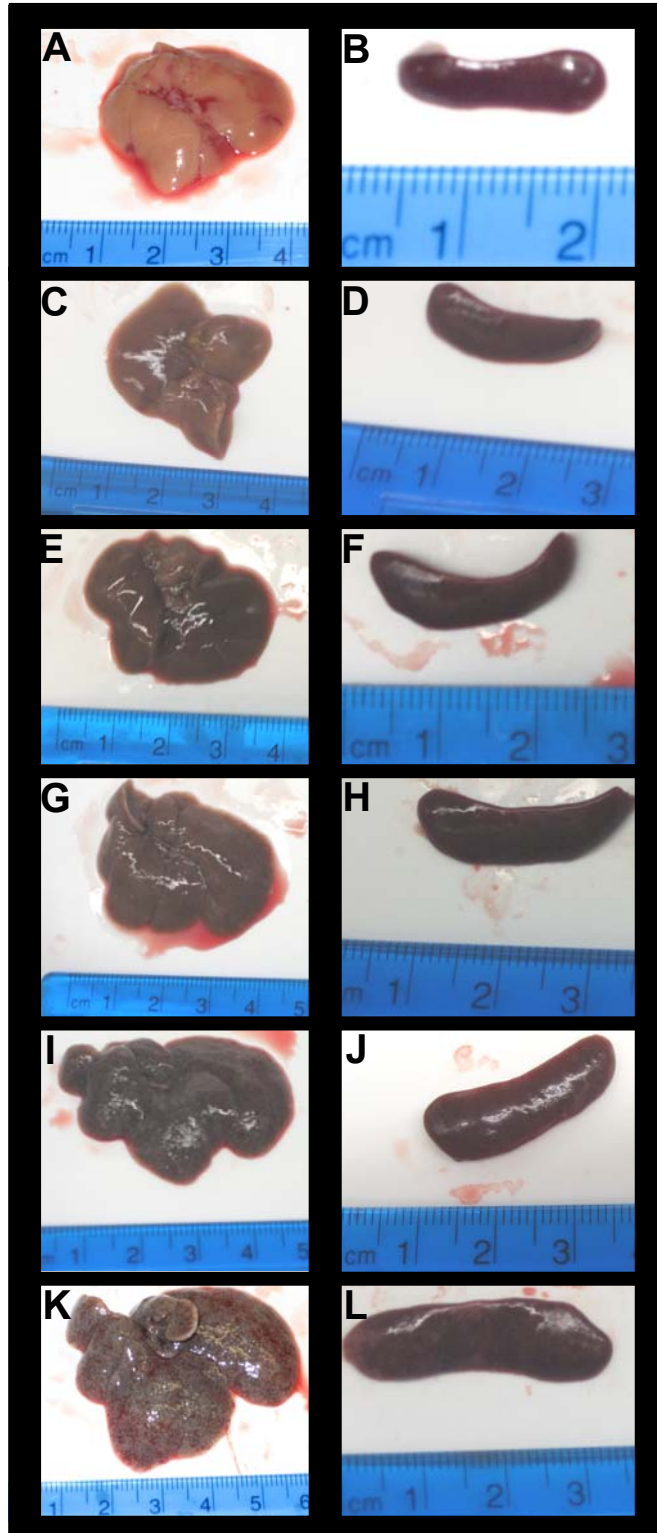


Figure 21 Growth of *S. mansoni*-infected livers and spleens through 8 weeks p.i. Collected livers were measured from weeks (C) 4, (E) 5, (G) 6, (I) 7 and (K) 8 p.i. as compared to (A) controls. Spleens were also measured from weeks (D) 4, (F) 5, (H) 6, (J) 7 and (L) 8 p.i. as compared to (B) controls. Compared to controls, livers were found to increase in size 67% and spleens 36%.

of the spleen was found to increase 36% in length from 2.5 cm to 3.4 cm during an 8 week infection.

Although the collected livers and spleens were shown to increase significantly in size, the weights of the mice were found to remain constant (Figure 22A). Their liver and spleen weights, however, increased 3-fold throughout the infection (Figure 22B&C). Much of this increase is believed to correlate to the increase in collagen deposited at the sites of the tissue-trapped eggs. Previous studies of female CF1 mice (~20 g) infected with 50 *S. mansoni* cercariae were shown to amass 20-fold more collagen in 9 weeks p.i. livers than uninfected mice.¹⁵⁹ Decreases in the surface area of functioning tissue are also thought to play a role in water-retention and swelling of the livers and spleens.

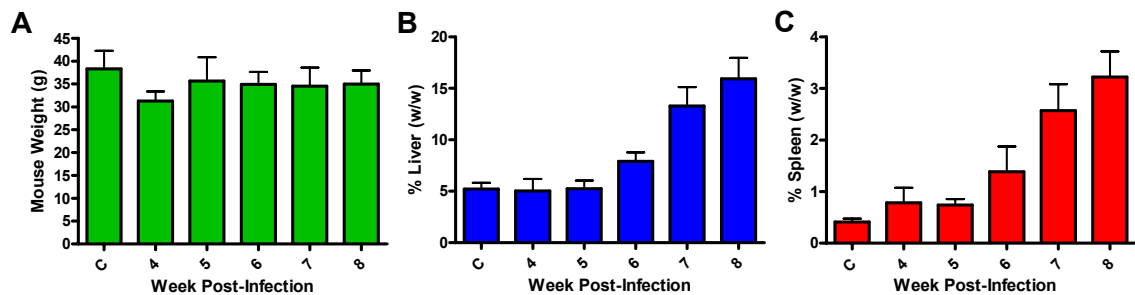


Figure 22 Variation in mice and organ weight. (A) Mouse weight was found to remain constant throughout the time study, averaging 30 g each. The (B) liver and (C) spleen weights, however, increased nearly 3-fold from week 4 to 8 p.i.

At weeks 4, 5, 6, 7 and 8 post-infection (p.i.) and uninfected controls, 5 μm thin tissue sections were taken of the collected livers and spleens. Hematoxylin and eosin (H&E) stains were applied to each week p.i., illustrating the degree of granuloma formation in the livers and megakaryocyte clustering in the spleens (Figure 23). In uninfected mice, healthy hepatocytes and splenocytes were observed. By week 6 p.i.,

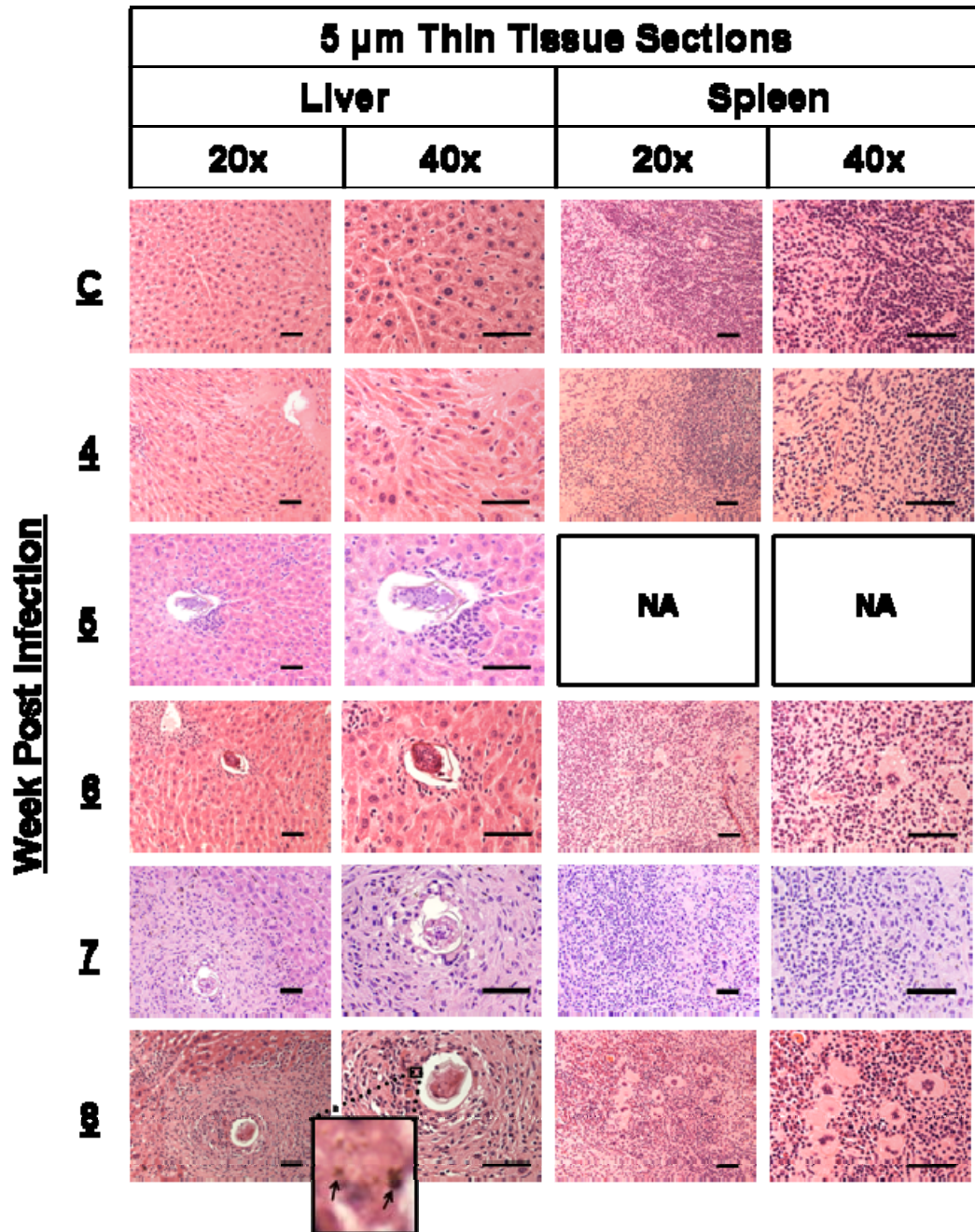


Figure 23 Hematoxylin and eosin (H&E) immunostaining of liver and spleen tissue sections. H&E stains were applied to the thin tissue sections of collected livers and spleens. The progressive formation of granulomas was observed in the liver sections, and the emergence of megakaryocytes was seen in the spleen sections. HZ (liver, week 8 insert arrows) was shown to accumulate in the surrounding phagocytes. Scale bars are 100 μ m.

however, a delayed type hypersensitivity to the liver-deposited schistosome eggs was observed, as denoted by the torrent of immune cells at the egg surface. This response

continued to escalate through week 8 p.i. in which a fibrous area containing leukocytes had formed around the eggs. Coarse to the touch and dark in color, the livers bore several granulomas and increasing amounts of HZ-laden cells. Scattered deposits of dark HZ pigment were discernible in the week 8 p.i. H&E stains (Figure 23 box insert and arrows). The deposits of HZ were absent from the H&E stains of the spleen, however, most likely due to the 2-fold less HZ in the spleen and the lower fibrotic density of cells found therein. Few megakaryocytes in the spleen were seen at week 6 p.i., but by week 8 p.i., large (4-cell) megakaryocyte clusters were observed, demonstrative of an acute disease state especially that found in helminth infections.

The suspected dark HZ pigment was isolated from the livers and spleens each week p.i. and characterized (Figure 24). The isolates' sharp Bragg peaks in the XRD spectra were indicative of a crystalline structure. The characteristic 2θ peaks and their respective 2:1 intensity between 7° and 21° , 24° were observed, confirming an identical structure to that of synthetic BH (Figure 24A). Additionally, SEM morphological comparisons between the HZ of the schistosome and that isolated from the livers and spleens yielded analogous images (Figure 24C&D). Although the HZ isolated from the host tissue required exhaustive processing to remove salt and other cellular debris prior to characterization, ultimately, the HZ from both the schistosome and the host organs were expected to appear near-identical since they were formed in the same environment of the schistosome gut. HZ isolated previously from the schistosome was shown to be amorphous in shape, ranging from 50 nm-3 μ m, and spherical in appearance.^{44,54} Indeed, this description is consistent with the images of the liver and spleen HZ isolates herein. This differs from other hemophagous parasites like the malarial *Plasmodium falciparum*

in which significant cellular processing within an infected RBC would be expected to and in fact, does yield packed, uniform brick-like aggregates within the cell.^{1,28} The sharpness of these “bricks” was seen in BH (Figure 24B), but the organization of these crystals appeared more varied than that seen in an infected RBC.

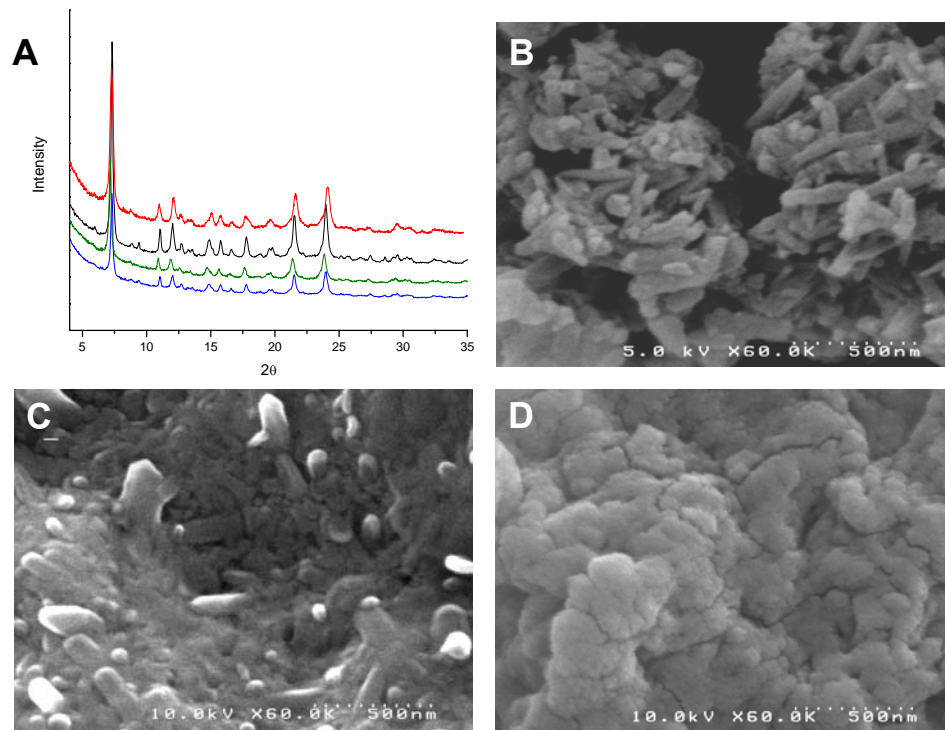


Figure 24 Physical characterization of isolated schistosomal HZ. (A) X-ray diffraction spectra of (red) BH, (black) HZ isolated from the schistosome, (green) HZ isolated from an *S. mansoni*-infected liver and (blue) HZ isolated from an *S. mansoni*-infected spleen. All spectra displayed the characteristic 2:1 intensity of the 2 θ peaks 7° to 21° and 24°. (B) SEM image of BH. (C) SEM image of HZ isolated from liver. (D) SEM image of HZ isolated from spleen.

The HZ isolated from each organ was quantified by measuring sample absorbance within the heme Soret band, specifically at 400 nm (Figure 25). The average schistosome age of sexual maturity is 5½ weeks p.i.,⁶¹ and the first trace of HZ was measured in the host liver to be $39.1 \pm 11.2 \mu\text{g}$ at 4 weeks p.i. (Figure 25A). By 6 weeks p.i., this quantity had doubled to $94.5 \pm 29.7 \mu\text{g}$ at the peak of schistosome maturity and doubled

again by 8 weeks p.i. to $203.8 \pm 51.1 \mu\text{g}$. Measurable quantities of HZ in the spleen were not reached until 5 weeks p.i., amassing to $25.6 \pm 4.3 \mu\text{g}$ (Figure 25B). This quantity held constant through schistosome maturity before tripling at 7 weeks p.i. to $84.9 \pm 15.6 \mu\text{g}$. Hence, the cumulative increase in host HZ at schistosome maturity from week 6 to 7 p.i. was estimated roughly at $125 \mu\text{g}$, attributing $1 \mu\text{g/day}$ to each adult worm pair. While the liver would be expected to trap and shoulder the majority of the burden from HZ regurgitated into the hepatic portal vein, both the liver and spleen were found to experience 3-fold increases in HZ content between weeks 5-8 p.i., further emphasizing the inability of leukocytes to break down and remove HZ.

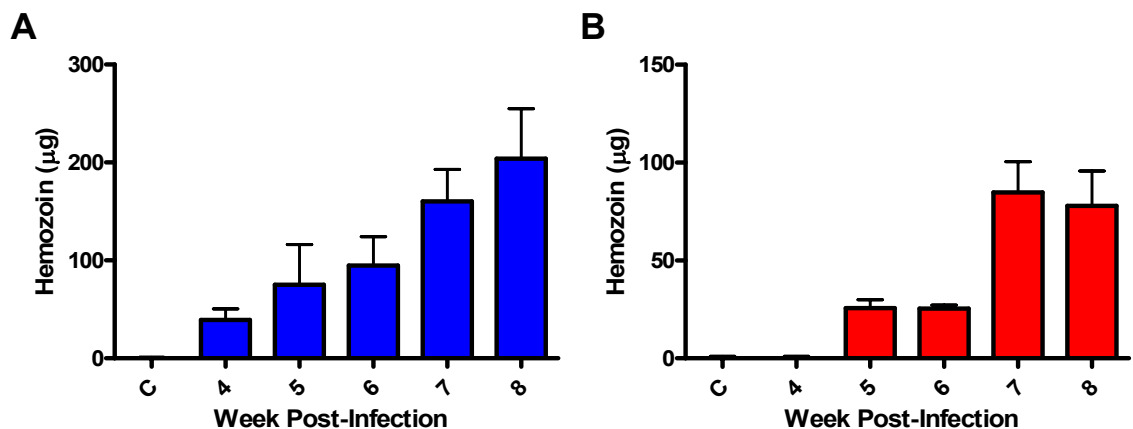


Figure 25 Quantification of HZ isolated from the livers and spleens of *S. mansoni*-infected mice. The HZ from collected (A) livers and (B) spleens was isolated and quantified by measuring its absorbance in the heme Soret band at 400 nm, ($\epsilon=1 \times 10^5 \text{ M}^{-1} \text{ cm}^{-1}$). A 3-fold increase in HZ deposited in the liver and spleen was observed between weeks 5 and 8 p.i.

Iron content of each organ was measured with ICP-MS (Figure 26). Changes over the course of infection in iron content were not distinguishable in the collected livers (Figure 26A). Although an observable change in HZ content was found, the iron composition of the biomineral is only 10% and therefore does not provide a significant

increase in total organ iron content. The dynamic changes in iron content of the spleen, however, are intriguing (Figure 26B). Like the liver samples, these changes in iron content would not be expected to originate from the increasing HZ content, but rather, a separate source. The total iron content in the spleen is nearly 8-fold greater at 6 weeks p.i. than the iron content of the liver, and this level then returned to a steady 4-fold greater than liver measurements for weeks 7 and 8 p.i. The significant change in spleen iron content is unclear but may be linked to a spike in enzymatic activity following schistosome maturity (6 weeks) and egg deposition. This also may be suggestive of RBC sequestration to the spleen during portal hypertension, hepatosplenomegaly, contributing to the common disease symptom of anemia.^{160,161} The development of anemia may also explain the drop in iron content at week 7 p.i.

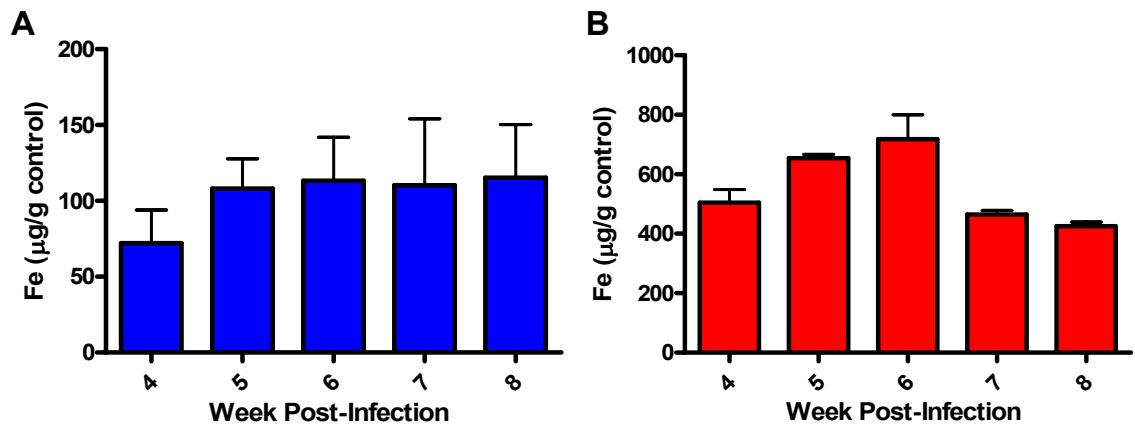
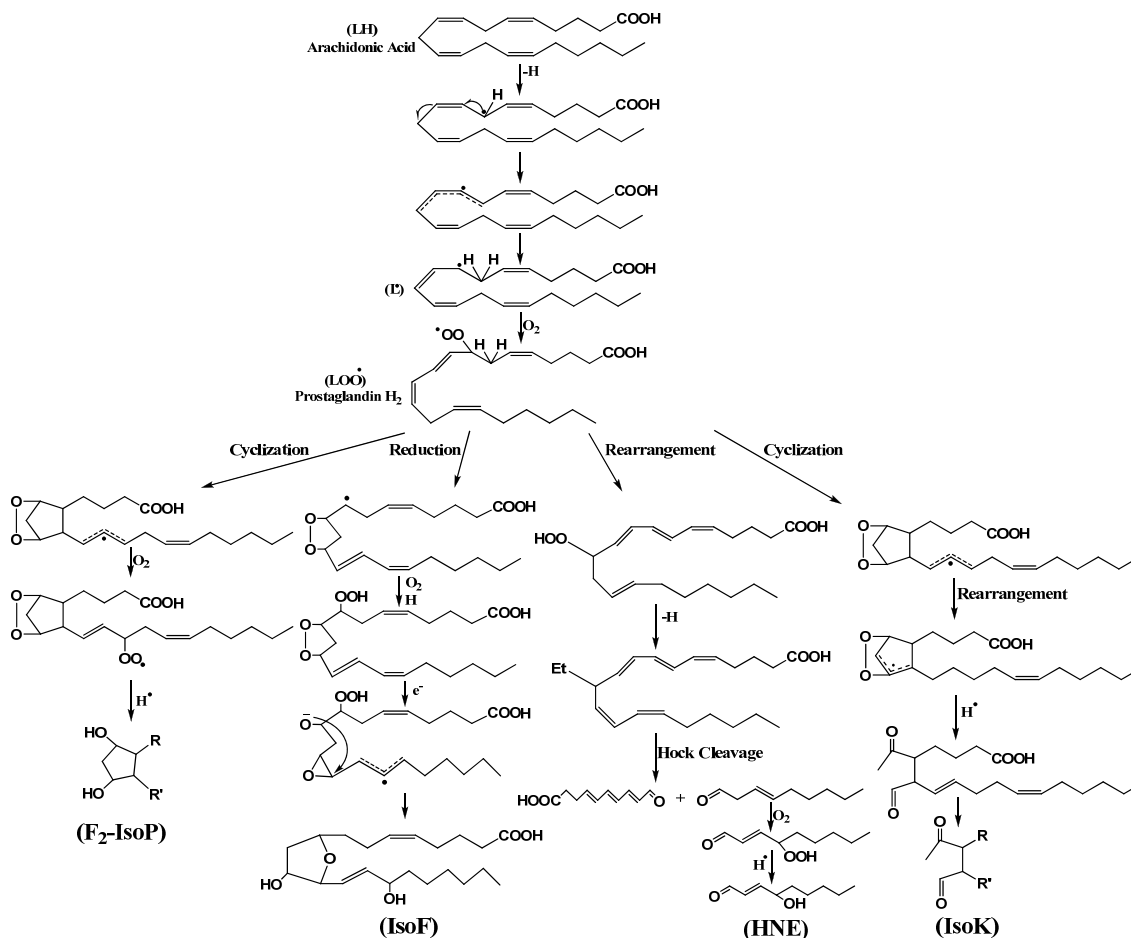


Figure 26 ICP-MS determined iron content of collected *S. mansoni*-infected livers and spleens. (A) Livers from the schistosomiasis time study were found to have an indistinguishable amount of iron per week p.i. (B) The iron content of the spleens collected was found to increase through week 6 p.i. and then falling at week 7 p.i.

Regardless of the iron content, the quantity of tissue-trapped HZ and deposited eggs was found to increase significantly. These observations were followed closely by a

desire to find a correlative detection method to evaluate the organ's induced oxidative stress. Since HZ and BH have been shown to mediate lipoxidation in a variety of fatty acids, it was proposed that a better understanding of HZ's presence in oxidative stress could be gained by monitoring the accumulation of a particular lipoxidation product.



Scheme 5 Potential lipid peroxidation products of arachidonic acid. Initiation of lipid peroxidation in arachidonic acid can lead to the non-enzymatic formation of several oxidized lipids in the prostaglandin 2-series pathway. Featured here are the prostaglandin H₂ (PG-H₂) products PG-F_{2α} isoprostanes (F₂-IsoP), PG-F_{2α} isofurans (F₂-IsoF), secondary oxidation product 4-hydroxy-2-nonenal (HNE) and the isomers of levuglandin E₂ γ-ketoaldehyde, isoketals (IsoK).

Several lipoxidation products are feasible upon HZ's reaction with arachidonic acid (Scheme 5), but of particular interest was the reactive secondary oxidation product HNE.

Therefore, thin tissue sections of the livers and spleens of uninfected through 8-week p.i. mice were subjected to immunostaining with a monoclonal anti-HNE antibody and the light visible AEC chromophore (Figure 27). The basal levels of HNE in the uninfected liver and spleen sections were very low, as depicted by the absence of red staining. By 6 weeks p.i., however, both the liver and spleen sections had a noticeable increase in HNE production. The amount of HNE continued to increase through week 8 p.i. in both organs. Several hotspots labeled for the presence of HNE were evident at the edges of deposited eggs and throughout the tissue as compared to controls. These hotspots are most likely attributed to the ROS and RNS attacks of surrounding leukocytes and the resultant lipoxidation of cellular fatty acids. There is probable reason to think that HZ would also contribute to this increase in HNE since its synthetic analog, BH, has been shown to mediate the oxidation of HNE *in vitro*,⁵⁸ and the native HZ from malaria infection has been reported to increase HNE levels 8-fold when incubated two hours with human monocytes.⁵⁹

As a tissue marker of oxidative stress, the immunostaining of HNE therefore suggests that the HNE identified outside of the imaged granulomas could be the oxidation product of an egg-independent response. While the diffusion of ROS outside of the granuloma is likely possible, there is significant literature precedent that steady-state monocyte levels of HNE are raised 50-fold in the presence of phagocytosed HZ.¹⁶² Likewise, other liver diseases such as hemochromatosis that have characteristically high iron tissue deposits generate high concentrations of HNE compared to controls.¹⁶³ In this study, the 3-fold increase of HZ measured between weeks 5 and 8 p.i. and the visible increase in antibody-labelled HNE of the liver and spleen thin sections suggest an

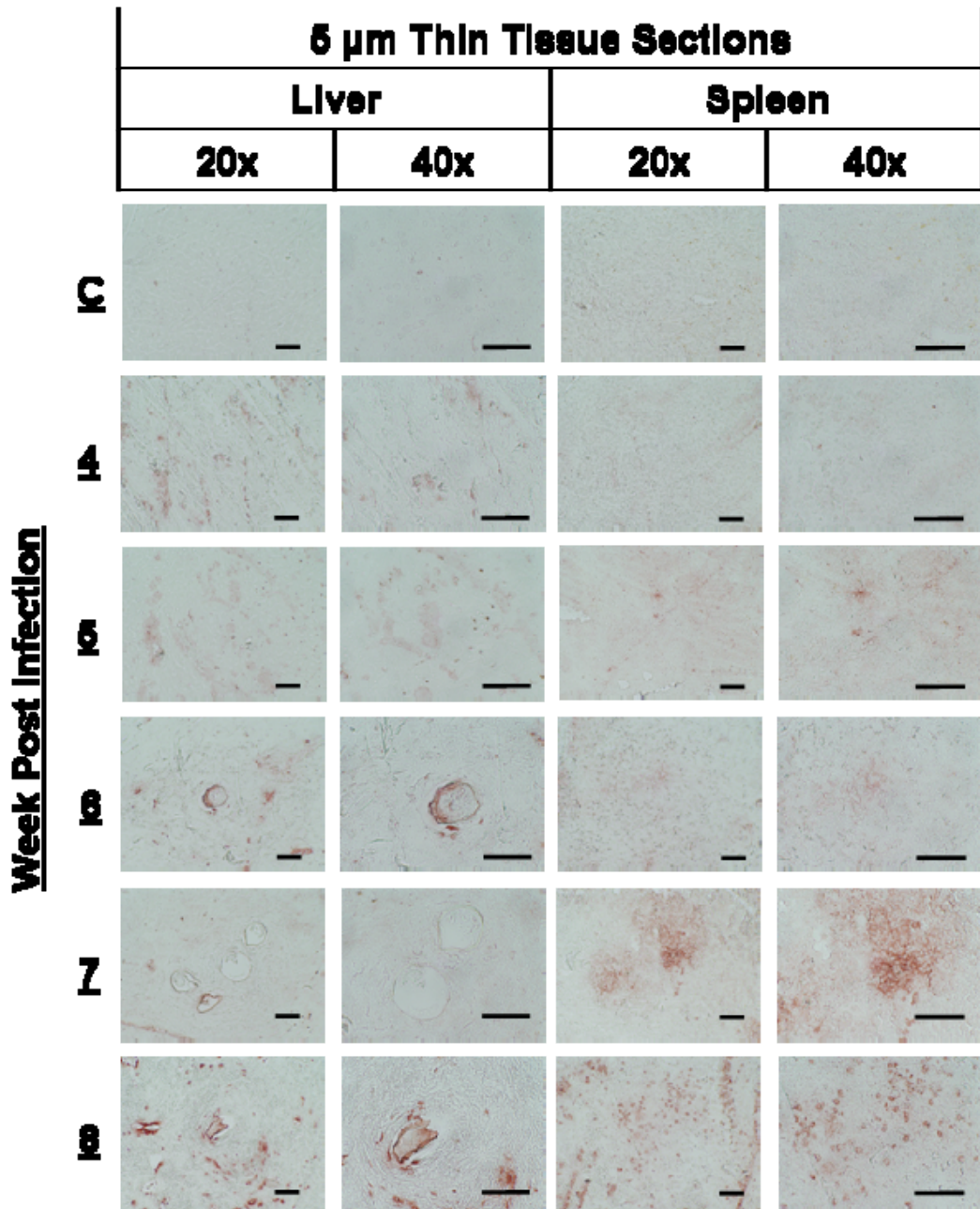


Figure 27 Anti-4-hydroxy-2-nonenal (Anti-HNE) antibody immunostaining of liver and spleen tissue sections from the schistosomiasis time study. The presence of HNE intensifies in both the livers and spleens throughout infection. Minimal staining was seen in the control tissue sections whereas hotspots and diffuse localization was found to increase over infection duration, hence identifying HNE as a marker of oxidative stress in progressive disease studies. Scale bars are 100 μ m.

increasing state of oxidative stress incapable of being reduced by normal antioxidant processes or cleared by the surrounding leukocytes.

While its exact contribution to oxidative stress remains elusive, BH has been shown to modulate temperature in rats¹⁶⁴ and upregulate chemokine and cytokine production in BALB/c mice upon inoculation.¹⁴⁷ Additionally, the intravenous injection of mice with BH also led to a dose-dependent upregulation in mRNA of liver expression of chemokines and cytokines.¹⁴⁷ Ultimately, these induced conditions modulate and in some cases, amplify the host's immune response. This potential role as an immunomodulatory agent is a more recent attribute of the biomineral.

As such, purified schistosomal HZ, washed of any lipid, protein or cellular debris, when incubated with arachidonic acid, should produce HNE. Support for this is seen from its identical, synthetic analog BH's ability to mediate the formation of HNE *in vitro*⁵⁸ as well as its formation of highly reactive γ -ketoaldehyde isomers or isoketals (IsoKs)¹⁶⁵ (Figure 28).

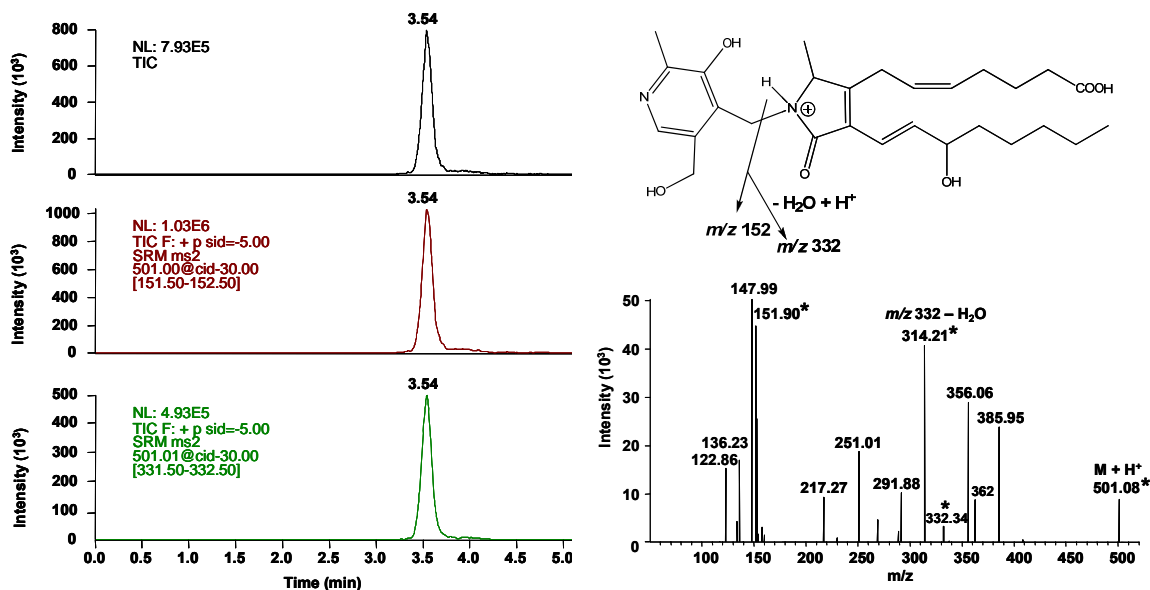


Figure 28 LC-MS/MS identification of IsoKs in the reaction of BH with arachidonic acid. Product scan spectra of the IsoK-pyridoxamine-lactam adduct at $[M+H^+]$ 501 m/z was confirmed by selective reaction monitoring of the ionization transitions at 152 m/z and 332 m/z . Compliments of Dr. Alexandra C. Schrimpe-Rutledge.

IsoKs are toxic to a variety of cultured cells, including Neura2A cells, RAW macrophage cells and lung fibroblasts, at nanomolar to low micromolar ranges.¹⁶⁶ Once formed in the cell, IsoKs are thought to resist clearance as evidenced by a 50% reduction in protein degradation upon reaction of 1 IsoK adduct per molecule of target protein.¹⁶⁷ This is of particular interest in disease states where oxidative stress is known to play a large role in inflammation and aggregates of damaged proteins are reported, as in Alzheimer's disease. In fact, plasma levels of IsoKs in atherosclerosis and end-stage renal disease were found to be approximately 2-fold higher than those of controls.¹⁶⁸

IsoK levels in this study were evaluated by staining the liver and spleen tissue sections (Figure 29). A significant change in labeled pigment could not be distinguished at lower magnifications, suggesting lower IsoK level changes in the tissue than that seen for the HNE stains. At 40X magnification, an increase in staining was observed between control and lower week p.i. as compared to the image at 8 weeks p.i. This visible increase at the interior of the granuloma and along the edges of the schistome egg may be attributed to first, the higher density of immune cells present and secondly, to the greater cellular toxicity of IsoKs as compared to HNE. Since the reactivity of IsoKs has been reported as an order of magnitude greater than that of HNE,¹⁶⁹ a smaller change would be expected than observed in the HNE stains and therefore only visually seen at higher magnifications. In fact, IsoK-induced cell death was observed in exogenously treated neuroglial cells at 100-fold less concentrations than those needed to gain the same effect with HNE treatment.¹⁶⁹ Minimal change was observed in the spleen tissue sections as might be expected in an organ indirectly affected by the granuloma and HZ deposition responses.

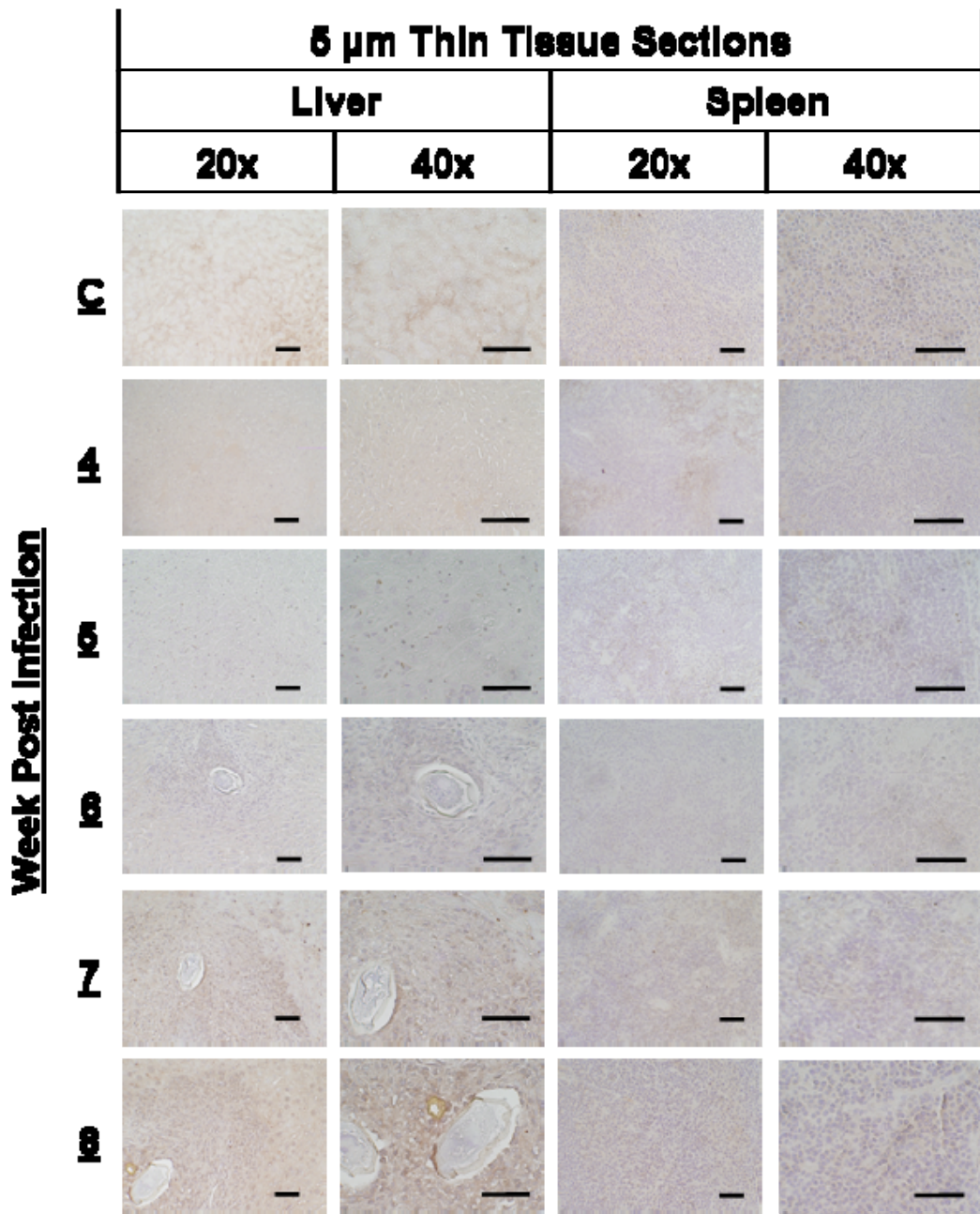


Figure 29 IsoK immunostaining of liver and spleen tissue sections collected during schistosomiasis infection. Thin tissue sections of liver and spleens were stained for the presence of IsoKs. Significant changes were not seen at lower magnifications due to lower concentrations of the reactive and low-level cytotoxic IsoKs. At 40X magnification, an increase in staining is observed in the liver from week 6 to 8 p.i. Scale bars are 100 μ m.

Also measured in this study were the prostaglandin- $F_{2\alpha}$ isoprostanes (IsoPs) and isofurans (IsoFs). These lipoxidation products of arachidonic acid and hence, markers of

oxidative stress *in vivo*, are formed either by preference for intramolecular attack or molecular oxygen, respectively. Therefore, IsoPs are found with greater prominence in environments of low oxygen tension and IsoFs at higher oxygen tension. This trend was observed in the liver homogenates of this study (Figure 30A&C). When the IsoP levels of the liver spike at schistosome maturity (5 weeks p.i.) and then decline when oxidative

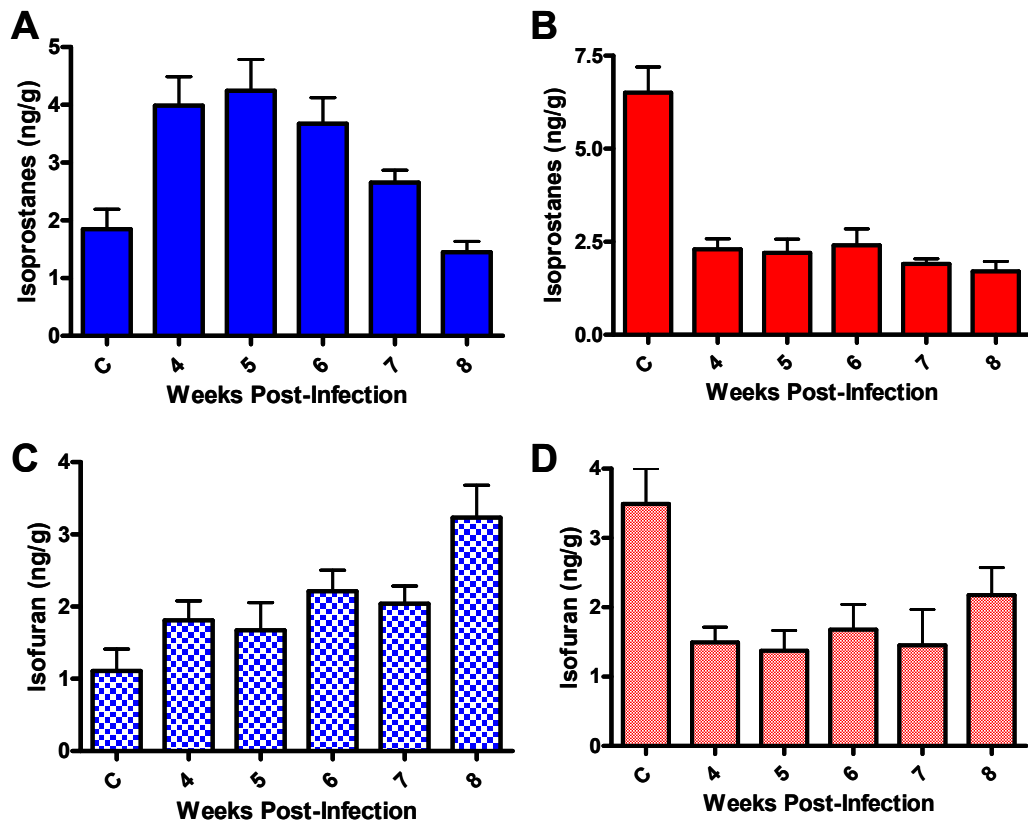


Figure 30 Measurement of IsoP and IsoF levels in liver and spleen samples throughout schistosomiasis infection. PG-F_{2α} isoprostane and isofuran were measured in *S. mansoni*-infected mice. As expected, (A) the liver IsoPs peaked at schistosome maturity (week 5 p.i.), and upon oxidative oxidative stress, dropped, leading to (C) an increase in IsoF formation. The spleens' (B) IsoP and (D) IsoF levels drop upon infection and do not recover throughout the time study.

stress escalates (Figure 30A), the IsoF levels gradually increase until they peak at 8 weeks p.i. (Figure 30C). This is not the trend observed in the collected spleens, however

(Figure 30B&D). The levels of IsoPs and IsoFs present in infected spleens are significantly reduced at week 4 p.i. and remain lower than controls throughout the study. The reason for this drift in the spleen is unclear. Earlier schistosomiasis studies found that treatment of splenic lymphoid cell populations with PG-F_{2α} augmented lymphocyte yields, especially those of NK cells and further upregulated the immune response seen in splenomegaly.¹⁷⁰ By whatever mechanism, the observed decrease in IsoPs and IsoFs in the collected spleens may be a host defense method of suppressing a similar immune response so evident in the upstream livers. Regardless, these metabolites have been shown to play an immunomodulatory role in the development of common symptoms like fever and headache in the hemophagous parasitic infection African trypanosomiasis, or sleeping sickness.¹⁷¹ In fact, the effects of these reactive molecules have been implicated in the oxidative stress found in a wide range of diseases, including atherosclerosis, cancer, Alzheimer's and generally, the aging process.¹⁷²

Conclusions

This study provides the first XRD crystal structure confirmation of schistosomal HZ isolated from *S. mansoni*-infected livers and spleens as the structural identical of the synthetic BH and malarial HZ. The biomineral's reactivity as evident by reaction with fatty acids *in vitro*^{39,58,59} and stimulant to immune response *in vivo*,¹⁴⁷ was explored further with the monitoring of known markers of oxidative stress *in situ*. The direct effect of HZ on host oxidative stress is not always certain, though. Further evaluation of these markers during schistosomiasis infection could reveal more clearly HZ's

immunomodulatory role in initiating lipid peroxidation and contributing to observed tissue inflammation. Recent inhibition of HZ formation with the heme-aggregation inhibitor chloroquine led to a decline in observed morbidity and schistosome viability.¹⁷³ By applying chloroquine treatment to the time study conducted herein, the reduction of HZ could be used to evaluate its subsequent effects on metabolite production. Various methods were developed herein to measure oxidative stress in this infection. Other antioxidant treatments could be employed as well in order to assess the severity of HZ's effect on disease symptoms and tissue function. Regardless, these preliminary studies provide an interesting look at schistosomal disease progression as it relates to oxidative stress and HZ accumulation.

CHAPTER V

LIPOPHILIC MEDIATED ASSAY FOR β -HEMATIN INHIBITORS¹⁷⁴

During malarial infection, the parasite catabolizes host hemoglobin to acquire amino acids therefore becoming exposed to the oxidative stress caused by liberated free heme.⁶ In order to avoid heme toxicity, the parasite sequesters heme into aggregates of dimeric ferriprotoporphyrin IX (Fe(III)PPIX) called hemozoin (HZ). Throughout history, HZ has been reported in association with malaria⁸ but was not structurally elucidated until the late 20th century.¹⁷⁵ These dimeric units aggregate via an extended network of hydrogen bonds between the propionate groups of the porphyrins. Native HZ and its synthetic analogue, β -hematin (BH), are crystallographically identical. The two structures are dimeric five-coordinate Fe(III)PPIXs with reciprocal monodentate carboxylate interactions.¹⁷⁵ While the structural makeup of HZ has been examined extensively,^{33,176-178} the crucial step of hemozoin formation in the parasite digestive food vacuole (DV) remains a mystery.

Over the years, several hypotheses have been proposed for the mechanism of HZ formation, including enzyme catalysis¹⁴⁶ or protein mediated formation,¹⁷⁹ lipid mediated formation^{26,180,181} and spontaneous formation¹⁸² or autocatalysis.¹⁸³ Recently, the weight of evidence has swung strongly towards a lipid mediated process. Transmission electron microscopy of the trophozoite stage of *Plasmodium falciparum* infected red blood cells revealed nanosphere lipid droplets containing HZ crystals.²⁹ These droplets consist of a blend of fatty acyl glycerides (specifically monostearic, monopalmitic, dipalmitic, dioleic

and dilinoleic glycerols). When extracted, they promoted the formation of BH both individually and as a blend.²⁹ BH crystallization may be favored in a hydrophobic environment in which hydrogen bonds between the hydrophilic Fe(III)PPIX's propionate linkages are preferred.^{28,184} This beneficial solubility in a lipophilic setting was also shown to hold true when the common laboratory surfactants SDS, Tween 80 and Tween 20 were used to mediate BH crystallization.^{26,185}

Conversion of these templates and subsequent reactions into a biologically relevant, yet robust, primary screen for compounds that inhibit the HZ pathway presents a

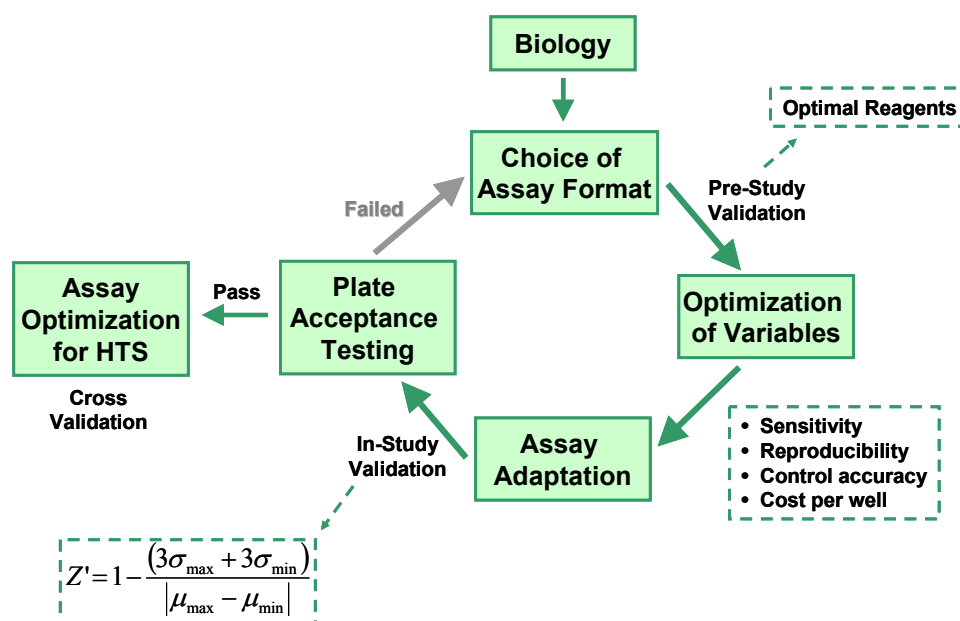


Figure 31 Assay development and validation pathway. Successful assays are fashioned after a biological system and designed to mimic the environment of the drug target. A series of optimization steps are used to obtain an assay that is sensitive, reproducible, robust and cost efficient. Optimized and validated assays are cross validated in a separate lab and then applied in high throughput screening programs. Adapted from the NIH Chemical Genomics Center.

challenge. Like many of its predecessors, the lipid-based assay must meet suitable performance criteria with regard to time, expense, resources and validation, which cumulatively dictate an assay's success and future applicability (Figure 31).^{179,182,186-189}

For instance, the radioactive hematin polymerization assay developed by Kurosawa *et al.* requires trophozoite lysates, overnight incubation and is subject to the expense and restrictions imposed on any assay containing a radio-labeled substrate.¹⁸⁷ While the assay was used to screen over 100,000 compounds for BH inhibition,¹⁸⁷ its practical use in other labs is limited to those with the training and resources to work with radioactive materials and *Plasmodium* cultures. Equally problematic, are assays incapable of quantifying the degree of BH crystallization¹⁸² or assays that require starting materials not commercially available.^{179,188}

By using the neutral lipid blend ratio found in trophozoite HZ extracts to mediate BH formation,²⁹ most, if not all, labs should be capable of mimicking the acidic and lipid-rich environment of the parasite's DV *in vitro*. The potential for further simplification of lipid-based assays was shown by Huy *et al.* with the use of the detergent Tween 20, curtailing not only the cost of the assay's lipophilic template but also the incubation time of the assay to 4 hr.¹⁸⁵ Both of these assays produced comparable amounts of BH under similar acidic and hydrophobic conditions. However, when used to generate concentration response curves of known BH inhibitor chloroquine, the drug IC₅₀ values from the Tween 20 mediated assay were approximately 10-fold higher than those obtained with the neutral lipid blend.^{29,185} This significant difference suggests that Tween 20 is not the most accurate mimic of the native neutral lipid blend. Herein, a series of lipophilic templates were surveyed for use in BH crystallization assays. The robustness of the assays was then tested in the preliminary screening of a small library of natural product extracts (NPEs).

Experimental

Dehydrohalogenation BH Synthesis. BH was prepared following the Bohle dehydrohalogenation method.¹⁹⁰ The reaction was protected from light and allowed to stand for 3 months. The final product was filtered and washed exhaustively with methanol, 0.1 M sodium bicarbonate (pH 9.1) and deionized water. Once purified, the BH was dried 48 hr at 150°C under vacuum and stored under desiccant.

Neutral Lipid Initiated BH Crystallization Assay. Lipid mediated BH formation was adapted from previous description.²⁹ A 25 mM hematin stock solution was prepared by dissolving 16.3 mg of hemin in 1.0 mL DMSO and filtering through a 0.22 µm PVDF membrane syringe driven filter unit. From this 25 mM solution, 177.8 µL was added to 20 mL of a 0.2 M ammonium acetate solution, pH 4.9 for a final 222.2 µM hematin stock. Lipids (1-Stearoyl-rac-glycerol; 1,2-Dipalmitoyl-rac-glycerol; 1,2-Dioleoyl-rac-glycerol; 1,3-Dilinoleoyl-rac-glycerol; or 3-Palmitoyl-sn-glycerol) were dissolved at 200 µM each in ethanol prior to addition to the assay. Final concentrations of 100 µM hematin, 0.1 M acetate buffer, 50 µM lipid solution, and 0-3.5 mM antimalarial (chloroquine or amodiaquine) were incubated in clear, 96-well round bottom plates at 37°C in a water bath and shaken at 55 rpm for 20 hr.

Detergent Initiated BH Crystallization Assay. Detergent mediated BH formation was adapted from previous description.¹⁸⁵ A 25 mM hematin stock solution was prepared by dissolving 16.3 mg of hemin in 1.0 mL DMSO and filtering through a 0.22 µm PVDF membrane syringe driven filter unit. From this 25 mM solution, 177.8 µL was added to 20 mL of the 2.0 M sodium acetate solution, pH 4.9 for a final 222.2 µM hematin stock.

Final concentrations of 100 μM hematin, 1.0 M acetate buffer, detergent (9.77 μM Tween 20, 30.55 μM NP-40, > 58.62 μM Triton X-100, 1.47 mM CHAPS, 0.29 mM SDS, or 14.88 μM Tween 80), and 0-3.5 mM antimalarial were incubated in clear, 96-well round bottom at 37°C in a water bath and shaken at 55 rpm for 4 hr.

Assay Analysis. Assays were removed from incubation and centrifuged at 1100 x g for 1 hr at 25°C in a Beckman Coulter AllegraX 22R, S2096 rotor. The supernatant was discarded and 200 μL of 0.15 M sodium bicarbonate, 2 % (w/v) SDS was added to each well. Centrifugation was repeated, and the supernatant, containing unreacted heme substrate, was removed. A final addition of 200 μL 0.36 M sodium hydroxide, 2% (w/v) SDS was used to dissolve the BH produced. The absorbance of the plates' contents was measured at 400 nm on a BioTek SynergyHT plate reader. A molar extinction coefficient of $1 \times 10^5 \text{ M}^{-1} \text{ cm}^{-1}$ was used to calculate the BH formed. Sigmoidal concentration response curves were generated using GraphPad Prism v5.0 (March 7, 2007) software.

Fermentation. Production cultures of the actinomycete strain *Nonomuraea kuesteri* were initiated by transfer of 3 mL of seed culture into a 250 mL Erlenmeyer flask containing 30 mL "ET" medium containing 60 g/L molasses, 20 g/L Difco soluble starch, 20 g/L fish meal, 0.1 g/L $\text{CuSO}_4 \cdot 5\text{H}_2\text{O}$, 0.5 mg/L sodium iodide and 2 g/L calcium carbonate dissolved in distilled water, adjusted to a pH 7.2 before autoclaving. Fermentation of the production cultures was allowed to proceed at 30°C for 7 days in a shaker incubator.

Natural Product Extraction. An equal volume of ethyl acetate was added to the production culture, an emulsion was created by agitation and the solution was shaken for 1 hr at 200 rpm. The extraction solution was transferred to a 50 mL Falcon tube and

centrifuged at 3000 x g for 30 minutes in a Sorvall Legend RT, TTH-750 rotor. The ethyl acetate layer was collected, dried over MgSO₄ and evaporated. Alternatively, an equal volume of methanol was added to the production culture and the solution was shaken for 1 hr at 200 rpm. The extraction solution was transferred to a 50 mL Falcon tube and centrifuged at 3019 x g for 30 minutes as before. The methanol/water mixture was collected and evaporated. The resulting residue was dissolved in 1mL of methanol, 0.2 µm filtered and subjected to LC-MS/MS analysis. *Cinchona officinalis* bark powder (0.5 g) was suspended in 10 mL 75% ethanol and shaken in a rotary shaker (200 rpm) at 30°C for 24 hrs. The extract was separated from bark by microcentrifugation at 14,000 rpm and the supernatant evaporated to dryness *in vacuo*.

LC-MS/MS of Ethyl Acetate Extracts. Mass spectrometry was performed using ThermoFinnigan LTQ linear ion trap mass spectrometer (Thermo Fisher Scientific, Waltham, MA) concurrently in negative and positive ion modes. Nitrogen was used both for the auxiliary and sheath gas. The auxiliary and sheath gases were set to 20 psi and 36 psi, respectively. For positive ion mode, capillary temperature 300°C; source voltage 5.0 kV; source current 100 µA; capillary voltage 21.0 V; tube lens 45.0 V; skimmer offset 0.00 V; activation time 50 ms with an isolation width 1 m/z. For negative ion mode, capillary temperature 300°C; source voltage 4.5 kV; source current 100 µA; capillary voltage -49.0 V; tube lens -148.30 V; skimmer offset 0.00 V; activation time 50 ms with an isolation width 1 m/z. Data acquisition and quantitative spectral analysis was conducted using the Thermo-Finnigan Xcaliber software, version 2.0 Sur 1. Samples were introduced by a Waters Acquity UPLC system (Waters, Milford, MA) with an injection volume of 10 µL. Secondary metabolites were separated on a Phenomenex Luna

5 μm C18 column (4.60 x 250mm, Phenomenex, Torrance, CA) with a linear water-acetonitrile gradient (ranging from 95:5 to 5:95 water:acetonitrile) containing 10 mM ammonium acetate over 48 minutes with a flow rate of 1 mL/min split with 900 $\mu\text{L}/\text{min}$ collected as fractions and 100 $\mu\text{L}/\text{min}$ subjected to mass spectral analysis. Fractions were collected every minute in 96-well deep well plates using a Gilson FC204 fraction collector (Gilson, Middleton, WI). Each 96-well deep well plate was separated into 100 μL aliquots into 96-well plates, evaporated and subjected to assay conditions.

Results and Discussion

A series of lipophilic templates were evaluated for use in BH crystallization assays. The neutral lipid blend (a ratio of 4:2:1:1:1 monostearoyl-, monopalmitoyl-, dipalmitoyl-, dioleoyl-, and dilinoleoyl glycerols, respectively) used by Pisciotta *et al.*, and the detergents studied by Shoemaker and Kamei represent biological and abiological controls.^{26,29,185} A variety of detergents were selected, differing in chemical structure and ionic character. Initial detergent assay concentrations were estimated using a ratio of the detergent's critical micelle concentration and the concentration of Tween 20 reported by Huy and coworkers.¹⁸⁵ The nonionic and non-denaturing detergents Triton X-100, NP-40, Tween 20 and Tween 80; the zwitterionic detergent, CHAPS; and an anionic, denaturing detergent, SDS, were examined for their ability to nucleate BH formation. The reaction products were evaluated by differential solubility, characteristic infrared spectroscopy stretches at 1664 cm^{-1} (C=O) and 1211 cm^{-1} (C-O) and powder x-ray diffraction (XRD). Comparison of the Bohle dehydrohalogenation BH product¹⁹⁰ and the

NP-40 mediated BH product by XRD revealed a strong match to the representative 7°, 21° and 24° 2θ peaks (Figure 32). The lipophilic mediators that were found to promote BH formation were evaluated in concentration response experiments with the antimalarials amodiaquine and chloroquine.

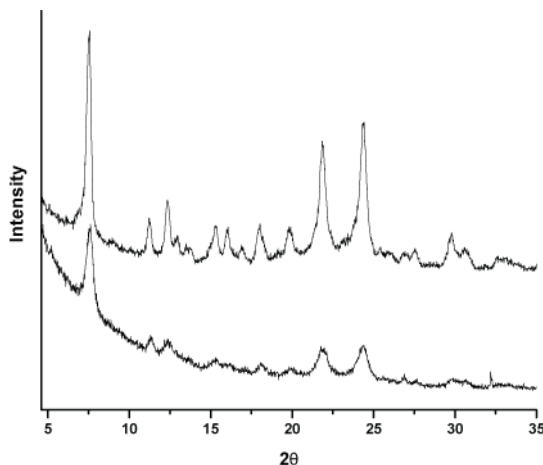


Figure 32 Powder x-ray diffraction (Cu K α radiation) of BH products. The XRD patterns of Bohle dehalogenation BH (top) and NP-40 mediated BH (bottom) were compared, and the characteristic 7°, 21° and 24° 2 θ peaks were observed.

Of the six detergents surveyed, the zwitterionic CHAPS, nonionic Triton X-100 and anionic SDS were found to be inefficient mediators of BH crystallization; while the nonionic surfactants Tween 20, 80 and NP-40 effectively mediated the formation of BH at $\geq 69\%$ yield (Table 1). Since HZ has been shown to aggregate in the presence of neutral lipid droplets in *P. falciparum* infected host red blood cells, the hydrophobic nature of the nonionic detergents is thought to effectively mimic the neutral lipid environment. This system allows the localization of high concentrations of heme, promoting dimer formation and aggregation. The analogous nature of the detergents and

neutral lipids is supported by the similar yields in BH crystallization between the Tween 20, 80 and NP-40 detergents and those of the neutral lipid blend (Table 1).

Table 1 Lipophilic Mediators of BH Formation.

Lipophilic Mediator	Mediator (μM)	BH Produced (nmol)	Percent Yield (%)
Neutral Lipid Blend	50	7.49	75
NP-40	30.6	7.44	74
Tween 20	9.77	7.11	71
Tween 80	14.9	6.92	69
SDS	1140	1.01	10
Triton X-100	58.6	0.74	7.4
CHAPS	1466	0.70	7.0

The adaptation of reaction parameters for optimal throughput and sensitivity was crucial in establishing assay viability for NP-40. The initial focus was directed at mediator concentration. A titration of neutral lipid and NP-40 was plotted against their respective BH yields (Figure 33A&B). For the neutral lipid blend, similar yields of BH were observed over a range of mediator concentrations from 50 nM to 50 μM (Figure 33A). These results illustrate the high efficiency of the native neutral lipid blend in mediating BH formation even at low nanomolar concentrations. In contrast, NP-40 demonstrated an optimal concentration for BH yields at 30.5 μM (Figure 33B). The reasons for the difference between the optimal template concentrations is unclear, but could be the result of a variation in the detergent's ability to encompass substrate heme prior to the formation of propionate bonds in the hydrophilic reaction buffer.

Detergents have long been reported as mimics for native membrane lipids given their capability of binding hydrophobic surfaces in a micelle-like manner and facilitating ordered packing.¹⁹¹⁻¹⁹⁵ Using neutron diffraction methods, Roth *et al.* showed that fatty acid detergents promoted protein crystallization by exerting interactions that mediate

effective molecular packing.^{196,197} By analogy, the detergent's role in BH crystallization could be its ability to segregate free heme optimally along the lipid-water interface^{29,198}.

As the fatty acyl glycerides used in the neutral lipid blend and NP-40 both contain

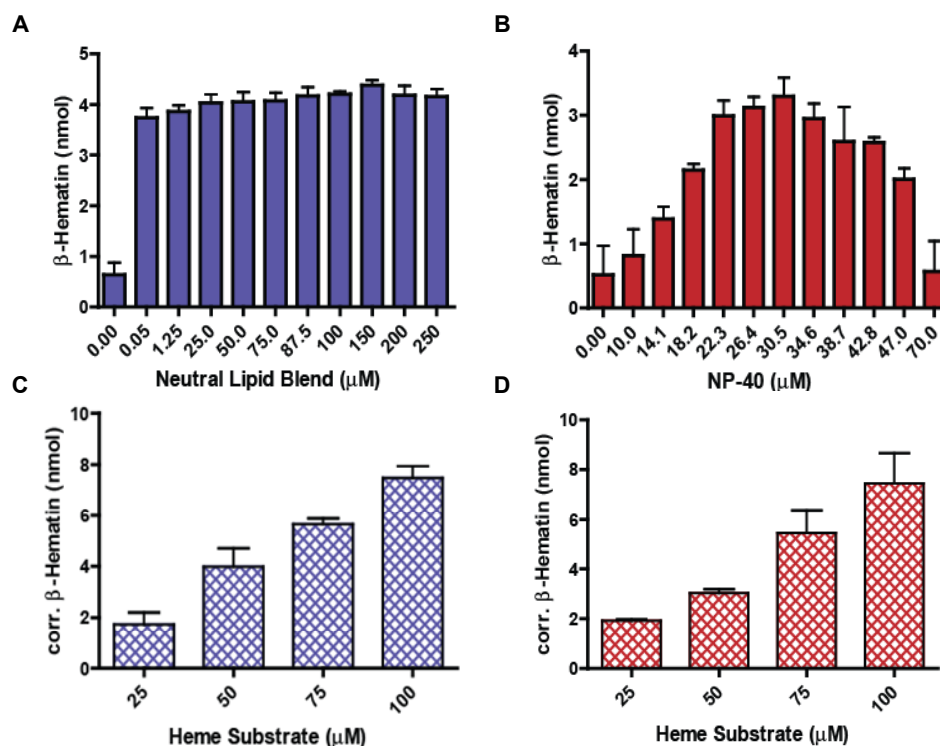


Figure 33 Assay optimization of substrate heme and lipophilic mediator. (A) Lipid blend mediator concentrations were varied between 50 nM and 250 μ M for optimal BH production. A specific concentration of neutral lipids was not observed. (B) A titration of NP-40 was also carried out. Here, the optimal concentration of 30.5 μ M showed the greatest yields of BH. (C) Substrate heme was added increasingly to the neutral lipid blend assay in order to determine the optimal range (100 μ M) without decreasing the assay's S/N. (D) Increasing amounts of heme were also added to the NP-40 assay and as seen in the neutral lipid assay, were not shown to hinder assay S/N at ranges up to 100 μ M heme.

hydrocarbon tails, it may simply be that the phenyl ring of the NP-40 changes the template packing enough that a more specific concentration of the detergent is required for optimal heme stacking and hence, BH assembly.

In order to optimize the assays' BH yields, the optimal substrate heme concentration was determined. For these experiments, increasing concentrations of substrate heme were added to the reactions until a decline in signal to noise (S/N) was

observed (Figure 33C&D). When heme concentrations exceeded 100 μM in both assays, a significant reduction (>70%) of S/N was observed due to the variability of a saturated system in which there was an increasing quantity of non-aggregated heme among the precipitate BH, yet the production of BH remained unchanged (data not shown). Scaling the substrate from 50 μM to 100 μM , however, improved the BH yields approximately 60% with a S/N value of 14, an increase of 1.8 fold. Consequently, final optimized assay conditions employed 100 μM substrate heme and 30.5 μM NP-40 or 50 μM neutral lipid mediator.

With established conditions for maximum BH formation, the efficacy of antimalarials known to inhibit BH crystallization was evaluated. Concentration response curves were generated for each of the lipophilic mediated assays in the presence of amodiaquine and chloroquine. The detergents Tween 20 and Tween 80 consistently exhibited 10-fold higher drug IC_{50} values than those for the DV neutral lipid blend (Table 2). In contrast, the NP-40 assay's IC_{50} values (within $\pm 1.5 \mu\text{M}$) closely resembled those of the neutral lipids' and thus, provided an accurate yet inexpensive and accelerated assay

Table 2 Efficacy of Known BH Inhibitors in the Lipophilic Mediated Assays.

Lipophilic Mediator	Amodiaquine IC_{50} (μM)	Chloroquine IC_{50} (μM)
Neutral Lipid Blend	23.07	85.26
NP-40	25.73	50.99
Tween 20	316.3	262.0
Tween 80	201.8	195.7
SDS	225.4	245.6
Triton X-100	N/A	N/A
CHAPS	N/A	N/A

mimic for BH crystallization (Figure 34A&B). Inhibition trends consistent with those observed from the native neutral lipid blend suggested that the NP-40 assay would be

capable of discerning other potential inhibitors of BH crystallization that were similar or greater in potency than the control drugs amodiaquine and chloroquine.

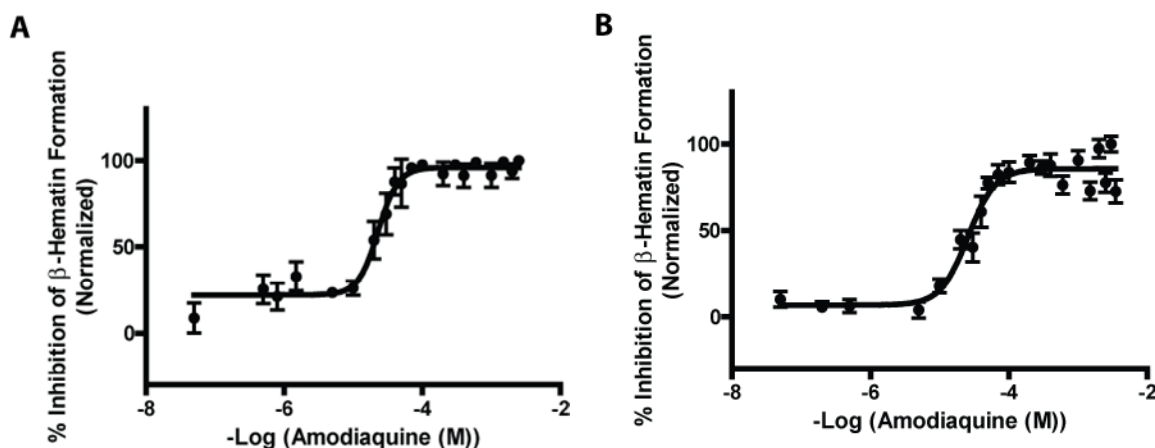


Figure 34 Amodiaquine concentration response curves of neutral lipid and NP-40 mediated BH formation assays. (A) The IC₅₀ value of amodiaquine in the neutral lipid mediated BH formation assay was 23.1 μM. (B) The IC₅₀ value of amodiaquine in the NP-40 mediated BH formation assay was 25.7 μM. Error was within ± 1.5 μM.

Assay performance and plate uniformity were then validated in order to evaluate future assay throughput. Initial studies were conducted in 96-well plates with a checkerboard pattern of wells containing the acetate buffer vehicle and the positive controls of assay substrates with amodiaquine at its reported IC₅₀ value (Figure 35). The drift responses calculated from both lipid blend- and NP-40-mediated sample signals were less than 12%, well under the generally accepted 20% threshold. Negligible drift and edge effects were confirmed using linear regressions of the vehicle and positive control data with slopes of less than 2.5×10^{-3} illustrating the minimal shift in data across the plate. These findings reinforced that compound response could be screened with equal significance across each assay plate.

In these multi-variable systems, there are often more contributing factors in an actual screen than accounted for by substrates alone. Therefore, assay performance was evaluated in the presence of possible interfering agents (Table 3). A number of potential contaminants were considered that might arise while screening a simple small molecule

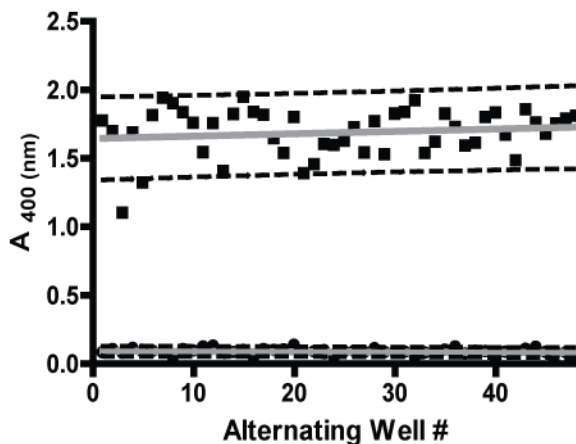


Figure 35 Assessment of plate uniformity. Reaction plates were ran with a checkerboard pattern of alternating wells of acetate buffer (negative control) and the assay substrates heme-acetate buffer, NP-40 and IC₅₀ 25.7 μ M amodiaquine (positive control). When plotted, the assay signal did not fluctuate along the edges of the plate nor across the plate, as confirmed by slopes of linear regression below 2.5×10^{-3} and low drift calculations of 12%.

drug library or a complex natural product extract. Organic solvents commonly used in extraction methods like methanol and ethyl acetate were found to be compatible at final assay concentrations of less than 5% (v/v). The separation solvent, acetonitrile, did not perturb assay S/N measurements or BH yields at levels below 20% (v/v). Dimethyl sulfoxide, a common drug delivery vehicle, did not hinder assay signal below a 10% (v/v) final concentration. Common tannins, thiols and chelating agents at low concentrations were observed to have little effect. Likewise, natural plant pigment chlorophyll *a* did not alter assay output when maintained at concentrations of less than 0.13 mM. Methanol and ethyl acetate extracts of various growth media were not expected to be present at

percentages higher than 0.02% (w/v) and no interference was observed at these levels. Cumulatively, these controls provided a high level of confidence that future “hits” would not be the result of common interfering agents.

Table 3 Evaluation of Common Interfering Agents.

Potential Interfering Agents	Range Tested	Observed Interference (≥)
Solvents		
(v/v)		
Methanol	0-30%	5.0%
Ethanol	0-30%	5.0%
Acetonitrile	0-30%	20%
Dimethyl sulfoxide	0-30%	10%
Acetone	0-50%	40%
Ethyl Acetate	0-30%	5.0%
Butanol	0-30%	5.0%
Chelating Agents		
EDTA	0-15 mM	15 mM
EGTA	0-15 mM	6.0 mM
Tannins		
Catechin	0-1.0 mM	0.26 mM
Gallic Acid	0-1.0 mM	0.13 mM
Tannic Acid	0-1.0 mM	0.13 mM
Thiol groups		
DTT	0-1.0 mM	0.13 mM
Cysteine	0-1.0 mM	0.97 mM
GSH	0-1.0 mM	0.26 mM
Pigments		
Chlorophyll a	0-1.0 mM	0.13 mM
Media Extracts		
(w/v)		
K26S with Ethyl Acetate	0-0.3%	0.15%
K26S with Methanol	0-0.3%	0.25%
ET with Ethyl Acetate	0-0.3%	0.05%
ET with Methanol	0-0.3%	0.10%

This high degree of optimization is crucial when the assay target is suspected to encounter a number of bioactive compounds during a screen. Such is the case when identifying potential drugs from crude natural products. Between 1981-2002, 52% of all new chemical entities introduced into the pharmaceutical pipeline was derived from natural products.¹⁹⁹ Even prior to this time period, alkaloids from the Cinchona tree and

peroxides from the Qinghao shrub gave rise to the vital antimalarials quinine and artemisinin, respectively.²⁰⁰ Unfortunately, parasite drug resistance continues to diminish what is left of the quinine derivatives' efficacy, and reports of resistance to artemisinin combination treatments have emerged.²⁰⁰ Since these antimalarials are currently the fore in combating the disease, the need for new effective drugs is paramount.

Given the importance of natural products as a source of effective antimalarials, the neutral lipid and NP-40 assays were subjected to trial screens of a small library of assembled natural product extracts (NPEs) from actinomycete and myxobacteria microorganisms.^{199,201} An extract of the cinchona tree, known to contain the BH inhibitor quinine, was also examined. These screens served as effective measures of the assays' applicability under "real-world" conditions. To ensure the proper interpretation of the results, all extracts were spiked with the known antimalarial drug amodiaquine at its IC₅₀. The NPEs were grown under various media conditions, extracted with either methanol or ethyl acetate, and all extracts were separated by an acetonitrile:water gradient using reverse phase liquid chromatography tandem mass spectrometry (RP-LC-MS/MS). One milliliter fractions of each sample were collected per minute in 96-deep well source plates and transferred to 96-well destination plates for screening, ensuring synchronization with the LC-MS/MS data to facilitate spectral identification of each well's compound(s). The amodiaquine (m/z 356 [M+H⁺]) was identified using MS/MS fragmentation and shown to elute at 21 minutes into well 22 (Figure 36A&B).

When the NPE plates were screened for activity, well 22 tested positive for approximately 50% BH inhibition, the predicted activity (Figure 36C). The apparent activity of other metabolites in the assay are under investigation but may need to be

further adapted in the assay with respect to an optimal concentration. Coupled with the observed activity of quinine from the cinchona bark extract (Figure 37), the neutral lipid

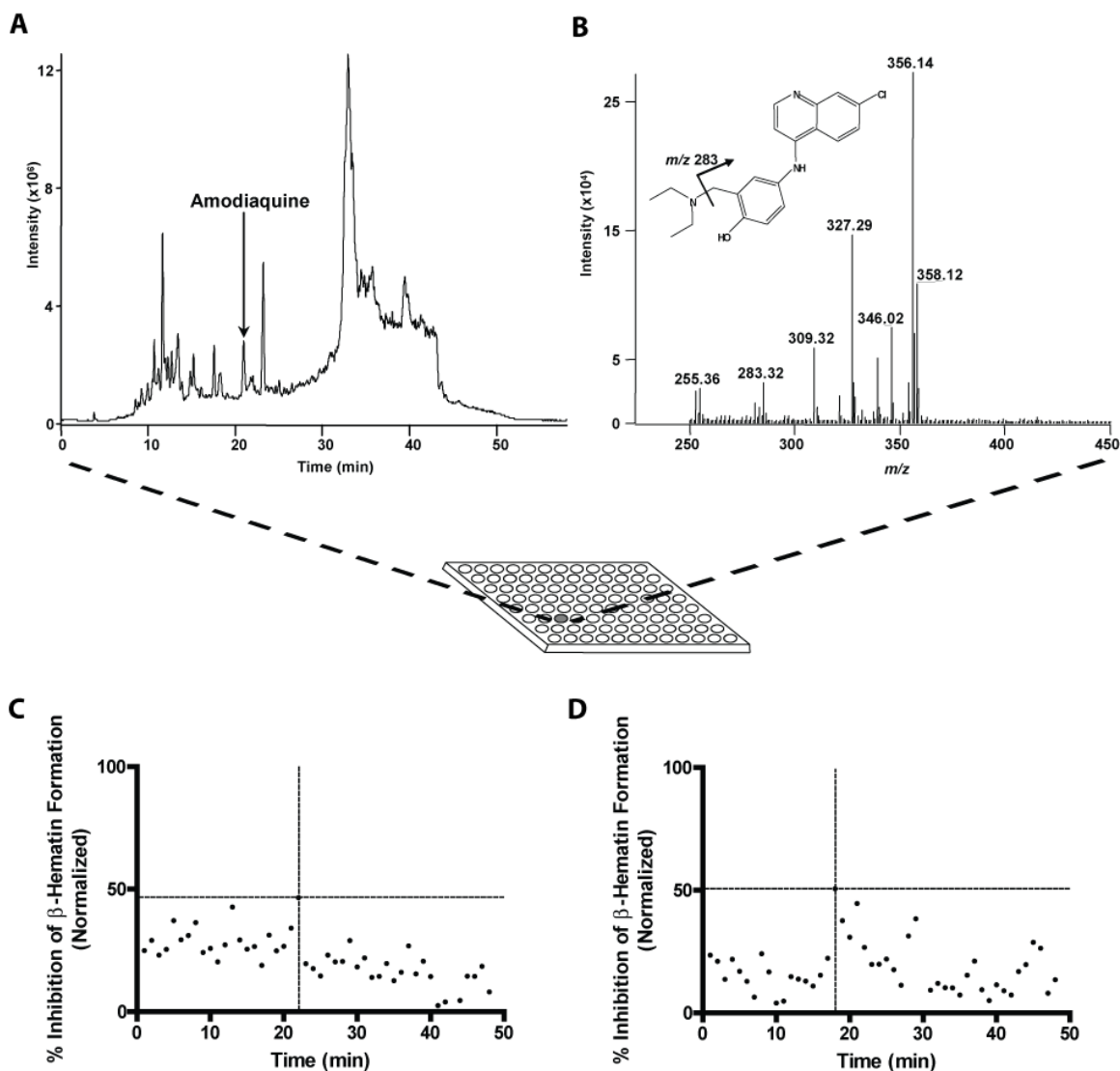


Figure 36 Natural product extracts in BH crystallization screens. (A) Separation of amodiaquine from spiked K26S ethyl acetate natural product extracts. Amodiaquine was shown to elute at 21 minutes into collection plate well number 22. (B) ESI⁺ spectra of amodiaquine. Amodiaquine's precursor ion was observed at m/z 356 [M+H⁺]. A ³⁷Cl isotopic ion was seen at m/z 358, and the characteristic MS/MS product ion from the 73 unit inductive cleavage of NH(C₂H₅)₂ was detected at m/z 283. (C) ET extracts in BH assay. Compounds collected from LC separation of ET natural product extracts were screened in the NP-40 mediated BH crystallization assay. The amodiaquine from the extract solution is indicated by the cross-hair dotted line. (D) Cinchona bark extract in BH assay. Compounds collected from LC separation of the Cinchona bark extract were also screened with the NP-40 mediated BH crystallization assay. Quinine activity was observed in well 19 (18 minute elutant) and is indicated by the cross-hair dotted line.

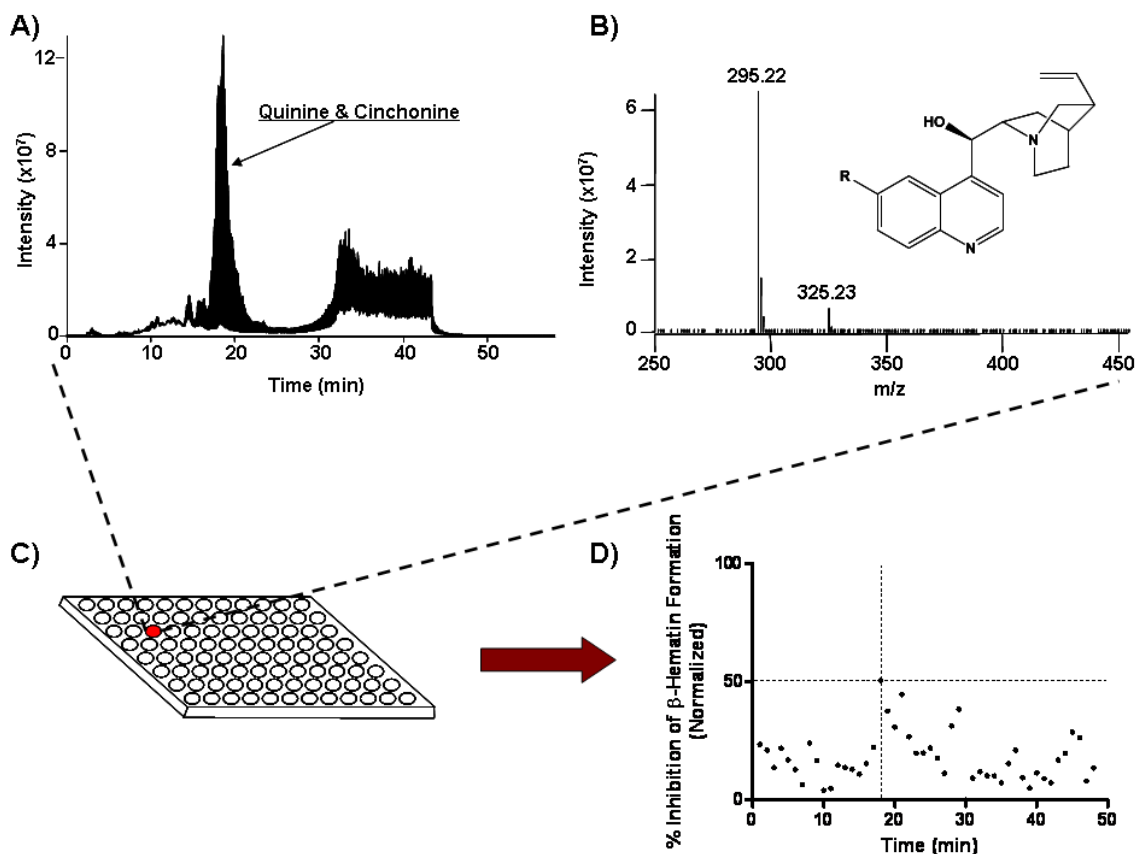


Figure 37 Red Cinchona bark extract in BH crystallization assay. **A)** Separation of quinine from Cinchona bark ethanol extracts. **B)** ESI⁺ spectra of quinine and cinchonine. Quinine's precursor ion was observed at m/z 325 [M+H⁺], where R is a CH₃O- group. Cinchonine was observed at m/z 295 [M+H⁺], where R is a H- substituent. **C)** Quinine was shown to elute at 18 minutes into collection plate well number 19. **D)** Cinchona bark extract in BH assay. Compounds collected from LC separation of the Cinchona bark extract were also screened with the NP-40 mediated BH crystallization assay. Quinine activity was observed in well 19 and is indicated by the cross-hair dotted line.

and NP-40 assays were shown to selectively discriminate between bioactive hits, ultimately substantiating their potential use in future antimalarial drug screening.

Conclusions

Despite almost universal resistance to chloroquine in *Plasmodium falciparum*, widespread mefloquine resistance and diminished efficacy of quinine, HZ remains a

uniquely suitable target for antimalarial drugs. There is no compelling evidence for any change in HZ formation in resistant strains, and analogs of chloroquine retain activity against chloroquine resistant parasites ²⁰²⁻²⁰⁴. However, the target pathway is complicated by the mystery of HZ's *in vivo* formation. Evidence for a lipid-rich biomineralization template was most recently acquired in the extraction of HZ-surrounded neutral lipid droplets from *P. falciparum* infected red blood cells. These extracted neutral lipids were shown to act as an effective scaffold for *in vitro* BH formation ²⁹. Herein, two optimized lipid-based assays were shown to provide a robust assay platform for the discrimination of BH inhibitors against both common chemical interferants and the complex milieu of natural product extracts. In particular, the surfactant NP-40 is a newly used BH aggregation scaffold that requires less expensive materials than the specific blend of neutral lipids and expedites the processing time by 16 hr. Validation studies and application in a preliminary screen of NPEs confirmed both the neutral lipid and NP-40 mediated assays' potential in future high throughput drug screens.

CHAPTER VI

HIGH THROUGHPUT SCREENS FOR LEAD SMALL-MOLECULE INHIBITORS OF β -HEMATIN CRYSTALLIZATION

The international costs of malaria are estimated to balloon upwards \$38-45 billion US dollars between 2006 and 2015.²⁰⁵ This increase is largely due to the decreasing efficacy of current drug therapies as they shudder under the pressures of parasite and vector resistance as well as distribution fraud and production costs. The worldwide clinical and financial burden of malaria is third only to HIV and tuberculosis infections. Once easily treated by an oral dose of the fail-safe chloroquine, many areas are now inhabited by chloroquine-resistant strains of *Plasmodium falciparum*.

The resistance of the parasite to chloroquine treatment was slow to develop given the complexity of the DV and the invulnerable nature of released heme.²⁰⁶ Current resistance is primarily attributed to mutations in the gene that encodes for the parasite's DV membrane protein, the *Plasmodium falciparum* chloroquine resistance transporter (PfCRT).²⁰⁷ The presence of PfCRT has been associated directly to a decrease of chloroquine concentration in the DV. This change in the drug delivery system of the parasite has not altered the heme detoxification mechanism against which chloroquine is active, however.

In fact, many studies are directed at restoring chloroquine's access to the DV by using chemosensitizers, or resistance-reversal agents, that act upon PfCRT. The most recent successes of these agents are of the acridone chemotype.²⁰⁸ The acridone structure is designed to both promote π - π stacking with heme via a tricyclic aromatic core as well

as obtain DV access via acid trapping with hydrogen bond acceptors on its side chain nitrogen moieties.²⁰⁸ Preliminary studies were successful in synergy with chloroquine, amodiaquine, quinine and piperaquine in the *P. falciparum* Dd2 strain.²⁰⁸ This renewed access to the DV heme target reinforces the continued success of and interest in targeting the parasite's heme detoxification system.

Specifically, the parasite is reliant on the biomineralization of heme into aggregates of dimeric ferriprotoporphyrin IX (Fe(III)PPIX), known as hemozoin (HZ). This process takes place along a neutral lipid scaffold in the acidic environment of the DV. By mimicking this environment, several research groups have established *in vitro* models from which potential antimalarial activity can be measured against HZ's synthetic analog, β -hematin (BH).^{23,29,35,174,185,189} As this synthetic analog is structurally, spectroscopically and crystallographically identical to HZ,³⁵ the results of these assays are indicative of the heme and drug molecular interactions expected *in vivo*. Few of these assays have been developed with true high throughput screening capabilities, however. Many are validated only to 96-well plates, contain centrifugation steps, extensive periods of incubation and costly radio-labeled substrates.

By introducing a pyridine reagent to the end step of the previously developed NP-40 mediated BH crystallization assay,¹⁷⁴ the centrifugation steps of the sodium bicarbonate washes were discontinued, reducing the assay's processing time by 2 hours. Further optimization of this assay to a 384-well plate format and cross-validation in a high throughput screening facility has enabled the screening of 38,400 small molecules to date. The development and validation of this assay are presented herein along with the analysis of its resultant 161 preliminary hits, and 136 of those further confirmed.

Experimental

*NP-40 mediated BH crystallization assay.*¹⁷⁴ In a Corning 384-well clear plate, each assay was prepared with a series of substrates added by a CombiChem liquid dispenser. The following order of distributions were added into each well: 14 μL of DI water, 30 μL of 222.2 μM heme in 2.0 M sodium acetate (pH 4.9), 5 μL of 0.0002 g/mL NP-40 and 15 μL of 100% acetone. The final assay contained a 100 μM heme solution in 1.0 M sodium acetate buffer with 30.5 μM NP-40 and 30% acetone. The assay was incubated 4 hours under constant agitation in a reciprocating water bath at 37°C, 55 rpm. When plates were removed from incubation, 8 μL of 50% pyridine, 20 mM HEPES buffer (pH 7.5) was added, and the plates were shaken for 15 minutes prior to taking absorbance readings at 405 nm. Amodiaquine and chloroquine stock controls were screened at an IC_{MAX} of 100 μM . Concentration response curves were designed at 0, 0.5, 1.0, 5.0, 10, 15, 20, 30, 50, 80 and 110 μM doses of preliminary hit compounds (N=2). Data were fitted to sigmoidal dose response (variable slope) curves using GraphPad Prism v. 4.0 software.

Small molecule screens. Small molecules were screened from the Vanderbilt University High Throughput Screening Facility and Institute of Chemical Biology. All samples were dissolved in 100% dry DMSO at 10 mM stock solutions. Molecules screened in the assay were screened at 19.3 μM , the approximate IC_{50} concentrations of amodiaquine and chloroquine in the assay. To do this, 125 nL of the stock samples were added to each test well prior to assay substrate addition and the molecules' absorbance

was read at 405 nm. This initial absorbance reading was subtracted from the final assay reading in order to prevent a high false positive rate.

Drug properties of hits. The preliminary assay hits were organized by their structural similarity to known antimalarial structures and their chemical properties as calculated using ChemAxon Marvin v.5.2.2 software. The partition coefficients, pKa and solubility constants were determined for each hit. Hits were labeled by their PubChem identification numbers.

Results and Discussion

The NP-40 BH assay was designed for its similarity to HZ formation *in vivo*, its low cost, robust nature and high reproducibility. Previously, the assay was used to screen natural product extracts for potential BH inhibitors.¹⁷⁴ Since then, the assay was reduced in volume to a 384-well plate compatible 60 μ L, and its analysis changed from the quantification of BH produced to the absorbance of heme substrate remaining after incubation. These changes required a complete re-validation of the assay and its parameters. A checkerboard distribution of the drugs chloroquine and amodiaquine at IC_{MAX} concentrations were prepared in the assay plates and their absorbance read at 405 nm upon pyridine buffer addition (Figure 38). The drift in the assays of both drugs was under 20%, indicating minimal variation between the wells across the plate. The Z' values for chloroquine and amodiaquine were 0.8824 and 0.7308, respectively. These calculations were used to evaluate the quality performance of the assay in terms of reproducibility within the plate and between plates.

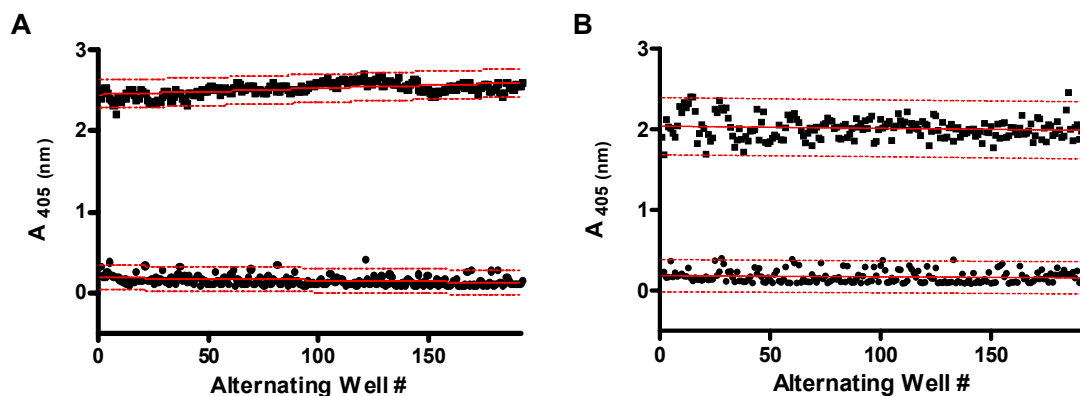


Figure 38 Calculation of Z' values during assay cross validation. Checkerboard plot of (A) chloroquine and (B) amodiaquine at IC_{MAX} 100 μ M (top line) and DMSO vehicle (bottom line). The 99.7% confidence intervals of each line are plotted above and below the data lines.

Cross validation of the assay in a concentration response curve was carried out with amodiaquine (Figure 39). The IC_{50} found for amodiaquine was 12.1 μ M with a calculated Z' value of 0.9430. This calculated IC_{50} for amodiaquine was most likely lower than the expected 20 μ M due to the decreased surface area in a 384 well plate as compared to a 96 well plate and hence an increase in molecular interactions between the

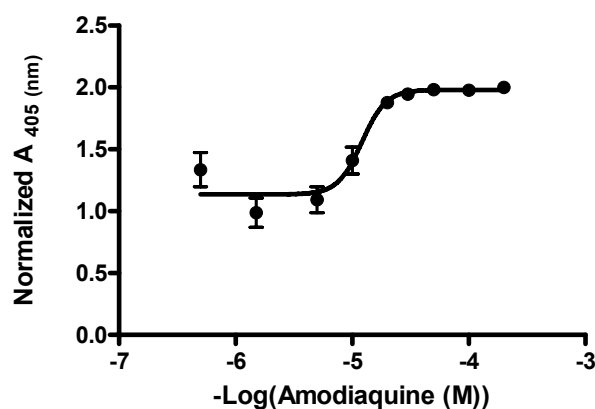


Figure 39 Concentration response curve of amodiaquine in the NP-40 BH assay. Increasing concentrations of amodiaquine were added to the BH assay and its IC_{50} determined. The IC_{50} value of amodiaquine was 12.1 μ M (error within ± 1.5 μ M), and the assay calculated Z' value was 0.9430.

drug and the {010} face of the heme moiety.

Library screens were carried out in 384-well plates containing 320 test compounds and outer columns filled of amodiaquine controls. Each plate contained a checkerboard of positive and negative controls from columns A1:P2 and A23:P24, while test samples were added to columns A3:P22. The amodiaquine control was added at an IC_{MAX} of 100 μ M for maximum inhibition of BH formation. The assay substrates without potential drugs were used as a negative control and background measurements. Collected data was plotted, containing linear regression averages with 99.7% confidence, at 3 standard deviations (Figure 40). To date, a total of 38,400 compounds were screened with a 0.42% hit rate of 161 potential leads (Appendix D). Of these hits, 15 were found to express activity at the level of amodiaquine's IC_{MAX} , giving a 0.04% IC_{MAX} hit rate (Scheme 6).

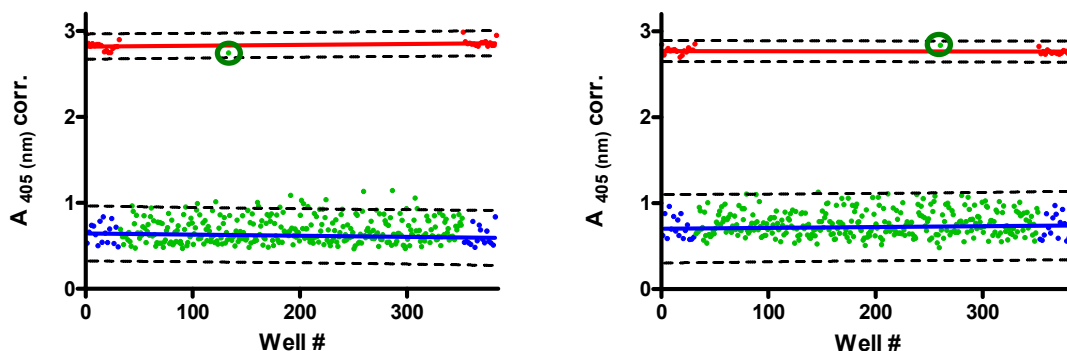
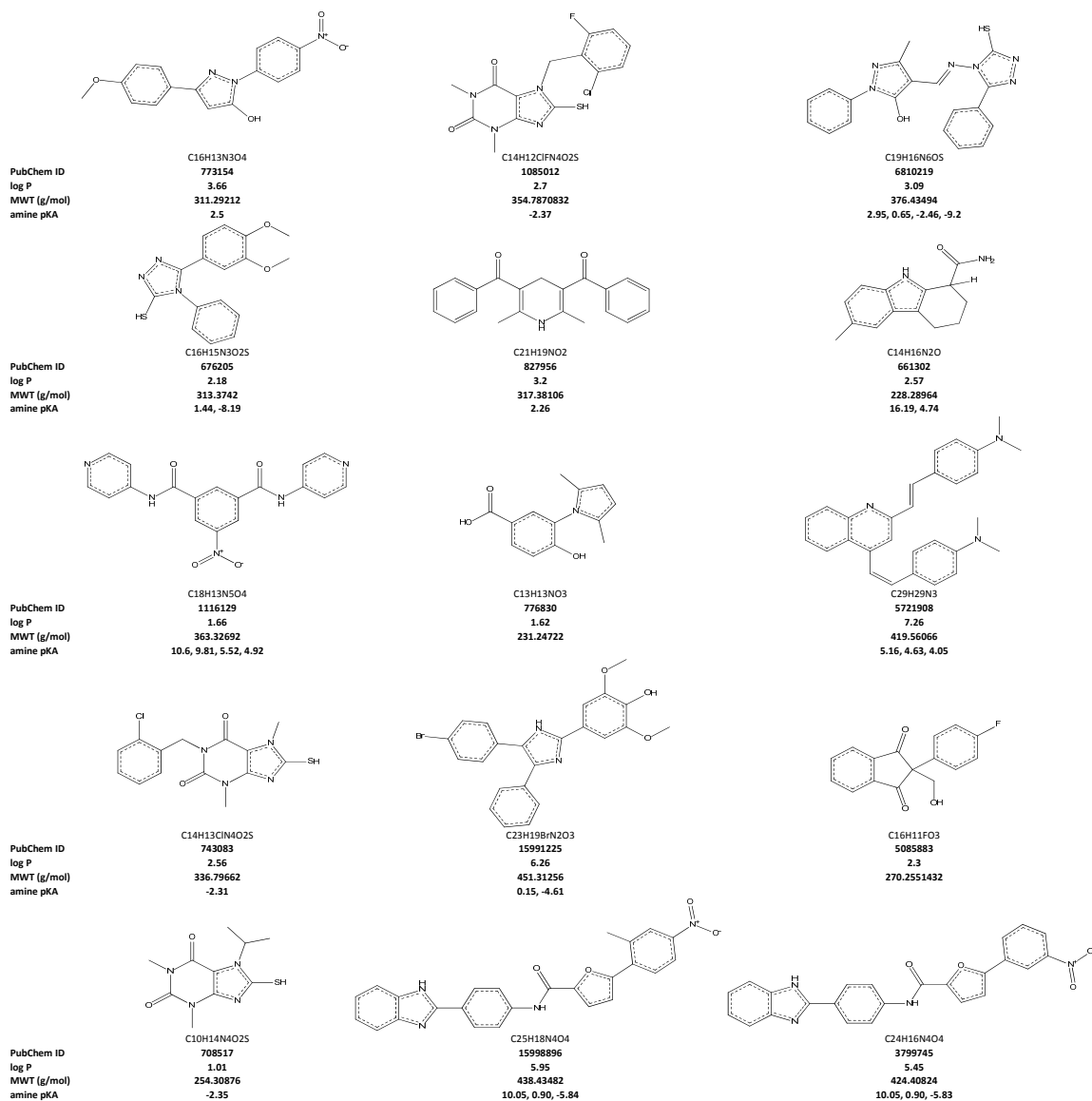


Figure 40 Small molecule library screens in the NP-40 BH crystallization assay. Library screens of 320 small molecules were carried out per plate (green), and the outer columns were filled with positive and negative controls of potentiator and vehicle, respectively. The potentiator was the amodiaquine at IC_{MAX} (red), and the vehicle was the BH assay without inhibitor (blue). Linear regressions were applied to each set of controls in order to calculate the drift across the plate as well as plot the 99.7% confidence interval from controls (dotted lines). Outliers from vehicle standard deviation were considered hits, and hits within the potentiator interval were considered IC_{MAX} hits, as marked with green rings.

PubChem identification and SMILES for the hits were obtained. The PubChem records for these hits were searched June 15, 2009, and none of the hits were found to have known antimalarial activity. The chemical properties (amine group pKa and log P values) of the hits were calculated using ChemAxon Marvin v.5.2.2 software. As compared to the control amodiaquine and chloroquine values (Scheme 7), a clear trend was not distinguishable.

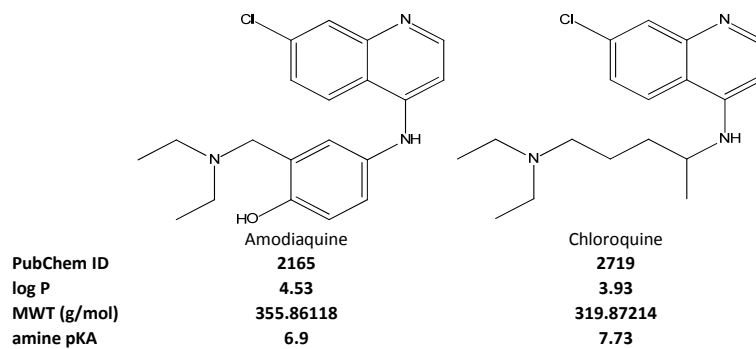
The pKa values of compounds' amine groups were considered for compatibility with the proposed acid-trapping mechanism of drugs entering and remaining in the acidic DV of the parasite. There are two proton pumps in the *P. falciparum* DV: a V-type H⁺-ATPase and a H⁺-pyrophosphatase.²⁰⁹ Weakly basic compounds are thought to gain access to the DV and hence, the heme target by protonation and subsequent trapping in the acidic vacuole, unable to efflux. While this route has been proposed as the means of drug access to the DV, it is not the *sine qua non* of antimalarial efficacy. In fact, manipulations of the DV by ± 1 pH unit were not found to result in significant changes in chloroquine accumulation as would be expected.²⁰⁹ DV permeability to charged species, however, has yet to be explored. Ultimately though, amodiaquine's moderately low pKa of 6.9 indicates that its nitrogen moiety can be protonated in an aqueous environment without high energy expenditures. This was also the case for several of the hits.

The move from potential leads to functioning drugs requires a number of considerations. Early reports of these standards by Lipinski *et al.* gave way to 'the rule of 5' well known in drug discovery and rational drug design.²¹⁰ These rules state that lead compounds are more likely to suffer from poor absorption and permeation as drugs if



Scheme 6 IC_{MAX} hits identified in the preliminary screens of the NP-40 BH assay. 15 hits with the activity of amodiaquine at an IC_{MAX} of 100 μM were identified. The PubChem ID of each compound is provided along with calculated log P, molecular weight, pKa values and the structure's chemical formula.

they possess >5 hydrogen bond donors, >10 hydrogen bond acceptors, molecular weights >500 g/mol and log P values >5.²¹⁰ Briefly, excessive hydrogen bond donors and acceptors lead to decreased membrane bilayer permeability.²¹¹ A molecular weight cutoff of 500 g/mol was established due to reported decreases in permeation rates through



Scheme 7 The physicochemical properties of the BH assay controls amodiaquine and chloroquine. The log P and pKa values for the assay controls amodiaquine and chloroquine were calculated and used as a source of comparison with the preliminary hits identified.

lipid bilayers²¹² and poorer permeability at the intestinal and blood brain barriers.²¹³ The lipophilicity of the leads, as measured by the ratio (log P) of their solubility in octanol as compared to aqueous medium, accounts for the compounds' absorption *in vivo*.²¹⁴ Fortunately, the majority of compounds in the Vanderbilt library screened heed these parameters.

The library of molecules screened was selected randomly, and upon inspection of the preliminary hit structures, they were organized structurally into 4 main groups for further evaluation: 1) Quinolines, 2) Azoles, 3) Perimidines and 4) Miscellaneous. Of the 161 hits, 6% had quinoline-like structures, 44% contained azole cyclic rings, 2% had perimidine privileged structures and the remaining 47% were grouped as miscellaneous due to the lack of a recognizable trend in their structures (Figure 41A). Of the 15 hits with IC_{MAX} activity (Scheme 6), 1 was quinoline-like in structure, 8 contained azole rings and the remaining 6 were of miscellaneous trends (Figure 41B). A large percentage (58%) of the 161 preliminary hits had structures containing joined, multi-cyclic rings and 54% of those were resonant structures. The strong presence of these resonant, multi-

cyclic structures supports the drug-heme binding model of π - π stacking of the drug at the {010} heme face.

This π - π stacking with heme is most likely the activity of the perimidines observed in these screens (Structure in Scheme 9). Perimidines are characteristically a 14 π -electron system containing 1 electron that is not delocalized and hence yields a reduction in aromaticity.²¹⁵ These molecules commonly form charge-transfer complexes with π -acids and have a high π -donor capacity.²¹⁵ While not reported for their antimalarial activity until now (2% of hits), this family of compounds has been reported as effective anti-ulcer, neurotropic, fungicidal and anti-helminthic agents.²¹⁵

Similarly, the π -binding quinolines were expected to exhibit activity in this BH inhibition assay given the previous performance of the 4-aminoquinoline controls chloroquine and amodiaquine. This family is also home to amopyroquine, tebuquine, mepacrine, pyronaridine, halofantrine, quinine, epiquinine, quinidine and bisquinoline. These drugs have been an effective source of BH inhibitors and consequently, antimalarials for over 300 years. An understanding of their mode of action was slower in coming, however. It is now thought that this group of antimalarials act by drug adsorption on the {001} and {011} crystal faces of BH, resulting in thinner crystal cross-sections.³¹ Inhibition from π - π stacking at the {010} heme face is also characteristic of the quinoline-heme complex. These compounds accumulate in the parasite DV at concentrations reaching millimolar ranges.⁶² The quinoline-heme complex prevents the formation of Fe-O propionate bonds needed between the dimeric subunits of HZ, resulting in an accumulation of toxic heme at near 400 mM concentrations.⁸⁷ The

buildup of free heme hinders metabolic function by generating oxidative free radicals, damaging DNA and inhibiting regulatory enzymes.⁶²

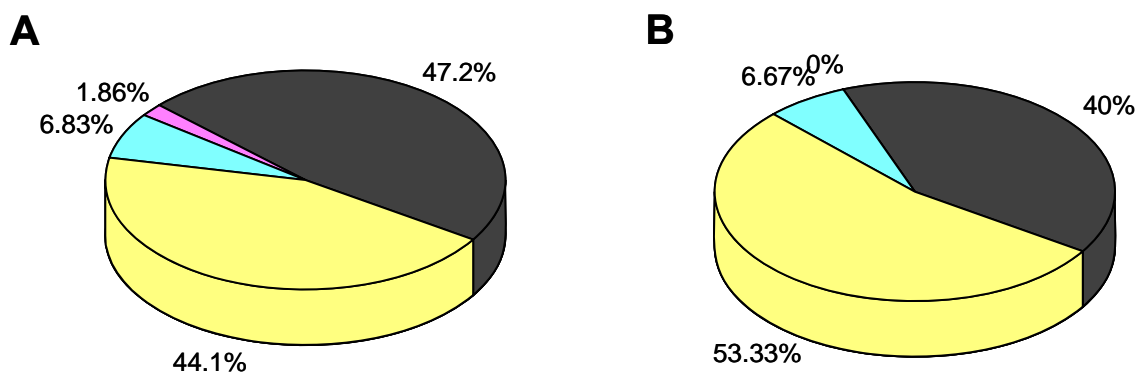
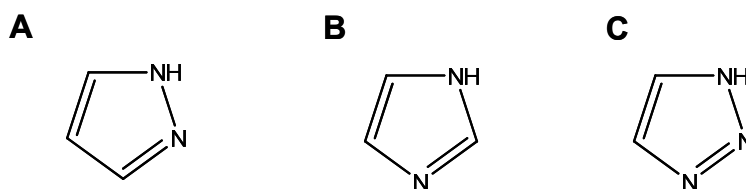


Figure 41 Structural trends in the preliminary hits from the NP-40 BH assay screens. Hits were organized structurally into 4 groups: (yellow) Azoles, (blue) Quinolines, (red) Perimidines and (black) Miscellaneous. The percent composition of these groups in (A) the 161 preliminary hits and (B) the 15 IC_{MAX} hits are shown.

The structure-function relationship of the quinolines varies. Compounds belonging to the 7-halo substituted 4-aminoquinolines are the most active antimalarials.²¹⁶ In fact, activity declines when the halogen is replaced by 7-amino and 7-chloro derivatives or when disubstitution at the quinoline nucleus occurs. Quinolines lacking the 7-chloro group still bind heme, but HZ crystallization is not blocked. When a Cl is substituted at the C-6 position, quinoline-heme binding is impeded.²¹⁶ The dialkylaminoalkylamino side groups are also crucial for optimal activity.²³ Bisquinolines, compounds containing 2 quinoline nuclei bound by aliphatic or aromatic linkers, are reportedly more potent than chloroquine although higher concentrations are required both *in vitro* and *in vivo*.^{216,217} This potency is attributed to the compounds' action as an antagonist against the heme sequestration process, possibly disrupting HZ's lipid-rich biomineralization platform.²¹⁷

Demonstrating a similar mode of BH inhibition are the azole-containing compounds. A more recent family of compounds with antimalarial activity, this group includes ketoconazole, miconazole and clotrimazole.²¹⁸ The antimycotic drug clotrimazole is the most potent of the group and exhibits antimalarial activity at low concentrations in *P. falciparum* cultures.²¹⁹ Both clotrimazole and miconazole have high binding affinities to the heme monomer, even preventing heme binding to the parasite



Scheme 8 Azole structures observed in preliminary hits of the NP-40 BH assay screens. The azole-containing compounds of the preliminary hits contained (A) pyrazole, (B) diazole and (C) triazole structures.

histidine rich protein, an early recognized protein template for HZ biomineralization.²²⁰ Clotrimazole's potency has also been attributed to its large molecular size and hydrophobicity in the induction of hemolysis.²²¹ Since HZ is thought to form along a scaffold of lipids, clotrimazole's noted hydrophobicity may improve its access to the heme in a lipid network.

A surprising number of the preliminary (44.7%) and IC_{MAX} (53%) hits were identified as azole-containing structures. Of these, there were three types of azoles observed: 1) pyrazoles, 2) diazoles and 3) triazoles (Scheme 8). The aforementioned ketocon-, micon- and clotrim-azoles contain diazole structures. A higher percentage (53%) of triazoles was observed in the preliminary hits than diazoles, yet 75% of the azoles in the IC_{MAX} hits were diazoles (Figure 42). The hydrophobicity, as evaluated

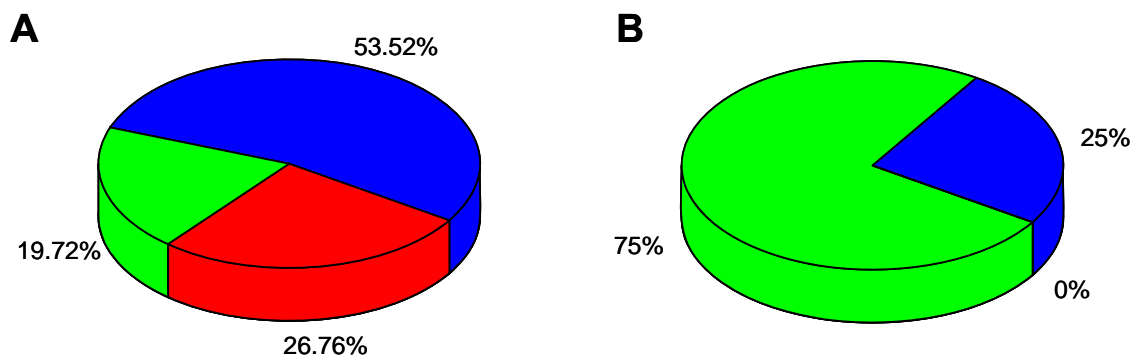
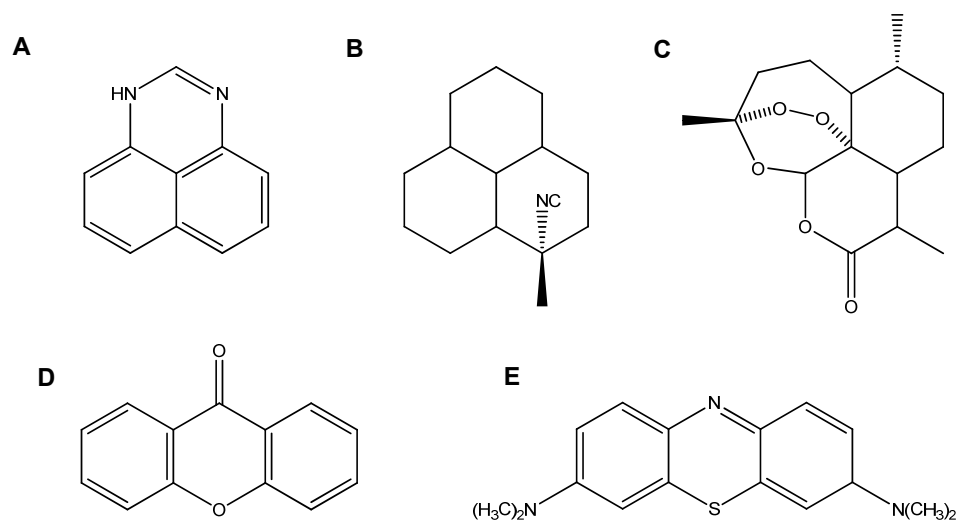


Figure 42 Azole structural trends in the preliminary hits from the NP-40 BH assay screens. Azole-containing hits were organized structurally into: (**red**) pyrazoles, (**green**) diazoles and (**blue**) triazoles. The percent composition of these groups in (A) the 161 preliminary hits and (B) the 15 IC_{MAX} hits are shown.

with calculated log P values, of the azole-containing hits was observed to increase when the immediate azole ring contained an electron withdrawing substituent, like a benzyl ring.

The remaining hits of these preliminary screens likely inhibit BH in the assay similarly, as that is the property for which this assay selects. While molecular trends were not recognized overtly in the miscellaneous group, this could change with further screening, potentially revealing a new privileged structure capable of inhibiting BH crystallization. The miscellaneous compounds were surveyed for the BH inhibitor xanthone-, methylene blue- and isonitrile-like structures (Scheme 9), but these were not evident. While the artemisinin derivatives are not noted primarily for their HZ inhibition activity, they have been implicated in the formation heme-adduct products incapable of aggregating to the dimeric Fe(III)PPIX biomineral.²²² For this reason, the compounds were also searched for artemisinin-like structures, and while 2 bridged structures were found, they did not contain the endoperoxide bridge essential to artemisinin's antimalarial activity.



Scheme 9 Structures searched in preliminary hits from NP-40 mediated BH assay screens. (A) Perimidines were identified in 2% of the preliminary hits. The hits were also searched for similar structures to the (B) isonitriles, (C) artemisinins, (D) xanthenes and (E) methylene blue derivatives but were not found.

All preliminary hits were screened in follow-up concentration response curves where N=2 (Figure 43). A complete list of these results is reported (Table 4). A false

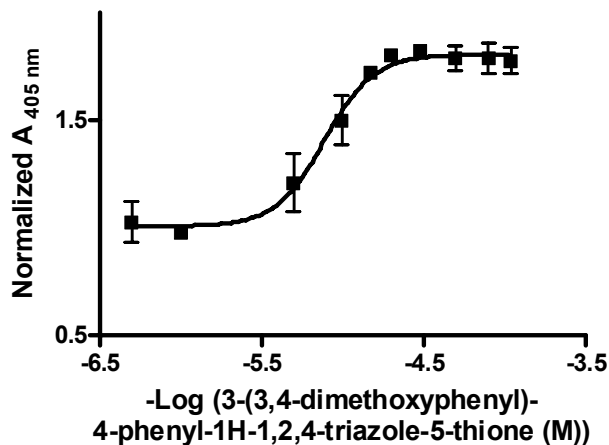


Figure 43 Concentration response curve of preliminary hit. PubChem CID 676205 was screened in a follow-up concentration response curve (N=2) and confirmed as a hit to be screened further. The compound's IC_{50} was $7.78 \pm 0.05 \mu M$ with a Z' calculation of 0.1746.

positive rate of 16% was observed, distinguished by orange highlighting. Curves were generated with 10 data points between 0 and 110 μM . This range was sufficient for hits with IC_{50} values similar to the control amodiaquine. Hits with higher IC_{50} values, and hence incomplete concentration response curves, were designated with yellow highlighting. The 136 confirmed hits from these screens will be screened in *P. falciparum* maturation assays in the near future.

Conclusions

Herein, a high throughput screening assay was developed that effectively mimics the lipophilic and acidic environment of the *P. falciparum* DV. As such, the assay was applied to screen a library of 38,400 small molecules for inhibitors to the parasite's heme detoxification pathway. While parasite resistance continues to grow, the drug target of this screen has proven invulnerable to change. These screens yielded a 0.42% preliminary hit rate, identifying 161 preliminary hits. Further, these hits contained 15 compounds with similar activity levels to the potentiator amodiaquine at IC_{MAX} . All hits were surveyed for structural trends, and 44% of the molecules were found to containazole rings, a more recent addition to the antimalarial families. The confirmed hit rate was 0.35% with 136 hits confirmed for secondary screening in *P. falciparum* maturation assays. When it is demonstrated that the hits are in fact leads with drug potential, a closer evaluation of their ADME (absorption, distribution, metabolism and excretion) properties and performance in PBPK (physiologically based pharmacokinetic) models will follow.

Table 4 Results of Follow-Up Screen Concentration Response Curves

PubChem CID	Z'	IC ₅₀ (μM)	±	PubChem CID	Z'	IC ₅₀ (μM)	±
783797	0.677966	12.45	0.06	991474	0.7819967	20.87	0.04
805136	0.49651	10.77	0.03	2197254	-0.9730862	4.86	0.05
751934	0.471088	29.22	0.12	930671	0.9017011	5.03	0.09
2933614	0.505247	23.65	0.18	2947540	-0.3946032	46.43	0.26
706129	0.727289	9.88	0.07	1085012	0.2907878	6.22	0.07
2931719	0.808408	67.84	1.02	931717	0.2975118	7.48	0.06
2931787	0.628934	39.62	0.31	677540	0.2574554	7.33	0.06
873167	0.136354	12.39	0.04	5721523	0.2695838	10.09	0.05
2256655				676205	0.1745512	7.78	0.05
6742706	0.811165	15.03	0.04	95445	0.6792867	10.27	0.05
6800421	-0.204941	8.98	0.07	667526	0.4496272	9.09	0.04
2057602				820006	0.9309869	6.06	0.04
1356910	0.227747	7.87	0.08	689492	0.7462937	11.57	0.05
1587948	0.43769	25.72	0.07	366	-0.6814497	8.65	0.1
892241	0.821423	5.99	0.07	300848	0.6783625	10.95	0.09
731870				3557264	0.6086307	11.42	0.07
748069	0.670988	5.62	0.06	5414628	0.9680207	7.12	0.07
2941849	0.80042	22.12	0.05	6777892	0.1373502	6.15	0.08
892098	0.527199	6.65	0.05	707204	0.0928293	5.88	0.05
702457				660813	0.3591574	5.93	0.06
748044	0.765649	7.47	0.06	2253328	0.0933446	23.83	0.05
748042	0.773259	13.37	0.05	6810219	0.6677377	8.89	0.07
3455308	0.273602	29.22	0.23	708517	0.5157961	32.33	0.24
729843	0.881729	19.8	0.05	3490666	0.8612433	14.25	0.05
6273261				5721908	0.3041729	20.5	0.05
764330	0.850526	8.51	0.09	2884112	0.8321099	10.59	0.05
6800179	0.428089	18.68	0.12	5731584	0.8108231	29.14	0.05
725824	0.872773	12.98	0.09	986302	0.5120991	14.96	0.08
3131870	0.837197	13.71	0.04	6809875	0.5909079	8.94	0.05
764331	0.781692	5.83	0.04	150718	0.107777	11.67	0.06
4670755				683639	0.8580982	48.99	0.23
5066435	0.429261	5.71	0.06	5898619	0.668525	5.86	0.05
690371	0.087854	5.83	0.08	6803142	0.7966663	56.16	0.27
870599	0.371238	6.34	0.1	2831725	0.8230734	27.53	0.05
574330	0.822699	4.74	0.07	774193	0.8203441	55.33	1.28
2248254	0.419496	11.53	0.03	991453	0.8665602	26.33	0.06
1556024	-0.265293	20.46	0.08	5550271	0.9512268	43.41	0.17
773154	-0.237286	7.18	0.08	2947757	0.5138404	32.9	0.08
2901657	0.696329	7.5	0.06	975838			
661205	0.853816	7.95	0.05	2947832	0.0224814	22.73	0.07
2897796	0.660458	66.27	0.41	830422			
2898021	-0.024032	7.01	0.06	2948389	0.4409473	23.34	0.11
2896732	0.850494	8.7	0.05	2949870	0.7335094	13.59	0.04

PubChem CID	Z'	IC ₅₀ (μM)	±	PubChem CID	Z'	IC ₅₀ (μM)	±
5739057	0.878833	15.3	0.06	555190	-1.590492	12.64	0.11
3799887				776836	0.738555	15.85	0.04
6796866	0.747734	28.06	0.05	3534454	0.766656	10.3	0.04
943060	0.643584	16.07	0.03	827956	-1.656443	8.77	0.24
757553				5724276	-3.219821	12.81	0.16
743083	0.534358	6.54	0.06	94022	0.787786	9.18	0.04
704537	0.520353	20.15	0.09	741829	0.538595	9.61	0.1
5336686	0.584344	11.23	0.06	2859344	0.357035	8.09	0.05
1226086	0.008623	8.42	0.08	661302	0.84382	12.34	0.17
3121854	0.679529	8.42	0.08	2858149	-0.8013	12.52	0.16
4365930	0.474188	21.16	0.13	3829096	0.258711	18.67	0.06
2918158	0.587352	16.97	0.06	695277	0.503433	14.53	0.04
2766102	0.802168	30.08	0.18	2888260	0.754397	8.17	0.06
15998154	0.007659	27.16	0.08	5085883			
3671746	0.249987	18.68	0.02	2158438			
6024818	0.901384	29.52	0.1	683639	0.682825	7.88	0.06
5740675				4435441	0.798934	13.66	0.02
6617298	0.707565	7.16	0.05	6751296	-0.798021	4.6	33.32
2761386	0.298912	6.11	0.05	15991628	0.936469	19.82	0.02
6824199	0.500856	49.36	0.21	3113707	0.884736	13.01	0.05
3762472	0.965874	8.38	0.07	3131467	0.867685	15.05	0.02
15991225	0.775061	7.25	0.06	15993120	0.512896	12.1	0.03
3275143				3134422	0.885663	50.81	0.2
4377684	0.380518	30.07	0.15	3109159			
2295553				5101675	0.8748	12.06	0.03
3746677	0.857208	9.43	0.07	1368402	0.525012	59.53	0.33
5189170	0.105935	9	0.09	2731017			
15998896	0.771507	12.4	0.13	211447			
5978130	0.229182	11.59	0.03	997968	0.86518	9.95	0.03
1098314				Unknown			
4436435				2337316			
6815125	0.606887	8.87	0.06	2921452			
3287443	0.872562	8.41	0.03				
15998274	0.778275	22.99	0.06				
3799745							
4104558							
4403626	0.428894	10.24	0.05				
3121968	0.679991	18.43	0.21				
3427810	0.064597	10.29	0.06				
4101678	0.046426	16.31	0.05				
3698429	0.328546	41.95	0.31				
Unknown	-0.125463	9.48	0.13				
1716517	-0.349886	11.47	0.05				

APPENDIX A

Cell and Tissue Culture Protocols and Assays

Cell Culture, Counting and Plating

Cell cultures were maintained in a Biosafety Level 2 laboratory. Biosafety hoods with two-way venting were used to prevent contamination of cell stocks and lab personnel. Hoods were sprayed with 70% isopropanol (IPA) and wiped down prior to and following use. Standard personal protective equipment was used, and gloves were sprayed with 70% IPA prior to contact with cell flasks (within incubator or hood). All bottles were sprayed with 70% IPA before placement in hoods. To avoid contamination of cell stocks, containers were not allowed to touch when transferring solutions or media, and all flask or bottle tops were placed top-up when sitting in the hood.

Three cell cultures were maintained in this work: Clone 15 HL-60 lymphoblast cells (ATCC CRL-1964), J774A.1 macrophage cells (ATCC TIB-67) and RAW 264.7 macrophage cells (ATCC TIB-71). Cells were incubated at 37°C, 5% CO₂. All cell lines were grown in RPMI complete media: 10% fetal bovine serum (FBS), 90% RPMI 1640, 100 U/mL penicillin and 100 U/mL streptomycin. Specifically, to every 1 L of RPMI 1640, 100 mL of FBS and 10 mL of a 10,000 U/mL stock of penicillin and streptomycin were added. This growth media was filtered through 0.45 µm pore size Nalgene filters to remove any contaminant bacteria or flora and stored at 4°C.

The murine macrophage-like J774 and RAW cell lines were maintained in a similar fashion. A freezing medium of 95% culture medium and 5% DMSO was used to

freeze down cells at a density of 6×10^6 cells/mL and volume of 1.5 mL. The HL-60 cells, however, were frozen down in 90% FBS and 10% glycerol. In general, if a sample has been pulled up from freeze, is growing healthily in a T75 flask and is at a low passage, more cells should be frozen down from these. Cells are frozen down in 2 mL cryogenic vials. The filled vials are placed in a Nalgene Cryo 1°C Freezing container (VWR 5100-0001) filled with 250 mL of 100% IPA. The container is placed in a -80°C freezer ≥ 4 hours undisturbed; the frozen vials are stored in a liquid nitrogen canister at -196°C.

To pull the cells up from freeze, thaw them rapidly (40-60 seconds) in a 37°C water bath. The neck of the vial should not be submerged in the water in order to prevent contamination. When removed from the water bath, the vials were sprayed thoroughly with 70% IPA. Cells were transferred via a 10 mL RPMI complete media suspension in a 15 mL Falcon centrifuge tube. Tubes were centrifuged at $430 \times g$ for 5 minutes. The supernatant was discarded, and the cell pellet was resuspended in 10 mL RPMI complete. The cells were centrifuged again, the supernatant removed and the pellet resuspended in 10 mL RPMI complete. The cell suspension was transferred to a T-25 flask and placed in the incubator. **J774 and RAW cells should be brought up from freeze every ~45 passages while HL60s should be brought up every ~26 passages (or 52 population doublings).**

All cell lines can be split 2 to 3 times a week as desired. Visual inspection of the cell medium color and cell-to-cell confluency will indicate the need for splitting. The medium contains phenol red which acts as a pH indicator. When the media is “salmon pink” in color, the pH is near 7.4, but as the nutrients from the growth media are

consumed and cell waste accumulates, the color changes to orange. If allowed to persist, the media will turn yellow from the acidity of cell waste and cause cell stress and eventually death. To split the adherent J774 and RAW cells and exchange their media, RPMI complete should be warmed at 37°C (15-20 minutes), the old media poured/aspirated away and enough fresh media added to cover the bottom of the flask (5 mL T25, 10 mL T75 and 20 mL T150) in order to scrape the cells loose from the flask bottom. Then, pipet off the loosened cells and transfer 1-2 mL of these to a new flask with ample fresh media (10 mL T25, 25-30 mL T75 and 50 mL T150). Under the inverted light microscope, these cells will appear as a floating suspension. The remaining cells may be discarded unless they are needed for plated experiments. Since HL-60 cells are non-adherent, 1-2 mL of these non-differentiated cell stocks may simply be transferred to a flask of fresh media as described for the RAWs and J774s but without the need for scraping. A non-differentiated stock of HL-60s must be maintained because they cannot be cultured long-term in their differentiated (neutrophil-like) state.

To differentiate the HL-60 cells, a similar process to splitting is used with the exception that the culture medium in the flask would be 98.7% RPMI complete media and 1.3% sterile, cell-tested DMSO (Sigma). Specifically, 5 mL of cells should be added to a T75 flask containing 25 mL RPMI complete media and 390 µL DMSO followed by incubation. Literature differentiation time is 5-7 days, but no difference was noted between 5 and 7 days for my experiments.

All cell lines were plated similarly. Once cells have been removed in a Falcon tube during splitting, the cells were centrifuged at 430 x g for 5 minutes, the supernatant was discarded and the cells were resuspended in desired media. Twenty microliters of

this cell suspension was placed in an autoclaved microcentrifuge tube (1.5mL) along with 20 μ L trypan blue and mixed by pipetting. The trypan blue is pumped out of live cells, but dead cells retain the dye and appear blue under a light microscope. A hemacytometer with two cell platform grids was used to count these cells (Figure 44).

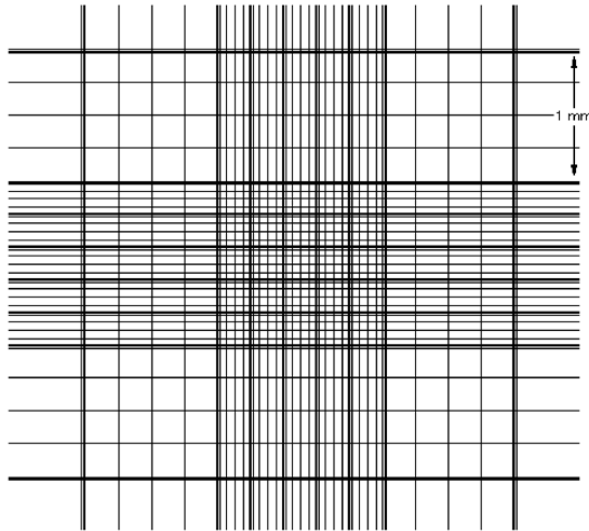


Figure 44 Hemacytometer grid. Live cells were counted in the four corner and center 1x1 mm quadrants of blocks. When cells came to rest on quadrant edges, they were only counted on the top and leftmost border lines.

Ten microliters of the trypan blue and cell mix were added to each platform. The hemacytomer was placed under a light microscope, and live cells were counted in the corner and centermost 1x1 mm grid quadrants. Cells resting along the borders of these quadrants were only counted when they were on the top- and left-most quadrant borders. The total number of cells for the two grids was then used to calculate the cell density of the suspension. For instance, a total of 92 cells would be divided by two (# of grid plates), equaling 46. This number would indicate a density of 4.6×10^6 cells/mL. To dilute this density to say 1×10^6 , simply use the $M_1V_1=M_2V_2$ for common dilutions:

4.6×10^6 cells/mL (5 mL cell suspension) = 1×10^6 cells/mL (V_2). The final volume of the diluted solution would be 23 mL; therefore, 18 mL of media would be used to dilute the 5 mL suspension of cells giving the desired 1×10^6 cells/mL density.

Four types of tissue culture plates were used for experiments: 6-well, 24-well, 96-well plates and 14 mm microwell dishes. The 6-, 24- and 96-well plates were used for cellular assays while the 35 mm MatTek-glass bottom 14 mm microwell dishes were used for cell studies with the confocal microscope. Cell plating for each of these plate types differed in obtaining the optimal cellular confluency (Table 5).

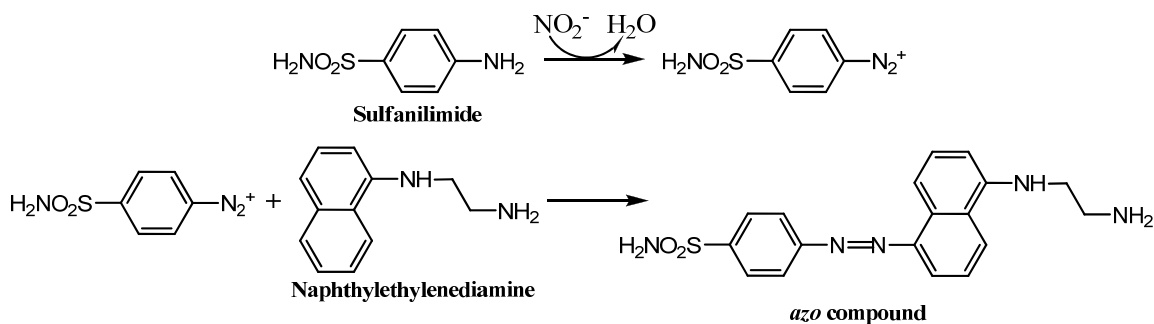
Table 5 Cell Plating Values for Optimal Cell Confluency.

Plate Type	Total Volume (mL)	Cell Density (cells/mL)	Total Cells (cells/well)
6-well	2.0	5×10^5	1×10^6
24-well	0.5	1×10^6	5×10^5
96-well	0.2	5×10^5	1×10^5
14 mm	3.0	5×10^5	5×10^4

Cell suspensions were added to each plate by lightly resting the pipet tip along the side of each well so that the transfer process had a softer impact on the cells. Cell transfer to the MatTek 14 mm microwell dishes was different in that only 100 μ L of a 5×10^5 cells/mL suspension was added to the center of the 14 mm microwell, incubated for 90 minutes and then diluted with 2.9 mL fresh media. This ensures that the cells are concentrated over the coverslip during confocal imaging. Stimulant treatments of plated cells are possible. When adding new stimulants, it is important that the stimulant dose be mixed thoroughly in the media to be applied and that the addition is made along the side of the plate well, avoiding direct impact on the cell layer. Likewise, the pipet tip used to aspirate off media should not make contact with the cell layer.

Griess Assay

The Griess assay is a standard assay⁶³ used to monitor the cellular production of nitric oxide (NO). This measurement is an indirect one since the Griess reaction actually quantifies the concentration of nitrite (NO_2^-), the stable byproduct of NO in the presence of O_2 . The amine group of the sulfanilimide reagent is converted to a diazonium ion upon nitrite addition and loss of a water molecule (Scheme 10). The diazonium ion quickly couples to the naphthylethylenediamine reagent to form an *azo* derivative that absorbs at 540 nm.



Scheme 10 Griess reaction scheme. Nitric oxide is measured in biological systems by measuring the amount of nitrite present. In reaction with sulfanilamide and naphthylethylenediamine, the presence of nitrite leads to the production of an *azo* compound that can be monitored at $\lambda=540$ nm.

This assay was used herein to measure the effects of HZ and polyunsaturated fatty acids on macrophage-like cells' inducible nitric oxide synthase (iNOS) activity. The assay can be used with the macrophage-like RAW and J774 cell lines but not with the neutrophil-like differentiated HL-60s since they are not a significant producer of nitric oxide. To set up this assay, Griess reagents were prepared. A solution of 0.1% naphthylethylenediamine dihydrochloride (NED) was prepared by dissolving 0.1 g of NED (Sigma N-9125, 259.2 g/mol) in 100 mL DI water, and 1.0% sulfanilimide in 5%

phosphoric acid was prepared by dissolving 1.0 g of sulfanilimide (Sigma S-9251, 172.21 g/mol) in 100 mL of 5% phosphoric acid (5 mL concentrated phosphoric acid in 95 mL DI water). Reagents were stored at 4°C in amber bottles for up to 6 months.

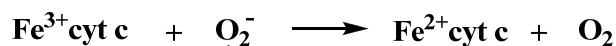
RAW cells were plated in 24-well plates at 1×10^6 cells/mL and allowed to incubate overnight. The media was aspirated, cells were washed lightly with 300 μ L phosphate buffer saline (PBS) containing Ca^{2+} and Mg^{2+} , followed by the addition of 390 μ L media and 10 μ L lipopolysaccharide (LPS) to activate the cells and another 100 μ L of stimulant dosed media. Note: It is important to prepare stimulant doses at 5 times their desired concentration since the final volume in the well will be 5 times that of the dose volume added. Plates were incubated at least 8 hours and the supernatants removed into autoclaved 1.5 mL microcentrifuge tubes and centrifuged at 16.1×10^3 g for 5 minutes to remove any cellular debris. Of the resultant supernatants, 100 μ L was added to clear 96-well plates along with the sequential additions of 50 μ L of sulfanilimide and 50 μ L of NED. After 5 minutes, the plates were read at $\lambda=540$ nm.

A standard curve of sodium nitrite (NaNO_2) was used to quantify the concentration of nitrite in the cell supernatants. A serial dilution of NaNO_2 was prepared from a stock solution of 100 mM (6.9 mg in 1.0 mL DI water) and diluted to ranges of 0-100 μ M.

Cytochrome C Superoxide Assay

The cytochrome c superoxide assay measures the classic reduction of cytochrome c by superoxide reactive oxygen species (ROS) in the presence and absence of anti-oxidant superoxide dismutase (SOD).¹⁰² The addition of SOD enables the

scavenging of extracellular superoxide when oxidative stress is induced. Differentiated HL-60 (neutrophil-like) cells were used in order to monitor the effects of a pro-oxidant 4-hydroxy-2-nonenal (HNE) on the nicotinamide adenine dinucleotide phosphate (NADPH) oxidase pathway of activated phagocytes. NADPH complexes within the mitochondrial membrane act as the major sources of ROS production during oxidative stress, serving as electron donors to cellular oxygen. In the presence of superoxide, ferric cytochrome c can be reduced to its ferrous state therefore oxidizing the ROS back to molecular oxygen (Scheme 11).



Scheme 11 Cytochrome c reduction by superoxide. Superoxide generated during phagocyte activation acts as an electron donor, reducing ferric cytochrome c to its ferrous state. The ferrous state absorbs at $\lambda=550$ nm and can be monitored spectroscopically as a measure of oxidative stress.

It is the ferrous form of the cytochrome c that can be monitored spectroscopically at 550 nm. Therefore, when SOD is added to solution, the extracellular superoxide is scavenged by the SOD and ferric cytochrome c is not reduced resulting in minimal absorbance change. The use of SOD in this assay ensures that the reduction of the cytochrome c observed is in fact due to superoxide.

This assay was carried out in sterile black 96-well clear bottom plates. A series of HNE dilutions were prepared from a 64 mM stock and added to each well to produce a concentration response curve ranging from 0-1 mM. The appropriate HNE dilutions were prepared in RPMI phenol red-free media and added to each well (x8). These additions were followed by a 50 μL volume of 2×10^6 cells/mL in phenol red-free media to each well ensuring a total cell count of 1×10^5 cells/well and incubated 3 hours. SOD

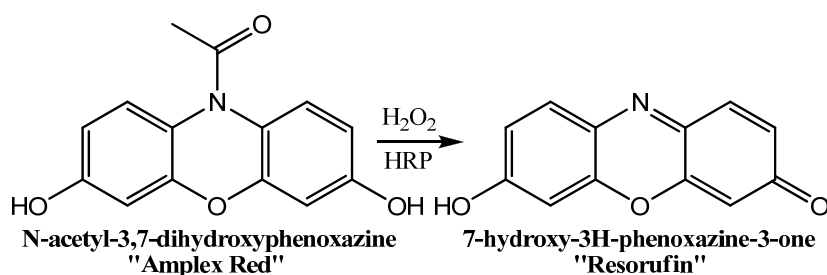
treated and SOD deprived reaction mixtures were then added to the wells (4 each of the 8 HNE doses). A 320 μM cytochrome c solution (64 mg in 16 mL Hank's Buffer Saline Solution (HBSS)) was made and 60 μL of 8.1 mM (5 mg/mL stock in 20 μL DMSO stored at -40°C) phorbol 12-myristate-13-acetate (PMA) added for a final solution concentration of 32 μM . PMA is a preferred pharmacological stimulant because it bypasses cell surface receptors and induces direct activation of NADPH oxidase, generally making stimulation quicker and more prominent. This 16 mL solution was then divided in two, and to one solution, 80 μL of 10,000 U/mL SOD (4 mg SOD in 500 μL HBSS) was added. Each HNE concentration then received 150 μL of each of these reaction mixtures (4x). The plate was incubated 37°C for 30 minutes, read at $\lambda=550$ nm and the concentration of superoxide calculated using a molar absorptivity constant of $2.1 \times 10^4 \text{ M}^{-1} \text{ cm}^{-1}$.

Physiological stimulants were also attempted with this assay; including zymosan (protein-carbohydrate complexes from the *Saccharomyces cerevisiae* cell wall), zymosan activated serum (ZAS, or zymosan incubated with FBS), opsonized zymosan particles (OZP, particulate from ZAS preparation) and N-formyl-methionyl-leucylphenylalanine (fMLP, oxidase activation via formyl-peptide receptors). These stimulants were prepared as follows and added to the 16 mL reaction mixture in the place of PMA. Zymosan was prepared at 2 mg/mL, or 32 mg per 16 mL solution. ZAS and OZP were prepared by incubating zymosan in FBS at 10 mg/mL 1 hour at 37°C and centrifuged at $2,000 \times g$ for 10 min. The supernatant and pellet were separated and heated at 56°C for 1 hour to inactivate endogenous alkaline phosphatase. The supernatant was the 10 mg/mL ZAS, and 3.2 mL of this was added to the 16 mL reaction solution for a final 2 mg/mL density.

The 150 mg pellet was OZP and was further washed in HBSS twice before resuspending in 5 mL of HBSS. A 2 mg/mL reaction solution was prepared by adding 1.07 mL of the OZP mixture. The fMLP was used at 32 μ M by adding 0.22 mg of the powder to the 16 mL reaction solution.

Amplex Red Hydrogen Peroxide Assay

The amplex red assay is a sensitive fluorescence assay used to measure hydrogen peroxide.²²³ The 96-well microplate assay is capable of detecting 5 pmol of hydrogen peroxide per 100 μ L sample. This assay was used herein to measure extracellular levels of hydrogen peroxide produced by differentiated (neutrophil-like) HL-60 cells upon stimulation with PMA and inhibition with HNE. In the assay, horseradish peroxidase (HRP) catalyzes the de-N-acetylation and oxidation of Amplex Red. In the presence of hydrogen peroxide, Fe(III)-HRP is oxidized to its Fe(IV) state as seen in the equation: $\text{Fe(III)-HRP} + 2\text{H}_2\text{O}_2 \rightarrow 2\text{H}_2\text{O} + \text{O}_2 + \text{HRP}^{\bullet}\text{-Fe(IV)} + 2\text{e}^-$. In turn, the reductant substrate, amplex red, is oxidized to its fluorescent derivative, resorufin (Scheme 12).



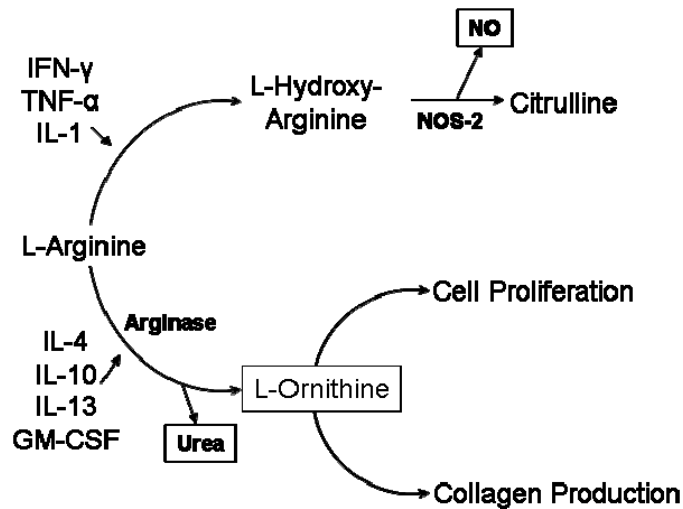
Scheme 12 Amplex red oxidation to fluorescent resorufin. In the presence of hydrogen peroxide, horseradish peroxidase catalyzes the de-N-acetylation and oxidation of amplex red to resorufin. This fluorescent product excites at 530/25 nm and emits at 590/35 nm, enabling an indirect measurement of hydrogen peroxide levels.

This fluorescence assay provides a sensitive method to monitor ROS production during oxidative stress and specifically, the measurement of hydrogen peroxide levels.

Coupled with the cytochrome c superoxide assay described previously, these assays provide a precise means of evaluating the effects of HNE on phagocyte function through the NADPH oxidase pathway. The assay was conducted on 5-day differentiated HL-60 cells. To sterile, black 96 well clear bottom plates, 20 μL of 7.5×10^5 cells/mL were added in phenol red-free RPMI 1640 for a total cell count of 1.5×10^4 cells/well. HNE 30 μL serial dilutions were added resulting in a final concentration range of 1 nM-100 μM and incubated 3 hours. A 10 mL reaction mixture was prepared in Krebs Ringer phosphate buffer (KRPB) of 20.5 μL of 7.81 mM PMA (final 16 μM), 50 μL of 10 mM amplex red (final 50 μM) and 100 μL of 10 U/mL HRP (1.68 mg in 50 mL KRPB) (final 0.1 U/mL). This mixture was added to each reaction well at a volume of 100 μL and incubated 30 minutes. Samples were excited at 530/25 nm and their fluorescence read at 590/35 nm. A 0-5 μM standard curve of hydrogen peroxide was prepared for quantitation.

Alternatively Activated Macrophages

Alternatively activated macrophages (AAMs) were attempted in murine RAW 264.7 cells.^{224,225} Activated macrophages are used to study innate immune responses while AAMs provide a model to study humoral immunity including repair processes. Macrophages possess two inducible enzymes, arginase and nitric oxide synthase-2 (NOS-2) (Scheme 13). Nitric oxide from the NOS-2 pathway was measured as described by the Griess assay when cells were challenged with LPS, a potent endotoxin that elicits the secretion of several pro-inflammatory cytokines. To study the arginase pathway, RAW cells were plated in 6-well plates at 1×10^6 cells/well (2 mL of 5×10^5 cells/mL RPMI complete media) and incubated overnight. Media was then aspirated and replaced by



Scheme 13 Th1 and Th2 stimulant response pathway in macrophage cells. Macrophages have two inducible enzymes where arginine is the substrate: arginase and NOS-2. Measurements were attempted of products highlighted by square borders. The top-most Th1 response was induced by LPS challenge and the bottom-most Th2 response was induced by ILs-4, 13 and 21.

Dulbecco's modified eagle medium (DMEM), low glucose 1X, 1 g/L D-glucose, L-glutamine, 110 mg/L sodium pyruvate, 1% FBS and 1% penicillin, streptomycin. Cells were incubated 20 hours. Media was aspirated and washed twice with PBS (without $\text{Ca}^{2+}/\text{Mg}^{2+}$). DMEM (2 mL) was added again but without FBS supplement. Cells were dosed with interleukins 4, 13 and 21 (IL-4, 13, 21) from 1-40 ng/mL, rotated by hand and incubated 48 hours. Measurements of arginase activity were attempted by monitoring the conversion of arginine to ornithine.

Cells were harvested and lysed with lysis buffer containing 0.5% triton solution with trypsin-chymotrypsin inhibitor (0.1 mg/mL), leupeptin (0.05 mg/mL), aprotinin (0.05 mg/mL) and pheynylmethonylsulfonyl fluoride (PMSF, 0.2 mM). After lysis, 25 μL of 10 mM MnCl_2 was added to 25 μL of lysate from each IL sample. Samples were incubated at 55°C for 20 minutes. Carbonate buffer (150 μL of 0.1 M) was added to each sample. Half of the samples received 50 μL of 100 mM L-arginine, incubated at 25°C 1

hour and the reaction stopped with addition of 750 μL of glacial acetic acid. A 250 μL aliquot of 2.5 g/L ninhydrin solution (in ethanol) was added to all samples and brought to a boil for 1 hour. Ornithine production was measured at 560 nm. Significant distinction between control and experimental samples was not established.

Measurement of urea levels was then attempted as previously described.^{226,227} In these experiments, RAW cells were plated in 96-well plates at 5×10^5 cells/well (200 μL of 2.5×10^6 cells/mL). Cells were incubated overnight. IL-21 was added to each well (0.4 μL of 10 $\mu\text{g/mL}$ stock, final density of 20 ng/mL) and incubated 6 hours. ILs-4 and -13 were added to the appropriate wells and incubated 6 hours. Cells were washed 3 times with PBS and lysed with 50 μL 0.1% Triton X-100 (15 μL of 10% Triton X-100 in 1.5 mL PBS, 1 protease inhibitor cocktail tablet). The plates were rotated 15 minutes at 4°C.

Aliquots of 50 μL of 10 mM manganese chloride and 50 mM TrisHCl, pH 7.5 (1.5 mL and 750 μL) were added to each well and incubated at 55°C for 10 minutes. Afterwards, 25 μL lysate was added to a new plate and wells already containing 25 μL of 0.5 M arginine (0.13065 g Arg in 1.5 mL 0.1 M sodium bicarbonate), pH 9.7. The plates were incubated at 37°C for 1 hour. A 100 μL solution of 1 sulfuric acid: 3 phosphoric acid: 7 water (v:v:v) was added to stop the reaction. An aliquot of 25 μL 9% (w/v) ISPF (α -isonitrosopropiophenone) in ethanol was added and incubated at 95°C for 3 hours. The absorbance of the samples was measured at 540 nm after cooling for 10 minutes. A 0-12 mM calibration curve of urea was treated in the same manner. Again, no significant distinction between control and sample wells was observed.

APPENDIX B

Schistosomiasis Study Protocols

Murine Model Infection

All stages of the *Schistosoma mansoni* life cycle are maintained at the Biomedical Research Institute in Rockville, Maryland, USA.⁶¹ There, cercariae were collected from *Biomphalaria glabrata* snail hosts and counted. Desired dilutions were made within 5 hours, and Swiss Webster mice were infected with 150 cercariae per mouse. To do this, mice were placed in individual plastic restraining tubes (Figure 45A). Their tails were positioned through the tube bottom and taped securely (Figure 45B). The restraining

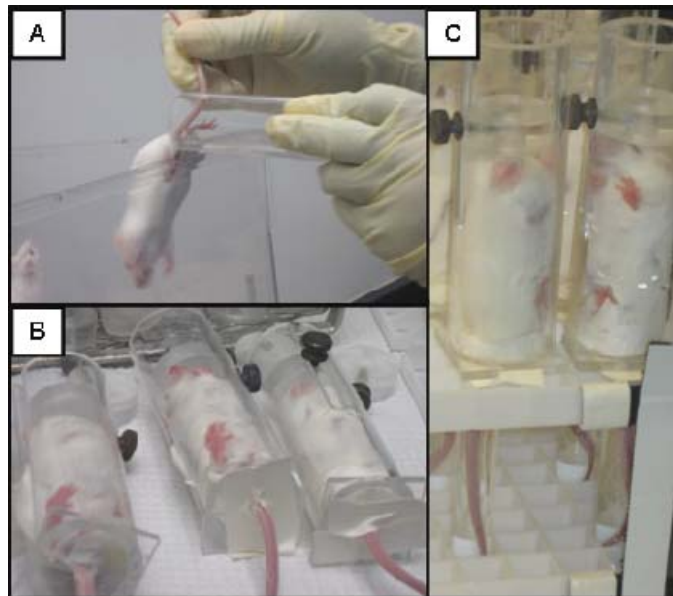


Figure 45 Percutaneous tail infection of Swiss Webster mice with *S. mansoni* cercariae. (A) Mice were placed in plastic restraining tubes. (B) Mouse tails were extended from the restraining tube bottoms and held in place by adhesive tape. (C) Mice restraining tubes were inverted over an exposure rack with *S. mansoni* cercariae dilution test tubes. The mice were infected via painless percutaneous tail exposure for 1 hour.

tubes were then inverted over an exposure rack containing 12 x 75 glass test tubes with the cercariae dilutions (Figure 45C). An absorbent kimwipe in each tube prevented mouse urine from reaching and killing the cercariae in the test tubes below. Mouse tails were wiped clean with water and then inserted into the cercariae dilutions for a 1 hour exposure time. Mice were removed from their tubes and placed back in their cages until desired time of schistosome collection. Cercariae infection numbers were estimated by staining the cercariae remaining in the test tubes with iodine and counting the stray bodies and tails under a light microscope.

Observed Disease Progression

Mice were evaluated at weeks 4, 5, 6, 7 and 8 p.i. and compared to uninfected controls. The abdomens of infected mice were observed to grow rotund as expected with the progression of the disease. A distended abdomen is characteristic of schistosomiasis infection. In severe chronic cases, portal shunts can be seen from the chest cavity to the abdomen as liver function and hence blood flow is dangerously reduced. Although, abdominal circumference was visually estimated to grow 23% (3.5 in. to 4.5 in.), mouse weight remained constant at ~30 g. Upon dissection, uninfected controls were found to contain healthy pink tissue, but infected mice were found to have larger, darker livers and spleens. Furthermore, the abdominal cavity was primarily taken up by the infected liver and spleen by weeks 7 and 8 p.i. (Figure 46).

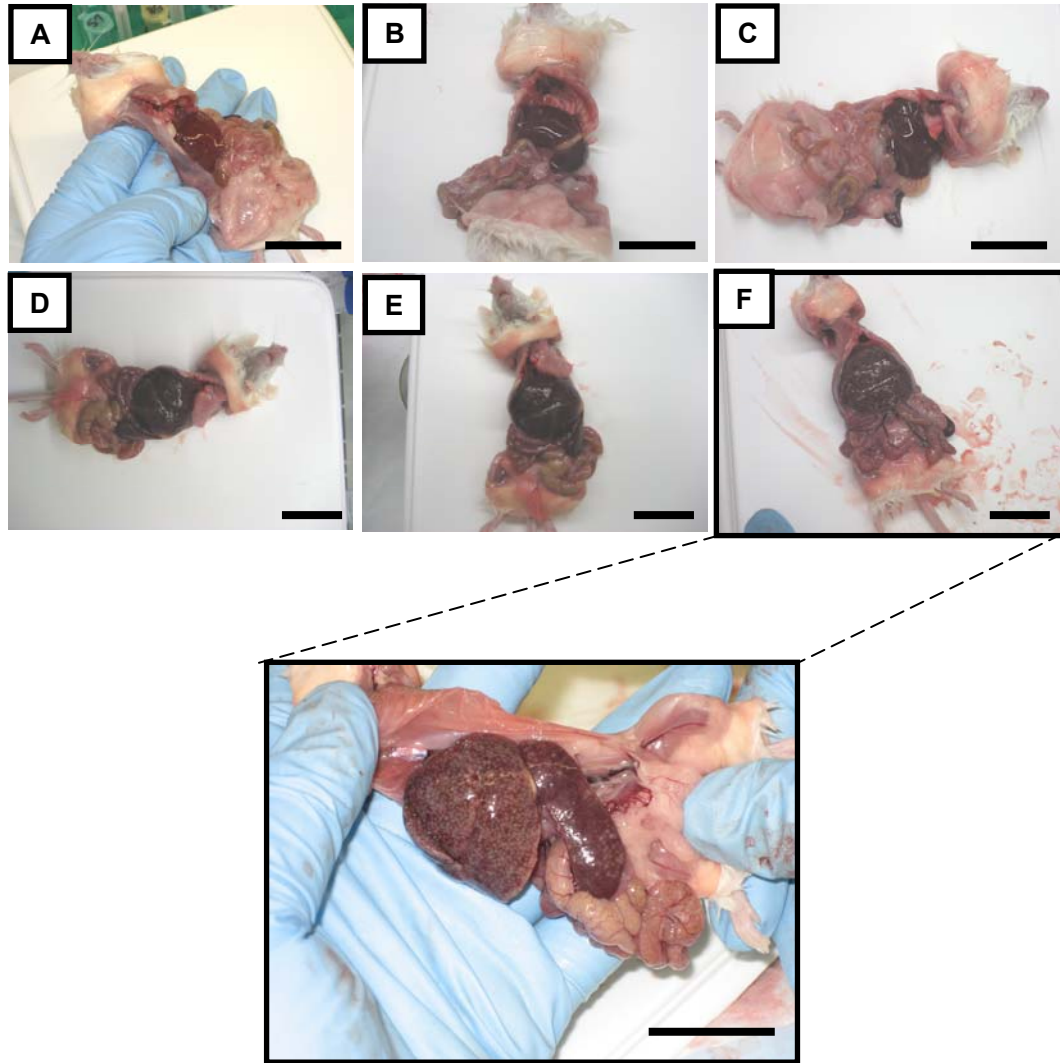


Figure 46 Increase in abdominal circumference in disease progression. Abdominal circumference of mice was observed to increase 23% progressively from (A) uninfected mice through weeks (B) 4, (C) 5, (D) 6, (E) 7 and (F) 8 p.i. Black scale bars are 5 cm.

Schistosome Perfusion

Schistosoma mansoni reach sexual maturity at 5½ to 6 weeks post-infection. Therefore, adult schistosomes are generally collected 6 to 7 weeks post-infection. The adult schistosomes reside in the hepatic portal vein, and perfusion of the descending aorta is used to extract them. First though, mice were weighed and euthanized with a 65 mg/mL sodium pentobarbital solution prepared from a 260 mg/mL stock of the controlled

substance Sleepaway. A 25 mL solution was prepared for the euthanasia of 60 mice. This solution included 2.5 mL of 260 mg/mL Sleepaway, 0.5 mL of 10 kU/mL heparin and 22 mL of sterile water. Each mouse received a 0.3 mL intraperitoneal injection of the pentobarbital solution with a 25_G^{5/8} syringe. After 30 minutes, mice were confirmed dead by toe pinch. The mice were then dipped in warm water and their coats smoothed. Scissors were used to make an incision through the abdomen coat, and the fur was removed from the abdominal and thoracic cavities. Mice were again submerged in warm water and another cut made to open the abdomen. The diaphragm was cut, and the ribs

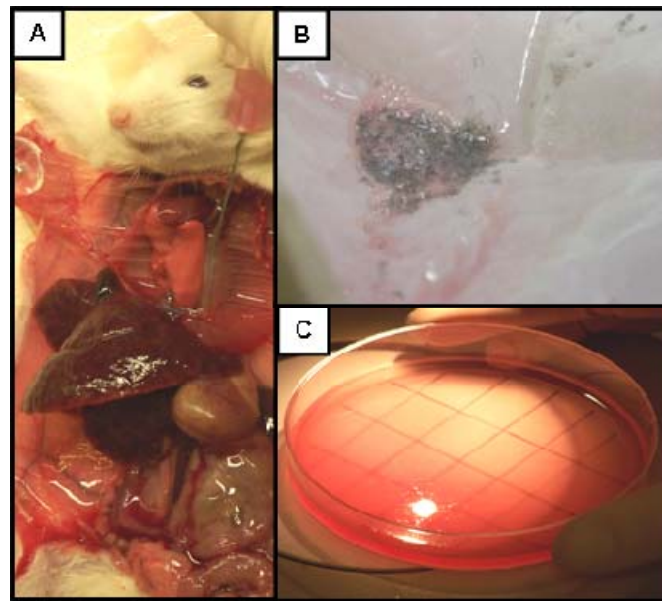


Figure 47 *S. mansoni* collection from infected Swiss Webster mice. (A) A 20_G needle was used to perfuse the descending aorta. (B) Adult schistosomes were collected on a mesh screen in order to wash away red blood cells. (C) Worms were counted in a grid-laden Petri dish and separated by gender.

of the left half thoracic cavity were severed. Below the liver, the hepatic portal vein was severed, and a 20_G needle attached to a peristaltic perfusion pump was inserted in the descending aorta, carefully avoiding completely puncturing the aorta and losing pressure (Figure 47A). Perfusion fluid (7.5 g trisodium citrate dihydrate and 8.5 g sodium

chloride per 1 L sterile water) was used to perfuse the schistosomes from the hepatic portal vein. The abdomen and intestines were carefully washed to ensure that all schistosomes were collected in the designated pan.

The infected livers and spleens were collected, weighed, wrapped in labeled aluminum foil, frozen in liquid nitrogen and stored at -80°C . The worms collected were washed onto a construction grade mesh screen and washed with perfusion fluid until no tissue, fur or red blood cells were visible (Figure 47B). Finally, the worms were placed in a gridded Petri dish (Figure 47C), separated by gender, counted, placed in cryo-tubes, frozen in liquid nitrogen and stored at -80°C .

Hemozoin Isolation

SmHZ was isolated from adult schistosomes by thawing frozen worms and adding them to an autoclaved 15 mL glass homogenizer and homogenizing into a homogenous mixture. The mixture was centrifuged at $1000 \times g$ for 1 minute and the supernatant containing the HZ removed. This process was repeated twice. The final supernatant was centrifuged at $5445 \times g$ for 2 hours. This supernatant was discarded and the precipitate resuspended in 10 mL of 150 mM phosphate buffer, pH 7.4. The mixture was centrifuged at $5445 \times g$ for 1 hour. The supernatant was discarded, and the dark brown precipitate was purified as described below.

SmHZ was also isolated from the livers and spleens collected. Organs were homogenized using hand-held electric homogenizer in a total of 50 mL deionized water. The solutions were centrifuged at $1,000 \times g$ for 2 minutes to remove some of the cellular debris. The supernatant was centrifuged at $5445 \times g$ for 2 hours. The supernatant was

discarded, and 1 mL of 150 mM phosphate buffer was added lightly. The pellet (two shades: lighter is tissue and darker is HZ) was vortexed gingerly to loosen the lightly colored tissue from the dark bottom pellet, and the supernatant was poured away. A series of 1:1 phosphate buffer and ethyl acetate washes (1 minute centrifugations at 1,000 x g) were repeated until the supernatant was clear. The HZ was further purified and quantified as described by Chen and coworkers.¹¹⁴

Briefly, the precipitate was resuspended in 5 mg/mL Proteinase K buffer (as purchased in Vanderbilt Core) and incubated at 37°C overnight. The pellet was washed 3 times with 2% SDS. The final pellet was resuspended in 6.0 M urea and incubated 3 hours at 37°C in a shaking water bath set at 80 rpm. The sample was again washed 3 times with 2% SDS, followed by 8 DI water washes. All purification washes as described were centrifuged at 16.1×10^3 g for 5 minutes.

The water suspension of the final wash was used to quantify the amount of HZ isolated by removing 10 μ L of the suspension and adding it to 990 μ L of 20 mM NaOH, 2% SDS. This solution sat at room temperature for 1 hour and its absorbance was measured at 400 nm, $\epsilon = 1 \times 10^5 \text{ M}^{-1} \text{ cm}^{-1}$. Beer's law was used to calculate the concentration of HZ in solution, and the final mass was determined by using the molar ratio of heme and HZ reported previously (25 μ g HZ/ 20 nmol heme).⁶² The final HZ pellet was blown dry under argon gas and stored under desiccant at -20°C.

Thromboxane Assay for Mouse Urine

Mouse urine was collected by bladder massage from uninfected (C), 4-, 5-, 6-, 7- and 8-weeks post-infection mice. Thromboxane levels in the urine samples were

measured as another measure of oxidative stress during infection. The assay measured the presence of 11-dehydro thromboxane B₂ (TxB₂) (Figure 48) using an internal

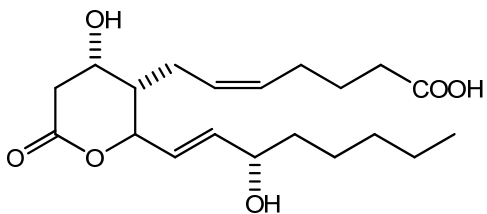


Figure 48 Structure of 11-dehydro-thromboxane B₂ (TxB₂).

standard of D₄-11-dehydroTxB₂. TxB₂ is the stable metabolite of the deleterious proaggregatory vasoconstrictor, thromboxane A₂ (TxA₂). Elevated levels of TxA₂ and hence TxB₂ have been found in tissues where arachidonate and its metabolites are upregulated, such as in inflammation and endotoxic shock.²²⁸ Therefore, an assay for TxB₂ was carried out as a measure of inflammation as it correlates to the lipoxidation of arachidonic acid. The assay was carried out as follows. A separate sample (100 μL urine and 150 μL DI water) from the assay was sent to the Vanderbilt comparative lab for creatinine levels. The internal standard D₄-11-dehydroTxB₂ (3 ng) was added to a tube of 3 mL pH 3.0 water and vortexed. A sample of urine (840 μL) was then added and vortexed. The sample acidity was adjusted to pH 3.0 with 1 N HCl (250 μL). A C18 SepPak column was preconditioned with 5 mL methanol followed by 5 mL of pH 3.0 water. The sample was loaded onto the column, rinsed with 10 mL of pH 3.0 water, then 10 mL 20% methanol (in pH 3.0 water) and finally eluted with ethyl acetate into a scintillation vial. The sample was dried over 1 scoop of sodium sulfate, transferred to a reactivial and dried under nitrogen gas. Methanol (25 μL) was added and vortex. The residue is not soluble. An addition of 400 μL pH 3.0 water and 5 μL 1 N HCl was made,

vortexed and the pH kept below 3.0. The sample was allowed to sit at room temperature for 30 minutes.

Extraction was made with 1 mL of ethyl acetate, transferred to a microcentrifuge tube, dried and reconstituted in 50 μ L ethyl acetate. A TLC plate was run in 97 ethyl acetate: 3 acetone: 2 acetic acid using 5 μ L prostaglandinD₂ (PGD₂) free acid as a standard. Bands were run to 13 cm (reference should be 0.40 cm) and scraped 1 cm on each side. Another 1 mL extraction of ethyl acetate was made. The extract was transferred to a glass vial and dried under nitrogen and pentafluorobenzylbromide (PFBB) at 37°C for 20 minutes. An addition of 40 μ L PFBB (in 10% acetonitrile) and 20 μ L of diisopropylethylamine (DIPE) (in 10% acetonitrile) was made, evaporated under nitrogen and reconstituted in 50 μ L ethyl acetate. Another TLC plate was run in 60 ethyl acetate: 40 heptane using 5 μ g PGD₂-PFBB ester as a standard. Bands were run 13 cm (reference should be 0.23 cm) and scraped 1.3 cm below center of band to 0.7 cm above center of band.

A 1 mL ethyl acetate extraction was made, dried and silylated with 20 μ L bis(trimethylsilyl)trifluoroacetamide (BSTFA) and 10 μ L of dimethylformamide (DMF). Samples were incubated at 37°C for 10 minutes. The samples were then dried and reconstituted in 10 μ L undecane when ready to run GC-MS analysis. Injections of 1-2 μ L were made and tracings were smoothed x1. A 15M DB 1701 column was used, monitoring 511-515, 190°-300°C, 20°C per minute, and a retention time of 9-10 minutes was seen. Normal human urine TxB₂ levels are 370 \pm 137 pg/mg of creatinine.

The TxB₂ levels for each week of the time study were measured, where N=1 (Figure 49). Small sample volumes and the lack of uniform sampling per mouse limited the accuracy and precision achieved with this assay. As schistosomes matured during

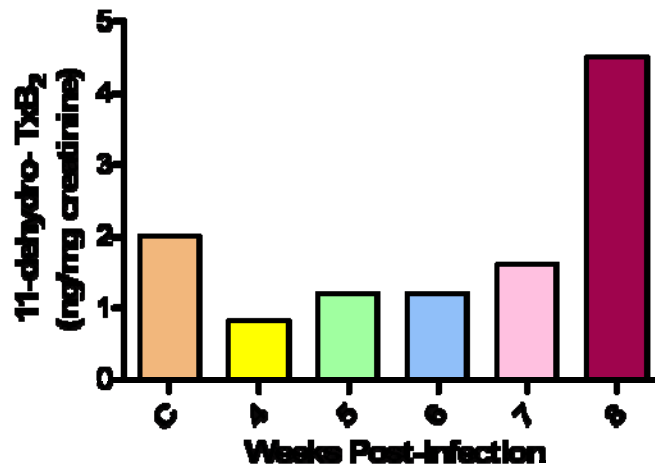


Figure 49 Mouse urine 11-dehydro-thromboxane B₂ levels during *S. mansoni* infection. Urine samples were collected from uninfected (C), 4-, 5-, 6-, 7- and 8-week post-infection mice. TxB₂ levels were measured (N=1) using a D₄- internal standard in GC-MS analysis and normalized to urine creatinine levels.

infection, more eggs would be expected to accumulate in the liver, causing the formation of fibrotic granulomas and an increase in tissue inflammation. HZ formed by adult worms would also be expected to accumulate over time, contributing to the lipoxidation of fatty acids and the upregulation of arachidonate metabolites.

Anti-HNE Immunostaining of Thin Tissue Sections

Thin tissue sections (5 μm thick) were taken of the livers and spleens collected from uninfected, 4-, 5-, 6-, 7- and 8-weeks post-infection mice. The sections were made by the Vanderbilt University Immunohistochemistry Core. Hemotoxylin and eosin (H&E) stains of these tissues were made by the core. Anti-HNE stains were made in my

lab using a similar method as referenced in previous literature.¹⁴⁹ Each slide obtained from the core had 2 tissue sections. For each sample treatment, a coverslip was used to uniformly cover the entire section (liquid tended to bubble over the paraffin-section). The R&D systems HRP-AEC System Cell and Tissue Staining kit was used, along with the R&D systems monoclonal anti-4-hydroxynonenal primary antibody. A 100 µg order of antibody was placed and was reconstituted in 4 mL sterile PBS (without Ca²⁺ or Mg²⁺) and then stored in 100 µL aliquots at -40°C. These aliquots are stable for 6 months. Specifically, the staining procedure was as follows:

Samples were covered with 2 drops of peroxidase blocking reagent for 5 minutes. The samples were rinsed with PBS (without Ca²⁺ or Mg²⁺) and then washed in PBS for 5 minutes. Washes must be gentle since hydrogen peroxidase may loosen the tissue sections from the slide. Samples were incubated with 2 drops of serum blocking reagent for 15 minutes. Slides were drained and excess blocking reagent was wiped away (no PBS rinse here). Samples were incubated with 2 drops of avidin blocking reagent for 15 minutes. Samples were rinsed with PBS, the slides drained and excess buffer wiped away. Samples were incubated with 2 drops of biotin blocking reagent for 15 minutes. Slides were rinsed again with PBS, drained and excess buffer wiped away. Samples were incubated at 37°C with primary antibody (25 µL of the 25 µg/mL stock) for 1 hour. The sample was rinsed with PBS and washed 3 times at 15 minute increments. Slides were drained and excess buffer was wiped away. Samples were then incubated at 37°C with 2 drops of biotinylated secondary antibody for 1 hour. The sample was rinsed with PBS and washed 3 times at 15 minute increments. Slides were drained and excess buffer was wiped away. Samples were incubated at 37°C with 2 drops of HSS-HRP for 30 minutes.

Slides were rinsed with PBS and washed 3 times at 2 minute increments (used pipet tip box lid and rotator to do this). Slides were drained and excess buffer removed.

The total volume of AEC chromagen needed for the entire reaction was calculated (20 μ L AEC chromagen in 480 μ L chromagen buffer, vortex). Two drops of freshly prepared AEC chromagen was added to the slides using small transfer pipets and incubated at 37°C for 1½ hours. The slides were rinsed with DI water and washed for 5 minutes (used pipet tip box lid and rotator to do this). Aqueous mounting medium (2 drops) was used to slowly and evenly position new coverslips over stained section, paying careful attention not to trap air bubbles over the samples. The slides were allowed to dry extensively. Samples were imaged on an Olympus BH2-RFCA light microscope with Olympus DP70 camera and DP controller software.

APPENDIX C

β -Hematin Assay Protocols

Dehydrohalogenation β -Hematin Synthesis

BH was prepared according to the dehydrohalogenation Bohle-Madsen method.³⁵ In three 240 mL round bottom flasks, 0.3 g of hemin chloride (Fluka $\geq 99.8\%$) was weighed out and a stir bar added. The flask neck was covered with a kimwipe held in place by a rubber band. Flasks were taken into a glovebox along with 3 24/40 glass stoppers, 3 pieces of 6 in. electrical tape and 3 pieces of aluminum foil to cover flasks completely. While stirring, 5.0 mL of 2,6-lutidine was added. In a graduated cylinder, 25 mL of DMSO and 25 mL of anhydrous methanol were mixed and added to the stirring flask. After 1 minute, stirring was stopped, and the flask was stoppered. The stopper was sealed with the electrical tape, and the flask was covered with aluminum foil. The flasks were stored in the glovebox 3 months.

Final products were removed from the glovebox and filtered on 0.45 μm filter paper. Samples were rinsed with methanol until filtrate was clear. Rinses continued with DI water. The sample was scraped from the filter paper and placed in a 50 mL centrifuge tube along with 25 mL of methanol, vortexed and centrifuged at 5445 x g for 30 minutes. Alternating washes of DI water and 0.1 M bicarbonate buffer, pH 9.0 were repeated until the absorbance of water supernatants were $<1 \times 10^{-2}$ at $\lambda=400$ nm (generally 3 months of daily washes following glovebox removal). Bicarbonate washes were rotated at room temperature for 1 hour while DI water washes were immediately centrifuged. Final

products were characterized by XRD, FT-IR and SEM and stored in the dark, under vacuum and desiccant. Since the faces of the crystal may degrade over time, the integrity of the stored sample may be tested by reading the absorbance of the sample in bicarbonate buffer. If an absorbance is observed, the crystal has degraded and should not be used for experiments.

Crystal Extension Assay

A BH crystal growth assay is used in which preformed BH seeds the extension of the BH aggregate with addition of hemin.¹⁸⁹ Since BH is used to seed further crystal growth, quantification of assay-formed BH requires a mass balance adjustment for the BH initially added to the assay. Drug concentrations in the range of 0-10 μM were effective in inhibiting the assay's aggregation of BH formation (Figure 50). Concentration-response curves were used to plot data from the assay, and IC_{50} values of 1.58 μM amodiaquine and 3.29 μM chloroquine were obtained, similar to those reported previously.¹⁸⁹ The Z' values for this assay range from 0.792 to 0.872, indicating its potential for use as a high throughput screen.

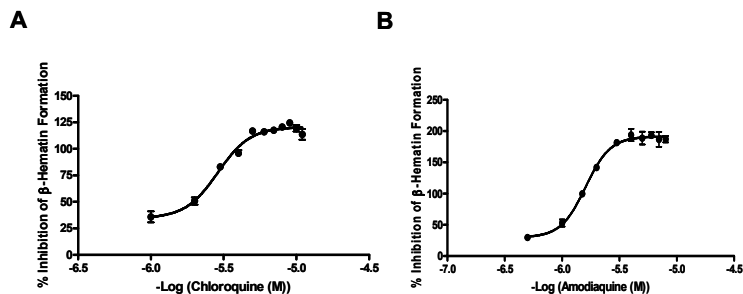


Figure 50 Concentration response curves from the BH crystal extension assay. (A) Chloroquine and (B) amodiaquine were evaluated for their IC_{50} concentrations in an assay of extension of BH growth from a preformed crystal.

A BH crystal extension assay was adapted from previous description.¹⁸⁹ A 25 mM hematin stock solution was prepared by dissolving hemin in DMSO and filtering through a 0.22 μm PVDF membrane syringe driven filter unit. From this solution, a 222.2 μM hematin stock solution was prepared in 0.1 M ammonium acetate solution. To each well, final concentrations of 50 μM hematin stock solution, 10 nmol preformed BH¹⁹⁰ and 0-10 μM antimalarial were incubated in clear, 384-well plates at 37 °C in a Thermo water bath and shaken at 40 rpm for 16 h. The plates were centrifuged in a Beckman Coulter AllegraX 22R, S2096 rotor, at 25 °C for 1 h at 1100 x g. Supernatant was removed and 0.15 M sodium bicarbonate, 2% SDS was used to dissolve free heme in the mixture. The plate was centrifuged again for 1 h and the supernatant removed. The remaining BH pellet was dissolved using 0.36 M NaOH, 2% SDS and its absorbance read at 400 nm.

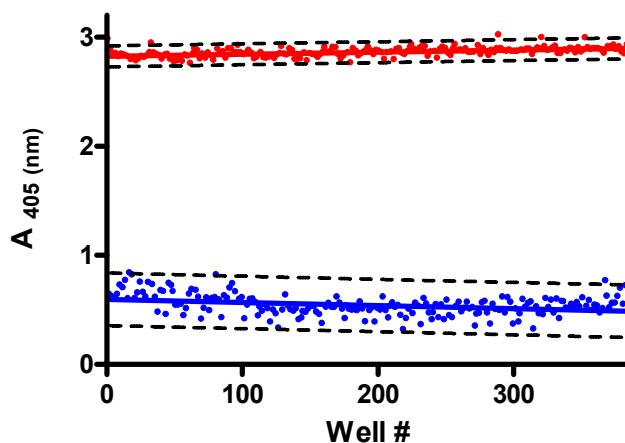


Figure 51 Cross validation of the BH crystal extension assay. The BH crystal extension assay was cross validated with checkerboard controls of (red) potentiator of amodiaquine at 10 μM and (blue) vehicle assay substrates. The assay had a strong Z' value of 0.8409.

Checkerboard cross validation experiments were carried out with this assay in order to provide a secondary assay for follow up confirmation of the preliminary hits from the NP-40 mediated BH crystallization assay (Figure 51). Confirmation of hits in this assay would ensure that the hits from the NP-40 assay were in fact targeting the heme surface rather than generating potential false positives from stronger interactions with the lipophilic detergent NP-40.

Lipid-Mediated Crystallization Assay

While the precise *in vivo* mechanism of HZ biomineralization is unknown, new evidence suggests that lipid-rich environments can act as templates for HZ crystallization. *In vitro* lipid-initiated BH crystallization was reported by Egan and coworkers using various glycerols.²²⁹ In a recent study, transmission electron microscopy (TEM) showed the localization of SmHz at the hydrophilic-hydrophobic interface of lipid droplets in the *S. mansoni* gut lumen.⁶⁴ Similarly, Pisciotta and coworkers proposed that neutral lipid nanospheres were the sites of HZ formation within the digestive food vacuole of *P. falciparum*.²³⁰ In both cases, lipid extracts from each organism provided a competent scaffold for HZ formation *in vitro*.^{64,230} Using the individual as well as the ratio of glycerols with the BH assay reported by Pisciotta *et al.*, we repeated the assay with a similar IC₅₀ value of 21.9 μ M for chloroquine. We also tested amodiaquine and found an IC₅₀ of 27.3 μ M (Figure 52). The resultant BH product was measured. This assay's Z' factor range of 0.602-0.755 demonstrates its suitability for high throughput screening.

Lipid mediated BH formation was adapted from previous description.²³¹ A 25 mM hematin stock solution was prepared by dissolving hemin (\geq 98%, Sigma-Aldrich, St.

Louis, MO) in DMSO and filtering through a 0.22 μm PVDF membrane syringe driven filter unit. From this solution, a 222.2 μM hematin stock solution was prepared in 0.2 M ammonium acetate solution. Lipids (1-Stearoyl-rac-glycerol [MSG]; 1,2-Dipalmitoyl-rac-glycerol [DPG]; 1,2-Dioleoyl-rac-glycerol [DOG]; 1,3-Dilinoleoyl-rac-glycerol [DLG]; or 3-Palmitoyl-sn-glycerol [MPG]; Sigma-Aldrich, St. Louis, MO) were dissolved in ethanol prior to addition to the assay. Final concentrations of 100 μM

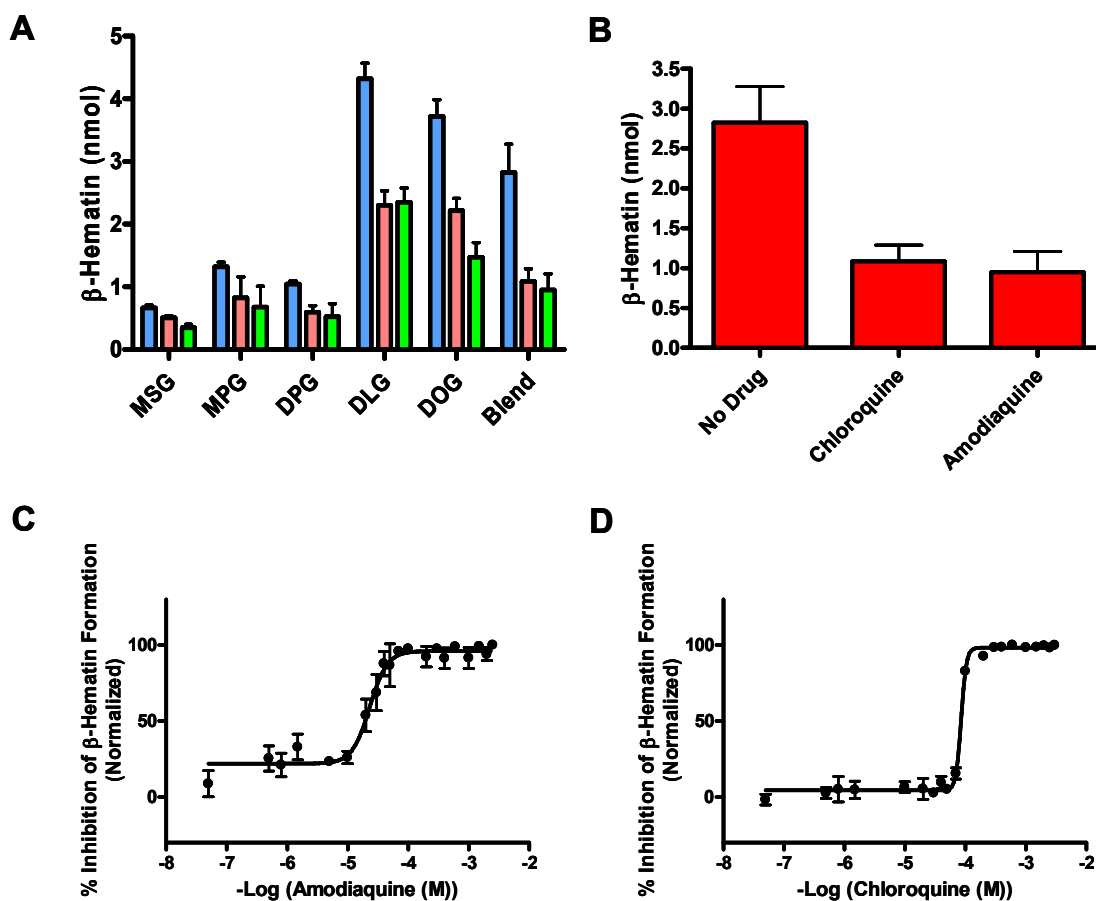


Figure 52 Inhibition studies of neutral lipid blend mediated BH assays. (A) BH production was measured by the individual glycerols of the neutral lipid blend (blue) without inhibitor, (red) with chloroquine at IC_{50} and (green) with amodiaquine at IC_{50} . (B) Specifically, the neutral lipid blend was found to form 3 nmol of BH at 50 μM hematin substrate and was inhibited 2-fold with the addition of chloroquine and amodiaquine at IC_{50} . (C) and (D) Concentration response curves of amodiaquine and chloroquine, respectively, in the NP-40 mediated BH assay.

hematin stock solution, 100 μ M lipid solution (a ratio of 4:2:1:1:1 monostearoyl-, monopalmitoyl-, dipalmitoyl-, dioleoyl-, and dilinoleoyl glycerols, respectively), and 0-100 μ M antimalarial (chloroquine or amodiaquine, Sigma-Aldrich, St. Louis, MO) were incubated in clear, 384-well plates at 37 °C in a Thermo water bath and shaken at 40 rpm for 20 h. The plates were centrifuged in a Beckman Coulter AllegraX 22R, S2096 rotor, at 25 °C for 1 h at 1100 x g. Supernatant was removed and 0.15 M sodium bicarbonate, 2% SDS was used to dissolve free heme in the mixture. The plate was centrifuged again for 1 h and the supernatant removed. The remaining BH pellet was dissolved using 0.36 M NaOH, 2% SDS and its absorbance read at 400 nm.

Detergent-Mediated Crystallization Assay

The detergent-mediated crystallization assay was designed to serve as a primary screen in the identification of potential antimalarials. The acidic and lipid-rich environment of the digestive food vacuole was mimicked *in vitro* and tailored to a 384-well plate format for high throughput screening. This assay uses an inexpensive detergent as an alternative to the more expensive lipid blend native to the parasite's digestive food vacuole, saving ~\$0.05/well. This assay also only requires an incubation time of 4 hours as compared to previously published ≥ 20 hour reactions.^{29,189} Several detergents are reported herein, but the detergent NP-40 was found to provide the growth platform that yielded the closest drug IC₅₀ values as those obtained by the native neutral lipid blend (Figure 53).

To set up the assay, a 2.0 M sodium acetate buffer, pH 4.9 was prepared (13.4039 g sodium acetate trihydrate and 5.799 mL glacial acetic acid in 100 mL deionized water). A 0.0002 g/mL NP-40 stock was prepared by adding 84.9 μ L of 10% NP-40 to 45 mL of deionized water and vortexed. Both of these solutions have been scaled-up for large

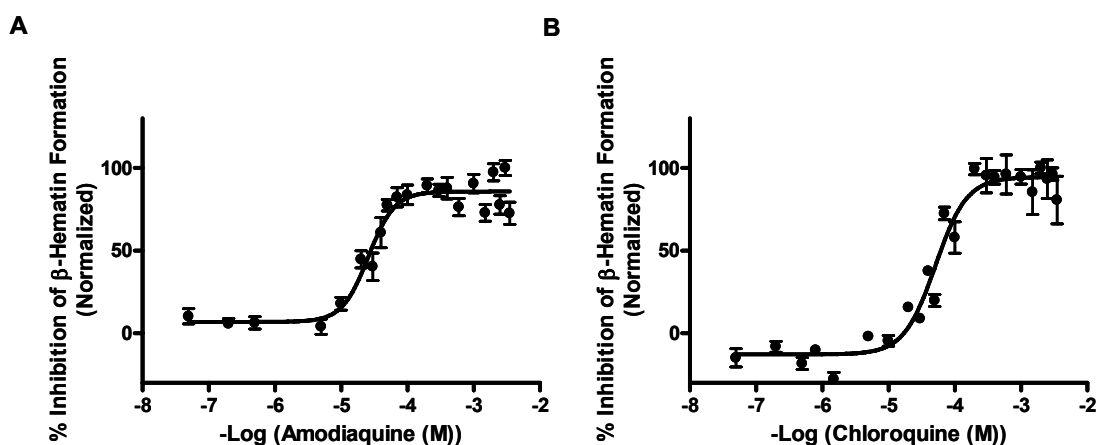


Figure 53 Concentration response curves of NP-40 mediated BH assays. The IC_{50} values of (A) amodiaquine and (B) chloroquine were calculated as 25 μ M and 50 μ M, respectively.

screens. A 25 mM heme solution was prepared by weighing out 16.3 mg of hemin (Fluka $\geq 99.8\%$) in a microcentrifuge tube and dissolving it in 1 mL DMSO. This solution was vortexed and sonicated before filtering through a 0.22 μ m PVDF Millex filter. A 177.8 μ L aliquot of the filtrate was added to 20 mL of the 2.0 M sodium acetate buffer for a final 222.2 μ M heme buffer solution. This solution was kept stirring during plate delivery; this is especially important when scaling up to volumes of ≥ 500 mL.

Control drug stocks (amodiaquine) were prepared at 51.6 mM in 100% DMSO. These additions resulted in a 100 μ M final concentration (IC_{MAX}) of drug in the final assay. Aliquots of 125 nL were made to designated wells, followed by 14 μ L of deionized water. The two outer columns of the plate A1:P2 and A23:P24 contained a checkerboard distribution of positive control amodiaquine and drug vehicle DMSO

(Figure 54). Library compounds (10 mM) were added (125 nL) to desired wells followed by 14 μ L of deionized water, resulting in a 19.3 μ M final concentration (the control drug's IC_{50}).

	1	2	3	4	5	6	7	8	9	10	11	12	13	14	15	16	17	18	19	20	21	22	23	24	
A	Red	Blue	Orange	Orange	Orange	Orange	Orange	Orange	Orange	Orange	Orange	Orange	Orange	Orange	Orange	Orange	Orange	Orange	Orange	Orange	Orange	Orange	Blue	Red	
B	Blue	Red	Orange	Orange	Orange	Orange	Orange	Orange	Orange	Orange	Orange	Orange	Orange	Orange	Orange	Orange	Orange	Orange	Orange	Orange	Orange	Orange	Orange	Red	Blue
C	Red	Blue	Orange	Orange	Orange	Orange	Orange	Orange	Orange	Orange	Orange	Orange	Orange	Orange	Orange	Orange	Orange	Orange	Orange	Orange	Orange	Orange	Orange	Blue	Red
D	Blue	Red	Orange	Orange	Orange	Orange	Orange	Orange	Orange	Orange	Orange	Orange	Orange	Orange	Orange	Orange	Orange	Orange	Orange	Orange	Orange	Orange	Orange	Red	Blue
E	Red	Blue	Orange	Orange	Orange	Orange	Orange	Orange	Orange	Orange	Orange	Orange	Orange	Orange	Orange	Orange	Orange	Orange	Orange	Orange	Orange	Orange	Orange	Blue	Red
F	Blue	Red	Orange	Orange	Orange	Orange	Orange	Orange	Orange	Orange	Orange	Orange	Orange	Orange	Orange	Orange	Orange	Orange	Orange	Orange	Orange	Orange	Orange	Red	Blue
G	Red	Blue	Orange	Orange	Orange	Orange	Orange	Orange	Orange	Orange	Orange	Orange	Orange	Orange	Orange	Orange	Orange	Orange	Orange	Orange	Orange	Orange	Orange	Blue	Red
H	Blue	Red	Orange	Orange	Orange	Orange	Orange	Orange	Orange	Orange	Orange	Orange	Orange	Orange	Orange	Orange	Orange	Orange	Orange	Orange	Orange	Orange	Orange	Red	Blue
I	Red	Blue	Orange	Orange	Orange	Orange	Orange	Orange	Orange	Orange	Orange	Orange	Orange	Orange	Orange	Orange	Orange	Orange	Orange	Orange	Orange	Orange	Orange	Blue	Red
J	Blue	Red	Orange	Orange	Orange	Orange	Orange	Orange	Orange	Orange	Orange	Orange	Orange	Orange	Orange	Orange	Orange	Orange	Orange	Orange	Orange	Orange	Orange	Red	Blue
K	Red	Blue	Orange	Orange	Orange	Orange	Orange	Orange	Orange	Orange	Orange	Orange	Orange	Orange	Orange	Orange	Orange	Orange	Orange	Orange	Orange	Orange	Orange	Blue	Red
L	Blue	Red	Orange	Orange	Orange	Orange	Orange	Orange	Orange	Orange	Orange	Orange	Orange	Orange	Orange	Orange	Orange	Orange	Orange	Orange	Orange	Orange	Orange	Red	Blue
M	Red	Blue	Orange	Orange	Orange	Orange	Orange	Orange	Orange	Orange	Orange	Orange	Orange	Orange	Orange	Orange	Orange	Orange	Orange	Orange	Orange	Orange	Orange	Blue	Red
N	Blue	Red	Orange	Orange	Orange	Orange	Orange	Orange	Orange	Orange	Orange	Orange	Orange	Orange	Orange	Orange	Orange	Orange	Orange	Orange	Orange	Orange	Orange	Red	Blue
O	Red	Blue	Orange	Orange	Orange	Orange	Orange	Orange	Orange	Orange	Orange	Orange	Orange	Orange	Orange	Orange	Orange	Orange	Orange	Orange	Orange	Orange	Orange	Blue	Red
P	Blue	Red	Orange	Orange	Orange	Orange	Orange	Orange	Orange	Orange	Orange	Orange	Orange	Orange	Orange	Orange	Orange	Orange	Orange	Orange	Orange	Orange	Orange	Red	Blue

Figure 54 HTS plate layout of the NP-40 mediated BH assay. The assay plate is organized by controls of (red) potentiator amodiaquine at IC_{MAX} 100 μ M and (blue) vehicle DMSO, and the orange wells contain 19.3 μ M test compounds.

To the plate containing drug and library compounds, 30 μ L of heme buffer solution was added, followed by 5 μ L of 0.0002 g/mL NP-40 stock and 15 μ L of acetone. Plates were incubated in a 37°C reciprocating water bath (55 rpm) for 4 hours. Meanwhile, a 20 mM 4-(2-hydroxyethyl)-1-piperzineethanesulfonic acid (HEPES) buffer, pH 7.5 was prepared by dissolving 2.383 g HEPES enzyme grade in 500 mL of deionized water. This buffer was used to prepare a 1:1 (v:v) solution of HEPES buffer to pyridine and was added (8 μ L) to plates following incubation. Plates were shaken 15 minutes and their absorbance read at 405 nm. The raw absorbance data was plotted against a logarithmic scale of drug in GraphPad Prism 5.0. Hits were identified as those data points lying three standard deviations outside of the control antimalarial in the screen.

BH Assay Development and Optimization

Several steps were undertaken in the optimization of each BH assay presented herein. One of the first inquiries was into the reaction buffer of each assay. The buffer of the neutral lipids was 0.1 M ammonium acetate while the buffer of the NP-40 assay was 1.0 M sodium acetate. Therefore, a series of experiments varying in pH and ionic strength were carried out (as summarized in Tables 6-8). A final reaction pH of 4.9 was

Table 6 Chloroquine-Inhibited Neutral Lipid BH Assay's Response to pH and Ionic Strength.

pH of Reaction Mixture	Buffer Ionic Strength (mM)	IC ₅₀ (μM) of CQ	R ²	Z'
4.1	22	2,020	0.8011	0.7026
	160	2,076	0.9162	0.7657
4.3	34	1,460	0.9741	0.6911
	160	3,153	0.9863	0.8434
4.5	50	748.2	0.9837	0.6766
	160	975.3	0.9573	0.6043
4.7	70	472.4	0.9950	0.7442
	160	484.1	0.9936	0.8028
4.9	93	190.4	0.9541	0.7145
	160	297.5	0.9970	0.8766
5.1	117	92.7	0.9955	0.6901
	160	99.3	0.9950	0.8062
5.4	139	41.3	0.9911	0.7271
	160	43.8	0.9905	0.6147
5.6	157	24.5	0.9730	0.7147
	160	19.3	0.9668	0.6655

Table 7 Amodiaquine-Inhibited Neutral Lipid BH Assay's Response to pH and Ionic Strength.

pH of Reaction Mixture	Buffer Ionic Strength (mM)	IC ₅₀ (μM) of AQ	R ²	Z'
4.5	50	136.1	0.9849	0.8724
	160	169.1	0.8556	0.6965
4.7	70	59.79	0.9651	0.8026
	160	72.93	0.9930	0.7740
4.9	93	34.47	0.9906	0.8457
	160	40.73	0.9903	0.7804
5.1	117	20.96	0.9834	0.8620
	160	20.41	0.9973	0.8679
5.4	139	14.78	0.9909	0.8041
	160	12.62	0.9968	0.7733
5.6	157	11.55	0.9831	0.7163
	160	10.70	0.9880	0.8487

maintained for all future assays. The ionic character was not found to cause significant change in the assay BH production as demonstrated in the neutral lipid mediated assay

Table 8 Chloroquine-Inhibited NP-40 BH Assay's Response to pH and Ionic Strength.

pH of Reaction Mixture	Buffer Ionic Strength (M)	IC ₅₀ (μM) of CQ	R ²	Z'
4.1	0.263	217.0	0.9532	0.6138
4.3	0.395	182.9	0.9514	0.8204
4.5	0.565	102.1	0.9756	0.7075
4.7	0.767	66.16	0.9775	0.6346
4.9	0.985	30.08	0.9626	0.7597
5.1	1.20	19.45	0.9647	0.6568
5.4	1.40	8.90	0.9864	0.8173
5.6	1.57	9.72	0.9475	0.4883

BH product (Figure 55A). The change in buffer concentration, however, between the NP-40 and neutral lipid assays was found to be of significance (Figure 55B). The BH produced from 4, 16, 20 and 24 hours in the various buffers were monitored, and the 1.0 M acetate buffers were found to consistently produce greater amounts of BH at 4 h, compared to the 0.1 M acetate buffers. It is possible that the greater salt concentration in the 1.0 M buffers provides a system with superfluous molecular interactions, supporting a faster formation time between substrates or even a faster sequestration of lipophilic mediator in the aqueous medium.

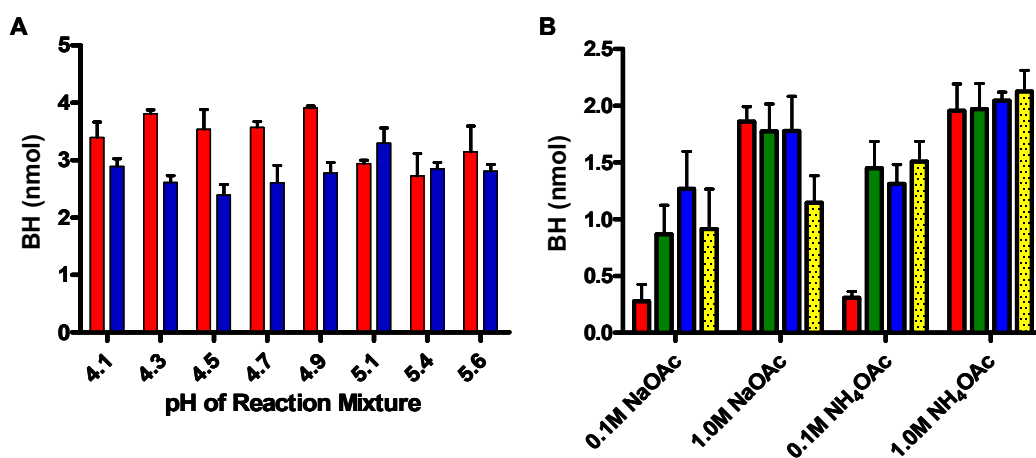


Figure 55 Quantification of BH formed at varying pH and buffer ionic strength. (A) The effects on BH production of varying ionic strength in the 0.1 M ammonium acetate, neutral lipid mediated BH assay were measured. These were minimal as observed between the buffers of (red) 160 mM and (blue) 22-157 mM ionic strengths. (B) The NP-40 assay was applied to varying concentrations of acetate buffer, where the 0.1 M buffers had an ionic strength 93 mM and the 1.0 M buffers are 985 mM. The 1.0 M buffers were found to support faster BH aggregation at the intervals: (red) 4, (green) 16, (blue) 20 and (yellow) 24 h.

Increasing concentrations of heme substrate at 16, 20 and 24 h intervals were also considered in each assay. Time was not found to be a factor in BH formation; product increased as substrate did. In the BH crystal extension assay (Figure 56A), an increase in BH was not observed because the quantity of preformed BH was not increased in the

assay. The lipophilic neutral lipid and NP-40 BH crystallization assays (Figure 56B&C), however, were found to mediate the formation of BH as the amount of heme was increased.

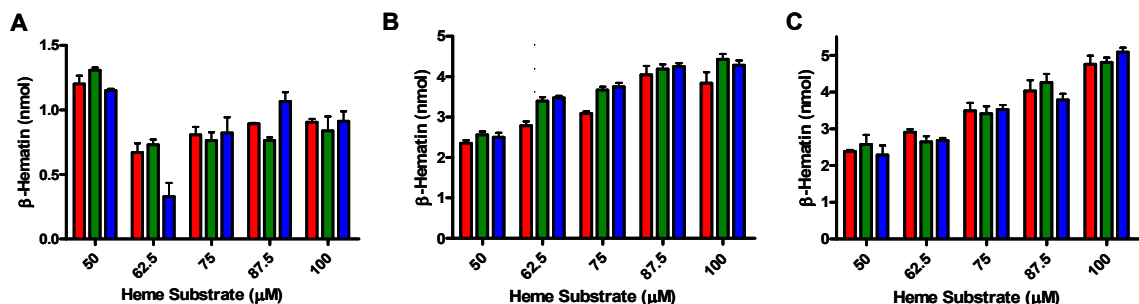


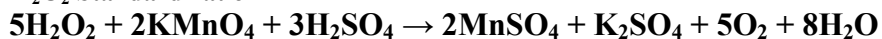
Figure 56 Kinetic and heme-dose response studies in the BH crystallization assays. The quantity of BH produced in the (A) BH crystal extension, (B) neutral lipid mediated and (C) NP-40 mediated BH assays was measured at (red) 16, (green) 20 and (blue) 24 h intervals as the concentration of heme substrate was increased.

Hydrogen Peroxide Degradation Assay^{41,100}

H₂O₂ degradation studies were carried out on Bohle, neutral lipid, extension and NP-40 prepared BH, similar to the studies used in chapter 3, but adapted to a 96-well plate format and with consideration of the various products of BH preparation. Prior to assay measurements, stock solutions were prepared and standardized. The 5 mM KMnO₄ (0.7902 g in 1 L DI water), 0.015 M Na₂C₂O₄ (0.5025 g in 250 mL DI water), 3 M sulfuric acid (16.7 mL 18 M H₂SO₄ in 100 mL DI water) and 4.5 M sulfuric acid (25 mL 18 M H₂SO₄ in 100 mL DI water) stocks were prepared. The standardization of KMnO₄ (Scheme 14) was began by preparing the analyte (25 mL of 0.015 M Na₂C₂O₄

Scheme 14 KMnO₄ Standardization



Scheme 15 H₂O₂ Standardization

and 15 mL of 3 M H₂SO₄ in 50 mL of DI water) and filling the buret with 5 mM KMnO₄ titrant. The H₂O₂ stock was standardized (Scheme 15) by preparing the analyte (15 mL of 4.5 M H₂SO₄, 50 mL of DI water and 25 μL of 30% H₂O₂ [newly opened]) and filling the buret with standardized KMnO₄ titrant.

Neutral lipid, extension and NP-40 BH assays were prepared as previously described (at 166 μL reactions volumes in round bottom 96-well plates). All assays were incubated at 37°C, 55 rpm for 20 h. The plates were centrifuged at 1100 x g for 1 hr at 25°C in a Beckman Coulter AllegraX 22R, S2096 rotor. The supernatant was removed, and HZ precipitate was washed with 200 μL of DI water, centrifuging again for 1 h. The supernatant was discarded, and the assay BH product (as well as a new plate of 2.0 mg/mL suspension of Bohle) was suspended in 100 mM sodium acetate buffer pH 4.8 with the appropriate concentration of standardized H₂O₂. These plates were incubated at 37° for 20 h. They were centrifuged 1 h and HZ precipitate was washed with 200 μL of DI water, centrifuging again for 1 h. To the remaining precipitate, 200 μL of 0.36 M NaOH, 2%SDS was added to each well. The absorbance of the plates' contents was measured at 400 nm on a BioTek SynergyHT plate reader. A molar extinction coefficient of 1x10⁻⁵ M⁻¹cm⁻¹ was used to calculate the BH remaining. These calculations were used to determine the EC₅₀ values of H₂O₂ in the degradation of BH.

The resultant dose response curves of Bohle BH, extension BH, lipid blend BH and NP-40 BH revealed stability strengths of the formed BH (Figure 57). As expected, the Bohle synthesis of BH had the highest EC₅₀ of 7.68 mM, followed by the neutral

blend BH at 5.95 mM, the NP-40 mediated BH at 4.13 mM and the extension formed BH at 3.37 mM. The BH formed in just acetate buffer was weaker and had EC₅₀ values of 1 mM.

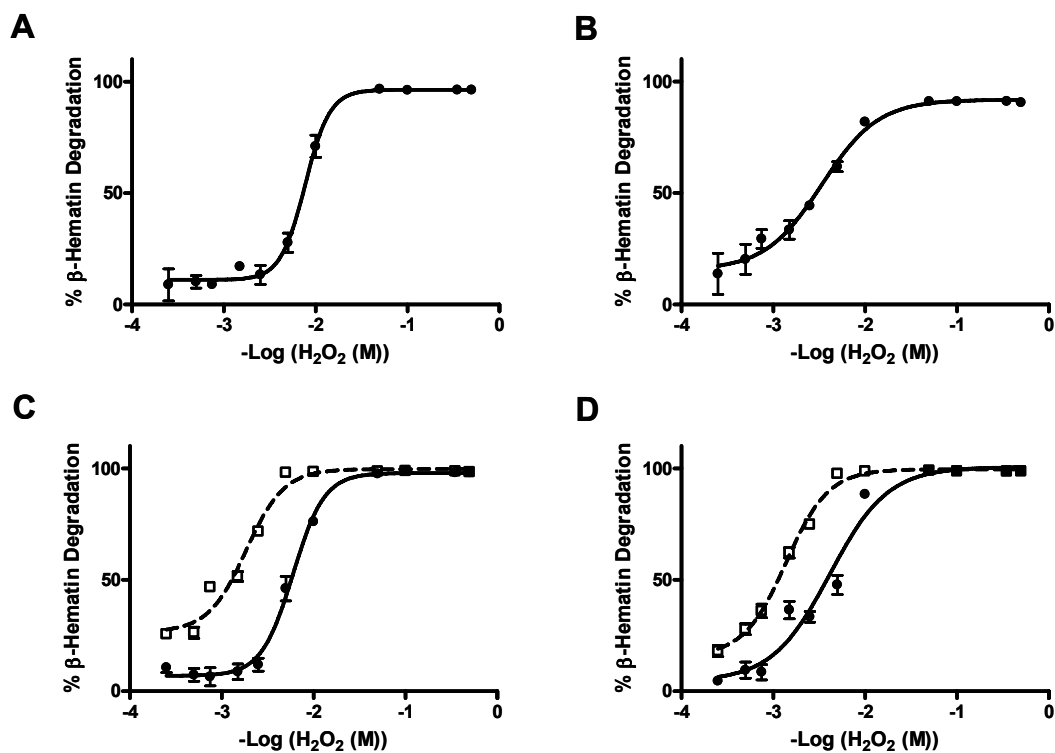


Figure 57 H₂O₂ Degradation of BH produced from varying templates. Concentration response curves of BH's degradation by H₂O₂ were generated for BH prepared from (A) the Bohle dehydrohalogenation method, (B) the BH crystal extension assay, (C) the neutral lipid blend mediated BH assay and (D) the NP-40 mediated BH assay. These plots generated H₂O₂ EC₅₀ values of 7.68 mM, 3.37 mM, 5.95 mM (1.84 mM) and 4.13 mM (1.38mM), respectively. In C and D, the -□- symbols represent assays where lipophilic mediator (whether glycerols or NP-40) were absent. The EC₅₀ values of these plots are given in the earlier parentheses.

APPENDIX D

HTS Preliminary Hits of the NP-40 Mediated BH Crystallization Assay

This appendix contains the graphical representation of the structural trends of the hits identified in the preliminary screens of the NP-40 mediated BH crystallization assay (Figure 56). The following pages of Scheme 16 contain the 161 hits (15 per page), labeled with their PubChem ID, calculated log P, molecular weight and amine pKa values. The compounds outlined with a black border are IC_{MAX} hits. Log P and pKa values were calculated using ChemAxon Marvin v.5.2.2 software.

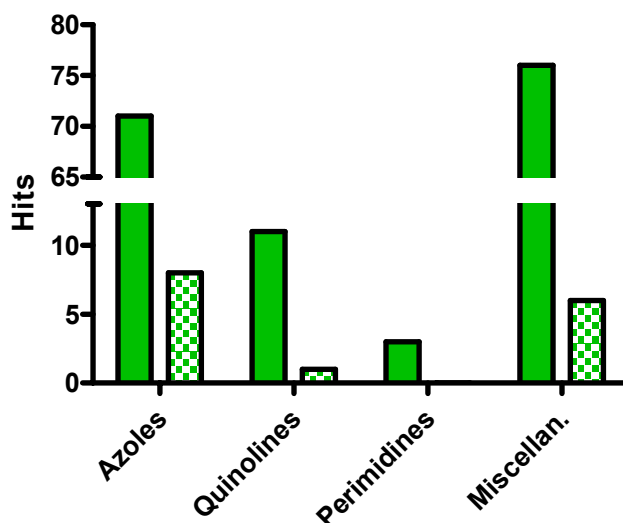
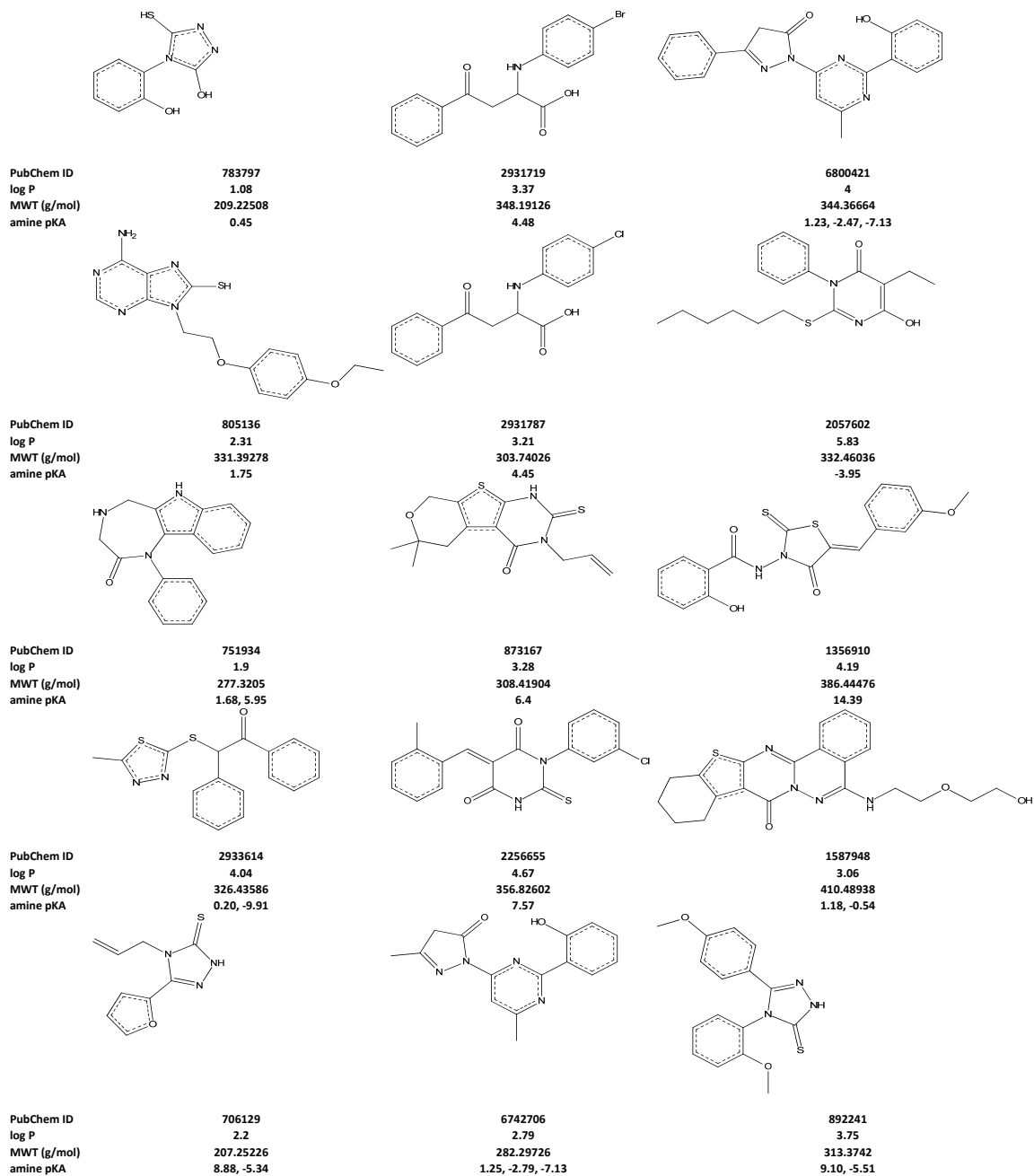
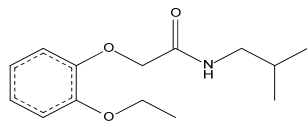


Figure 58 Graphical representation of the structural trends identified from the preliminary screens of the NP-40 mediated crystallization assay. (solid green) The total preliminary hits belonging to each structure category. (checker green) The number of IC_{MAX} hits belonging to each structure category.

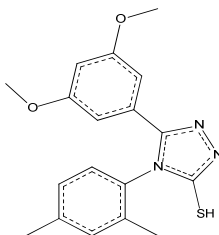
Scheme 16 Complete list of preliminary hits identified in the NP-40 mediated BH crystallization assay small molecule library screens.



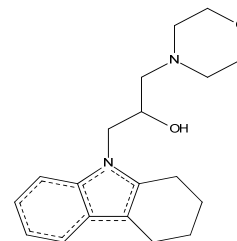


PubChem ID
log P
MWT (g/mol)
amine pKA

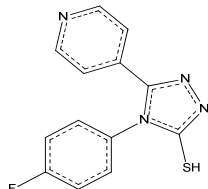
731870
2.15
251.32144
15.17



748044
3.11
341.42736
1.34, -8.25

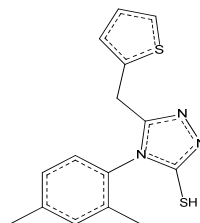


3131870
2.68
314.42194
7.31

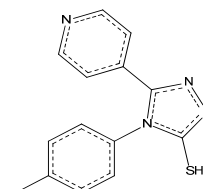


PubChem ID
log P
MWT (g/mol)
amine pKA

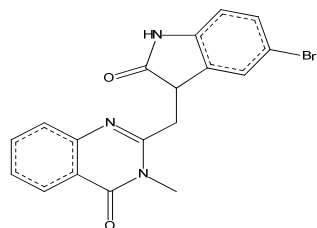
748069
1.51
272.3007632
3.78, 0.42, -8.91



748042
3.62
301.4297
1.83, -7.81

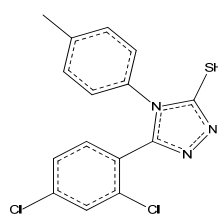


764331
1.84
268.33688
3.78, 0.42, -8.91

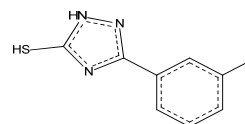


PubChem ID
log P
MWT (g/mol)
amine pKA

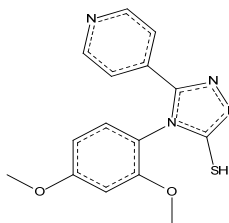
2941849
2.73
384.22666
2.44, 12.9



764330
4.19
336.23894
1.23, -8.21

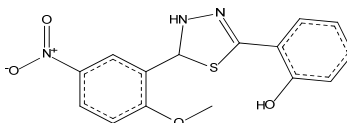


690371
2.63
191.25286
-2.94

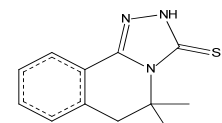


PubChem ID
log P
MWT (g/mol)
amine pKA

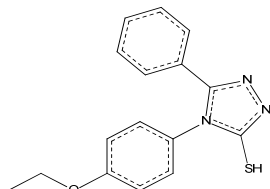
892098
0.87
314.36226
3.77, 0.41, -8.96



6800179
3.44
331.34642
19.77, 1.24, -8.23

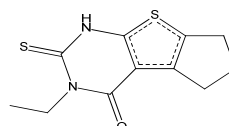


870599
3.14
231.31672
9.37, -2.56

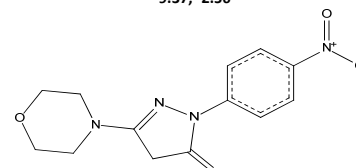


PubChem ID
log P
MWT (g/mol)
amine pKA

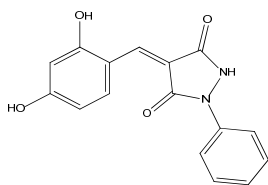
702457
2.77
297.3748
1.43, -8.14



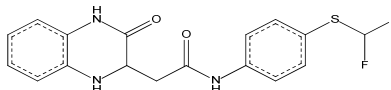
725824
3.3
252.35578
6.45



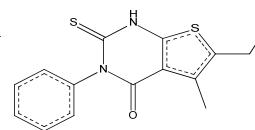
574330
0.71
290.27466
-2.31



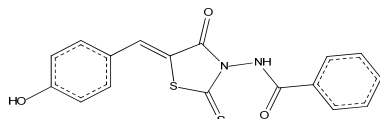
PubChem ID 2248254
 log P 1.82
 MWT (g/mol) 296.27748
 amine pKA 3.65



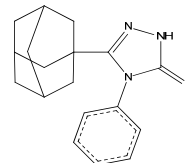
2897796
 3.43
 363.3817064
 13.97, 13.91, 13.03, 1.44



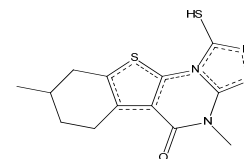
930671
 5.07
 302.41446
 5.41



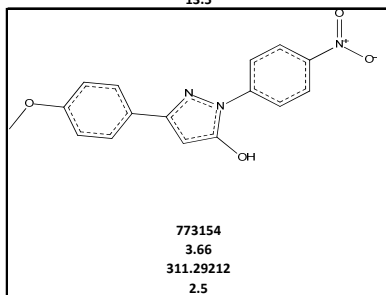
PubChem ID 1556024
 log P 3.7
 MWT (g/mol) 356.41878
 amine pKA 13.5



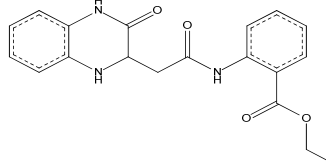
2898021
 4.81
 311.44444
 9.01, -5.4



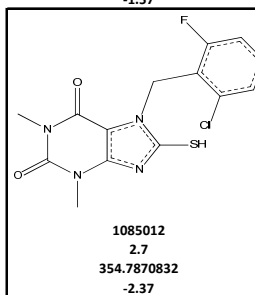
2947540
 1.73
 306.40646
 -1.57



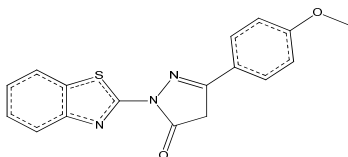
PubChem ID 773154
 log P 3.66
 MWT (g/mol) 311.29212
 amine pKA 2.5



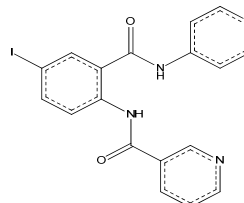
2896732
 2.76
 353.37186
 13.91, 13.2, 12.29, 1.44



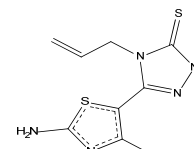
1085012
 2.7
 354.7870832
 -2.37



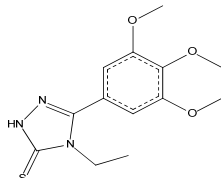
PubChem ID 2901657
 log P 3.62
 MWT (g/mol) 323.36902
 amine pKA - 1.21, -2.61



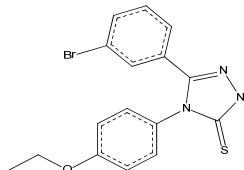
991474
 2.65
 444.22589
 10.51, 9.58, 5.22, 3.5



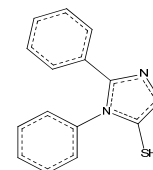
931717
 1.92
 253.34714
 9.1, 3.87, -4.5



PubChem ID 661205
 log P 2.29
 MWT (g/mol) 295.35738
 amine pKA -3.1

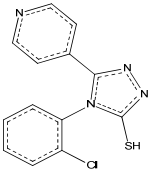
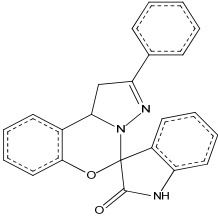
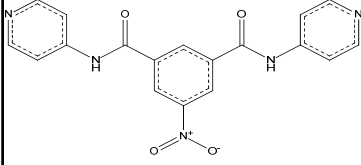
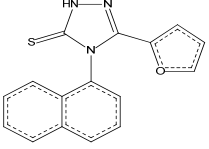
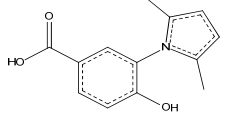
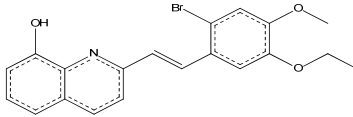
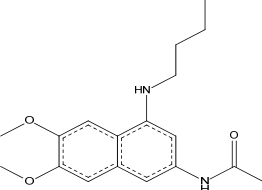
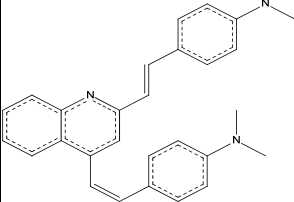
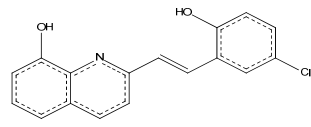
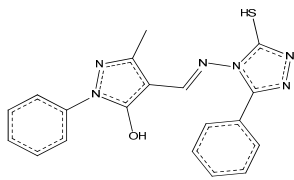
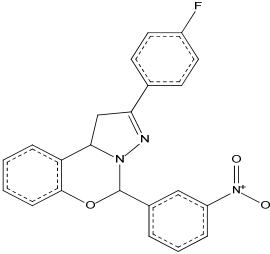
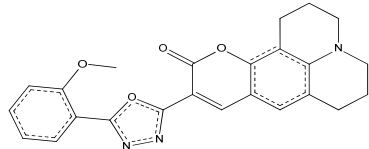
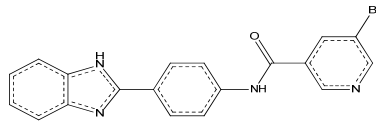
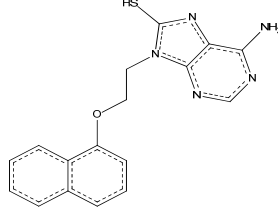
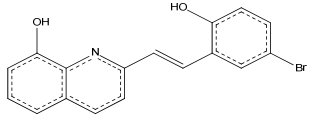


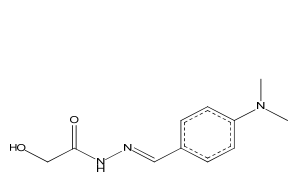
2197254
 5.03
 376.27086
 9.18, -5.73



677540
 2.68
 253.32224
 1.43, -8.14

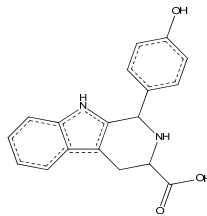
PubChem ID	676205	827956	661302
log P	2.18	3.2	2.57
MWT (g/mol)	313.3742	317.38106	228.28964
amine pKA	1.44, -8.19	2.26	16.19, 4.74
PubChem ID	95445	5724276	2858149
log P	1.6	3.66	3.24
MWT (g/mol)	232.23528	409.43512	276.76128
amine pKA	9.18	1.97	14.76, 4.48
PubChem ID	667526	94022	5414628
log P	2.87	2.86	2.78
MWT (g/mol)	267.34882	241.2851	296.34698
amine pKA	1.95, -8.11	3.72	0.68, -0.99, -9.20
PubChem ID	820006	741829	6777892
log P	1.74	1.43	4.45
MWT (g/mol)	237.27824	242.25984	335.37972
amine pKA	-2.93	- 0.35, - 2.28, - 9.62	9.16, -5.49

			
<p>PubChem ID log P MWT (g/mol) amine pKA</p>	<p>707204 1.89 288.75536 3.77, 0.41, -8.92</p>	<p>3490666 4.33 367.39998 2.11</p>	<p>1116129 1.66 363.32692 10.6, 9.81, 5.52, 4.92</p>
			
<p>PubChem ID log P MWT (g/mol) amine pKA</p>	<p>660813 4.12 293.34304 8.62, -7.41</p>	<p>776830 1.62 231.24722</p>	<p>5731584 5.21 400.26582 3.37</p>
			
<p>PubChem ID log P MWT (g/mol) amine pKA</p>	<p>2253328 2.68 316.39476 14.11, 4.22</p>	<p>5721908 7.26 419.56066 5.16, 4.63, 4.05</p>	<p>6809847 4.77 297.73568 3.37</p>
			
<p>PubChem ID log P MWT (g/mol) amine pKA</p>	<p>6810219 3.09 376.43494 2.95, 0.65, -2.46, -9.2</p>	<p>2884112 4.94 389.3791432 1.57</p>	<p>986302 3.67 415.44124 3.55, -2.3</p>
			
<p>PubChem ID log P MWT (g/mol) amine pKA</p>	<p>1207571 4.44 393.23672 10.82, 1.89, 0.85, -5.84</p>	<p>963506 3.1 337.3989 4.95, 1.75, -5.87</p>	<p>6809875 4.87 342.18668 3.37</p>

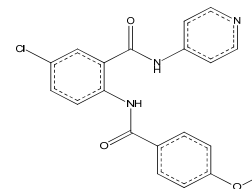


PubChem ID
log P
MWT (g/mol)
amine pKA

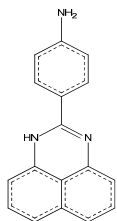
5406135
0.4
221.2557
9.93, 4.16, 1.9



2829105
2.8
308.33124
7.79, 3.32

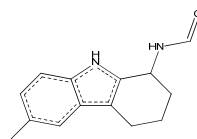


991453
3.39
381.81234
11.68, 9.94, 5.21

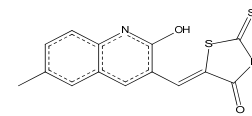


PubChem ID
log P
MWT (g/mol)
amine pKA

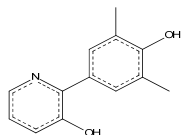
777097
3.31
259.30522
5.88, 3.04



2831725
2.43
228.28964
15.73, 4.6

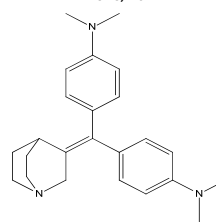


5550271
3.7
302.3714
7.48, 1.75, -5.66

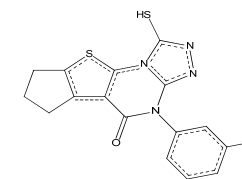


PubChem ID
log P
MWT (g/mol)
amine pKA

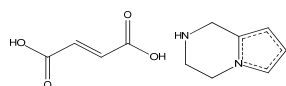
5898619
3.21
215.24782
5.07



1070499
4.2
361.52304
8.57, 4.62, 4.01

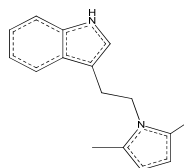


1306410
3.15
354.44926
-1.73

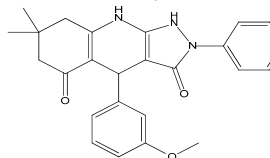


PubChem ID
log P
MWT (g/mol)
amine pKA

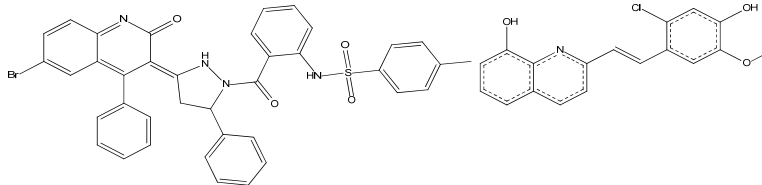
5717183
0.76
238.23986
0.53



774193
3.52
238.32752
5.17



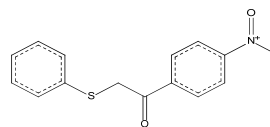
2947757
3.39
415.4843
6.68, -9.59



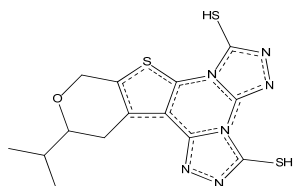
PubChem ID
log P
MWT (g/mol)
amine pKA

6803142
5.99
717.63026
7.27, -1.24

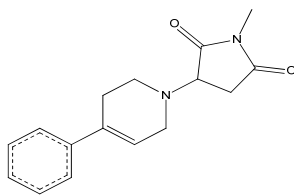
6796866
4.54
327.76166
3.37



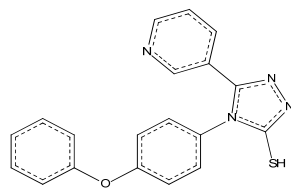
975838
3.46
273.30704



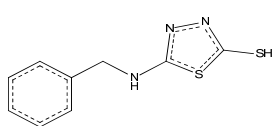
PubChem ID 2947832
log P 1.45
MWT (g/mol) 378.49556
amine pKA 0.45, -0.54, -8.57



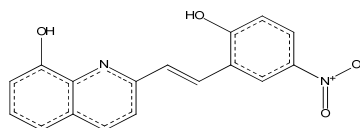
3799887
1.38
270.32632
6.62



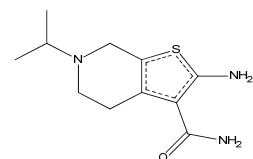
939004
2.8
346.40566
3.94, 0.86, -8.21



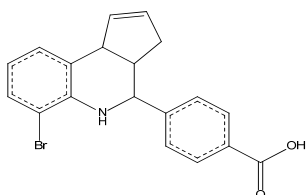
PubChem ID 830422
log P 2.41
MWT (g/mol) 223.31786
amine pKA 16.22, 0.1, -9.4



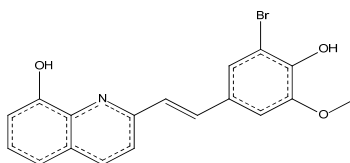
6801973
4.04
308.28818
3.37



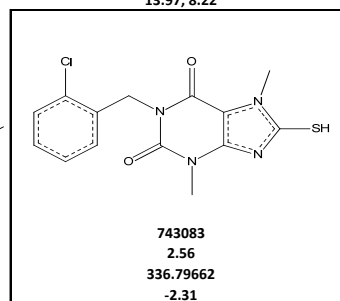
757553
1.48
239.33718
13.97, 8.22



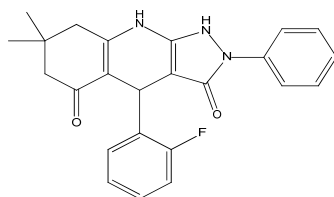
PubChem ID 2948389
log P 4.41
MWT (g/mol) 370.23984
amine pKA 19.95, 2.19



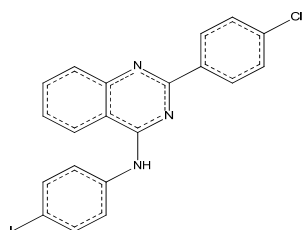
6845036
4.71
372.21266
3.38



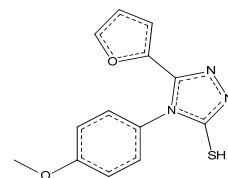
743083
2.56
336.79662
-2.31



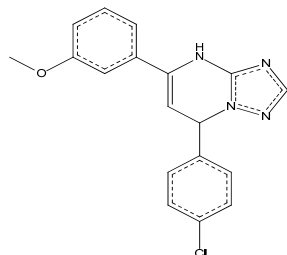
PubChem ID 2949870
log P 3.69
MWT (g/mol) 403.4487832
amine pKA 6.62, -5.22



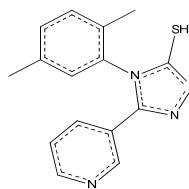
1592012
7.16
457.69479
15.94, 4.2, -1.51, -6.3



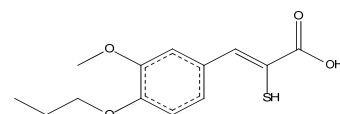
704537
1.38
273.31034
0.51, -9.81



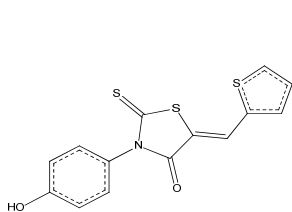
PubChem ID 5739057
log P 3.67
MWT (g/mol) 338.7909
amine pKA 17.87, 2.78, -6.56, -5.81



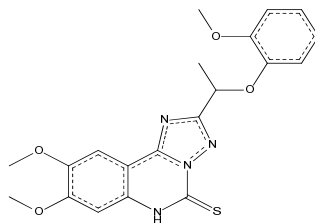
943060
2.31
282.36346
3.94, 0.86, -8.44



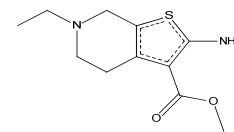
5336686
2.69
268.32874



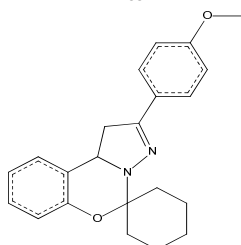
PubChem ID 1226086
log P 4.23
MWT (g/mol) 319.42176
amine pKA -2.58



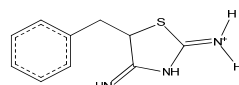
15998154
1.519663
412.4622



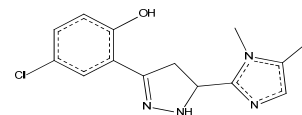
2761386
2.21
240.32194
18.8, 7.98, -7.84



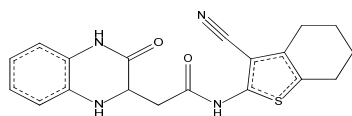
PubChem ID 3121854
log P 4.49
MWT (g/mol) 348.43816
amine pKA 3.13



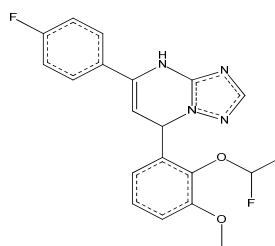
3671746
0.019000
206.28738



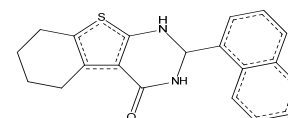
6824199
2.14
311.16658
19.94, 4.74, 2.26, -7.4



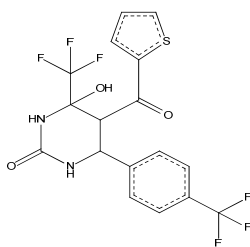
PubChem ID 4365930
log P 3.13
MWT (g/mol) 366.43682
amine pKA 13.91, 13.12, 10.47, 1.44



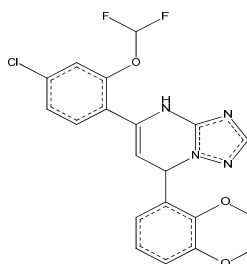
6024818
3.468510
388.3432096



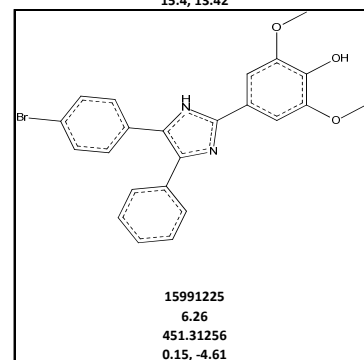
3762472
5.57
334.43472
15.4, 13.42



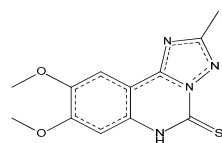
PubChem ID 2918158
log P 3.73
MWT (g/mol) 438.3441992
amine pKA 19.82, 10.33



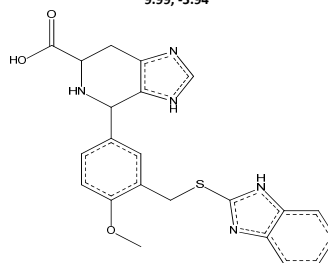
5740675
4.2
434.8237864
9.99, -5.94



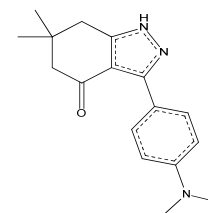
15991225
6.26
451.31256
0.15, -4.61



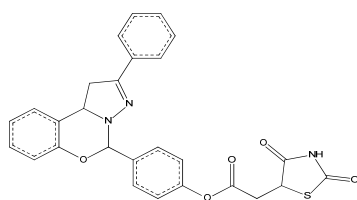
PubChem ID 2766102
log P 2.39
MWT (g/mol) 276.31428
amine pKA 10.03, -3.38



6617298
3.34
435.49884
7.01, 1.46, -0.15, -6.34, -6.93

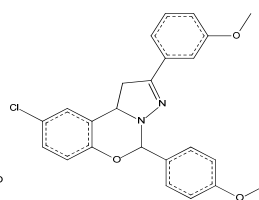


3275143
2.36
283.36814
3.88, 0.49

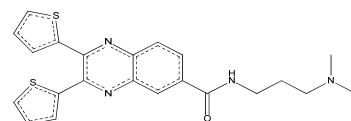


PubChem ID
log P
MWT (g/mol)
amine pKA

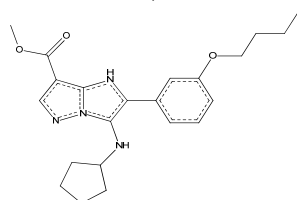
4377684
4.34
499.53774
6.31, 2.18



5066435
5.15
420.88814
1.78

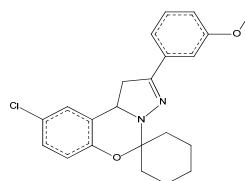


3698429
4.07
422.56628
14.76, 9.3, -0.95, -5.98

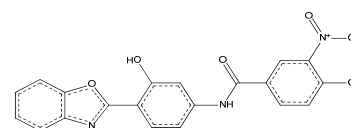


PubChem ID
log P
MWT (g/mol)
amine pKA

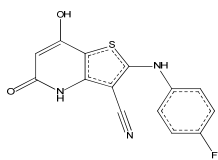
3455308
4.44
396.48272
4.49, -2.06, -7.83



4403626
5.09
382.88322
2.51

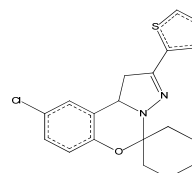


Unknown
4.59
409.77938
12.19, 0.02

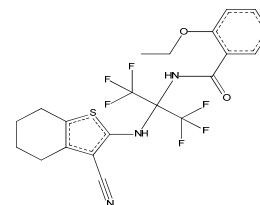


PubChem ID
log P
MWT (g/mol)
amine pKA

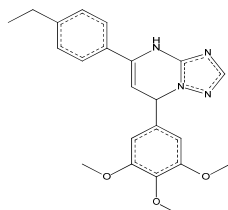
729843
2.36
301.2956232
15.24, 9.76, -8.89



3121968
5.17
358.88496
1.47

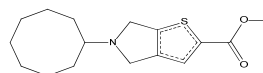


1716517
6.38
491.4498792
14.12, 10.12

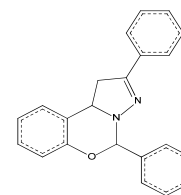


PubChem ID
log P
MWT (g/mol)
amine pKA

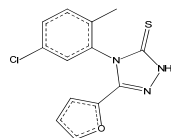
6273261
3.71
392.45096
18.02, 2.78, -5.99, -6.14



3427810
4.4
293.42432
7.73

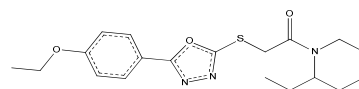


555190
4.86
326.39112
3.07

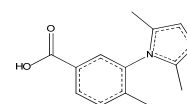


PubChem ID
log P
MWT (g/mol)
amine pKA

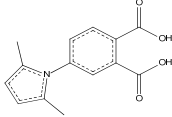
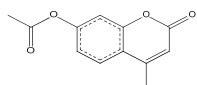
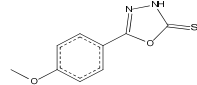
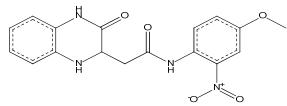
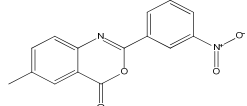
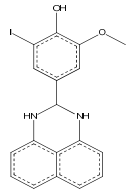
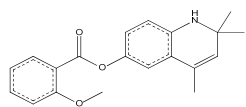
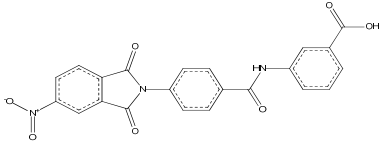
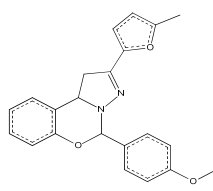
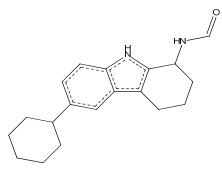
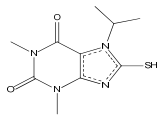
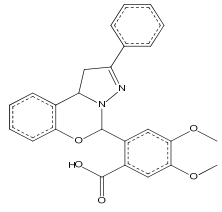
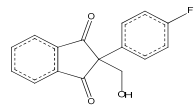
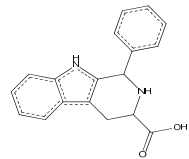
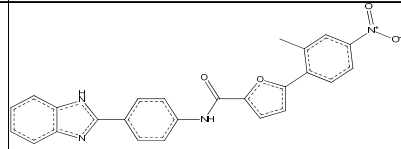
4670755
4.24
291.756
8.65, -8.12

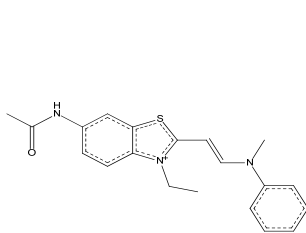


4101678
3
375.4851
-2.03

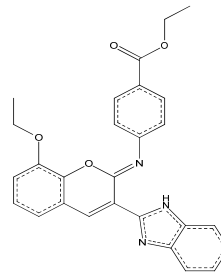


776836
2.37
229.2744

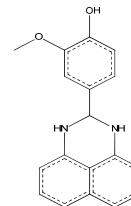
 PubChem ID log P MWt (g/mol) amine pKa	3534454 1.42 259.25732	 PubChem ID log P MWt (g/mol)	366 1.67 218.2054	 PubChem ID log P MWt (g/mol) amine pKa	683639 2.39 208.23702 8.67, -0.54, -1.97
 PubChem ID log P MWt (g/mol) amine pKa	3829096 1.53 356.33274 13.91, 13.14, 11.76, 1.44	 PubChem ID log P MWt (g/mol) amine pKa	300848 3.81 282.2509 -2.19	 PubChem ID log P MWt (g/mol) amine pKa	2295553 4.25 418.22837 18.90, 1.57, 0.36
 PubChem ID log P MWt (g/mol) amine pKa	695277 4.31 323.38564 19.26, 4.14	 PubChem ID log P MWt (g/mol) amine pKa	3557264 3.26 431.35452 12.23	 PubChem ID log P MWt (g/mol) amine pKa	3746677 3.96 360.4058 0.26
 PubChem ID log P MWt (g/mol) amine pKa	2888260 4.04 296.40666 15.75, 4.56	 PubChem ID log P MWt (g/mol) amine pKa	708517 1.01 254.30876 -2.35	 PubChem ID log P MWt (g/mol) amine pKa	5189170 4.2 430.45258 1.95
 PubChem ID log P MWt (g/mol) amine pKa	5085883 2.3 270.2551432	 PubChem ID log P MWt (g/mol) amine pKa	150718 3.11 292.33184 6.56, 3.5	 PubChem ID log P MWt (g/mol) amine pKa	15998896 5.95 438.43482 10.05, 0.90, -5.84



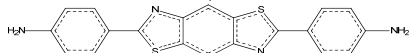
PubChem ID 5978130
 log P 0.2
 MW (g/mol) 352.47318
 amine pKa 13.79, -0.34



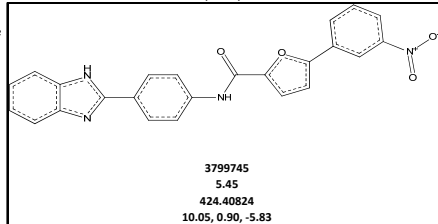
15998274
 6.86
 453.48922
 0.83, -0.66, -5.91



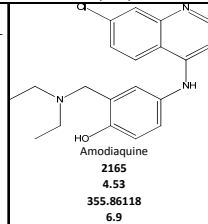
760603
 3.33
 292.33184
 18.90, 1.57, 0.36



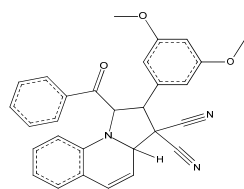
PubChem ID 1098314
 log P 4.48
 MW (g/mol) 374.48196
 amine pKa 3.39, 2.78, 0.96, 0.23



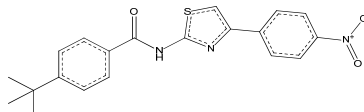
3799745
 5.45
 424.40824
 10.05, 0.90, -5.83



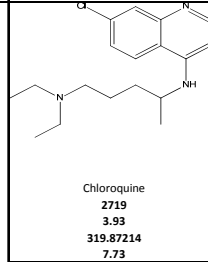
2165
 4.53
 355.86118
 6.9



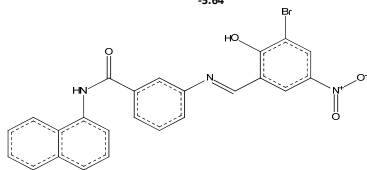
PubChem ID 4436435
 log P 4.78
 MW (g/mol) 461.51122
 amine pKa -5.64



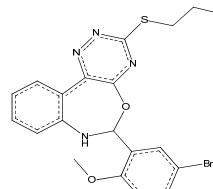
4104558
 5.93
 381.44816
 9.57, -1.04



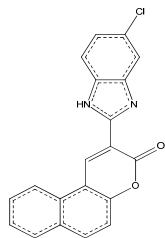
2719
 3.93
 319.87214
 7.73



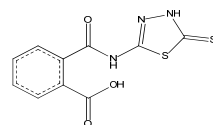
PubChem ID 6815125
 log P 6.33
 MW (g/mol) 490.30554
 amine pKa 11.49, 0.77



2858622
 5.59
 459.35946
 12.61, 8.91, -0.25, -1.96



PubChem ID 3287443
 log P 5.22
 MW (g/mol) 346.76654
 amine pKa 0.64, -6.09



3238973
 2.31
 281.31088
 12.70, 8.48, -4.05, -5.49

BIBLIOGRAPHY

- (1) Carter, M. D.; Hoang, A. N.; Wright, D. W. In *Wiley Encyclopedia of Chemical Biology*; John Wiley & Sons, Inc.: 2008.
- (2) Reprinted from *Wiley Encyclopedia of Chemical Biology*, ed. Tadhg P. Begley, Carter, M.D.; Hoang, A.N.; Wright, D.W., Hemozoin: a paradigm for biominerals in disease, 2009, with permission from Wiley.
- (3) Mann, S. *Biomineralization: Principles and Concepts in Bioinorganic Materials Chemistry*; Oxford University Press: Oxford, 2001.
- (4) Nakata, P. A. *Plant Science* **2003**, *164*, 901-909.
- (5) De Yoreo, J. J.; Vekilov, P. G. In *Reviews in Mineralogy and Geochemistry*; Dove, P. M., De Yoreo, J. J., Weiner, S., Eds.; The Mineralogical Society of America: Washington, D.C., 2003; Vol. 54, p 57-90.
- (6) Ziegler, J.; Linck, R.; Wright, D. W. *Current Medicinal Chemistry* **2001**, *8*, 171-189.
- (7) Bonilla, J. A.; Moura, P. A.; Bonilla, T. D.; Yowell, C. A.; Fidock, D. A.; Dame, J. B. *International Journal for Parasitology* **2007**, *37*, 317-327.
- (8) Haas, L. *Journal of Neurology, Neurosurgery, and Psychiatry* **1999**, *67*, 520.
- (9) Scheibel, L.; Sherman, I. In *Malaria: Principles and Practice of Malariology*; Wernsdorfer, W., McGregor, I., Eds.; Churchill-Livingstone: Edinburgh, 1988.
- (10) Knoll, A. H. In *Reviews in Mineralogy and Geochemistry*; Dove, P. M., De Yoreo, J. J., Weiner, S., Eds.; The Mineralogical Society of America: Washington DC, 2003; Vol. 54, p 329-350.
- (11) Rodriguez-Navarro, A. B.; Cabraldmelo, C.; Batista, N.; Morimoto, N.; Alvarez-Lloret, P.; Ortega-Huertas; Fuenzalida, V. M.; Arias, J. I.; Wiff, J. P.; Arias, J. L. *Journal of Structural Biology* **2006**, *156*, 355-362.
- (12) He, G.; Ramachandran, A.; Dahl, T.; George, S.; Schultz, D.; Cookson, D.; Veis, A.; George, A. *The Journal of Biological Chemistry* **2005**, *280*, 33109-33114.

- (13) Bozec, L.; de Groot, J.; Odlyha, M.; Nicholls, B.; Nesbitt, S.; Flanagan, A.; Horton, M. *Ultramicroscopy* **2005**, *105*, 79-89.
- (14) Perry, C. C. In *Reviews in Mineralogy and Geochemistry*; Dove, P. M., De Yoreo, J. J., Weiner, S., Eds.; The Mineralogical Society of America: Washington DC, 2003; Vol. 54, p 304-323.
- (15) Nie, S.; Emory, S. R. *Science* **1997**, *275*, 1102-1106.
- (16) Lowenstam, H. A. *Science* **1981**, *211*, 1126-1131.
- (17) Mann, S. *Nature* **1988**, *332*, 119-124.
- (18) Gibbs, J. *Trans. Connect. Acad. Sci.* **1878**, *16*, 343-524.
- (19) Hohenberg, P. C.; Halperin, B. I. *Reviews of Modern Physics* **1977**, *49*, 435-475.
- (20) Mann, S. *Nature* **1993**, *365*, 499-505.
- (21) Sullivan, D. J. *Int J Parasitol* **2002**, *32*, 1645-1653.
- (22) Ziegler, J.; Change, R.; Wright, D. *J Am Chem Soc* **1999**, *121*, 2395-2400.
- (23) Egan, T.; Mavuso, W. W.; Ncokazi, K. K. *Biochemistry* **2001**, *40*, 204-213.
- (24) Carney, C. K.; Harry, S. R.; Sewell, S. L.; Wright, D. W. In *Biomineralization I: Crystallization and Self-Organization Process*; Naka, K., Ed.; Springer: Verlag, 2007; Vol. 270, p 155-185.
- (25) Schneider, E. L.; Marletta, M. A. *Biochemistry* **2005**, *44*, 979-986.
- (26) Fitch, C.; Cai, G.-z.; Chen, Y.-F.; Shoemaker, J. D. *Biochimica et Biophysica Acta* **1999**, *1454*, 31-37.
- (27) Hemplemann, E.; Motta, C.; Hughes, R.; Ward, S.; Bray, P. *Trends Parasitol* **2003**, *19*, 23-26.
- (28) Egan, T. J.; Chen, J. Y.-J.; de Villiers, K. A.; Mabothe, T. E.; Naidoo, K. J.; Ncokazi, K. K.; Langford, S. J.; McNaughton, D.; Pandiancherri, S.; Wood, B. R. *FEBS Letters* **2006**, *580*, 5105-5110.

- (29) Pisciotta, J. M.; Coppens, I.; Tripathi, A. K.; Scholl, P. F.; Shuman, J.; Bajad, S.; Shulaev, V.; Sullivan Jr., D. *Biochem. J.* **2007**, *402*, 197-204.
- (30) Kuman, S.; Guha, M.; Choubey, V.; Maity, P.; Bandyopadhyay, U. *Life Sciences* **2007**, *80*, 813-828.
- (31) Solomonov, I.; Osipova, M.; Feldman, Y.; Baetz, C.; Kjaer, K.; Robinson, I. K.; Webster, G. T.; McNaughton, D.; Wood, B. R.; Weissbuch, I.; Leiserowitz, L. *J Am Chem Soc* **2007**, *129*, 2615-2627.
- (32) Ridley, R. *Trends Microbiol* **1996**, *4*, 253.
- (33) Slater, A.; Swiggard, W.; Orton, B.; Flitter, W.; Goldberg, D.; Cerami, A.; Henderson, G. *Proceedings of the National Academy of Sciences USA* **1991**, *88*, 325-329.
- (34) Noland, G.; Briones, N.; Sullivan Jr., D. *Mol Biochem Parasitol* **2003**, *130*, 91-99.
- (35) Pagola, S.; Stephens, P.; Bohle, D.; Kosar, A.; Madsen, S. *Nature* **2000**, *404*, 307-310.
- (36) Schwarzer, E.; Kuhn, H.; Valente, E.; Arese, P. *BLOOD* **2003**, *101*, 722-728.
- (37) Cheng, Z.; Li, Y. *Chem Rev* **2007**, *107*, 748-766.
- (38) Green, M.; Xiao, L.; Lal, A. *Mol Biochem Parasitol* **1996**, *83*, 183-188.
- (39) Carter, M. D.; Harry, S. R.; Wright, D. W. *Biochemical and Biophysical Research Communications* **2007**, *363*, 867-872.
- (40) Parroche, P.; Lauw, F. N.; Goutagny, N.; Latz, E.; Monks, B. G.; Visintin, A.; Halmen, K. A.; Lamphier, M.; Olivier, M.; Bartholomeu, D. C.; Gazzinelli, R. T.; Golenbock, D. T. *PNAS* **2007**, *104*, 1919-1924.
- (41) Carney, C. K.; Schrimpe, A. C.; Halfpenny, K.; Harry, S. R.; Miller, C. M.; Broncel, M.; Sewell, S. L.; Schaff, J. E.; Deol, R.; Carter, M. D.; Wright, D. W. *J Biol Inorg Chem* **2006**, *11*, 917-929.
- (42) Fenaille, F.; Guy, P. A. *J. Am. Soc. Mass Spectrom* **2003**, *14*, 215-226.

- (43) Skorokhod, O. A.; Alessio, M.; Mordmuller, B.; Arese, P.; Schwarzer, E. *J. Immunol.* **2004**, *173*, 4066-4074.
- (44) Reprinted from Biochemical and Biophysical Research Communications, 363, Carter, M.D.; Harry, S.R.; Wright, D.W., Identification of hydroxyeicosatetraenoic acid components of schistosomal hemozoin, 867-872, 2007, with permission from Elsevier.
- (45) McManus, D. P. *Immunological Reviews* **1999**, *171*, 149-161.
- (46) Pearce, E. J.; MacDonald, A. S. *Nature Reviews* **2002**, *2*, 499-511.
- (47) In *WHO Technical Report Series 912* Geneva, 2002.
- (48) van der Werf, M. J.; de Vlas, S. J.; Brooker, S.; Looman, C. W. N.; Nagelkerke, N. J. D.; Habbema, J. D. F.; Engels, D. *Acta Tropica* **2003**, *86*, 125-139.
- (49) Lawrence, J. D. *The Journal of Parasitology* **1973**, *59*, 60-3.
- (50) Brindley, P. J.; Kalinna, B. H.; Dalton, J. P.; Day, S. R.; Wong, J. Y. M.; Smythe, M. L.; McManus, D. P. *Molecular and Biochemical Parasitology* **1997**, *89*, 1-9.
- (51) Chou, A. C.; Fitch, C. D. *The Journal of Clinical Investigation* **1981**, *68*, 672-677.
- (52) Francis, S. E.; Sullivan Jr., D. J.; Goldberg, D. E. *Annual Review of Microbiology* **1997**, *51*, 97-123.
- (53) Oliveira, M. F.; d'Avila, J. C. P.; Torres, C. R.; Oliveira, P. L.; Tempone, A. J.; Rumjanek, F. D.; Braga, C. M. S.; Silva, J. R.; Dansa-Petretski, M.; Oliveira, M. A.; Souza, W. d.; Ferreira, S. T. *Molecular and Biochemical Parasitology* **2000**, *111*, 217-221.
- (54) Oliveira, M. F.; Kycia, S. W.; Gomez, A.; Kosar, A. J.; Bohle, D. S.; Hemplemann, E.; Menezes, D.; Vannier-Santos, M. A.; Oliveira, P. L.; Ferreira, S. T. *FEBS Letters* **2005**, *579*, 6010-6016.
- (55) Schwarzer, E.; Turrini, F.; Ulliers, D.; Giribaldi, G.; Ginsburg, H.; Arese, P. *Journal of Experimental Medicine* **1992**, *176*.
- (56) Urban, B. C.; Roberts, D. J. *Current Opinion in Immunology* **2002**, *14*, 458-465.

(57) Giribaldi, G.; Ulliers, D.; Schwarzer, E.; Roberts, I.; Piacibello, W.; Arese, P. *Haematologica* **2004**, *89*, 492-493.

(58) Miller, C. M.; Carney, C. K.; Schrimpe, A. C.; Wright, D. W. *Inorganic Chemistry* **2005**, *44*, 2134-2136.

(59) Schwarzer, E.; Muller, O.; Arese, P.; WSiems, W. G.; Grune, T. *FEBS Letters* **1996**, *388*, 119-122.

(60) Bohle, D. S.; Helms, J. B. *Biochemical and Biophysical Research Communications* **1993**, *193*, 504-508.

(61) Lewis, F. In *Current Protocols in Immunology*; John Wiley & Sons: 1998, p 19.1.1-19.1.28.

(62) Sullivan Jr., D. J.; Gluzman, I. Y.; Russell, D. G.; Goldberg, D. E. *Proceedings of the National Academy of Sciences, USA* **1996**, *93*, 11865-11870.

(63) Nagano, T. *Luminescence* **1999**, *14*, 283-290.

(64) Soares, J. B. R. C.; Maya-Monteiro, C. M.; Bittencourt-Cunha, P. R. B.; Atella, G. C.; Lara, F. A.; d'Avila, J. C. P.; Menezes, D.; Vannier-Santos, M. A.; Oliveira, P. L.; Egan, T. J.; Oliveira, M. F. *FEBS Letters* **2007**, *581*, 1742-1750.

(65) Hada, T.; Swift, L. L.; Brash, A. R. *Biochimica Biophysica Acta* **1997**, *1346*, 109-119.

(66) Jiang, Z. D.; Gerwick, W. H. *Lipids* **1997**, *32*, 231-235.

(67) Jiang, Z. D.; Ketchum, S. O.; Gerwick, W. H. *Phytochemistry* **2000**, *53*, 129-133.

(68) Hawkins, D. J.; Brash, A. R. *Journal of Biological Chemistry* **1987**, *262*, 7629-7634.

(69) Coffa, G.; Hill, E. M. *Lipids* **2000**, *35*, 1195-1204.

(70) Boeglin, W. E.; Kim, R. B.; Brash, A. R. *Proceedings of the National Academy of Sciences, USA* **1998**, *95*, 6744-6749.

(71) Yamamoto, S.; Suzuki, H.; Ueda, N. *Progress in Lipid Research* **1997**, *36*, 23-41.

- (72) Samuelsson, B.; Dahlen, S. E.; Lindgren, J. A.; Rouzer, C. A.; Serhan, C. N. *Science* **1987**, *237*, 1171-1176.
- (73) Burger, F.; Krieg, P.; Marks, F.; Furstenberger, G. *Biochemical Journal* **2000**, *348*, 329-335.
- (74) Secor, W. E.; Powell, M. R.; Morgan, J.; Wynn, T. A.; Funk, C. D. *Prostaglandins & Other Lipid Mediators* **1998**, *56*, 291-304.
- (75) Delcroix, M.; Medzihradsky, K.; Caffrey, C. R.; Fetter, R. D.; McKerrow, J. H. *Molecular and Biochemical Parasitology* **2007**, *154*, 95-97.
- (76) GeneDB, Sanger Institute; Vol. 2007.
- (77) Porter, N. A.; Logan, J.; Kontoyiannidou, V. *Journal of Organic Chemistry* **1979**, *44*, 3177-3181.
- (78) Schwarzer, E.; Ludwig, P.; Valente, E.; Arese, P. *Parassitologia* **1999**, *41*, 199-202.
- (79) With kind permission from Springer Science+Business Media: Journal of Biological Inorganic Chemistry, The basis of immunomodulatory activity of malaria pigment (hemozoin), 11, 2006, 917-929, Carney, C. K.; Schrimpe, A. C.; Halfpenny, K.; Harry, S. R.; Miller, C. M.; Broncel, M.; Sewell, S. L.; Schaff, J. E.; Deol, R.; Carter, M. D.; Wright, D. W.
- (80) Bremen, J. *American Journal of Tropical Medicine and Hygiene* **2001**, *64*, 1-11.
- (81) World Health Organization, 2002.
- (82) Sherman, I.; ASM Press: Washington, 1998.
- (83) Greenwood, B.; Mutabingwa, T. *Nature* **2002**, *415*, 670-672.
- (84) Goldberg, D. E. *Semin Cell Biol* **1993**, *4*, 355-358.
- (85) Oliveira, M. R.; Timm, B. L.; Machado, E. A.; Kildare, M.; Attias, M.; Silva, J. R.; Dansa-Petretski, M.; de Oliveira, M. A.; De Souza, W.; Pinhal, N. M.; Sousa, J. J. F.; Vugman, N. V.; Oliveira, P. L. *FEBS Letters* **2002**, *512*, 139-144.
- (86) Atamna, H.; Ginsberg, H. *Mol Biochem Parasitol* **1993**, *61*, 231-241.

- (87) Orjih, A. U.; Banyal, H. S.; Chevli, R.; Fitch, C. D. *Science* **1981**, *214*, 667-669.
- (88) Carney, C. K.; Harry, S. R.; Sewell, S. L.; Wright, D. W. In *Naka K*; Springer: Berlin Heidelberg New York, 2006; Vol. Biomineralization.
- (89) Hurst, J. K.; Lymar, S. V. *Acc Chem Res* **1999**, *32*, 520-528.
- (90) Schwarzer, E.; Bellomo, G.; Giribaldi, G.; Ulliers, D.; Arese, P. *Parasitology* **2001**, *123*, 125-131.
- (91) Reiner, N. E. *Immunol Today* **1994**, *15*, 374-381.
- (92) Schwarzer, E.; Alessio, M.; Ulliers, D.; Arese, P. *Infect Immun* **1998**, *66*, 1601-1606.
- (93) Fiori, P. L.; Rappelli, P.; Mirkarimi, S. N.; Ginsberg, H.; Arese, P.; Capuccinelli, P.; Turrini, F. *Parasite Immunol* **1993**, *15*, 647-655.
- (94) Pichyangkul, S.; Saengkrai, P.; Webster, H. *American Journal of Tropical Medicine and Hygiene* **1994**, *51*, 430-435.
- (95) Prada, J.; Malinowsky, J.; Muller, S.; Bienzle, U.; Kremsner, P. *Eur Cytokine Netw* **1995**, *6*, 109-112.
- (96) Sherry, B. A.; Alava, G.; Tracey, K. J.; Martiney, J.; Cerami, A.; Slater, A. F. G. *J Inflamm* **1995**, *45*, 85-96.
- (97) Taramelli, D.; Basilico, N.; Pagani, E.; Grande, R.; Monti, D.; Ghionew, M.; Olliaro, P. *Experimental Parasitology* **1995**, *81*, 501-511.
- (98) Taramelli, D.; Basilico, N.; De Palma, A. M.; Sarasella, M.; Ferrante, P. *Trans. R. Soc. Trop. Med. Hyg.* **1998**, *92*, 57-62.
- (99) Taramelli, D.; Recalcati, S.; Basilico, N.; Olliaro, P.; Cairo, G. *Lab. Invest.* **2000**, *80*, 1781-1788.
- (100) Huckaba, C. E.; Keys, F. G. *J Am Chem Soc* **1948**, *70*, 1640-1644.
- (101) Ditz, H.; Rudolf, M. *Z. Anal. Chem.* **1930**, *79*, 333-345.

- (102) Teufelhofer, O.; Weiss, R.-M.; Parzefall, W.; Schulte-Hermann, R.; Micksche, M.; Berger, W.; Elbling, L. *Toxicological Sciences* **2003**, *76*, 376-383.
- (103) Mohanty, J. G.; Jaffe, J. S.; Schulman, E. S.; Raible, D. G. *Journal of Immunological Methods* **1997**, *202*, 133-141.
- (104) Derham, B. K.; Ellory, J. C.; Bron, A. J.; Harding, J. J. *Eur. J. Biochem.* **2003**, *270*, 2605-2611.
- (105) Steck, T. L.; Kant, J. A. *Methods Enzymol.* **1974**, *31*.
- (106) Babior, B. M. *Blood* **1999**, *93*, 1464-1476.
- (107) Vignais, P. V. *Cell Mol. Life Sci.* **2002**, *59*, 1428-1459.
- (108) De Leo, F. R.; Quinn, M. T. *J. Leukoc. Biol.* **1996**, *60*, 677-691.
- (109) Jaramillo, M.; Godbout, M.; Olivier, M. *J. Immunol.* **2005**, *174*, 475-484.
- (110) Jaramillo, M.; Gowda, D. C.; Radzioch, D.; Olivier, M. *J. Immunol.* **2003**, *171*, 4243-4253.
- (111) Keller, C. C.; Kremsner, P. G.; Hittner, J. B.; Misukonis, M. A.; Weinberg, J. B.; Perkins, D. J. *Infect Immun* **2004**, *72*, 4868-4873.
- (112) Prada, J.; Malinowsky, J.; Muller, S.; Bienzle, U.; Kremsner, P. G. *American Journal of Tropical Medicine and Hygiene* **1996**, *54*, 620-624.
- (113) Tenhunen, R.; Marver, R. S. *J. Biol. Chem.* **1969**, *244*, 6388-6394.
- (114) Chen, M. M.; Shi, L.; Sullivan Jr., D. J. *Molecular and Biochemical Parasitology* **2001**, *113*, 1-8.
- (115) Schaefer, W. H.; Harris, T. M.; Guengerich, F. P. *Biochemistry* **1985**, *24*, 3254-3263.
- (116) Groves, J. T.; Haushalter, R. C.; Nakamura, M.; Nemo, T. E.; Evans, B. J. *J Am Chem Soc* **1981**, *103*, 2884-2886.
- (117) Nagababu, E.; Rifkind, J. M. *Antioxid. Redox Signal* **2004**, *6*, 967-978.

- (118) Nakamoto, K. In *Infrared and Raman spectra of inorganic and coordination compounds Part B*; Nakamoto, K., Ed.; Wiley: New York, 1997, p 319-377.
- (119) Decatur, S. M.; Franzen, S.; Depillis, G. D.; Dyer, R. B.; Woodruff, W. H.; Boxer, S. G. *Biochemistry* **1996**, *35*, 4939-4944.
- (120) Bohle, D. S.; Kosar, A. D.; Stephens, P. *Can. J. Chem.* **2003**, *81*, 1285-1291.
- (121) Albrich, J. M.; McCarthy, C. A.; Hurst, J. K. *Proceedings of the National Academy of Sciences USA* **1981**, *78*, 210-214.
- (122) Arese, P.; Schwarzer, E. *Ann. Trop. Med. Parasitol.* **1997**, *91*, 501-516.
- (123) Schwarzer, E.; De Matteis, F.; Giribaldi, G.; Ulliers, D.; Valente, E.; Arese, P. *Mol. Biochem. Parasitol.* **1999**, *100*, 61-72.
- (124) Neely, M. D.; Amarnath, V.; Weitlauf, C.; Montine, T. J. *Chem. Res. Toxicol.* **2002**, *15*, 40-47.
- (125) Dianzani, C.; Parrini, M.; Ferrara, C.; Fantozzi, R. *Cell Biochem. Funct.* **1996**, *14*, 193-200.
- (126) Poli, G.; Schaur, R. J. *Life Sciences* **2000**, *50*, 315-321.
- (127) Schwarzer, E.; Turrini, F.; Giribaldi, G.; Cappadoro, M.; Arese, P. *Biochimica Biophysica Acta* **1993**, *1181*, 51-54.
- (128) Stenson, W. F.; Parker, C. W. *The Journal of Immunology* **1980**, *124*, 2100-2104.
- (129) Goldie, P.; Roth, E. F.; Oppenheim, J.; Vanderberg, J. P. *American Journal of Tropical Medicine and Hygiene* **1990**, *43*, 584-596.
- (130) Coban, C.; Ishii, K. J.; Hemmi, H.; Sato, S.; Uematsu, S.; Yamamoto, M.; Takeuchi, O.; Itagaki, S.; Kumar, N.; Horri, T.; Akira, S. *Journal of Experimental Medicine* **2005**, *201*, 19-25.
- (131) Millington, O. R.; Di Lorenzo, C.; Phillips, R. S.; Garside, P.; Brewer, J. M. *Journal of Biology* **2006**, *5*, 5.

- (132) Thompson, D.; Chitsulo, L. *Schistosomiasis*, World Health Organization, 2007.
- (133) Bilharz, T.; Kean, B. H.; Mott, K. E.; Russell, A. J. *Reviews of Infectious Diseases* **1982**, *4*, 727-732.
- (134) Levesque, M. A.; Sullivan, A. D.; Meshnick, S. R. *The Journal of Parasitology* **1999**, *85*, 570-573.
- (135) Stenger, R. J.; Warren, K. S.; Johnson, E. A. *The American Journal of Tropical Medicine and Hygiene* **1967**, *16*, 473-482.
- (136) Boyd, M. F. *American Journal of Tropical Medicine* **1924**, *s1-4*, 49-67.
- (137) Gryseels, B.; Polman, K.; Clerinx, J.; Kestens, L. *Lancet* **2006**, *368*, 1106-1118.
- (138) Caffrey, C. R. *Current Opinion in Chemical Biology* **2007**, *11*, 433-439.
- (139) El-Sokkary, G. H.; Omar, H. M.; Hassanein, A.-F. M. M.; Cuzzocrea, S.; Reiter, R. J. *Free Radical Biology & Medicine* **2002**, *32*, 319-332.
- (140) Bedossa, P.; Houglum, K.; Trautwein, C.; Holstege, A.; Chojkier, M. *Hepatology* **1994**, *19*, 1262-1271.
- (141) Parola, M.; Leonarduzzi, G.; Robino, G.; Albano, E.; Poli, G.; Danzani, M. U. *Free Radical Biology & Medicine* **1996**, *20*, 351-359.
- (142) Halliwell, B.; Gutteridge, J. M. C. *Biochemical Journal* **1984**, *219*, 1-14.
- (143) Monnier, V. M. *The Journal of Clinical Investigation* **2001**, *107*, 799-801.
- (144) Laggner, H.; Hermann, M.; Sturm, B.; Gmeiner, B. M. K.; Kapiotis, S. *FEBS Letters* **2005**, *579*, 6486-6492.
- (145) Molina, J. A.; Jimenez-Jimenez, F. J.; Aguilar, M. V.; Meseguer, I.; Mateos-Vega, C. J.; Gonzalez-Munoz, M. J.; de Bustos, F.; Porta, J.; Orti-Pareja, M.; Zurdo, M.; Barrios, E.; Martinez-Para, M. C. *Journal of Neural Transmission* **1998**, *105*, 479-488.
- (146) Slater, A.; Cerami, A. *Nature* **1992**, *355*, 167-169.

(147) Jaramillo, M.; Plante, I.; Ouellet, N.; Vandal, K.; Tessier, P. A.; Olivier, M. *The Journal of Immunology* **2004**, *172*, 3101-3110.

(148) Brown, H. S. *Hematoxylin & eosin (The routine stain)*, Sigma-Aldrich Corporation, 2002.

(149) Majima, H. T.; Nakanishi-Ueda, T.; Ozawa, T. In *Methods in Molecular Biology: Oxidants and Antioxidants: Ultrastructure and Molecular Biology Protocols* 2002; Vol. 196, p 31-34.

(150) Morrow, J. D.; Roberts II, L. J. In *Methods in Enzymology*; Academic Press: 1999; Vol. 300, p 3-12.

(151) Fessel, J. P.; Porter, N. A.; Moore, K. P.; Sheller, J. R.; Roberts II, L. J. *Proceedings of the National Academy of Sciences of the United States of America* **2002**, *99*, 16713-16718.

(152) Eboumbou, C.; Steghens, J. P.; Abdallahi, O. M. S.; Mirghani, A.; Gallian, P.; Van Kappel, A.; Qurashi, A.; Gharib, B.; De Reggi, M. *Acta Tropica* **2005**, *94*, 99-106.

(153) Berhe, N.; Halvorsen, B. L.; Gundersen, T. E.; Myrvang, B.; Gundersen, S. G.; Blomhoff, R. *American Journal of Tropical Medicine and Hygiene* **2007**, *76*, 943-949.

(154) Eissa, L. A.; Gad, L. S.; Rabie, A. M.; El-Gayer, A. M. *Annals of Hepatology* **2008**, *7*, 235-244.

(155) Gharib, B.; Abdallahi, O. M. S.; Dessein, H.; De Reggi, M. *Journal of Hepatology* **1999**, *39*, 594-602.

(156) Salim, E. I.; Morimura, K.; Menesi, A.; Eli-Lity, M.; Fukushima, S.; Wanibuchi, H. *International Journal of Cancer* **2008**, *123*, 601-608.

(157) Rizk, M.; Fayed, T. A.; Badawy, M.; El-Regal, N. S. *Medical Journal of Islamic World Academy of Sciences* **2006**, *16*, 25-34.

(158) Hanna, S.; Gharib, B.; Lepidi, H.; Montet, J. C.; Dumon, H.; De Reggi, M. *Parasitology Research* **2005**, *95*, 6-11.

(159) Dunn, M. A.; Rojkind, M.; Warren, K. S.; Hait, P. K.; Rifas, L.; Seifter, S. *The Journal of Clinical Investigation* **1977**, *59*, 666-674.

- (160) Woodruff, A. W.; al., e. *Trans. R. Soc. Trop. Med. Hyg.* **1966**, *60*, 343-351.
- (161) Friedman, J. F.; Kanzaria, H. K.; McGarvey, S. T. *Trends in Parasitology* **2005**, *21*, 386-392.
- (162) Schwarzer, E.; Muller, O.; Arese, P.; Siems, W. G.; Grune, T. *FEBS Letters* **1996**, *388*, 119-122.
- (163) Poli, G.; Schaur, R. J.; Siems, W. G.; Leonarduzzi, G. *Medicinal Research Reviews* **2008**, *28*, 569-631.
- (164) Sherry, B. A.; al., e. *Journal of Inflammation* **1995**, *45*, 85.
- (165) Davies, S. S.; Amarnath, V.; Roberts II, L. J. *Chemistry and Physics of Lipids* **2004**, *128*, 85-99.
- (166) Murthi, K. K.; Friedman, L. R.; Oleinick, N. L.; Salomon, R. G. *Biochemistry* **1993**, *32*, 4090-4097.
- (167) Davies, S. S.; Amarnath, V.; Montine, K. S.; Bernoud-Hubac, N.; Boutaud, O.; Montine, T. J.; Roberts II, L. J. *FASEB J.* **2002**, *16*, 715-717.
- (168) Salomon, R. G.; Batyreva, E.; Kaur, K.; Sprecher, D. L.; Schreiber, M. J.; Crabb, J. W.; Penn, M. S.; DiCorleto, A. M.; Hazen, S. L.; Podrez, E. A. *Biochimica Biophysica Acta* **2000**, *1485*, 225-235.
- (169) Davies, S. S.; Amarnath, V.; Montine, K. S.; Bernoud-Hubac, N.; Boutaud, O.; Montine, T. J.; Roberts II, L. J. *The FASEB Journal* **2002**, *16*, 715-717.
- (170) Chensue, S. W.; Remick, D. G.; Higashi, G. I.; Boros, D. L.; Kunkel, S. L. *American Journal of Pathology* **1986**, *125*, 28-34.
- (171) Kubata, B. K.; Duszenko, M.; Kabututu, Z.; Rawer, M.; Szallies, A.; Fujimori, K.; Inui, T.; Nozaki, T.; Yamashita, K.; Horii, T.; Urade, Y.; Hayaishi, O. *Journal of Experimental Medicine* **2000**, *192*, 1327-1337.
- (172) Fessel, J. P.; Roberts II, L. J. *Antioxid. Redox Signal* **2005**, *7*, 202-209.
- (173) Oliveira, M. F.; d'Avila, J. C. P.; Tempone, A. J.; Soares, J. B. R. C.; Rumjanek, F. D.; Ferreira-Pereira, A.; Ferreira, S. T.; Oliveira, P. L. *The Journal of Infectious Diseases* **2004**, *190*, 843-852.

- (174) Carter, M. D.; Phelan, V. V.; Sandlin, R. D.; Bachmann, B. O.; Wright, D. W. *Combinatorial Chemistry & High Throughput Screening* **2009**.
- (175) Pagola, S.; Stephens, P. W.; Bohle, D. S.; Kosar, A. D.; Madsen, S. K. *Nature* **2000**, *404*, 307-310.
- (176) Fitch, C.; Kanjanangulpan, P. *J Biol Chem* **1987**, *262*, 15552-15555.
- (177) Bohle, D.; Conklin, B.; Cox, D.; Madsen, S.; Paulson, S.; Stephens, P.; Yee, G. *ACS Symp Ser* **1994**, *572*, 497-515.
- (178) Bohle, D.; Dinnebier, R.; Madsen, S.; Stephens, P. *J. Biol. Chem.* **1997**, *272*, 713-716.
- (179) Sullivan Jr., D. J.; Gluzman, I. Y.; Russell, D. G.; Goldberg, D. E. *Proc. Natl. Acad. Sci. U.S.A.* **1996**, *93*, 11865-11870.
- (180) Bendrat, K.; Berger, B.; Cerami, A. *Nature* **1995**, *378*, 138-139.
- (181) Dorn, A.; Vippagunta, S.; Matile, H.; Bubendorf, A.; Vennerstrom, J.; Ridley, R. *Biochem Pharmacol* **1998**, *55*, 737-747.
- (182) Egan, T. J.; Ross, D. C.; Adams, P. A. *FEBS Letters* **1994**, *352*, 54-57.
- (183) Dorn, A.; Stoffel, R.; Matile, H.; Bubendorf, A.; Ridley, R. *Nature* **1995**, *374*, 269-271.
- (184) Huy, N. T.; Maeda, A.; Uyen, D. T.; Trang, D. T. X.; Sasai, M.; Shiono, T.; Oida, T.; Harada, S.; Kamei, K. *Acta Tropica* **2007**, *101*, 130-138.
- (185) Huy, N. T.; Uyen, D. T.; Maeda, A.; Trang, D. T. X.; Oida, T.; Harada, S.; Kamei, K. *Antimicrobial Agents and Chemotherapy* **2007**, *51*, 350-353.
- (186) Parapini, S.; Basilico, N.; Pasini, E.; Egan, T. J.; Olliaro, P.; Taramelli, D.; Monti, D. *Experimental Parasitology* **2000**, *96*, 249-256.
- (187) Kurosawa, Y.; Dorn, A.; Kitsuji-Shirane, M.; Shimada, H.; Satoh, T.; Matile, H.; Hofheinz, W.; Masciadri, R.; Kansy, M.; Ridley, R. G. *Antimicrobial Agents and Chemotherapy* **2000**, *44*, 2638-2644.
- (188) Ziegler, J.; Pasierb, L.; Cole, K. A.; Wright, D. W. *Journal of Inorganic Biochemistry* **2003**, *96*, 478-486.

- (189) Chong, C. R.; Sullivan, D. J. *Biochemical Pharmacology* **2003**, *66*, 2201-2212.
- (190) Bohle, D. S.; Helms, J. B. *Biochemical and Biophysical Research Communications* **1993**, *193*, 504-508.
- (191) Michel, H.; Oesterhelt, D. *Proceedings of the National Academy of Sciences USA* **1980**, *77*, 1283-1285.
- (192) Garavito, R. M.; Rosenbusch, J. P. *The Journal of Cell Biology* **1980**, *86*, 327-329.
- (193) Michel, H. *J. Molec. Biol.* **1982**, *158*, 567-572.
- (194) Michel, H. *Trends in biochemical sciences* **1983**, *8*, 56-59.
- (195) Garavito, R. M.; Markovic-Housley, Z.; Jenkins, J. A. *Journal of Crystal Growth* **1986**, *76*, 701-709.
- (196) Roth, M.; Lewit-Bentley, A.; Michel, H.; Deisenhofer, J.; Huber, R.; Oesterhelt, D. *Nature* **1989**, *340*, 659-662.
- (197) Roth, M.; Arnoux, B.; Ducruix, A.; Reiss-Husson, F. *Biochemistry* **1991**, *30*, 9403-9413.
- (198) Barber, J. *Nature* **1989**, *340*, 601.
- (199) Chin, Y.-W.; Balunas, M. J.; Chai, H. B.; Kinghorn, A. D. *The AAPS Journal* **2006**, *8*, E239-E253.
- (200) White, N. J. *Science* **2008**, *320*, 330-334.
- (201) Barton, H. A.; Jurado, V. In *Microbe* 2007; Vol. 2, p 132-138.
- (202) De, D.; Krogstad, F. M.; Cogswell, F. B.; Krogstad, D. J. *American Journal of Tropical Medicine and Hygiene* **1996**, *55*, 579-583.
- (203) Biot, C.; Glorian, G.; Maciejewski, L. A.; Brocard, J. S. *Journal of medicinal chemistry* **1997**, *40*, 3715-3718.
- (204) O'Neill, P. M.; Mukhtar, A.; Stocks, P. A.; Randle, L. E.; Hindley, S.; Ward, S. A.; Storr, R. C.; Bickley, J. F.; O'Neill, I. A.; Maggs, J. L.; Hughes, R. H.;

Winstanley, P. A.; Bray, P. G.; Park, B. K. *Journal of medicinal chemistry* **2003**, *46*, 49333-4945.

(205) Kiszewski, A.; Johns, B.; Schapira, A.; Delacollette, C.; Crowell, V.; Tan-Torres, T.; al., e. *Bull World Health Organ* **2007**, *85*, 623-630.

(206) Foley, M.; Tilley, L. *J. Parasitol.* **1997**, *27*, 231-240.

(207) Cooper, R. A.; al., e. *Mol. Pharmacol.* **2002**, *61*, 35-42.

(208) Kelly, J. X.; Smilkstein, M. J.; Brun, R.; Wittlin, S.; Cooper, R. A.; Lane, K. D.; Janowsky, A.; Johnson, R. A.; Dodean, R. A.; Winter, R.; Hinrichs, D. J.; Riscoe, M. K. *Nature* **2009**, *459*, 270-273.

(209) Hayward, R.; Saliba, K. J.; Kirk, K. *Journal of Cell Science* **2006**, *119*, 1016-1025.

(210) Lipinski, C. A.; Lombardo, F.; Dominy, B. W.; Feeney, P. J. *Advanced Drug Delivery Reviews* **2001**, *46*, 3-26.

(211) Abraham, M. H.; Chadha, S. H.; Whiting, G. S.; Mitchell, R. C. *J. Pharm. Sci.* **1994**, *83*, 1085-1100.

(212) Cohen, B. E.; Bangham, A. D. *Nature* **1972**, *236*, 173-174.

(213) Pardridge, W. M. *Advanced Drug Delivery Reviews* **1995**, *15*, 5-36.

(214) Testa, B.; Carrupt, P.-A.; Gaillard, P.; Billois, F.; Weber, P. *Pharm. Res.* **1996**, *13*, 335-343.

(215) Pozharskii, A. F.; Dal'nikovskaya, V. V. *Russian Chemical Reviews* **1981**, *50*, 1559-1600.

(216) Kumar, S.; Guha, M.; Choubey, V.; Maity, P.; Bandyopadhyay, U. *Life Sciences* **2007**, *80*, 813-828.

(217) Raynes, K.; Foley, M.; Tilley, L.; Deady, L. W. *Biochemical Pharmacology* **1996**, *52*, 551-559.

(218) Chong, C. R.; Sullivan Jr., D. J. *Biochemical Pharmacology* **2003**, *66*, 2201-2212.

- (219) Tiffert, T.; Ginsburg, H.; Krugliak, M.; Elford, B. C.; Lew, V. L. *Proceedings of the National Academy of Sciences of the United States of America* **2000**, *97*, 331-336.
- (220) Huy, N. T.; Kamei, K.; Yamamoto, T.; Kondo, Y.; Kanaori, K.; Takano, R.; Tajima, K.; Hara, S. *The Journal of Biological Chemistry* **2002**, *277*, 4152-4158.
- (221) Huy, N. T.; Takano, R.; Hara, S.; Kamei, K. *Biological & Pharmaceutical Bulletin* **2004**, *27*, 361-365.
- (222) Loup, C.; Lelievre, J.; Benoit-Vical, F.; Meunier, B. *Antimicrobial Agents and Chemotherapy* **2007**, *51*, 3768-3770.
- (223) Towne, V.; Will, M.; Oswald, B.; Zhao, Q. *Analytical Biochemistry* **2004**, *334*, 290-296.
- (224) Konarska, L.; Tomaszewski, L. *Clinica Chimica Acta* **1986**, *154*, 7-18.
- (225) Chinard, F. P. *Journal of Biological Chemistry* **1952**, *199*, 91-95.
- (226) Thompson, R. W.; Pesce, J. T.; Ramalingam, T.; Wilson, M. S.; White, S.; Cheever, A. W.; Ricklefs, S. M.; Porcella, S. F.; Li, L.; Ellies, L. G.; Wynn, T. A. *PLOS Pathogens* **2008**, *4*, e1000023(1-17).
- (227) Corraliza, I. M.; Campo, M. L.; Soler, G.; Modolell, M. *Journal of Immunological Methods* **1994**, *174*, 231-235.
- (228) Cook, J. A.; Wise, W. C.; Halushka, P. V. *Journal of Clinical Investigation* **1980**, *65*, 227-230.
- (229) Egan, T. J.; Chen, J. Y.-J.; de Villiers, K. A.; Mabotha, T. E.; Naidoo, K. J.; Ncokazi, K. K.; Langford, S. J.; McNaughton, D.; Pandiancherri, S.; Wood, B. R. *FEBS Letters* **2006**, *580*, 5105-5110.
- (230) Pisciotta, J. M.; Coppens, I.; Tripathi, A. K.; Scholl, P. F.; Shuman, J.; Bajad, S.; Shulaev, V.; Sullivan Jr., D. J. *Biochemistry Journal* **2007**, *402*, 197-204.
- (231) Pisciotta, J. M.; Coppens, I.; Tripathi, A. K.; Scholl, P. F.; Shuman, J.; Bajad, S.; Shulaev, V.; Sullivan, D. J. *Biochemistry Journal* **2007**, *402*, 197-204.

Melissa D. Carter
Graduate Research Assistant
VU Station B 351822
Department of Chemistry, Vanderbilt University
Nashville, TN 37235-1822
Lab: (615) 322-5516; Fax: (615) 343-1234
melissa.d.carter@vanderbilt.edu

Research Interest

My dissertation is comprised of a multi-disciplinary body of work including inorganic chemistry, physical methods for characterization, mammalian tissue culture, animal models and HTS assay development and screening. The uniting factor among these topics is the reactive chemistry preceding and following the formation of a heme-derived biomineral called hemozoin. Hemozoin is a detoxification byproduct found in hemophagous parasitic diseases such as malaria and schistosomiasis, and its presence has been implicated in host immunomodulation. Once formed and engulfed by professional phagocytes, the host immune system cannot rid itself of these aggregates; they accumulate as a dark pigment in the already fibrotic tissue of the host and lead to cellular dysfunction by way of hemozoin-mediated lipid peroxidation. A *Schistosoma mansoni* infected Swiss Webster murine model was used to study the oxidative stress imposed by hemozoin. The oxidation products extracted were assessed using UPLC-MS/MS and high-resolution TOF MS/MS. Lipids were also shown to play a role in the formation of hemozoin. Unlike the oxidized lipids observed following hemozoin formation, a blend of neutral lipids were found to form nano-droplets within the digestive food vacuole of the malaria parasite and the gut lumen of the schistosome in which heme could then accumulate and form hemozoin. Using these findings, a lipophilic *in vitro* 384-well HTS assay was developed that could support the reproducible screening of compounds for their potential as inhibitors of hemozoin formation like the well-known antimalarials chloroquine and amodiaquine.

Education

Vanderbilt University

Ph.D. degree in Bioinorganic Chemistry, August, 2009

Transylvania University

B.A. degree in Chemistry, June 2005
Minors in Biology and Music

Professional and Research Experience

Graduate Research Assistant	August 2005-current	Vanderbilt University
Undergraduate Research Assistant	Summer 2004	NASA, Langley
Undergraduate Research Assistant	Summer 2003	Transylvania University
Undergraduate Research Assistant	Summer 2002	University of Kentucky

Fellowships and Awards

The American Institute of Chemists Student Award	2005
Langley Aerospace Research Summer Scholars Program	2004
Transylvania University John Kenan Research Grant Recipient	2003
EPSCoR Research Grant Recipient	2002

Professional Societies and Activities

American Chemical Society (member)	2006-current
President of the Transylvania University Student Affiliate Chapter	2001-2005
American Association for the Advancement of Science (member)	2007-current

Teaching

Vanderbilt University

Teaching Assistant for:

- General Chemistry Labs (Chem 104A&B) – Fall 2005, Fall 2006, Spring 2007, Fall 2007
- Analytical Chemistry Lab (Chem 212A) – Spring 2006
- Introduction to Bioinorganic Chemistry (Chem 202) – Spring 2008
- Chemical Literature (Chem 250) – Spring 2008

Transylvania University

National Science Tutoring Program	2003-2004
General Chemistry Workshop Peer Team Leader	Fall 2002

Selected Service Activities

Vanderbilt University

Vanderbilt University Graduate Student Chemistry Steering Committee	2006-2008
Vanderbilt University Medical Center Volunteer Services	2008-current

Transylvania University

Student Programming Fund Allocation Committee	2003-2004
Transylvania Science Day	2001-2003
Lexington Children's Museum Science Fair	2003

Publications

Carter, M.D.; Sandlin, R.D.; Wright, D.W. High Throughput Screens for Inhibitors of β -Hematin Crystallization. *In progress*.

Carter, M.D.; Gliga, B.; Scott, V.J.; Roberts, L.J.; Wright, D.W. Hemozoin-Mediated Lipid Peroxidation in Schistosomiasis. *In progress*.

Carter, M.D.; Phelan, V.V.; Sandlin, R.D.; Bachmann, B.O.; Wright, D.W. Lipophilic Mediated Assays for β -Hematin Inhibitors. *Comb. Chem. High Throughput Screen*. **Accepted** March 24, 2009.

Carter, M.D.; Hoang, A.N.; Wright, D.W. Hemozoin: A Paradigm for Biominerals in Disease. *Wiley Encyclopedia of Chemical Biology*. John Wiley and Sons, Inc. **2008**. 11pp. DOI: 10.1002/9780470048672.webc649.

Carter, M.D.; Harry, S. Reese; Wright, D.W. Identification of Hydroxyeicosatetraenoic Acid Components of Schistosomal Hemozoin. *Biochem. Biophys. Res. Commun.* **2007**, 363(3), 867-872.

Carney, C.K.; Schrimpe, A.C.; Halfpenny, K.C.; Harry, S.R.; Miller, C.M.; Broncel, M.; Sewell, S.L.; Schaff, J.E.; Deol, R.; Carter, M.D.; Wright, D.W. The Basis of Immunomodulatory Activity of Malaria Pigment (Hemozoin). *J. Biol. Inorg. Chem.* **2006**, 11(7), 917-929.

Presentations

“A High Throughput Screen for Beta-Hematin Inhibitors” Melissa D. Carter, R.D. Sandlin, David W. Wright. Oral Presentation at the 60th Southeast Regional Meeting of the American Chemical Society, November 12-15, 2008 in Nashville, Tennessee.

“*In Situ* Isolation of Schistosomal Hemozoin” Melissa D. Carter, Brooke Gliga, Vanessa J. Scott, L. Jackson Roberts, David W. Wright. Oral Presentation at the 60th Southeast Regional Meeting of the American Chemical Society, November 12-15, 2008 in Nashville, Tennessee.

“Schistosomal Hemozoin-Mediated Lipid Peroxidation” Melissa D. Carter, S. Reese Harry, David W. Wright. Oral Presentation at the 235th National Meeting of the American Chemical Society, April 6-10, 2008 in New Orleans, Louisiana.

“Hemozoin Mediated Immunosuppression: A Role in Schistosomiasis?” S. Reese Harry, Melissa D. Carter, David W. Wright. Poster Presentation at the Keystone Symposia Meeting on *The Macrophage: Homeostasis, Immunoregulation and Disease (D2)*, April 11-16, 2007 in Copper Mountain, Colorado.

“Atmospheric Plume Modeling of Class 2 Liquefied Compressed Gases” Melissa Carter, Norman Loney, Gowri Rao, Megan Seals, Biongo Bosuku, Brian Tisdale, Russell Clark, Traci Chisholm, Petra Harvey. Poster Presentation at the 229th National Meeting of the American Chemical Society, March 13-17, 2005 in San Diego, California.

“Screening of Freshwater Algae for Possible Anticancer Activity” Melissa Carter, Carl E. Heltzel. Poster Presentation at the 227th National Meeting of the American Chemical Society, March 28-April 1, 2004 in Anaheim, California.

“Ti(II)-Mediated Cyclotrimerization of Alkynes” Rebecca H. Huyck, Melissa Carter, Carl E. Heltzel, Folami Ladipo. Poster Presentation at the 225th National Meeting of the American Chemical Society, March 23-27, 2003 in New Orleans, Louisiana and the 9th Annual EPSCoR Conference, May 12, 2003 in Lexington, Kentucky.